NONLINEAR FINITE ELEMENT ANALYSIS OF

REINFORCED CONCRETE COUPLED SHEAR WALLS

by

SALAH EDDINE DJELLAB

Ingenieur d'Etat en Genie Civil

Ecole Nationale Polytechnique d'ALGER

A Thesis submitted for the Degree of

Master of Science

Department of Civil Engineering,

University of Glasgow.

JUNE, 1991.

In the name of God, Most Gracious, Most Merciful

Read *In the name of thy Lord who created*

He created man from a clot

Read *and thy Lord is Most Bountiful*

He who taught with the **Pen**,

Taught man that what he knew not.

TO MY PARENTS AND THE MARTYRS OF THE ALGERIAN REVOLUTION

FOR INDEPENDANCE.

SUMMARY

This thesis is concerned with the development of an inelastic material model to be used in conjunction with the finite element technique to simulate the behaviour of reinforced concrete shear—walls under lateral loads. The proposed computational model is capable of tracing the entire nonlinear response up to ultimate load conditions. The main features of the nonlinear behaviour of concrete and steel are incorporated in the numerical model. These include cracking, nonlinear biaxial stress—strain relationships in concrete up to crushing and yielding of steel.

The investigation first considers the linear elastic behaviour of coupled shear—walls then a consistent material model that matches the existing experimental evidence for the behaviour of plain concrete under monotonic biaxial loading is considered. The reinforcing steel is idealized as bilinear uniaxially stressed material.

The individual material models are combined with the finite element technique to demonstrate their applicability. To check the validity and accuracy of the numerical model, finite element calculations are compared with experimental results for shallow and deep beams, shear panels subjected to monotonic loading. Finally, various hypothetical coupled shear—walls and tested microconcrete shear walls were analysed highlighting the history of crack propagation, deflections, crushing of concrete and yielding of steel up to failure.

The resulting model should prove to be a simple useful research tool for use in the study of any reinforced concrete structure which may be considered to be in a state of plane stress.

ACKNOWLEDGEMENTS

CONTENTS

CHAPTER THREE : NUMERICAL MODELLING OF CONCRETE AND STEEL

3-1 Introduction

3-2 Mechanical behaviour of concrete

    3-2-1 Uniaxial compressive stress-strain response

    3-2-2 Uniaxial tensile stress-strain response

    3-2-3 Biaxial behaviour

3-3 Constitutive modelling of concrete

    3-3-1 Elasticity based models

    3-3-2 Plasticity based models

    3-3-3 Plastic-Fracturing models

    3-3-4 Endochronic base models

3-4 Cracked concrete models

    3-4-1 Discrete cracking models

    3-4-2 Smeared cracking models

    3-4-3 Fracture mechanics

3-5 Present model for concrete

    3-5-1 Concrete in compression

        3-5-1-1 Elastic concrete

        3-5-1-2 Inelastic concrete

        3-5-1-3 Crushed concrete

    3-5-2 Concrete in tension

        3-5-2-1 Singly cracked concrete

        3-5-2-2 Doubly cracked concrete

    3-5-3 Tension stiffening

    3-5-4 Shear retention across cracks

3-6 Constitutive modelling of steel bars

    3-6-1 Elastic perfectly plastic model

CHAPTER SIX: APPLICATIONS TO COUPLED SHEARWALLS

CHAPTER SEVEN: CONCLUSION AND SUGGESTIONS FOR FUTURE WORK

CHAPTER 1

INTRODUCTION

1-1 GENERAL :

Reinforced concrete is by far one of the most commonly used construction materials with applications in many types of structures such as tall buildings, bridges, cooling towers, nuclear containment and pressure vessels, etc. Despite this widespread use of concrete as a structural material, knowledge about its physical properties and behaviour under general multiaxial stress states is still incomplete or rather deficient. The main reason for this is that this composite material demonstrates a highly nonlinear behaviour caused by cracking, aggregate interlock at crack interfaces, dowel action in bars crossing cracks, bond—slip phenomenon between steel and concrete, crushing of inelastic concrete and yielding of steel among others. Therefore it becomes apparent that formulation of rational analytical procedures is very difficult. To overcome these limitations, both analytical and experimental studies of reinforced concrete members, as basic components of complete structural systems, have been the focus of a number of investigators for many years and continue to be so. These early studies, by necessity, concentrated on the behaviour of isolated members such as beams, columns, joints, slabs, etc. As facilities developed and computing hardware capability expanded, the scope broadened to include entire systems such as full scale three dimensional buildings. These developments in the power of modern computing systems along with the accumulated data from tests, have made possible the inclusion of the complex material behaviour under multiaxial stress conditions into methods of analysis.

Present day linear analysis methods are generally considered adequate in engineering design practice, because structures designed on the basis of these simplified analysis methods have, by and large, behaved satisfactorily, and the complexity of reinforced concrete behaviour has left little other choice. However,

the adequacy of these traditional methods have been questioned in a number of applications. Foremost is the construction of nuclear power plants. A second application for which the standard design methods may be inadequate is the design of tall concrete structures to safely withstand strong lateral loads induced by earthquake ground motions for which ductility and energy absorbtion capacity, associated with large inelastic deformations is to be activated. In a more general sense, there exists a fundamental inconsistency in current analysis and design practice. While structures are generaly analysed using linear elastic methods, they are designed on the basis of ultimate uniaxial strength conditions. In contrast, the material within these structures is nonlinear and in a multiaxial state of stress.

The most powerful and general method now available in structural analysis, by which a complete detailed study can be performed, is the finite element method. Its basic concepts are now well estabilished and have been widely published. Its generality and versatility are particularly essential for structural systems that fall outside the experimental database, because physical experiments to determine the sequence of formation and location of failure modes were not easy to conduct. The scaling of these structures made the construction of physical models of the size to fit into laboratories very difficult, demanding and expensive. Such problems are also seen in the case where the number of necessary experimental test specimens is extremly large in accordance with the variety of loading and boundary conditions. This is particularly important for reinforced concrete shear walls which have usually been tested using small scale models of microconcrete mix or perspex materials. Because full scale experimental studies on reinforced concrete coupled shear walls are difficult and costly, if not impossible at the moment, the use of the finite element methods incorporating the main features of the nonlinear behaviour of the constituent materials, concrete and steel, is a well justified alternative for simulating the behaviour of such systems up to failure. This prompted the so called numerical experiments being adopted in this study.

1-2 SCOPE AND PURPOSE :

Computer aided structural analysis of reinforced concrete structures has been the object of extensive research for almost three decades. The usual method of modelling reinforced concrete systems is to make use of finite element models with various degrees of sophistication that have been used successfully for predicting the response of reinforced concrete beams, slabs and shells, etc.

The purpose of this study is an attempt to demonstrate the possibility of predicting the history of stresses, deflections and crack propagation, crushing of concrete and yielding of steel up to failure of reinforced concrete coupled shear walls. Therefore, the first objective was to develop a nonlinear plane stress finite element program which can analyse a wide range of reinforced concrete systems in plane stress conditions and subjected to short term loading up to failure. The ultimate purpose of this study was to estabilish an economical computer program and procedures to undertake a parametric study of shear wall behaviour.

A review of the available analytical and computational methods of analysis is given in Chapter 2, in which numerical investigations using these methods were deemed necessary to carry out a parametric study on coupled shear walls. Studies on the degree of accuracy of each of the following methods, namely, continuum shear analogy, wide-column frame analogy and finite element techniques have been carried out.

In Chapter 3 , a survey of available literature on the experimental behaviour of concrete and steel and their mathematical modelling is given along with a description of the mathematical model used to simulate their experimental behaviour in this study. An orthotropic biaxial model of concrete is used to represent various aspects of concrete behaviour suited to two dimensional plane stress problems. It simulates the behaviour of concrete in the compression-compression zone up to crushing type of failure, and in the tension-tension and combined tension-compression up to cracking type of failure. For cracking and post cracking behaviour of concrete, the smeared approach is used, including tension stiffening

due to bond between steel and concrete, and a variable shear retention factor simulating dowel action and friction at the interfaces of an open crack. For steel reinforcement a bilinear uniaxial model with or without strain hardening is employed.

In chapter 4 , nonlinear methods of solution are discussed and a description of the method adopted in this study is presented.

The validity and accuracy of the finite element model is tested and reported in chapter5 by comparing the results obtained from the present analysis with carefully conducted experimental tests on various concrete structures.

Chapter 6 presents some numerical applications of reinforced concrete shear walls including the influence of the degree of coupling, position of the openings, stiffening beam in the top, stiffening beam at midheight, on the ultimate load, crack propagation and mode of failure including the sequence of yielding of steel and crushing of concrete in the lintel beams and walls.

Finally, general conclusions and recommendations for future work are presented in chapter 7.

CHAPTER 2

ANALYTICAL AND COMPUTATIONAL METHODS OF ANALYSIS

2-1 INTRODUCTION :

The structural analysis of tall shear wall buildings has been treated extensively in technical literature in recent years as most designers are aware of the benefits that shear walls can offer in the lateral load resistance of multistorey buildings. The most frequent causes of horizontal loads are due to wind, blasts and earthquake actions. For tall buildings the effect of lateral loads is very significant, from both the ultimate strength and serviceability points of view, and it is important to ensure adequate strength and stiffness to resist these horizontal loads.

Because a large portion of the lateral load on a building, if not the whole amount, and the resulting shear force from the load, are often resisted by such structural elements, they have been called shear walls. However, it should be noted that rarely is the critical mode of resistance associated with shear. As multistorey buildings have become taller and more slender, the trend for the use of shear walls is almost imperative in certain high rise buildings to control overall lateral deflections and interstorey drift. The observed behaviour of well designed shear walls has convincingly shown their potential in damage control, providing safety and protection against nonstructural damage during moderate seismic disturbances.

Buildings comprising such structural systems are commonly of 10 to 30 storeys, and their behaviour is influenced by the shape of the walls whether planar, flanged or cores, and their position. The plan distribution of walls should be such that the building is torsionally as well as flexurally stiff. In its simplest form the shear wall consists of a single monolithic cantilever wall and can be classified as, short, squat or cantilever according to its height to depth ratio, Fig (2-1). However, in general reinforced concrete shear walls are often interrupted by vertical bands of openings

for doors, windows and corridors, yielding highly indeterminate structures from the point of view of stress analysis, Fig (2—2). In such cases the behaviour is much more complicated. The practical importance to the designer of obtaining accurate methods of analysis of such coupled wall structures has emerged as a critical design item reflected in the large number of papers devoted to this subject.

Three main distinct methods have been developed for the efficient and accurate analysis of such structures, Fig (2—3):

1— The continuum method (Analytical).

2— The wide—column frame analogy (Computational).

3— The finite element technique (Computational).

In this chapter, the various analytical and computer based methods for the analysis of tall shear wall buildings are discussed. Numerical investigations using the above three techniques are presented, and wherever possible, comparison of the accuracy of results due to these different methods is made. Special emphasis on structural features such as local deformations and stress concentrations at beam—wall junctions, degree of rigidity of the coupling are incorporated in the analysis. This will provide valuable information on the main factors affecting the response of shear walls in the simple case of linear elastic theory, before a study of these systems loaded up to collapse can be pursued, using the experimentally based constitutive laws of concrete and steel.

2-2 CONTINUUM SHEAR CONNECTION ANALOGY :

In this method the discrete system of connections, formed by lintel beams or floor slabs are replaced by an equivalent substitute continuous medium Fig (2-4). By assuming that the lintel beams coupling the walls have a point of contraflexure at midspan and do not deform axially, conditions of compatibility and equilibrium yield a governing differential equation of the second order, enabling a closed mathemetical solution to the problem to be obtained for specific loading functions (uniform, triangular or point loads).

The continuum technique appears to have been first used by Chitty and Wan 1947 , in the analysis of a cantilever composed of a number of parallel beams interconnected by cross bars. This was later used by Beck 1962 , who applied this technique to coupled shear walls taking the shear forces in the connecting medium as the basic statically indeterminate redundant to investigate the behaviour of a single case of coupled shear walls on rigid foundations subjected to uniformly distributed load. Rosman 1964 subsequently extended the method to cope with various boundary conditions at the lower end, and derived solutions for a wall system with one or two symmetric bands of openings under both a uniformly distributed load and a single point load at the top. Many other researchers in the field such as Coull and al. in the U.K, Tso and his colleagues in Canada, Gluck and Gellert in palestine have all contributed a good deal to the development and extension of this approach using a similar procedure. Explicit theoretical solutions have been presented for the common practical cases using this technique which are in good agreement with experimental tests conducted on model structures. Further developments of the method are reviewed below:

(a) Variation of cross section :

Traum 1967 used the continuous connection method to analyse symmetrical coupled shear walls pierced by one band of openings and with a single stepped variation in cross section and considered the upper zone of the wall as elastically supported on the lower one at the discontinuity. The lower zone was then analysed being subjected to axial forces, bending moment and shearing force at its top together with the horizontal external loading. Using the same approach Coull and Puri 1967 presented another type of discontinuity by considering a stepped variation in the thickness of the walls, and presented in 1968 a simpler analysis of the problem considered by Traum 1967, but applied the loads simultaneously and included the effects of shear deformations in the walls.

(b) Multi- bay shear wall structures:

Most of the published work deals with two wall structures, in which case, the set of equations ensuring compatible deformations and equilibrium degenerates into a single differential equation comprising the redundancies. Hussein 1972 presented a method based on a continuous media technique for the analysis of multi- bay shear wall structures resting on rigid foundations. This required formulation of governing simultaneous second order coupled differential equations, for which numerical solution was sought by the matrix orthogonalization method. In the case of shear walls with slender connecting beams, good agreement was obtained between the theoretical and experimental results conducted on perspex models. Coull and Subedi 1972 presented an explicit solution for the case of shear wall containing either two asymmetrical or three symmetrical bands of openings, and theoretical deflection profiles and bending stress distributions have been compared with results obtained from tests. Elkholy and Robinson 1973 extended the problem to deal with multi- bay structures resting on rigid and elastic foundations.

(c) Beam—wall joint flexibility:

The importance of beam—wall joint flexibility and the local deformations due to high stress intensities have been analysed by Michael 1967 who considered the wall as a semi—infinite elastic plane and took the effect of the local deformations by reducing the beam stiffnesses by factors depending on the geometric proportions of the beams. Further refined work was done by Bhatt 1973 who conducted an investigation of the local deformations using the finite element technique and suggested modifications presented in graphical and tabular forms which could be applied to the continuous technique to take into account the effect of local deformations.

(d) Elastoplastic analysis:

It appears that, while the procedure has many limitations, the continuum idealization has proved sufficiently accurate to allow study of the basic behaviour of coupled systems. For wind loading on tall structures, such elastic analysis is generally adequate, since the criterion governing design is usually the deflection. However, for strong seismic excitation, the walls as well as the connecting elements may experience extensive yielding, and nonlinear behaviour results.

Ultimate analysis employing the above continuous connection method was first introduced by Winokur and Gluck 1968. They considered symmetrical and unsymmetrical coupled shear walls with uniform or abrupt changes in cross section. They assumed a complete collapse mechanism, by formation of plastic hinges at points of contact of all connecting beams and the shear—wall, and at the base of the latter. Extensive work by Paulay (1970,1971), resulted in an approximate stagewise procedure in which a fixed sequence of partial failure mechanisms involving the walls and beams is assumed prior to collapse. He included the effect of cracking of both connecting beams and piers by making an arbitrary reduction in their stiffness, and traced the post—elastic performance of the structure by

means of a step by step procedure. Gluck's formulation 1973 of the elastoplastic behaviour of the coupling continuum, with walls assumed elastic, provided lateral capacity based on the rotational yield limitation in the connecting beams. Elkholly and Robinson 1974 presented a finite difference method to solve the resulting differential equation of the continuum shear analogy for elastic and inelastic analysis of coupled shear walls resting on rigid, elastic or inelastic foundations, with constant or variable cross section. The effects of cracking of the reinforced concrete elements as well as the gravity loads were included in the analysis. Coull and Choo 1982 presented a simplified version of a technique described by Pekau and Gocevski 1978 for the elasto−plastic analysis of coupled shear walls with top stiffening beam.

Finally, a completely new aspect of the analysis of shear walls using the shear connection analogy was presented by Ungureanu 1976 who proposed a structural model by which the horizontal elements coupling the vertical members are replaced by a connection of variable stiffness according to a periodic law. This is an attempt to take into account more efficiently the local effects at the joints between horizontal and vertical elements. The concept of periodic continuous connection as proposed by Ungureanu who neglected axial deformations in the walls, needs further investigation as compared to the widely used simple constant stiffness distribution. The continuum method is the only method amenable to hand calculations for regular systems, although in many cases the use of a small computer is advisable.

2-3 WIDE-COLUMN FRAME ANALOGY :

The analysis of coupled shear walls by the wide-column frame analogy is basically an extension of the stiffness method. The first of the frame analogies is the equivalent frame method used by Green 1952, who replaced the walls by line members along their centroidal axes and assumed points of contraflexure at midpoints of all members. He neglected axial deformations of the walls and the influence of the finite width of the walls compared to the centre line distances, both of which may be of major importance in tall slender structures. An improvement on the equivalent frame method is the so called wide-column frame idealization. In this method a planar coupled shear wall can be idealized as a frame in which the walls and beams are represented by line elements of corresponding stiffness along their centroidal axes Fig (2-5). The influence of the finite width of the walls is incorporated by a stiff arm connecting the end of the beams to the centroidal axis of the wall Fig (2-5). By formulating the stiffness matrix relating displacements and external applied forces at the nodes a solution is derived using standard matrix procedures. MacLeod 1967 used the stiffness method to obtain a solution by incorporating infinitely stiff end sections. A variation of the method, was presented by Shwaighofer and Microys 1969 who considered the rigid arms as members with high but finite values of cross section area and moment of inertia.

The wide-column frame analogy method is relatively more versatile than the continuum method in that, variations in wall thickness, storey height, loading function and opening sizes may be taken into account easily.

In the present study a computer program **WFRAME** based on the wide-column frame analogy has been developed for the analysis of coupled shear walls under lateral loads. Incorporation of a transformation matrix procedure has been adopted to include the effect of the rigid ends which account for the finite

dimensions of the much stiffer walls. This allows consideration of the lintel beams along with the rigid arms as a single member.

A wall element between two consecutive floors is usually represented by a frame element with three degrees of freedom per node, Fig (2—5), corresponding to axial, lateral deflection and rotation. The stiffness matrix of which, taking into account axial and shear deformations effects, not to be neglected due to the large height to depth ratio is expressed as :

$$
[K_w] =
\begin{array}{cccccc}
u_i & v_i & \theta_i & u_j & v_j & \theta_j \\
\end{array}
$$

$$
[K_w] = \left[
\begin{array}{cccccc}
\dfrac{EA}{h} & & & & & \\[2ex]
0 & \dfrac{12EI}{(1+\alpha)h^3} & & & & \\[2ex]
0 & \dfrac{6EI}{(1+\alpha)h^2} & \dfrac{(4+\alpha)EI}{(1+\alpha)h} & & & \\[2ex]
\dfrac{-EA}{h} & 0 & 0 & \dfrac{EA}{h} & & \\[2ex]
0 & \dfrac{-12EI}{(1+\alpha)h^3} & \dfrac{-6EI}{(1+\alpha)h^2} & 0 & \dfrac{12EI}{(1+\alpha)h^3} & \\[2ex]
0 & \dfrac{6EI}{(1+\alpha)h^2} & \dfrac{(2-\alpha)EI}{(1+\alpha)h} & 0 & \dfrac{-6EI}{(1+\alpha)h^2} & \dfrac{(4+\alpha)EI}{(1+\alpha)h}
\end{array}
\right] \qquad (2\text{-}1)
$$

The term $\alpha = 12EIk/h^2 GA$ deals with shear deformations effects, k is the shape factor which is equal to 1.2 for rectangular sections.

The beams are usually assumed to be axially rigid and therefore, only four degrees of freedom are associated with each beam element Fig (2— 5), and the stiffness matrix is

$$[K_b^*] = \frac{EI}{(1+\alpha)}
\begin{matrix}
v_A^* & \theta_A^* & v_B^* & \theta_B^* \\
\end{matrix}
\begin{bmatrix}
\dfrac{12}{L^3} & & & \\[2ex]
\dfrac{6}{L^2} & \dfrac{(4+\alpha)}{L} & & \\[2ex]
\dfrac{-12}{L^3} & \dfrac{-6}{L^2} & \dfrac{12}{L^3} & \\[2ex]
\dfrac{6}{L^2} & \dfrac{(2-\alpha)}{L} & \dfrac{-6}{L^2} & \dfrac{(4+\alpha)}{L}
\end{bmatrix}
\qquad \ldots\ldots(2\text{-}2)$$

In addition to the shear deformations effects included through the term α, which may be important for deep coupling systems, the presence of the arm implies that the node of a beam does not coincide with the node of the connecting wall element Fig (2-5) , and therefore, appropriate coordinate transformations have to be carried out which relates the displacements $\{ D \}$ at A and B, Fig (2-5), to the displacements $\{ D^* \}$ at A* and B* by geometry as follows :

$$\{ D^* \} = [H] [D] \qquad \ldots\ldots (2\text{-}3)$$

where

$$[H] = \begin{bmatrix}
1 & a & 0 & 0 \\
0 & 1 & 0 & 0 \\
0 & 0 & 1 & -b \\
0 & 0 & 0 & 1
\end{bmatrix} \qquad \ldots\ldots(2\text{-}4)$$

is the transformation matrix. It follows that the stiffness matrix of a beam with rigid arms including shear deformations can be given by :

$$[K_b] = [H]^T [K_b^*] [H] \qquad \ldots\ldots (2\text{-}5)$$

which can be given explicitly as :

$$
[K_b^*] = \frac{EI}{1+\alpha}
\begin{array}{cccc}
\quad v_A & \quad \theta_A & \quad v_B & \quad \theta_B
\end{array}
$$

$$
[K_b^*] = \frac{EI}{1+\alpha}
\left[
\begin{array}{cccc}
\dfrac{12}{L^3} & & & \\[2ex]
\dfrac{6}{L^2}+\dfrac{12a}{L^3} & \dfrac{4+\alpha}{L}+\dfrac{12a}{L^2}+\dfrac{12a^2}{L^3} & & \\[2ex]
\dfrac{-12}{L^3} & \dfrac{-6}{L^2}-\dfrac{12}{L^3} & \dfrac{12}{L^3} & \\[2ex]
\dfrac{6}{L^2}+\dfrac{12}{L^3} & \dfrac{2-\alpha}{L}+\dfrac{6(a+b)}{L^2}+\dfrac{12ab}{L^3} & \dfrac{-6}{L^2}-\dfrac{12b}{L^3} & \dfrac{4+\alpha}{L}+\dfrac{12b}{L^2}+\dfrac{12b^2}{L^3}
\end{array}
\right] \qquad (2\text{-}6)
$$

The beam and wall stiffness matrices are assembled in a standard manner and solved for the displacements, which in turn can be used to yield the internal forces in all members. Here the assembly process is defined as the operation of adding the coefficients of the element equations into the proper locations in the global system equations.

2-4 THE FINITE ELEMENT TECHNIQUE / GENERAL :

As with any major development in enginering mechanics, the early history of the finite element method can be traced along several paths, because the method makes use of many theories drawn from mathematics and continuum mechanics. The name finite element was first introduced by Clough 1960. Since then, more individuals and organizations began working with this engineering tool. At present the finite element technique has emerged as the most powerful general method for structural analysis, and has provided engineers with a tool of very wide capability. For reinforced concrete, in particular, the phenomena of cracking, tension stiffening, nonlinear multiaxial behaviour and other effects previously ignored or treated in a very approximate manner can now be considered more rationally. Four finite element models are currently employed in structural analysis :

        (a) The displacement model

        (b) The equilibrium model

        (c) The mixed model

        (d) The hybrid model

Most structural analyses in common use are based on the displacement model, in which, assumed displacement fields and the principle of minimum potential energy functional are used to solve various structural mechanics problems. A number of different variational principles, other than the principle of minimum potential energy, can be used to derive different types of finite elements, namely; the principle of minimum complementary energy and the principle of stationary Reissner energy. The displacements are the primary unknowns in this model, and the displacement field is chosen to satisfy compatibility of deformations both within and across the boundaries of elements.

Similarly, equilibrium elements are based on an assumed stress field instead of displacements, and the principle of minimum complementary energy is used to compute the nodal values of stresses or forces, treated as primary unknowns of the discretized structure. The stress field is selected such that internal equilibrium is satisfied with continuous stress transmission between elements.

In mixed finite element models, which make use of the principle of stationary Reissner energy, both displacements and stresses are treated as field variables. This will require more degrees of freedom to achieve a given accuracy. This shortcoming can be avoided in hybrid based models in which the assumed displacement and stress fields are independant. Hybrid elements are obtained if in addition to one field variable, displacement or stress, other variable, stress or displacement, are introduced and the parameters that correspond to the additional variable are eliminated at the element stage level before assembling.

In general, the displacement approach predictions are too stiff compared to the exact solution, whereas equilibrium based models are too flexible. However, both models converge to the exact solution as the number of elements used to model a situation increases.

In the present study, the displacement based model along with the principle of minimum potential energy has been used. This is due partly to the large library of available elements using this concept, and also to its simplicity. As the standard procedure of the finite element method is well known Zienkiewicz 1977, Cook 1981, Bathe 1981, Desai 1979, Brebbia 1974 and Gallagher 1975 ... no attempt will be made to describe it in detail, but in order to define terms, a brief review of the method will be presented instead.

2-5 FINITE ELEMENT DISPLACEMENT APPROACH :

The finite element displacement method can be viewed as an extension of the stiffness method of skeletal structures but applied to two and three dimensional problems in structural mechanics. However, unlike skeletal structures, there are no well defined joints and the actual number of degrees of freedom in any continuum can essentially be considered as infinite. As a numerical approach an approximate solution is made by assuming the continuum is divided into a series of elements which are connected at a finite number of joints known as nodal points. This process is known as discretization, converting a problem with an infinite number of degrees of freedom to one with a finite number. The resulting continuum is composed of a finite number of sub-regions or elements of simple geometry defined by selected key points where conditions of equilibrium and compatibility are to be enforced.

In the finite element displacement approach, the displacements at any general point within an element are dependant only upon the unknown nodal displacements, being related by means of interpolation functions, as follows :

$$\{ \delta \} = [N] \{ \delta^e \} \qquad \dots\dots \quad (2-7)$$

Here, $[N]$ denotes a rectangular matrix containing the shape functions that relate displacements $\{ \delta \}$ at any point within an element to the element nodal displacements $\{ \delta^e \}$. The strains within any element can then be expressed in terms of the element nodal displacements. The strain displacement relationship is obtained by differentiation of the displacements $\{ \delta \}$. For problems involving small linear strains, the process is expressed by applying a linear differential operator to Eq. (2-7), thus:

$$\{ \ \epsilon \ \} = [\ B \ ] \{ \ \delta^e \ \} \qquad \ldots\ldots \quad (2-8)$$

where $[\ B \ ]$ is the strain matrix composed of derivatives of the shape functions. The stresses may be related to the strains by making use of the elastic constitutive laws :

$$\{ \ \sigma \ \} = [\ D \ ] \{ \ \epsilon \ \} \qquad \ldots\ldots \quad (2-9)$$

where, $[\ D \ ]$ is the material constitutive or stiffness matrix relating stresses $\{ \ \sigma \ \}$ to strains $\{ \ \epsilon \ \}$:

The equations of equilibrium are obtained by minimizing the total potential energy of the system. The total potential energy, Π_s, is expressed as:

$$\Pi_s = \frac{1}{2}\int\limits_{(v)} \{ \ \sigma \ \}^T \{ \ \epsilon \ \} \ dv - \int\limits_{(v)} \{ \ \delta \ \}^T \{b\} \ dv - \int\limits_{(s)} \{ \ \delta \ \}^T \{q\} \ ds \quad \ldots \ (2-10)$$

where $\{ \ \sigma \ \}$ and $\{ \ \epsilon \ \}$ are the stress and strain vectors respectively, $\{ \ \delta \ \}$ the displacement at any point, $\{ \ b \ \}$ the body force per unit volume, and $\{ \ q \ \}$ the applied surface loads.

The right hand side terms of Eq. (2-10) represent the strain energy of internal stresses, the work of external actions due to body forces and distributed surface loads. Integrations are taken over the whole structure, and will be the sum of the energy contribution of each individual element, thus:

$$\Pi_s = \Sigma \ \Pi_e \qquad \ldots\ldots \quad (2-11)$$

where Π_e represents the total potential energy of element (e) which, using Eq.(2—10) can be written as:

$$\Pi_e = \frac{1}{2} \int_{(V_e)} \{ \delta^e \}^T [B]^T [D] [B] \{ \delta^e \} \, dv$$

$$- \int_{(V_e)} \{ \delta^e \}^T [N]^T \{b\} \, dv - \int_{(S_e)} \{\delta^e\}^T [N]^T \{q\} \, ds \qquad \ldots \ldots (2\text{-}12)$$

Minimizing the potential energy results in:

$$\frac{\partial \Pi_e}{\partial \delta^e} = \int_{(V_e)} [B]^T [D] [B] \, dv$$

$$- \int_{(V_e)} [N]^T \{b\} \, dv - \int_{(S_e)} [N]^T \{q\} \, ds \qquad \ldots \ldots \ldots (2\text{-}13)$$

where

$$\{ F^e \} = \int_{(V_e)} [N]^T \{b\} \, dv - \int_{(S_e)} [N]^T \{q\} \, ds \qquad \ldots \ldots (2\text{-}14)$$

are the equivalent nodal forces for the element, and

$$[K_e] = \int_{(V_e)} [B]^T [D] [B] \, dv \qquad \ldots \ldots \ldots (2\text{-}15)$$

is termed the element stiffness matrix.

The summation of the terms in Eq. (2—13) over all elements results in:

$$\frac{\partial \Pi_s}{\partial \delta} = [K_s] \{ \delta \} - \{ F \} \qquad \ldots \ldots (2\text{-}16)$$

where $[K_s]$ is the global structural stiffness matrix and $\{ F \}$ the global loading vector obtained by summation of Equations (2—15) and (2—14) respectively.

For an equilibrium to be stable, the total potential enenrgy Π_s of the system must be a minimum, therefore:

or
$$\frac{\partial \Pi_s}{\partial \delta} = 0$$

$$[\; K_s \;] \; \{ \; \delta \; \} - \{ \; F \; \} = 0 \qquad\qquad \text{........} \quad (2-17)$$

The result is a system of equilibrium equations in which, the nodal displacements $\{ \; \delta \; \}$ of the overall structure are related to the externally applied load $\{ \; F \; \}$ through the global structural stiffness matrix $[\; K_s \;]$. These linear simultaneous equations are then solved by standard techniques to yield the unknown nodal displacements. The strains and therefore the stresses within each element can becomputed from the displacements using equations $(2-8)$ and $(2-9)$ respectively.

2-6 SHEAR WALL DISCRETIZATION BY FINITE ELEMENT :

It is apparent from section $(2-5)$ that the finite element method with the direct stiffness formulation involve three levels of idealization: material, element and structural as indicated in Fig $(2-6)$.

The material model is represented by a constitutive matrix $[\; D \;]$, which relates stresses to strains. Its quality depends on the assumed material constitutive laws and how they describe the real material behaviour.

The finite element represented by the element stiffness $[\; K_e \;]$, describes the behaviour of a portion of the structure with an assumed displacement function and a given material stiffness. Its accuracy depends primarily on the type of displacement functions used.

The structural model represented by the structural stiffness [K_s], describes the global behaviour of the structure. It reflects all of the assumptions made at the material and element levels. In addition, the structural model is affected by the choice of the finite element mesh. The predicted response of the structure is therefore influenced by approximations made at all three levels.

2-6-1 MATERIAL IDEALIZATION :

It is through the constitutive matrix [D] in Eq. (2-9) that nonlinear effects are introduced into the element stiffness relation Eq. (2-15). Stresses and strains are investigated at integration points. Cracking, yielding and crushing of concrete are thus determined from the stress and strain evaluations at these points.

In this chapter and for a preliminary study, a linear elastic material has been assumed to permit a simple parametric study of shear wall behaviour in the simple elastic case before a more refined nonlinear model will be introduced in Chapter (3).

2-6-2 ELEMENT IDEALIZATION :

Several types of plane stress elements are commonly used, Fig (2-7). Constant strain triangular elements have enjoyed considerable appeal for their simplicity as well as their ability to idealize structures with irregular boundaries. The main disadvantage of these elements stems from their uniform strain field and hence uniform stress field. Another type of plane element used in practice is the linear isoparametric quadrilateral element. Improved stress predictions can be obtained since the strains, and therefore the stresses vary linearly within each element. This element however, suffers the disadvantage of poor behaviour in representing in- plane bending.

Higher order parabolic isoparametric elements are now extensively used for plane stress problems. In fact most of the standard finite element packages have this element in their library routines. However, this element suffers from spurious shear effects when applied to certain classes of problems as reported recently by Jeyachandrabose and Kirkhope 1983; For instance, the analysis of cantilever beam under uniform loading. Although the computed deflections and axial stresses are in excellent agreement with theoretical ones, the shear stresses show a parabolic oscillation within each element, thus providing a poor representation of the actual stress. Although substitute shape functions have been derived using least square stress/strain smoothing techniques to eliminate the spurious shear modes, many investigators still use this popular element.

In addition to the uniform stress and strain fields in the constant strain triangle, the poor bending behaviour of the linear isoparametric element, the spurious shear effect of the popular parabolic isoparametric element, these elements are in general, not suitable for the analysis of shear walls if interaction with frames, or when modelling slender lintels as beam elements are considered. Special elements to deal with this situation and more suitable for shear walls have been developed. Abu Ghazaleh 1965, MacLeod 1969, Sisodiya, Lin et al. 1971 and Cheung and Ghali 1973 have proposed rectangular elements with additional rotational degrees of freedom, Fig(2−8). They assumed different displacement functions for the two translational degrees of freedom { u,v } and expressed the additional rotational degree of freedom as:

Abu−Ghazaleh's 1965 element Fig (2−8a):

$$\theta_i = 1/2 \ (\ \partial v/\partial x \ - \ \partial u/\partial y \ ) \quad i = 1,2,3,4. \qquad \ldots\ldots\ldots \quad (2-18)$$

The displacement u is linear in ξ and cubic in η .

MacLeod's 1969 element Fig (2—8b):

$$\theta_1 = \theta_3 = -\partial u/\partial y \qquad \theta_2 = \theta_4 = \partial v/\partial x$$

or $\quad \theta_1 = \theta_3 = \partial v/\partial x \qquad \theta_2 = \theta_4 = -\partial u/\partial y \qquad \ldots\ldots\ldots$ (2—19)

The displacement u is assumed linear in ξ and quadratic in η, whereas v is assumed quadratic in ξ and linear in η.

Lin et al's 1971 element Fig (2—8c):

$$\theta_i = \partial v/\partial x \qquad i = 1,2,3,4. \qquad \ldots\ldots\ldots\ldots \text{(2—20)}$$

The displacement u is linear in both ξ and η directions whereas v is cubic in ξ and linear in η.

Sisodiya and Cheung 1971 element Fig (2—8d):

$$\theta_i = -\partial u/\partial y \quad i = 1,2,3,4. \qquad \ldots\ldots\ldots\ldots\ldots \text{(2—21)}$$

The displacement u is linear in the ξ direction and cubic in the η direction, whereas v is linear in both directions, which would lead to a linear distribution of vertical stresses on horizontal sections of the wall.

Most rotational degrees of freedom in the elements above, are either biased around one of the axes, or induce a lack of symmetry in truly symmetrical cases.

A more refined element suitable for the analysis of shear walls when compared to the previously mentioned elements was presented by Oakberg and Weaver 1969. Four degrees of freedom are assumed at each node, Fig (2—9), two translations in the x and y directions and two slopes of horizontal and vertical lines at each edge expressed as partial derivatives of the translational displacements.

In this study, the element used to discretize a shear wall is the higher order element of Oakberg and Weaver 1969. The displacement functions assumed for this element are:

Translations :

$$u = \alpha_1 + \alpha_2 \xi + \alpha_3 \eta + \alpha_4 \xi\eta + \alpha_5 \eta^2 + \alpha_6 \xi\eta^2 + \alpha_7 \eta^3 + \alpha_8\xi\eta^3$$

$$v = \alpha_9 + \alpha_{10}\xi + \alpha_{11}\eta + \alpha_{12}\xi\eta + \alpha_{13}\xi^2 + \alpha_{14}\xi^2\eta + \alpha_{15}\xi^3 + \alpha_{16}\xi^3\eta \quad (2-22)$$

Rotations :

$$\theta_x = \partial v/\partial x = 1/a \ (\partial v/\partial \xi)$$

$$= 1/a \ (\alpha_{10} + \alpha_{12}\eta + 2\alpha_{13}\xi + 2\alpha_{14}\xi\eta + 3\alpha_{15}\xi^2 + 3\alpha_{15}\xi^2\eta \ )$$

$$\theta_y = -\partial u/\partial y = -1/b \ (\partial u/\partial \eta)$$

$$= -1/b \ (\alpha_3 + \alpha_4 \xi + 2\alpha_5\eta + 2\alpha_6\xi\eta + 3\alpha_7\eta + 3\alpha_8\xi\eta \ ) \ \dots \quad (2-23)$$

This is written in matrix form as:

$$
\begin{Bmatrix} u \\ v \\ \theta_x \\ \theta_y \end{Bmatrix} =
\begin{bmatrix}
1 & \xi & \eta & \xi\eta & \eta^2 & \xi\eta^2 & \eta^3 & \xi\eta^3 & 0 & 0 & 0 & 0 & 0 & 0 & 0 & 0 \\
0 & 0 & 0 & 0 & 0 & 0 & 0 & 0 & 1 & \xi & \eta & \xi\eta & \xi^2 & \xi^2\eta & \xi^3 & \xi^3\eta \\
0 & 0 & 0 & 0 & 0 & 0 & 0 & 0 & 0 & 1 & 0 & \eta & 2\xi & 2\xi\eta & 3\xi^2 & 3\xi^2\eta \\
0 & 0 & 1 & \xi & 2\eta & 2\xi\eta & 3\eta^2 & 3\xi\eta^2 & 0 & 0 & 0 & 0 & 0 & 0 & 0 & 0
\end{bmatrix}
\begin{Bmatrix} \alpha_1 \\ \alpha_2 \\ \vdots \\ \vdots \\ \vdots \\ \alpha_{16} \end{Bmatrix} \quad (2-24)
$$

The unknown vector coefficients $\{ \ \alpha_1,\alpha_2,\dots,\alpha_{16} \ \}^T$ defining the assumed displacement functions are obtained by expressing Eq (2-24) for each node in turn, which results in a set of 16 simultaneous equations. Solution of the system defines completely the shape functions [N] for each node, summarized in Fig (2-9). To compute the translations u(ξ,η), v(ξ,η) and rotations θ_x(ξ,η), θ_y (ξ,η) at any point (ξ,η) within the element, use is made of Eq (2-7) which takes the form :

$$u \ (\xi,\eta) = \sum_{i=1}^{4} N_{i1}(\xi,\eta) \ u_i \qquad v \ (\xi,\eta) = \sum_{i=1}^{4} N_{i2}(\xi,\eta) \ v_i$$

$$\dots \quad (2-25)$$

$$\theta_x(\xi,\eta) = \sum_{i=1}^{4} N_{i3}(\xi,\eta) \ \theta_{xi} \qquad \theta_y(\xi,\eta) = \sum_{i=1}^{4} N_{i4}(\xi,\eta) \ \theta_{yi}$$

The strain displacement relationships Eq (2—8) may be written as:

$$
\left\{
\begin{array}{c}
\epsilon_x \\[2em]
\epsilon_y \\[2em]
\gamma_{xy}
\end{array}
\right\}
=
\sum_{i=1}^{4}
\left[
\begin{array}{cccc}
\dfrac{\partial N_{i1}}{\partial x} & 0 & 0 & \dfrac{\partial N_{i2}}{\partial x} \\[1.5em]
0 & \dfrac{\partial N_{i2}}{\partial y} & \dfrac{\partial N_{i3}}{\partial y} & 0 \\[1.5em]
\dfrac{\partial N_{i1}}{\partial y} & \dfrac{\partial N_{i2}}{\partial x} & \dfrac{\partial N_{i3}}{\partial x} & \dfrac{\partial N_{i4}}{\partial y}
\end{array}
\right]
\left\{
\begin{array}{c}
u_i \\[1em]
v_i \\[1em]
\theta_{xi} \\[1em]
\theta_{yi}
\end{array}
\right\}
\qquad \dots \text{(2-26)}
$$

or simply: $\qquad \{ \epsilon \} = \sum_{i=1}^{4} [B_i] \{ \delta_i \}$ $\qquad \dots\dots\dots\dots\dots$ (2-27)

in which ϵ_x, ϵ_y are the normal strain components, γ_{xy} is the shear strain component; $[B_i]$ is the 3x4 strain matrix which contains the cartesian derivatives of the shape functions at node (i).

Since the shape functions $[N]$ are defined in terms of the local coordinates (ξ, η) of the element, a transformation from local to global coordinates (x,y) is required to obtain the $[B]$ matrix in Eq (2—26). This is done through the well known Jacobian matrix as follows:

$$
\frac{\partial N_i}{\partial x} = \frac{\partial N_i}{\partial \xi} \frac{\partial \xi}{\partial x} + \frac{\partial N_i}{\partial \eta} \frac{\partial \eta}{\partial x}
$$

$$
\frac{\partial N_i}{\partial y} = \frac{\partial N_i}{\partial \eta} \frac{\partial \eta}{\partial y} + \frac{\partial N_i}{\partial \xi} \frac{\partial \xi}{\partial y}
$$

or in matrix form:

$$
\left\{
\begin{array}{c}
\dfrac{\partial N_i}{\partial x} \\[1.5em]
\dfrac{\partial N_i}{\partial y}
\end{array}
\right\}
=
\left[
\begin{array}{cc}
\dfrac{\partial \xi}{\partial x} & \dfrac{\partial \eta}{\partial x} \\[1.5em]
\dfrac{\partial \eta}{\partial y} & \dfrac{\partial \xi}{\partial y}
\end{array}
\right]
\left\{
\begin{array}{c}
\dfrac{\partial N_i}{\partial \xi} \\[1.5em]
\dfrac{\partial N_i}{\partial \eta}
\end{array}
\right\}
= [J]
\left\{
\begin{array}{c}
\dfrac{\partial N_i}{\partial \xi} \\[1.5em]
\dfrac{\partial N_i}{\partial \eta}
\end{array}
\right\}
\qquad \dots \text{(2-28)}
$$

where $[J]$ is the Jacobian matrix.

From the theory of elasticity, for isotropic material in a plane stress condition

without initial strain and stress, the stress are related to the strains through the elasticity matrix [D] as follows:

$$
\begin{bmatrix} \sigma_x \\ \sigma_y \\ \tau_{xy} \end{bmatrix} = \frac{E}{(1-\nu^2)} \begin{bmatrix} 1 & \nu & 0 \\ \nu & 1 & 0 \\ 0 & 0 & 1-\nu/2 \end{bmatrix} \begin{Bmatrix} \epsilon_x \\ \epsilon_y \\ \gamma_{xy} \end{Bmatrix} \qquad \dots\dots\dots (2\text{-}29)
$$

Having defined [B] and [D], the element stiffness matrix can therefore be evaluated:

$$
[K_e] = \int_{(V_e)} [B]^T [D] [B] \, dv \qquad \dots\dots\dots\dots (2\text{-}30)
$$

where $dv = t \, dx \, dy$, t being the thickness of the plane element.

Transformation from global to local coordinates systems results in

$$
dv = \det [J] \, d\xi \, d\eta
$$

Analytical integration of equation (2-30) is possible. However, in this study some form of numerical integration is resorted to. Gaussian quadrature rules have been used because of their higher efficiency over other forms of quadrature. A 3x3 gauss rule has been used for the numerical integration of Eq.(2-30), although 2x2 and 4x4 are also available.

2-6-3 STRUCTURAL IDEALIZATION :

The use of a two dimensional formulation for structural analysis of reinforced concrete shear walls requires appropriate pre-processing facilities due to the high amount of input data needed for the discretization of the continuum. Therefore, since most of the finite element calculations involve a great deal of time and effort to generate numerical data such as node numbers, nodal point coordinates and element connectivity, automatic mesh generation schemes are very useful and important to finite element applications, especially when a large number of

elements or very complex geometries are encountered.

Several techniques are available such as, the superelement mesh generation method first introduced by Zienkiewicz and Phillips 1971 and used by Durocher and Gasper 1979 who included automatic bandwidth reduction. The method of superelement mesh generation, also known as isoparametric generation, is a method generating finite element meshes by dividing large superelements into smaller mesh elements. Another procedure known as a mapping technique is obtained by using two successive transformations. First, a conformal mapping regularizes the shape of the body ie. removing geometrical singularity. This transformed regular body is then subdivided into a number of zones and by using isoparametric transformation a mesh of the mapped body is generated.

In this study a straightforward mesh generation scheme has been developed for the automatic generation of nodal coordinates and automatic numbering of nodes and element connectivities based on a minimum amount of user supplied data. The procedure can discretize shearwalls with any configuration of the openings and with any refinement in critical regions. This automation reduces errors and spares the user a long tedious chore. The scheme is simpler than the techniques mentioned above but leads to less input data in the specific case of shearwalls. The wall is assumed as one unit and by introducing the openings re—ordering and renumbering is followed.

2-7 APPLICATIONS TO COUPLED SHEARWALLS :

Without implying lack of generality in regard to the applicability of the finite element method, only typical coupled shearwalls are considered.

Various examples of shearwall problems have been analysed and these illustrate the simplicity, versatility and accuracy of this method as compared to the results of other available methods. Because the amount of input data required for the discretization of the shearwall is very high, an automatic mesh generation procedure has been developed using the linear cubic finite element. A plot of the generated mesh before loading and after deformation is used to check both the correctness of the generated mesh (node numbering and element connectivity) and gives an overall behaviour of the wall when deformed. A reasonably accurate analysis requires a fine division of the wall, particularly in the neighbourhood of openings and it is essential to save computer storage as much as possible. The number of unknown displacements to be handled will frequently be of the order of thousands. The band matrix solution procedure used in this study is essential and efficient if proper node numbering has been generated. This was achieved by numbering the nodes across the width of the wall rather than across the height in order to minimize the bandwidth in all the coupled shearwalls analysed in this study.

2-7-1 CONVERGENCE STUDY :

The finite element method is an approximate numerical tool, and as mentioned in section (2-6), approximations are introduced at the material, element and structural levels. The material is assumed elastic for a preliminary study and using a higher order element, it follows that to obtain reliable and accurate solutions the structural idealization is crucial as it is user defined. Therefore, two coupled shearwalls will be analysed using various finite element mesh refinements.

The purpose is to perform a convergence study as the mesh is refined and to gain experience with the linear cubic element Fig (2—9), to assess how much refinement is needed to obtain reliable results for other shearwalls.

First, an eight story symmetrical coupled shearwall previously analysed by Almahaidi et al. 1975 with five different mesh configurations shown in Fig (2—10) is studied.

	Nodes	Elements	Degrees of freedom
Mesh A :	272	208	1088
Mesh B :	336	256	1344
Mesh C :	402	320	1608
Mesh D :	498	384	1992
Mesh E :	658	512	2632

The structure's flexibility is plotted against the number of degrees of freedom as shown in Fig (2—11). Assuming that the exact solution is approached asymptotically as the finite element mesh is refined and considering the bound characteristics of the finite element displacement approach, The flexibility predicted by this method is less than the exact one. In the absence of an exact solution to this problem the continuum and wide column—frame analogies as shown in Fig (2—11) reveal that the coarse meshes (A) and (B) need further refinement to obtain reliable results.

Second, a 21 story coupled shearwall analysed by Chan and Cheung 1979 with two appropriate discretizations Fig 2—12) has been analysed and good agreement is observed with mesh refinement, Fig (2—13).

An important behaviour to be noted from the overall displacement diagram Fig (2—13) would be the local distortions caused between the junctions of the lintel beams and the walls. This will depend on the stiffness of the lintel beams and will be studied in the next two sections.

2-7-2 PARAMETRIC STUDY :

One of the factors most influencing the distribution of stress and deformation in a coupled shearwall system is the stiffness of the lintel beams. Consequently, the depth of lintel beams is varied, and its influence on the variation of the overall behaviour is studied.

The geometry and loadings of an example shear wall problem of a six story building is shown in Fig (2-14). The effect of the degree of coupling is studied by varying the depth of lintel beams, d = 50, 90 and 150 cm, corresponding to what may be considered as weak, moderate and stiff coupling respectively.

The finite element discretizations for the coupled shear wall with weak, moderate and stiff coupling along with the vertical stress distribution at intermediate height levels are shown in Fig (2-15), Fig (2-16) and Fig (2-17) respectively. It can be noticed that the stress distribution is not linear as would be predicted by the continuum shear connection and wide-column frame analogies. However, at the base of the walls, the wide-column frame analogy results in satisfactory prediction for engineering and design purposes as shown in Fig (2-18) to Fig (2-20). If one analyses the distribution of vertical stresses at the base of the wall, it can be concluded that with slender (d=50cm) lintel beams Fig (2-18), the vertical stress at the base of the wall agrees well with simple bending theory. This weak coupling results in high bending moments in the walls and low axial forces in the walls as both walls tend to behave as separate units. On the other hand, with stiff coupling (d=150cm) high axial forces in the walls are induced Fig (2-20).

The forces acting on the lintel beams can be calculated from either the stress or deformation of the beams. The bending moments at the ends of lintel beams are calculated from the slopes at the ends Fig (2-21) and the relative vertical dispacements at the ends Fig (2-22). For the rotations at the ends of lintel beams Fig (2-21) it can be noticed that the wide-column frame analogy predicts

satisfactory results compared to the finite element method. On the other hand, the relative vertical displacements at the ends of the lintel beams reveal that the wide column frame analogy is not reliable in the case of moderate and stiff coupling for which a large scatter is observed. This is due mainly to local high distortions at the junction lintel beams— wall and to the assumption of rigid arms which is in a case of stiff coupling not valid.

When the lintel beams are slender (d= 50cm), the bending moments in all six beams are almost the same Fig (2— 23). As the depth of lintel beams increases (d= 150cm) the maximum bending moment occured in the lintel beam at level 2. The lateral deflection along the height of the wall for various degrees of coupling is shown in Fig (2— 24). The stiffness of the lintel beams, therefore has considerable influence on the stress distribution and the deformation characteristics of the entire structure.

Due to space limitations and because the purpose of this investigation is the nonlinear behaviour of reinforced concrete coupled shear walls, other elastic analyses are not included, however a more realistic study will be performed in chapter 6 including the effects of cracking and nonlinear concrete and steel behaviour.

From this preliminary study the following conclusions may be drawn:

In the absence of an elastic solution to a particular shear wall structural action, the continuum shear connection and wide— column frame analogies can be used to assess if further refinement of a finite element mesh is needed in order to obtain reliable results. The solution predicted by the finite element method is more flexible with an appropriate selection of finite element mesh.

The continuum shear connection and wide— column frame analogies are considered sufficiently accurate for engineering design purposes to predict internal actions and deformations in coupled shearwalls.

The use of the wide column— frame analogy to predict the stress variation at

intermediate levels or for the computation of bending moments at the ends of deep lintel beams is not reliable.
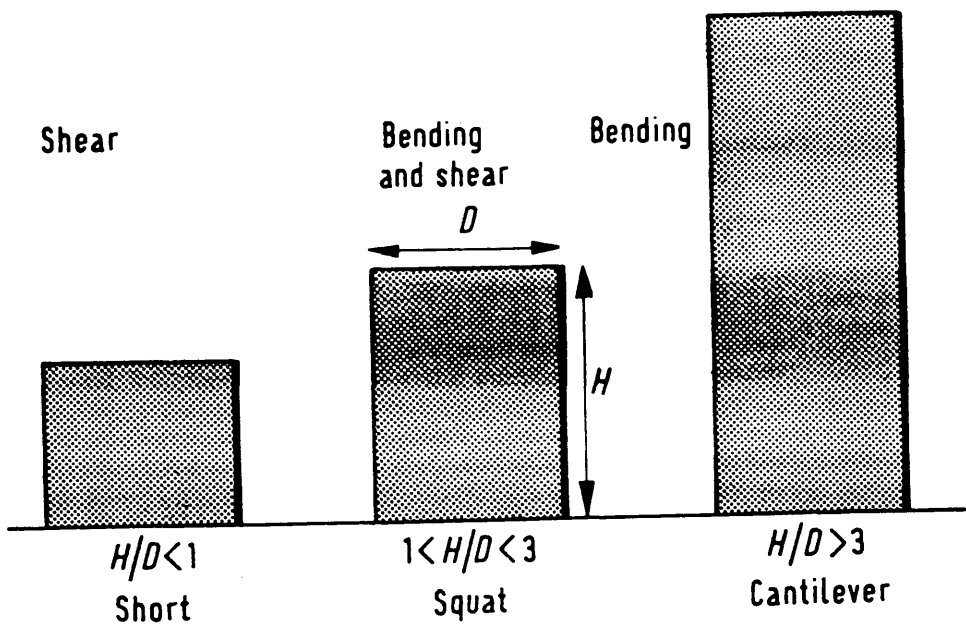
Fig (2-1) Shape of shear walls
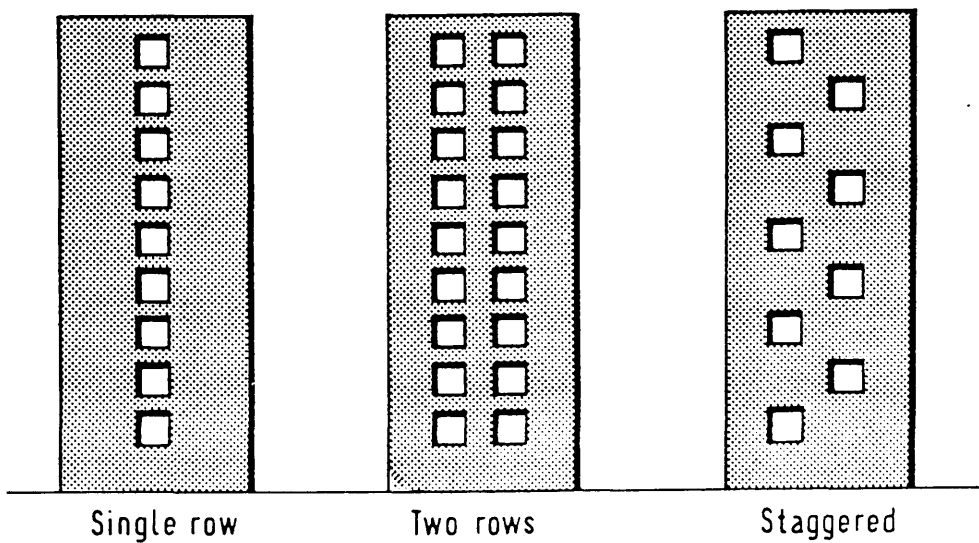
Fig (2-2) Forms of openings in shear walls
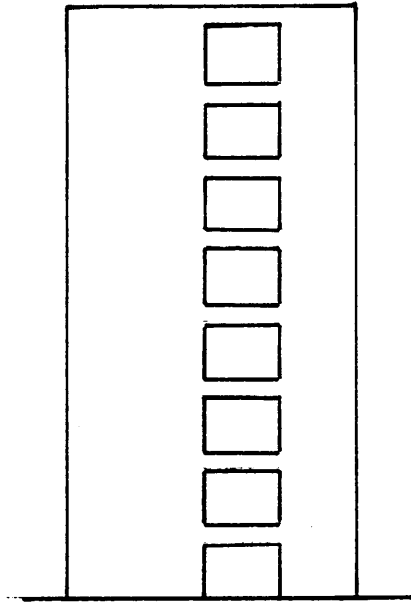
Typical shear wall

Continuum analogy   Wide–column frame   Finite element
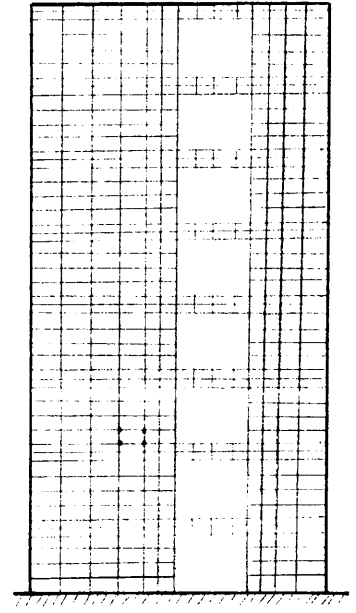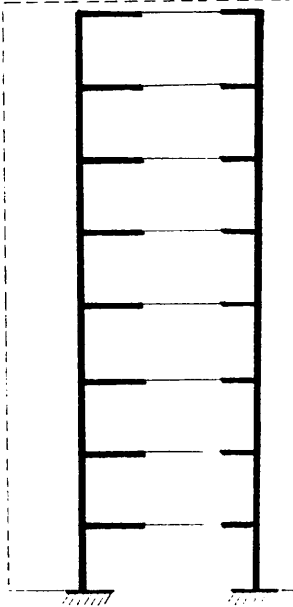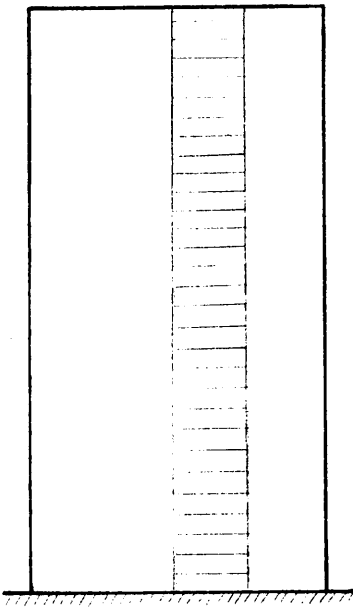
Fig (2-3) Methods of shear walls modelling

Typical shear wall   Continuum analogy

Equilibrium conditions
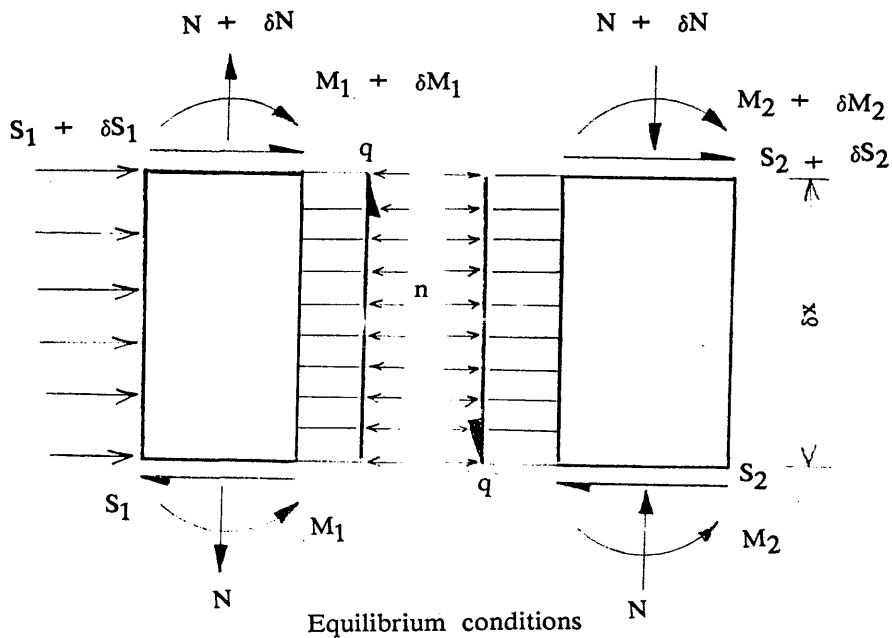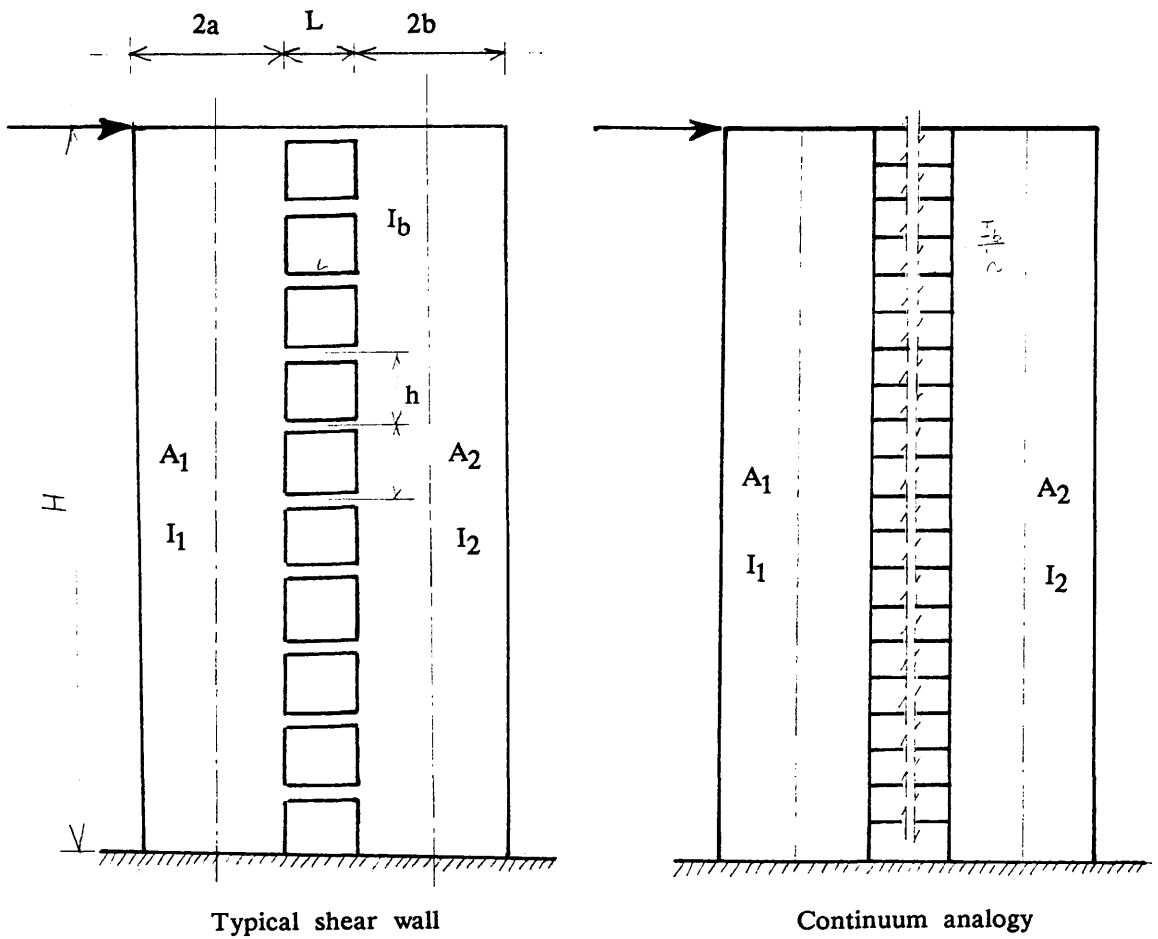
Fig (2-4) Continuum shear connection analogy
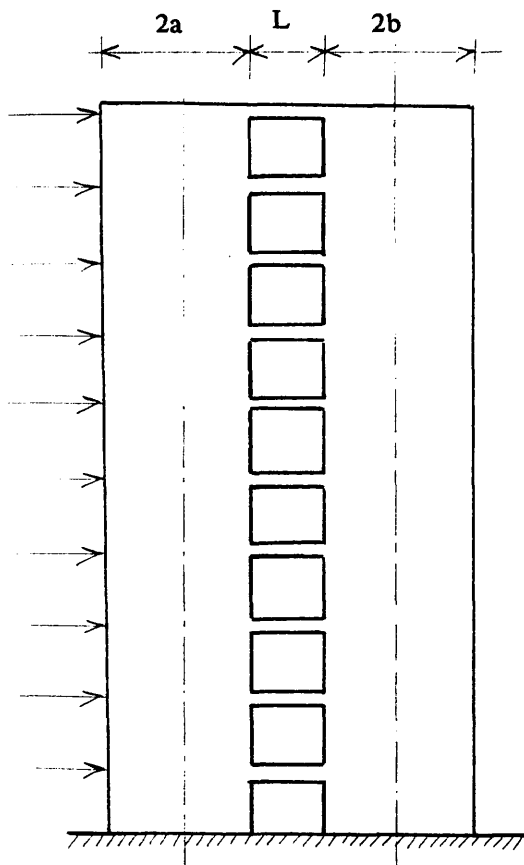
Typical shear wall
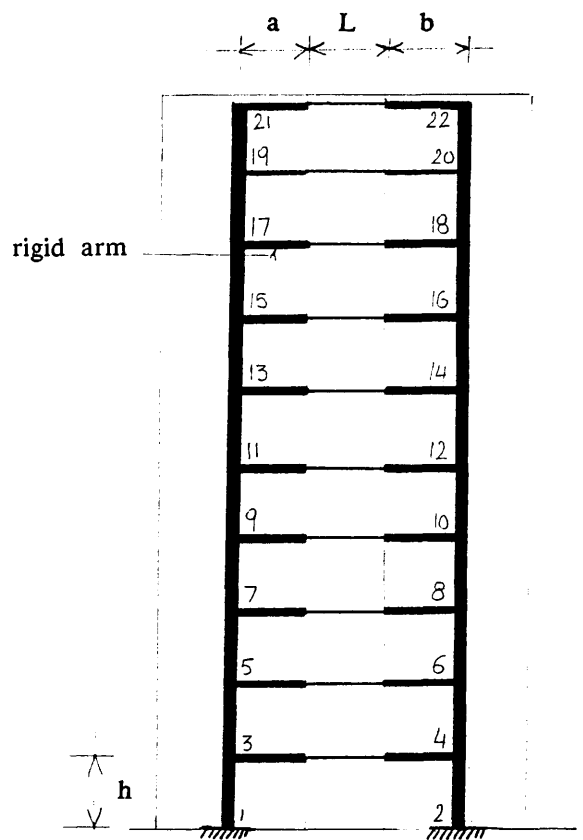
Wide—column frame model
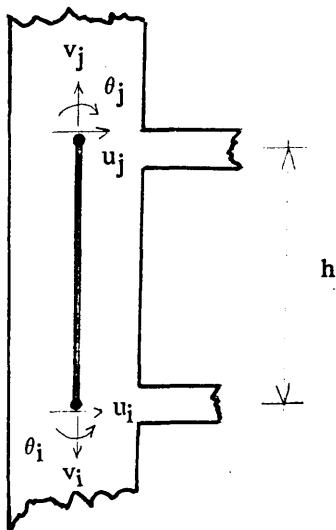
Wall element
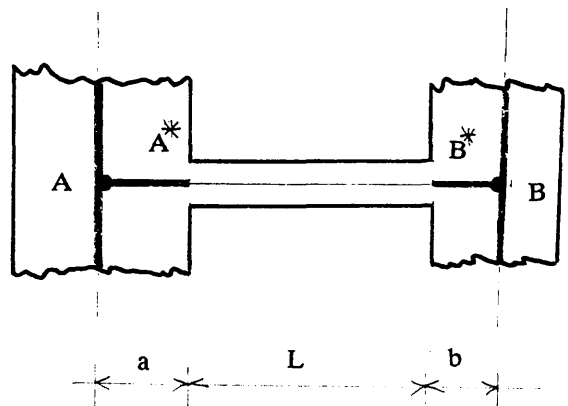
Beam element with rigid arms

Fig (2-5) Wide-column frame analogy

Material

Material constitutive law

— Elastic
— Elastoplastic
— ....

$$\{ \sigma \} = [D] \{ \epsilon \}$$

Element

Element shape functions

$$[K_e] = \int_{(v)} [B][D][B]^T dv$$

Structure

Choice of grid

$$[K_s] = \sum [K_e]$$
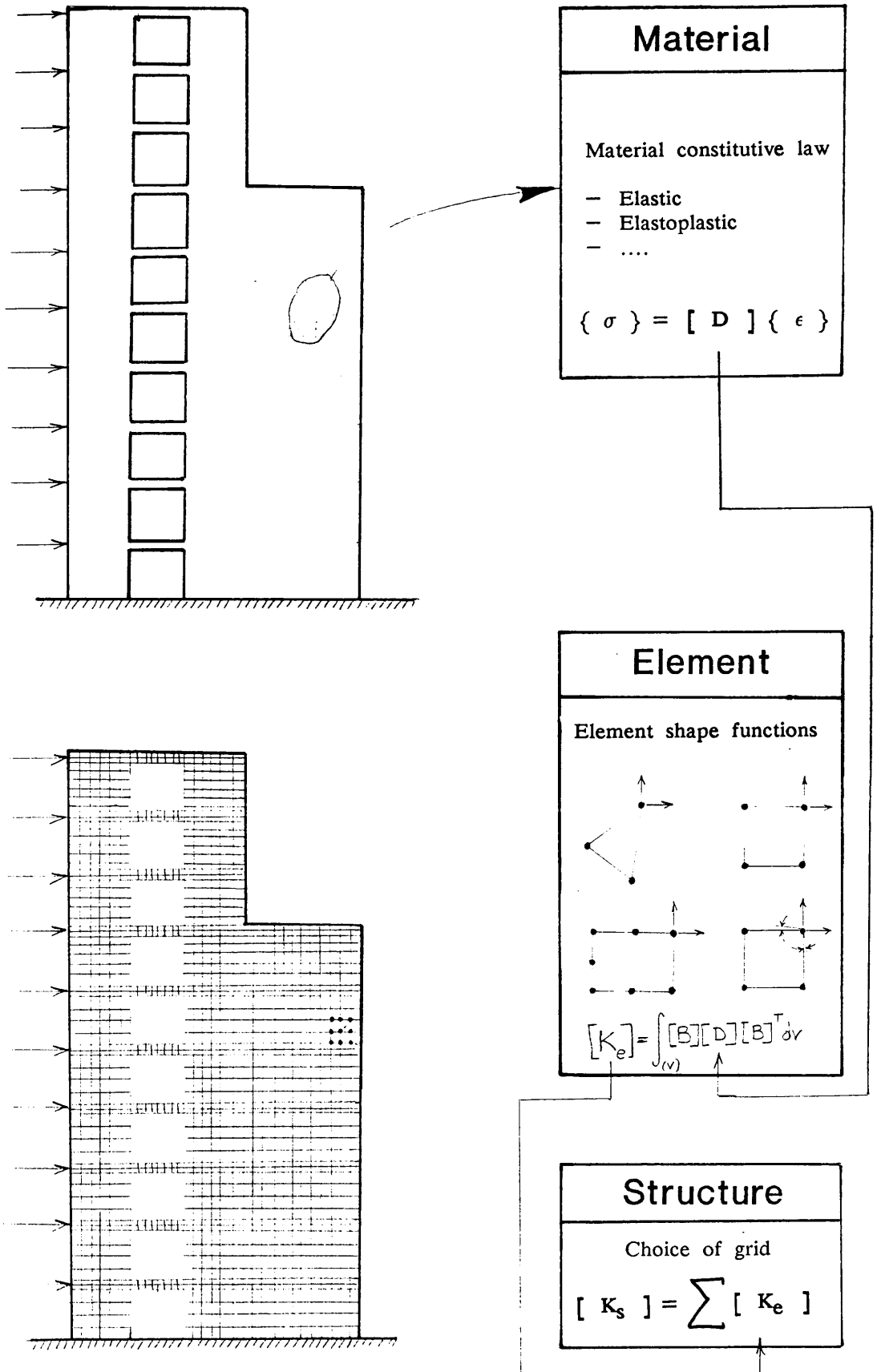
Fig (2-6) Levels of approximation in the finite element method
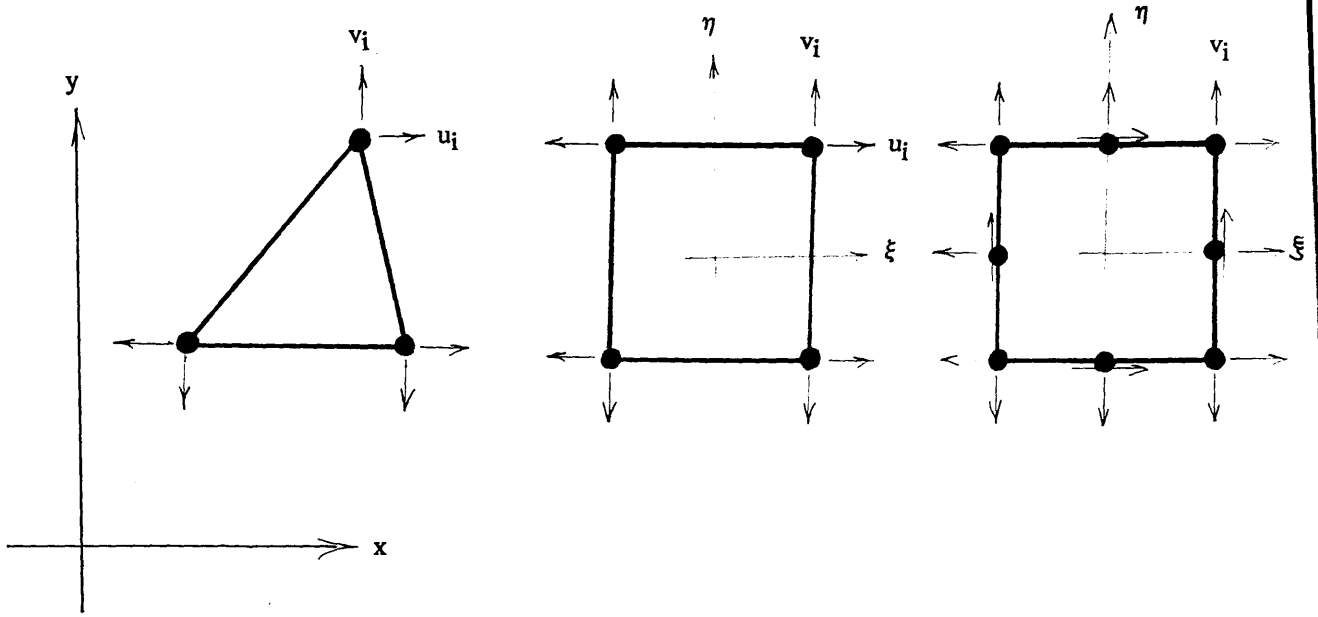
Fig (2-7) COMMON PLANE STRESS FINITE ELEMENTS

$\theta_i = \frac{1}{2}\left(\frac{\partial v}{\partial x} - \frac{\partial u}{\partial y}\right)$

Abu-Ghazaleh's element

$\theta_1 = \theta_3 = \frac{-\partial u}{\partial y}$

$\theta_2 = \theta_4 = \frac{\partial v}{\partial x}$

$\theta_1 = \theta_3 = \frac{\partial v}{\partial x}$

$\theta_2 = \theta_4 = \frac{-\partial u}{\partial y}$

MacLeod's element

$\theta_i = \frac{\partial v}{\partial x}$

Lin et al. 1971

$\theta_i = -\frac{\partial u}{\partial y}$

Sisodiya and Cheung's element
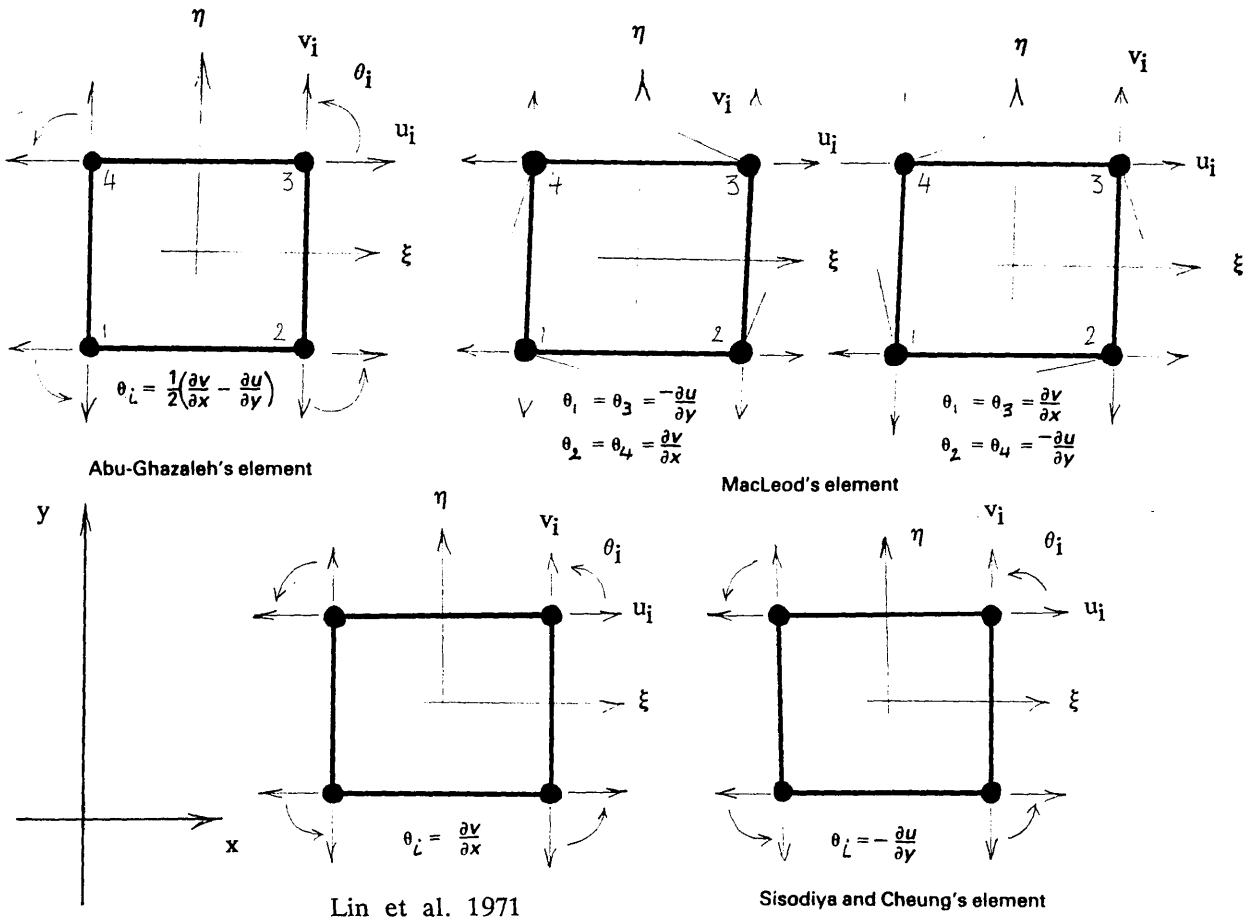
Fig (2-8) SPECIAL FINITE ELEMENTS USED FOR SHEAR WALLS
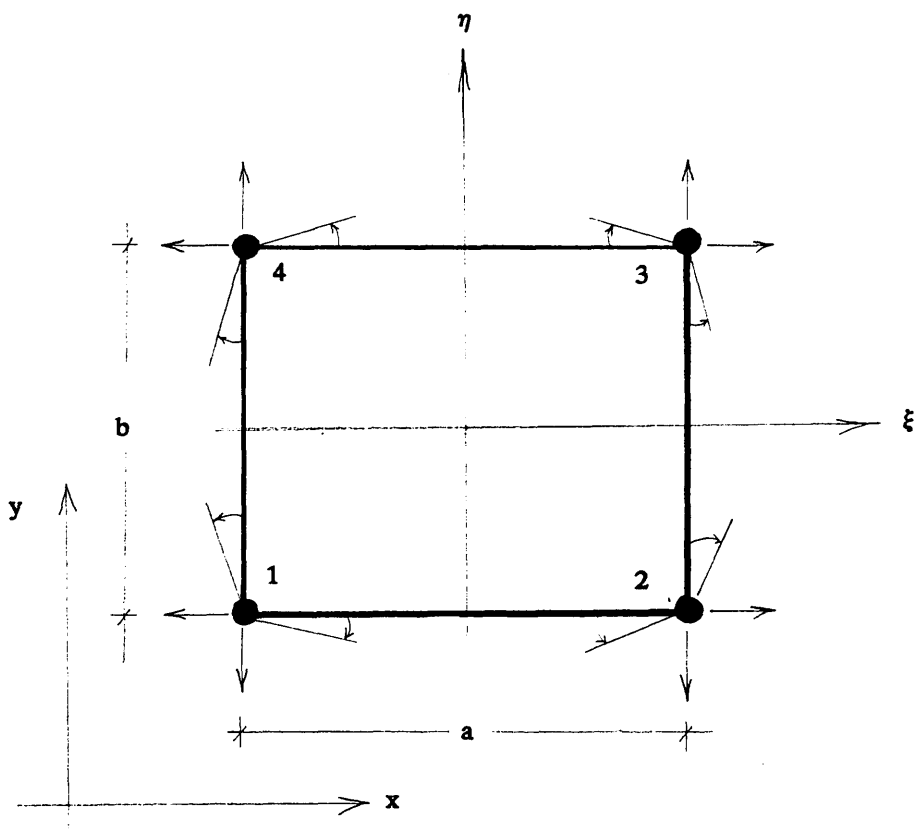
	Shape functions
1	$(1-\xi)\,(\eta-1)^2\,(2+\eta)/4$ $(\xi-1)^2\,(2+\xi)\,(1-\eta)\,/4$ $(\xi-1)^2\,(1+\xi)\,(1-\eta)\,a/4$ $-(1-\xi)\,(\eta-1)^2\,(1+\eta)\,b/4$
2	$(1+\xi)\,(\eta-1)^2\,(2+\eta)/4$ $(\xi+1)^2\,(2-\xi)\,(1-\eta)\,/4$ $-(\xi+1)^2\,(1-\xi)\,(1-\eta)\,a/4$ $-(1+\xi)\,(\eta-1)^2\,(1+\eta)\,b/4$
3	$(1+\xi)\,(\eta+1)^2\,(2-\eta)/4$ $(\xi+1)^2\,(2-\xi)\,(1+\eta)\,/4$ $-(\xi+1)^2\,(1-\xi)\,(1+\eta)\,a/4$ $(1+\xi)\,(\eta+1)^2\,(1-\eta)\,b/4$
4	$(1-\xi)\,(\eta+1)^2\,(2-\eta)/4$ $(\xi-1)^2\,(2+\xi)\,(1+\eta)\,/4$ $(\xi-1)^2\,(1+\xi)\,(1+\eta)\,a/4$ $(1-\xi)\,(\eta+1)^2\,(1-\eta)\,b/4$

FiG (2-9) FINITE ELEMENT USED IN THE STUDY
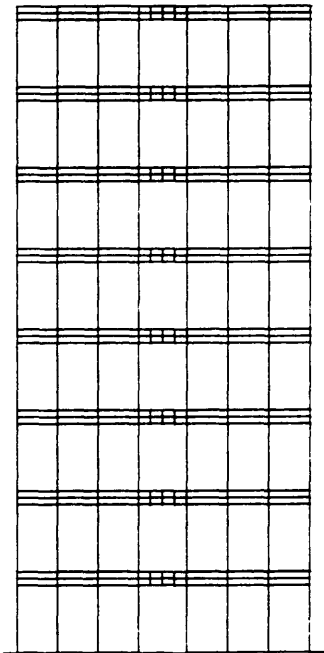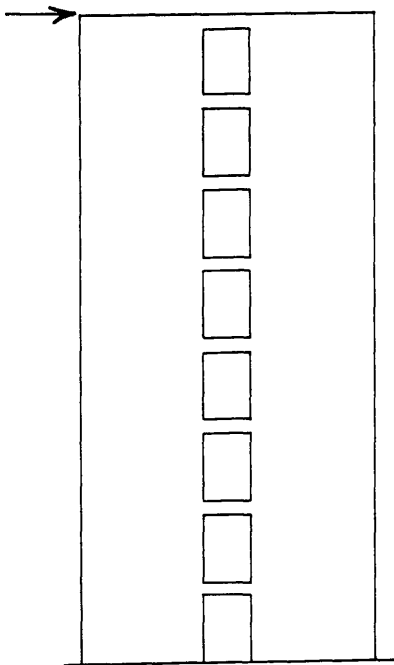
Mesh (A)
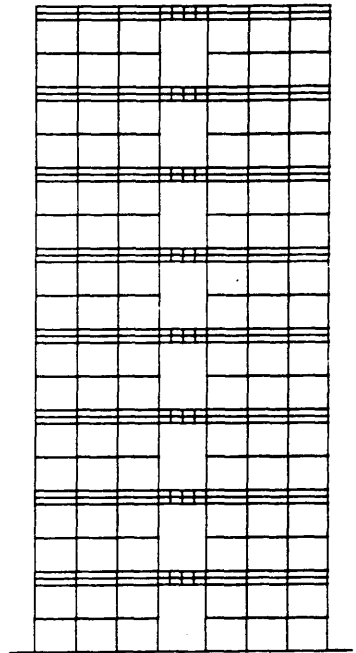
Mesh (B)
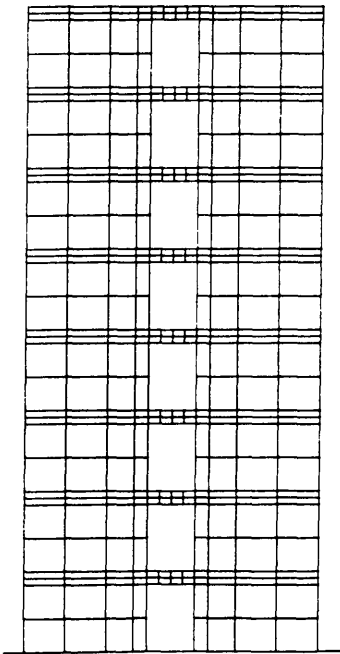
Mesh (C)
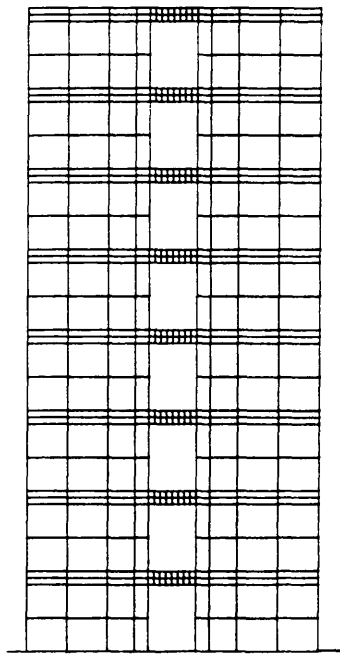
Mesh (D)
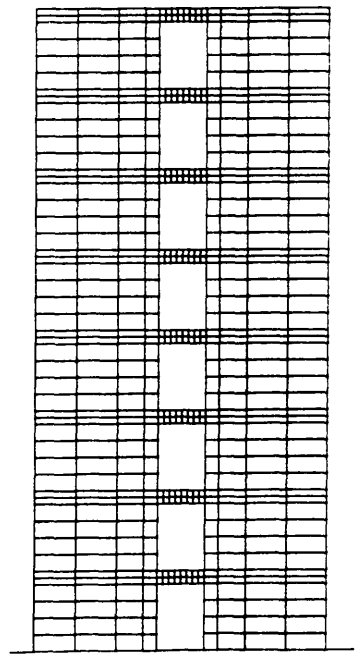
Mesh (E)

Fig (2-10) EIGHT STOREY COUPLED SHEAR WALL

	Nodes	Elements	Degrees of freedom
Mesh A :	272	208	1088
Mesh B :	336	256	1344
Mesh C :	402	320	1608
Mesh D :	498	384	1992
Mesh E :	658	512	2632

Finite element method ———

Wide—column frame —·—·—

Continuum shear connection —··—··—

Flexibility $EI\delta/P$

Number of degrees of freedom
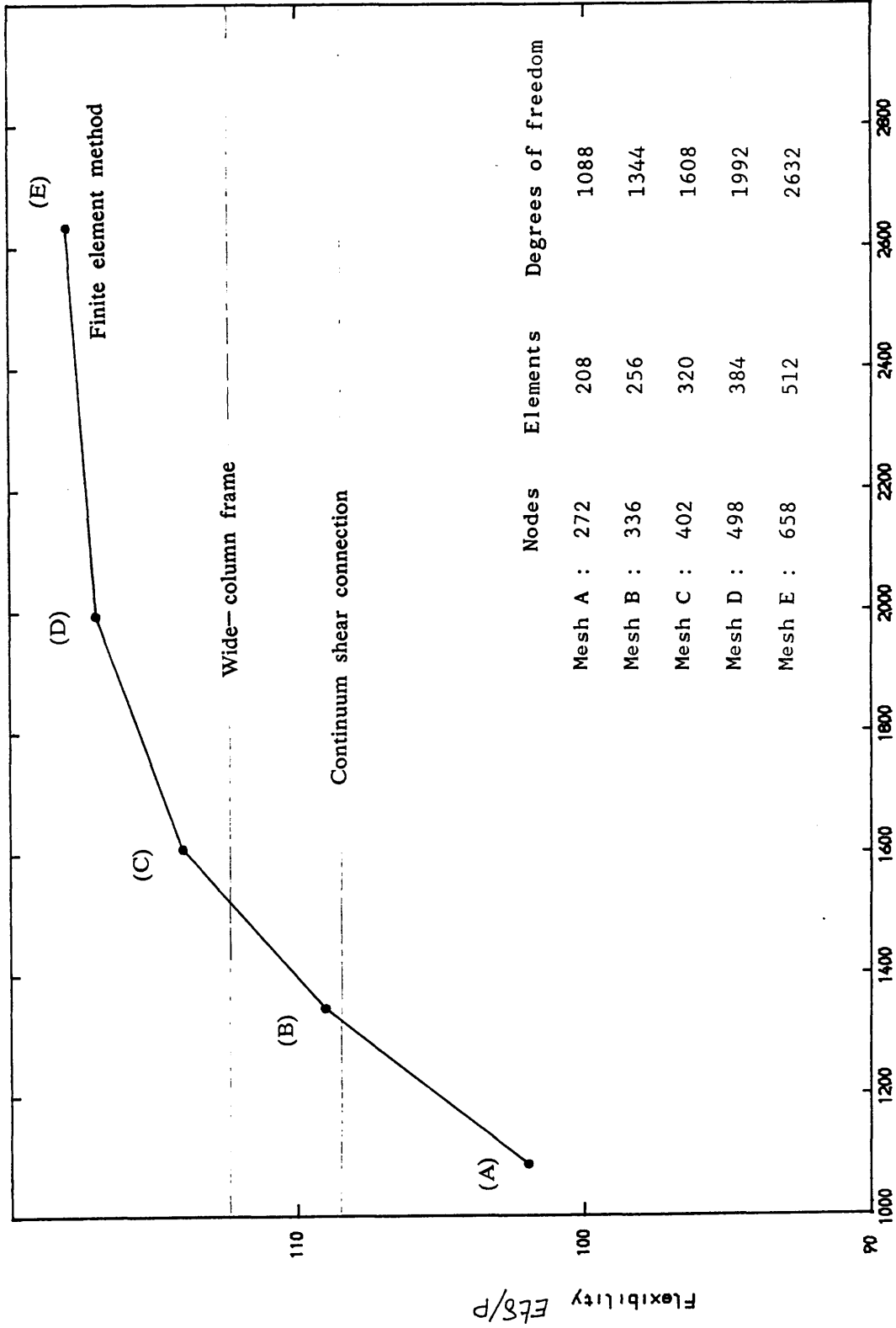
Fig (2-11) CONVERGENCE CURVE WITH MESH REFINEMENT

1165 Nodes, 924 Elements
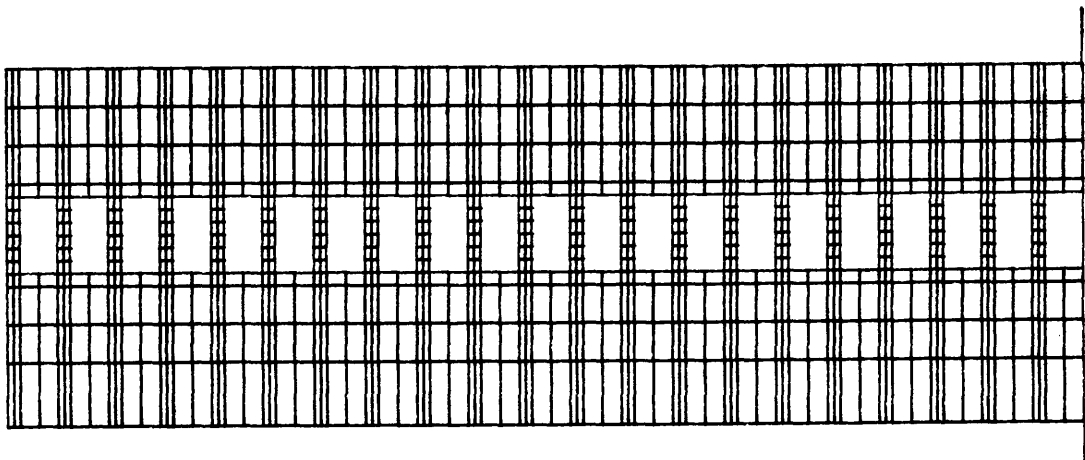
955 Nodes, 756 Elements

21 in.

Mesh (B)   4660 d.o.f

Mesh (A)   3820 d.o.f

3   1.5   2.5

u.d.l = 1 lb/in²
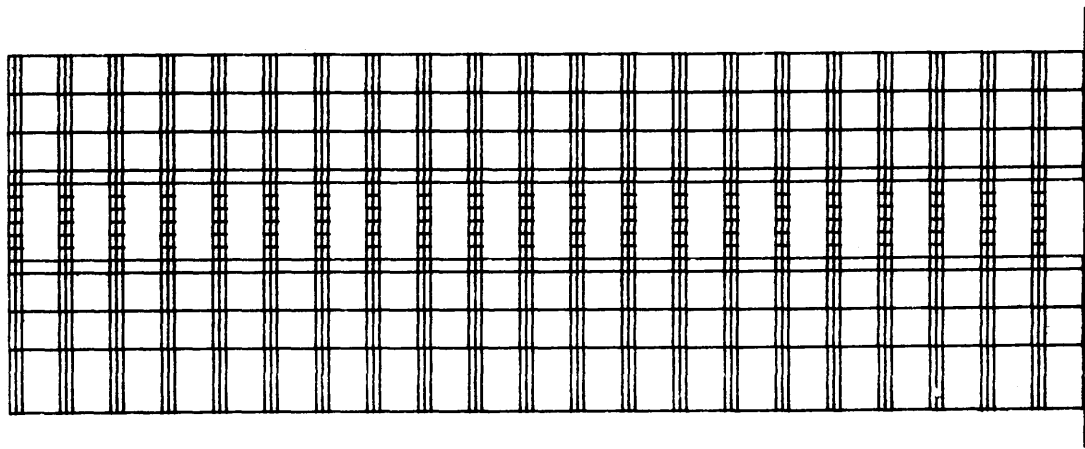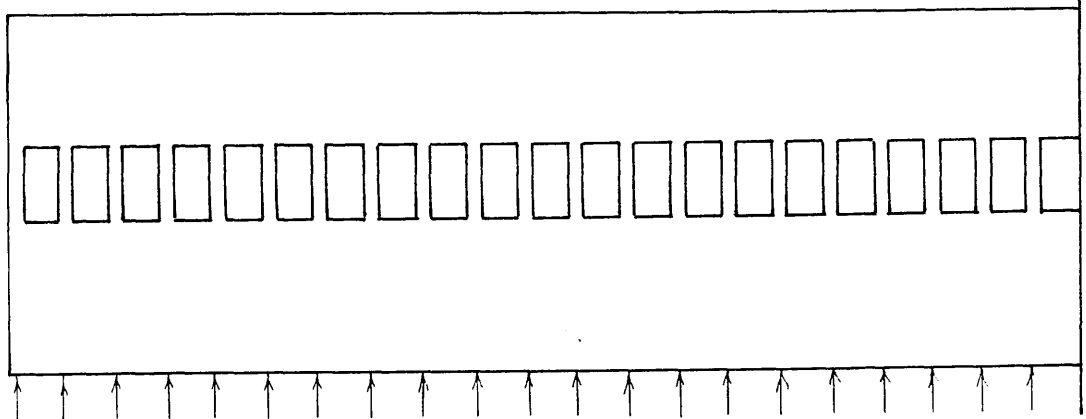
Fig (2-12) TWENTY ONE STOREY COUPLED SHEAR WALL

Mesh (B)

Mesh (A)

Height, in.

Deflection, x 10⁻³ in.

Experimental
Coull and Puri
Cheung and Chan
Present study
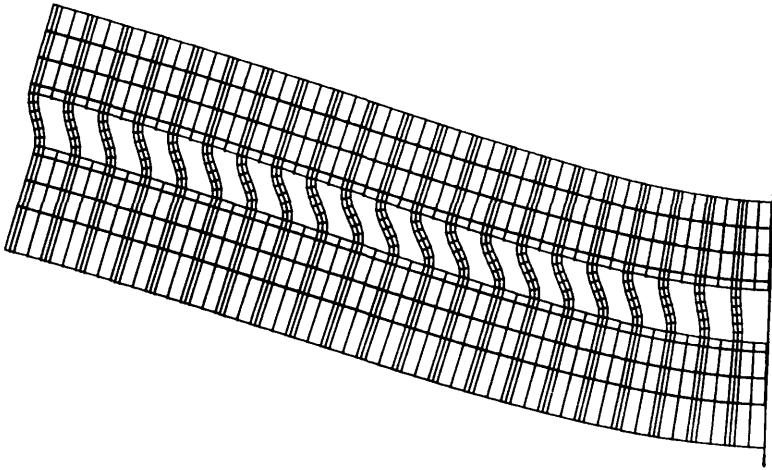
Deformed finite element mesh (B)
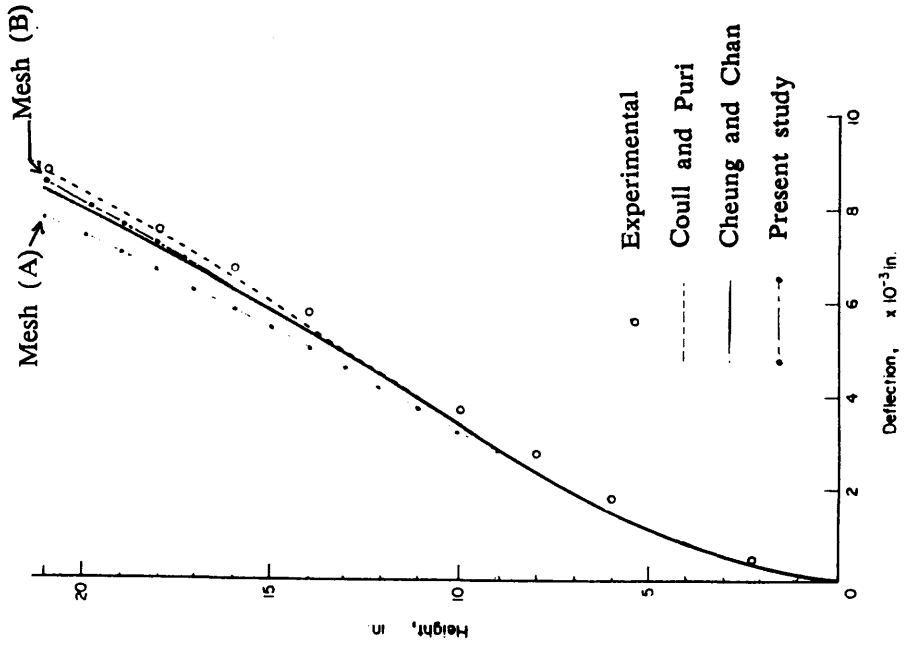
Fig (2-13) LATERAL DEFLECTION FOR 21 STOREY WALL
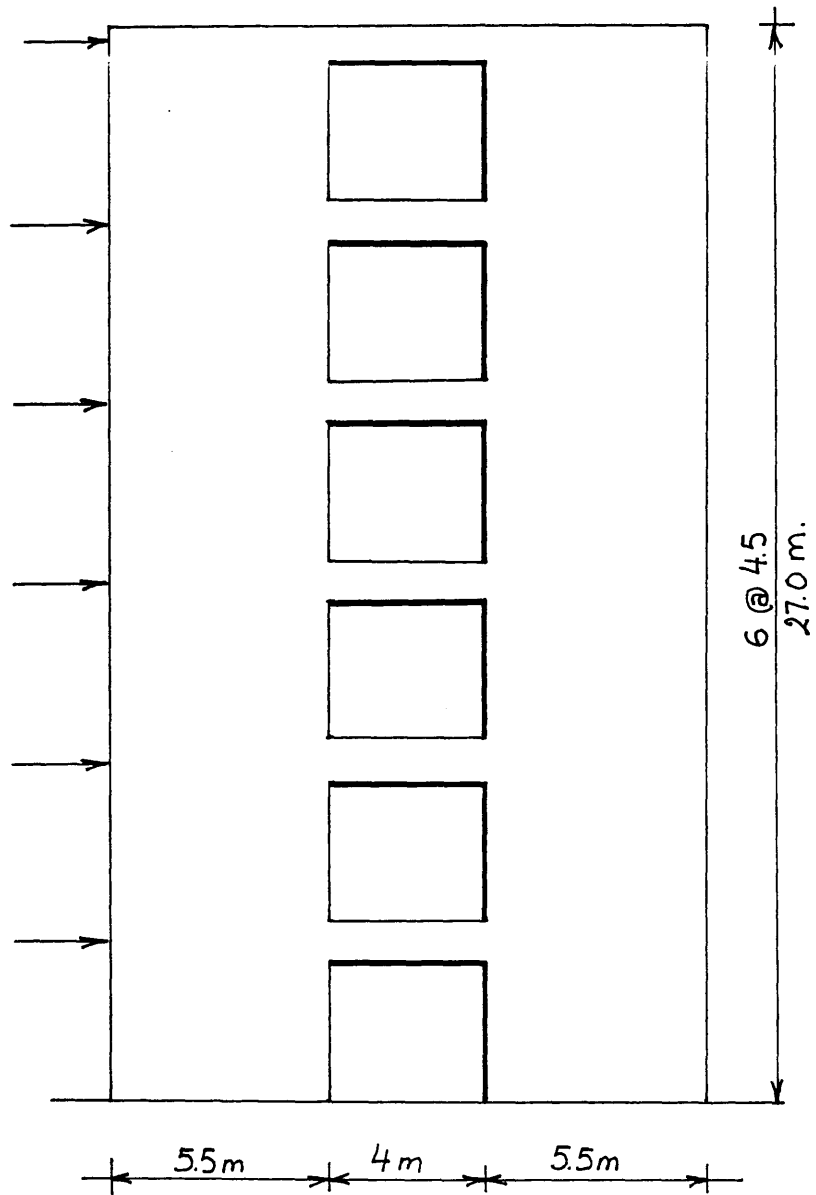
FIG (2-14) SIX STOREY COUPLED SHEARWALL

Vertical stress along the height

20 kg/cm²
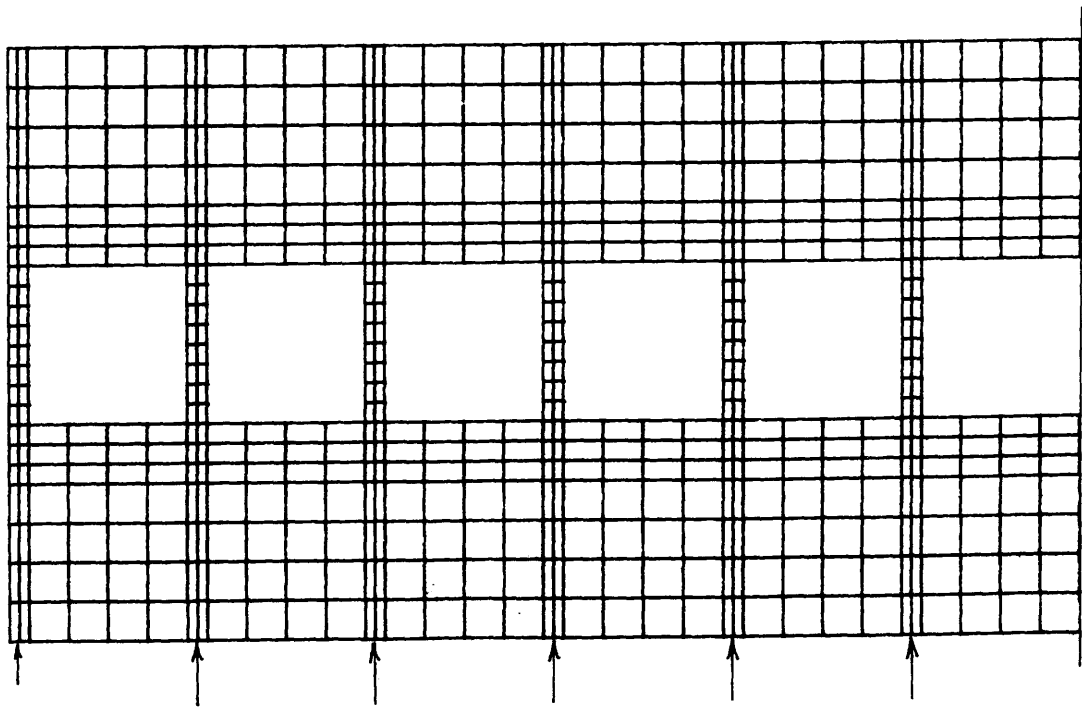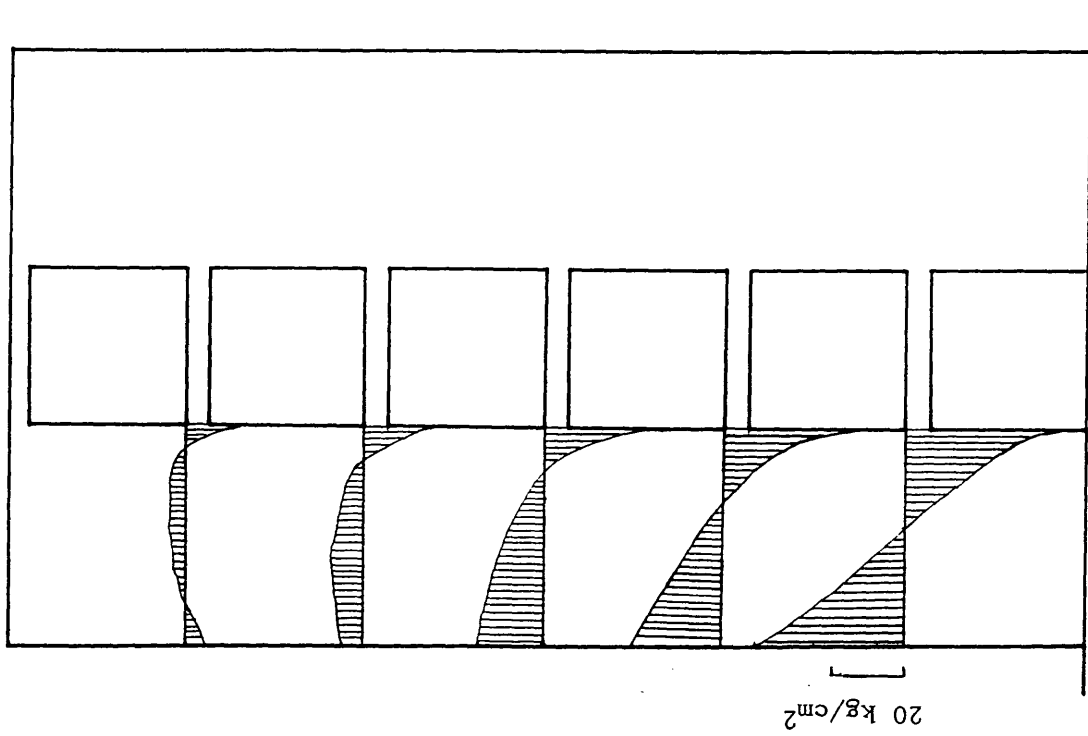
Finite element representation

Fig (2-15) SIX STOREY WALL WITH WEAK COUPLING

Vertical stress along the height

20 kg/cm²
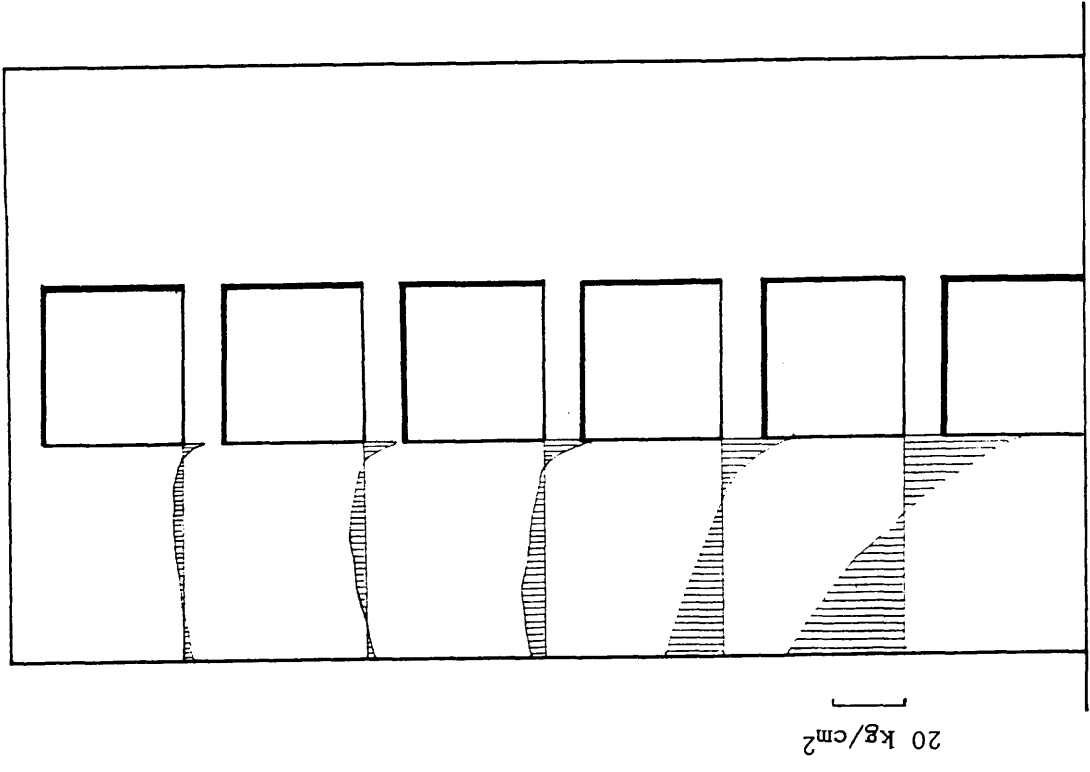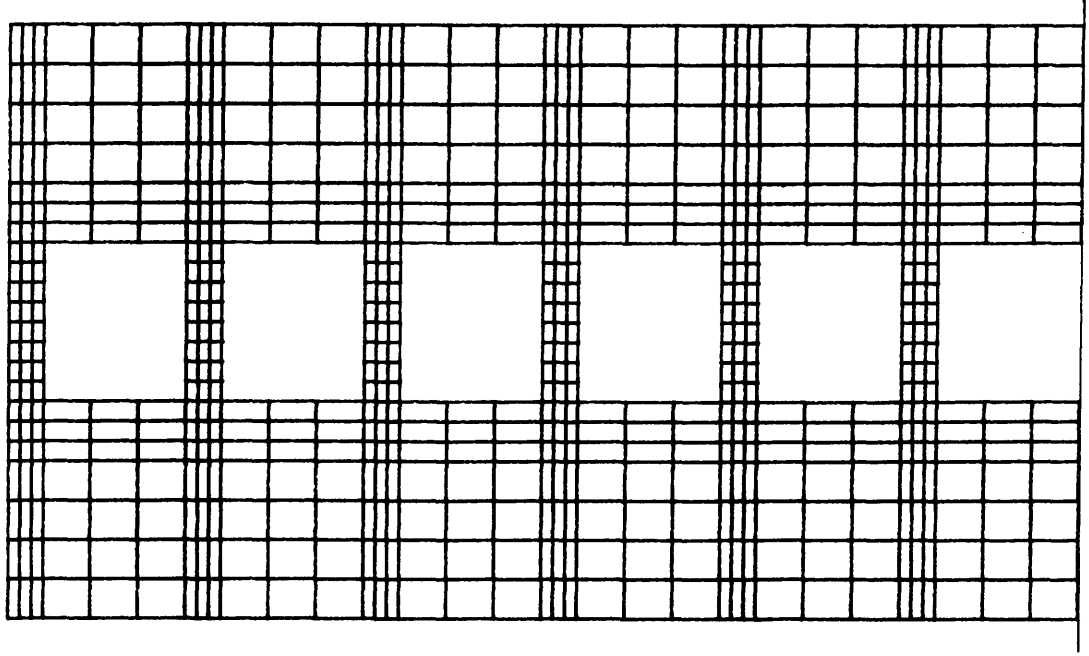
Finite element representation

Fig (2-16) SIX STOREY WALL WITH MODERATE COUPLING

Vertical stress along the height

20 kg/cm²
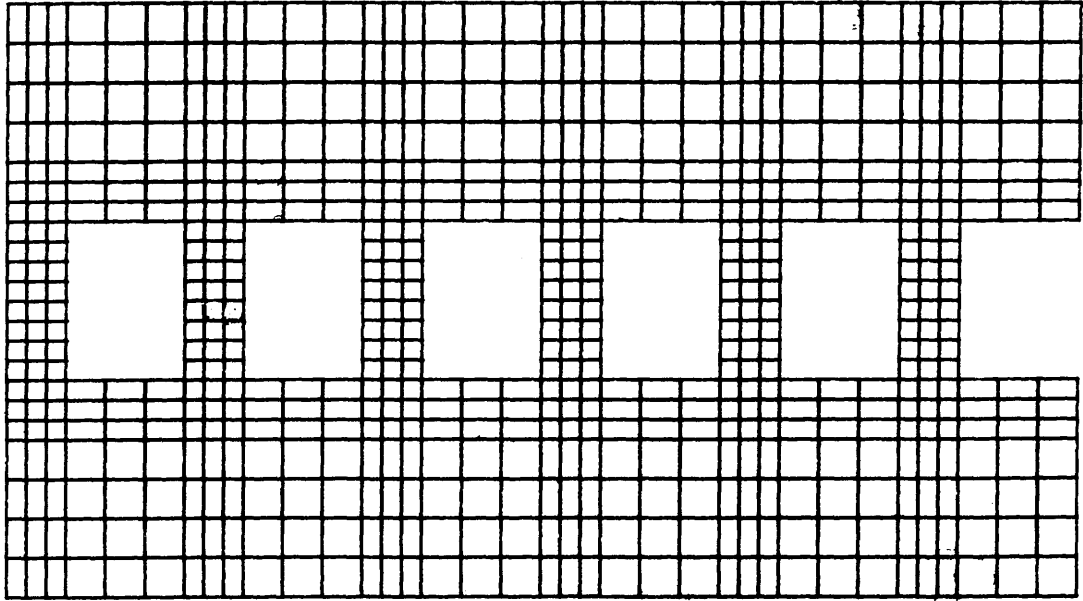
Finite element representation
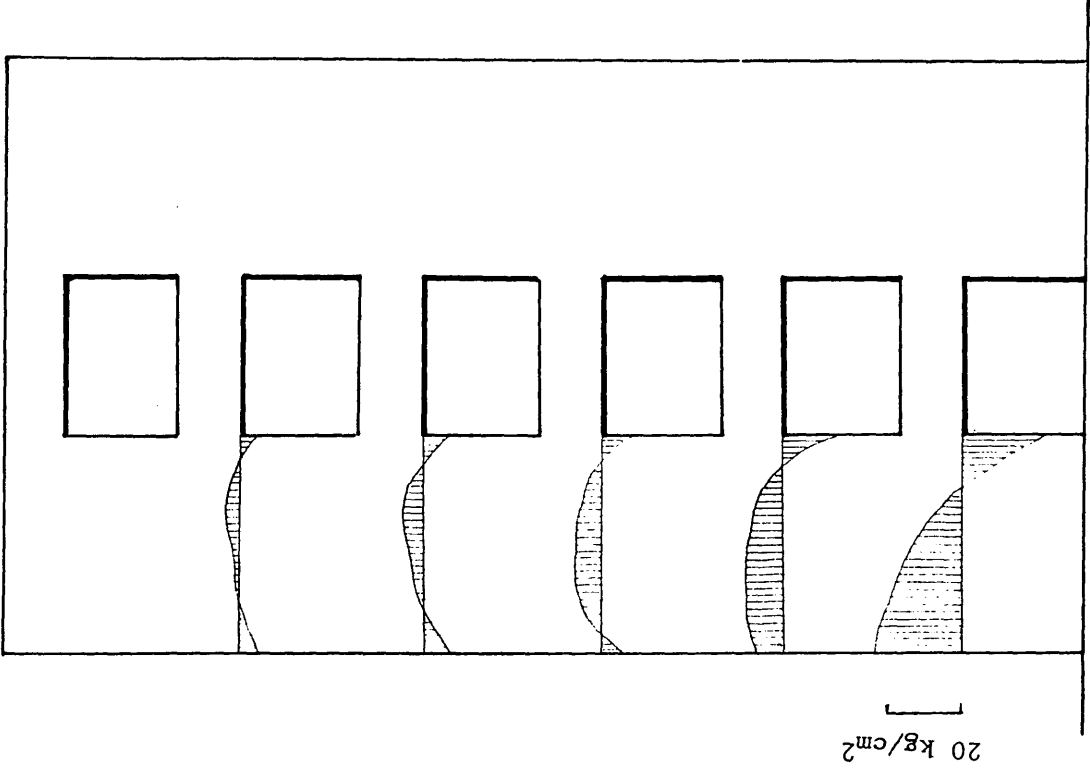
Fig (2-17) SIX STOREY WALL WITH STIFF COUPLING

Stress (Kg/cm)

Fibre distance (cm)

—— Finite element.

------- Wide frame.
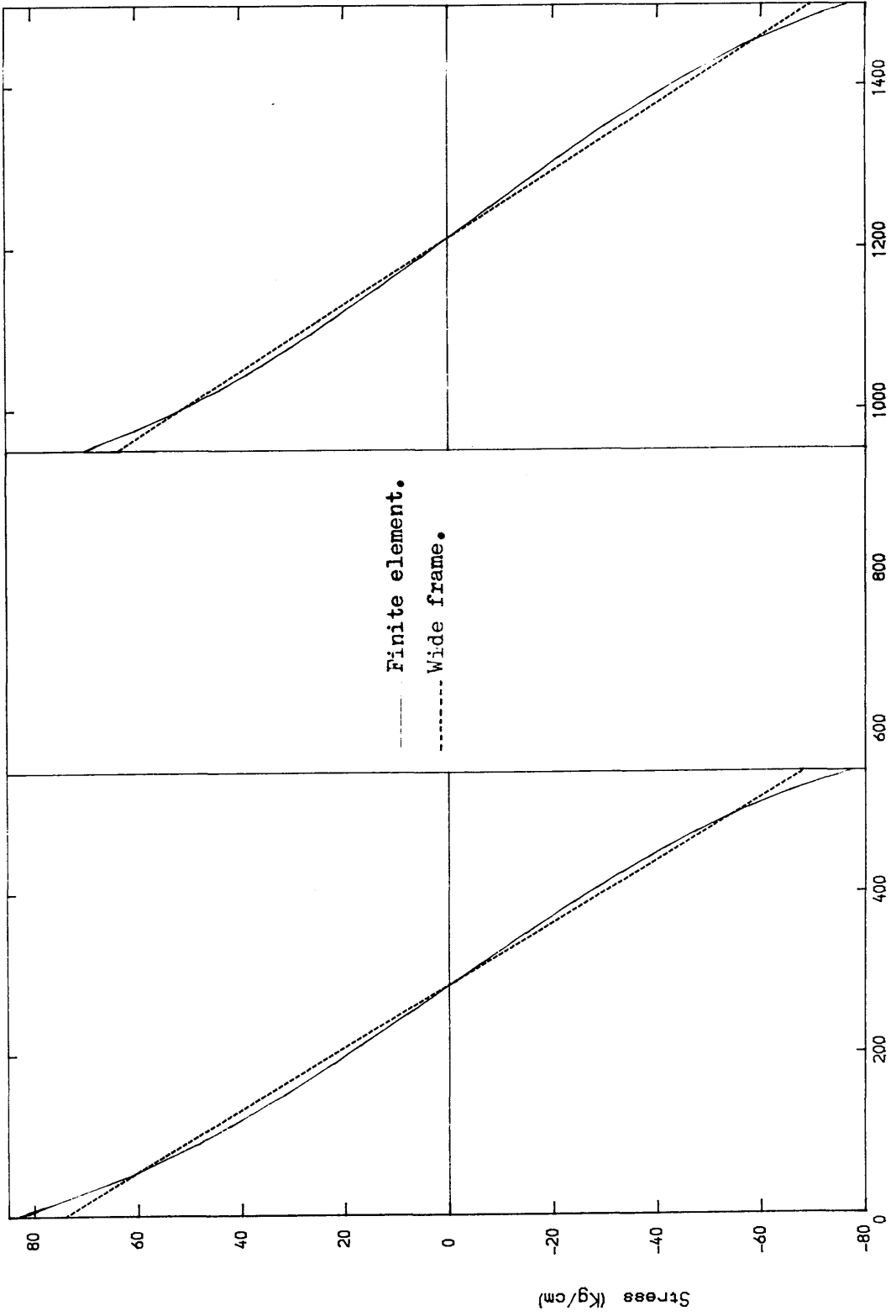
FIG (2-18) NORMAL STRESS AT THE BASE OF THE WALL WITH WEAK COUPLING (d=50cm)
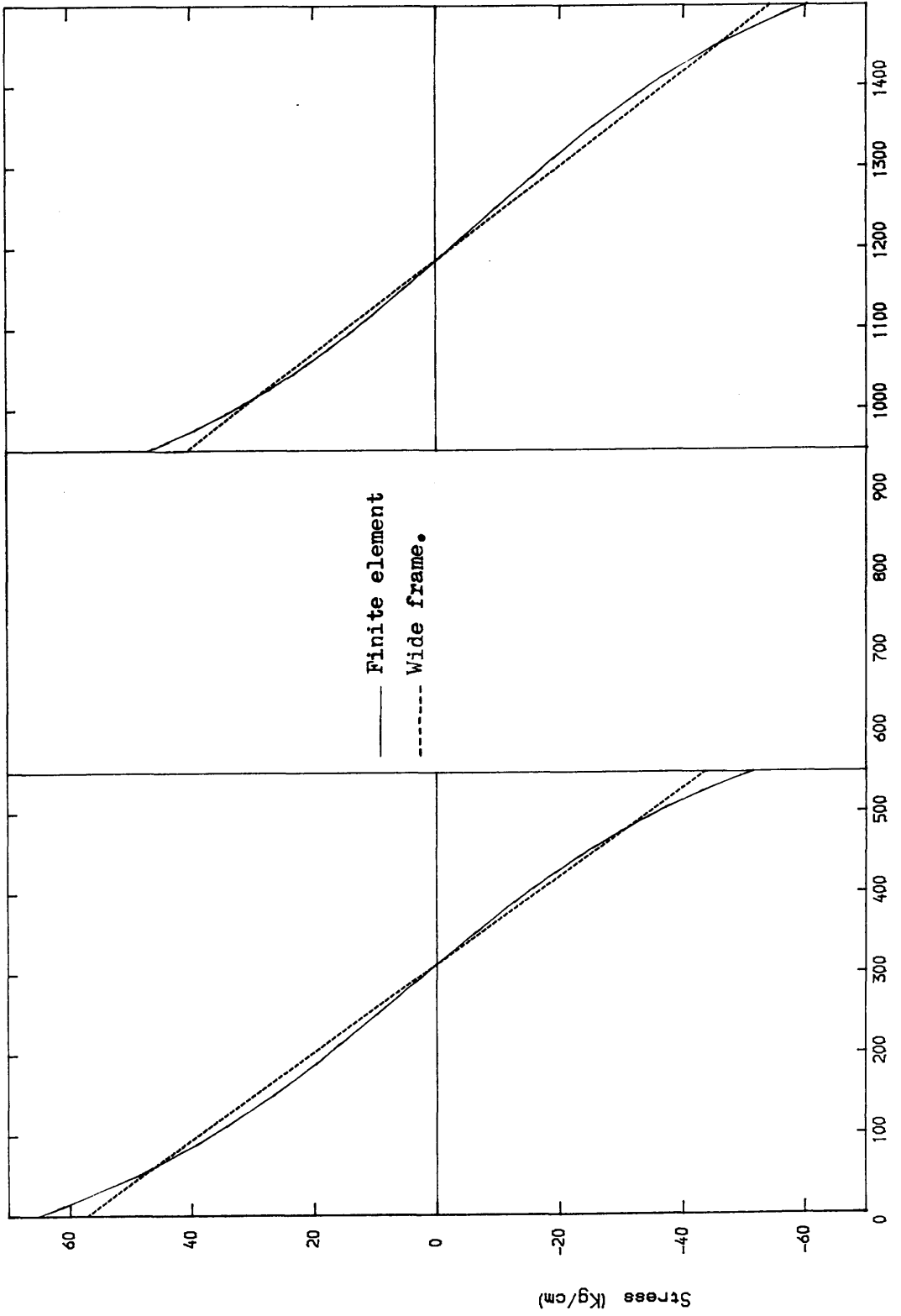
FIG (2-19) NORMAL STRESS AT THE BASE OF THE WALL WITH MODERATE COUPLING (d=90cm).
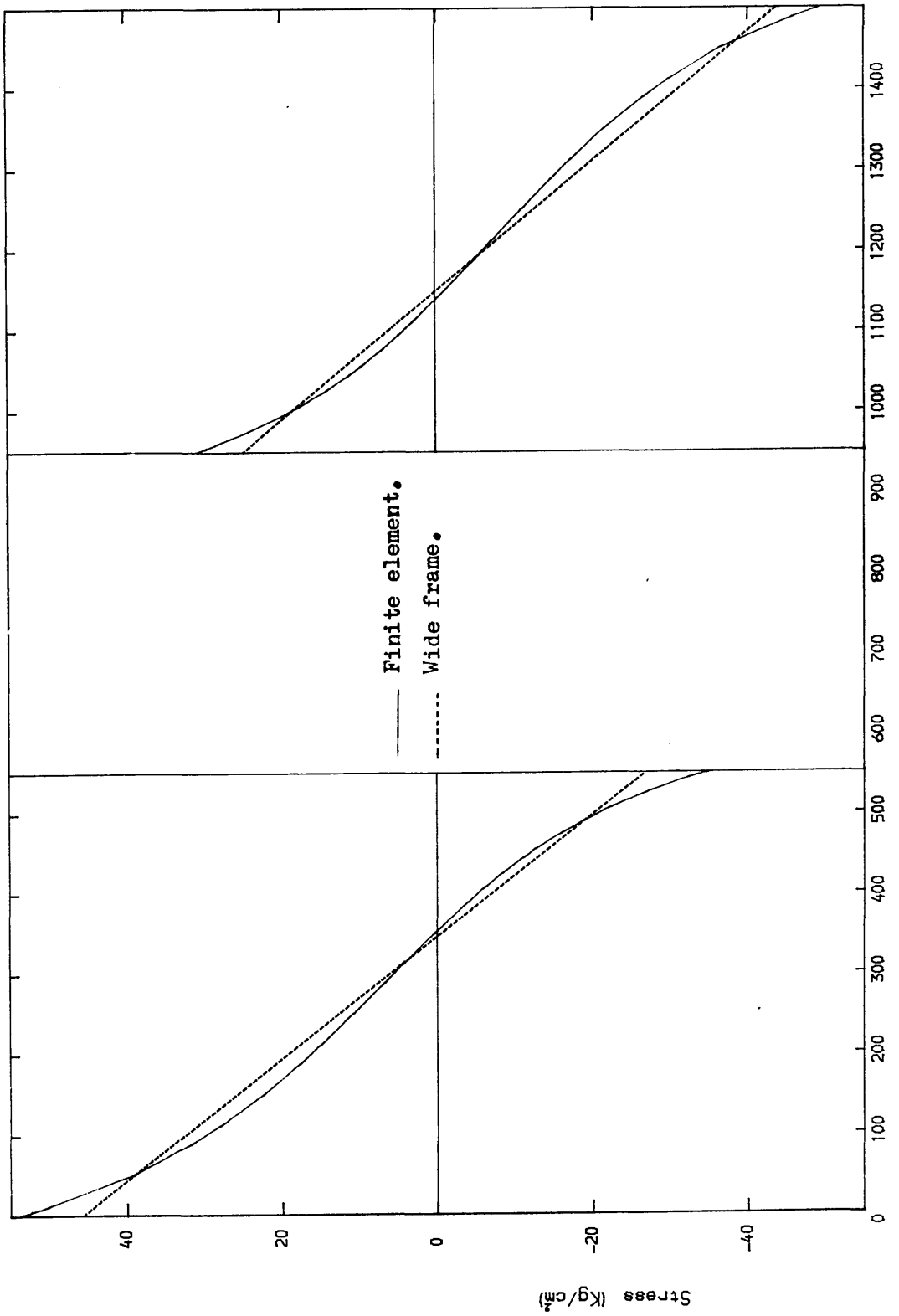
FIG (2-20) NORMAL STRESS AT THE BASE OF THE WALL WITH STIFF COUPLING (d=150cm).
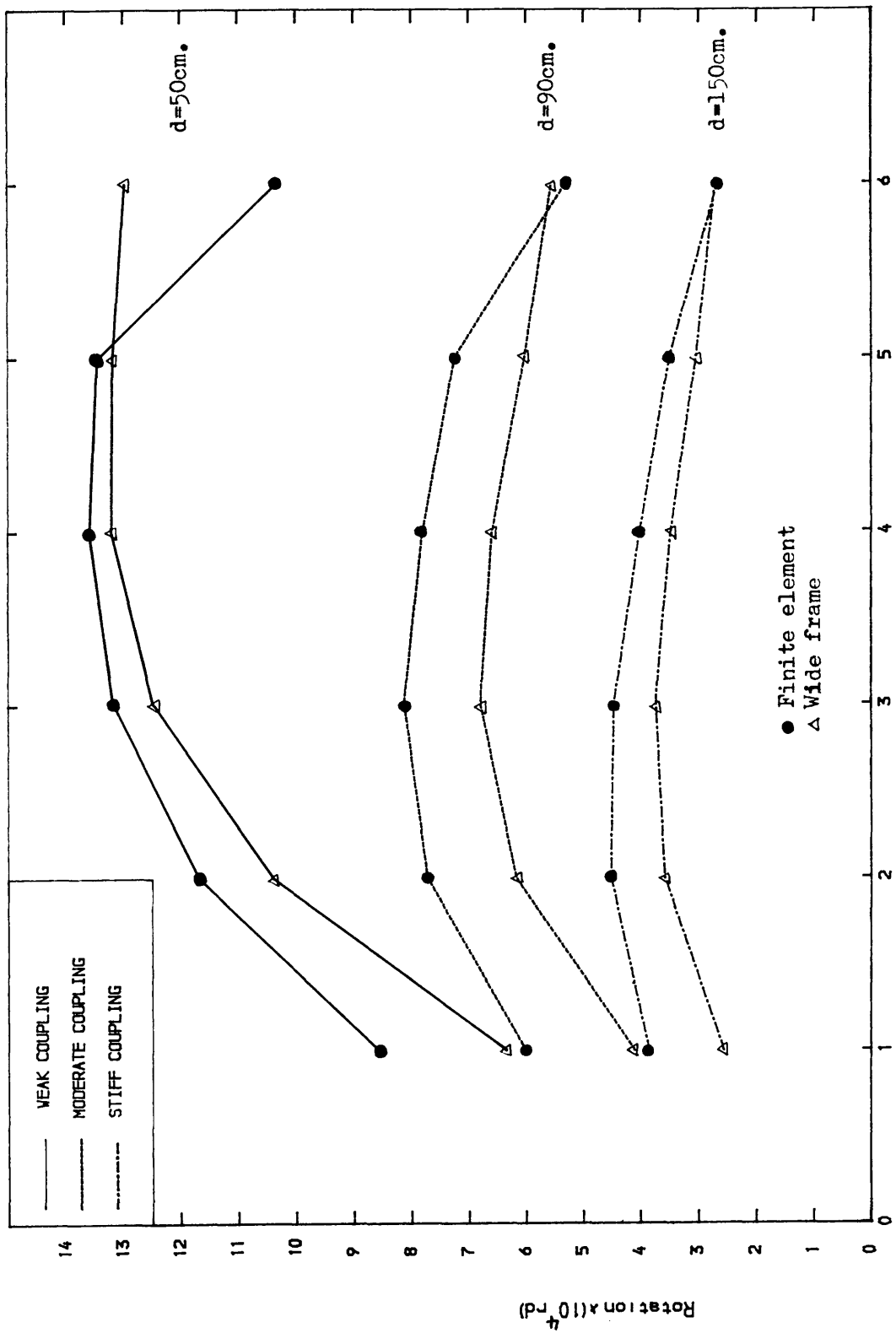
FIG (2-21) ROTATIONS IN THE LINTEL BEAMS (Finite element/Wide frame analogy).

Displacement (cm)

WEAK COUPLING
MODERATE COUPLING
STIFF COUPLING

Finite element
Wide—column
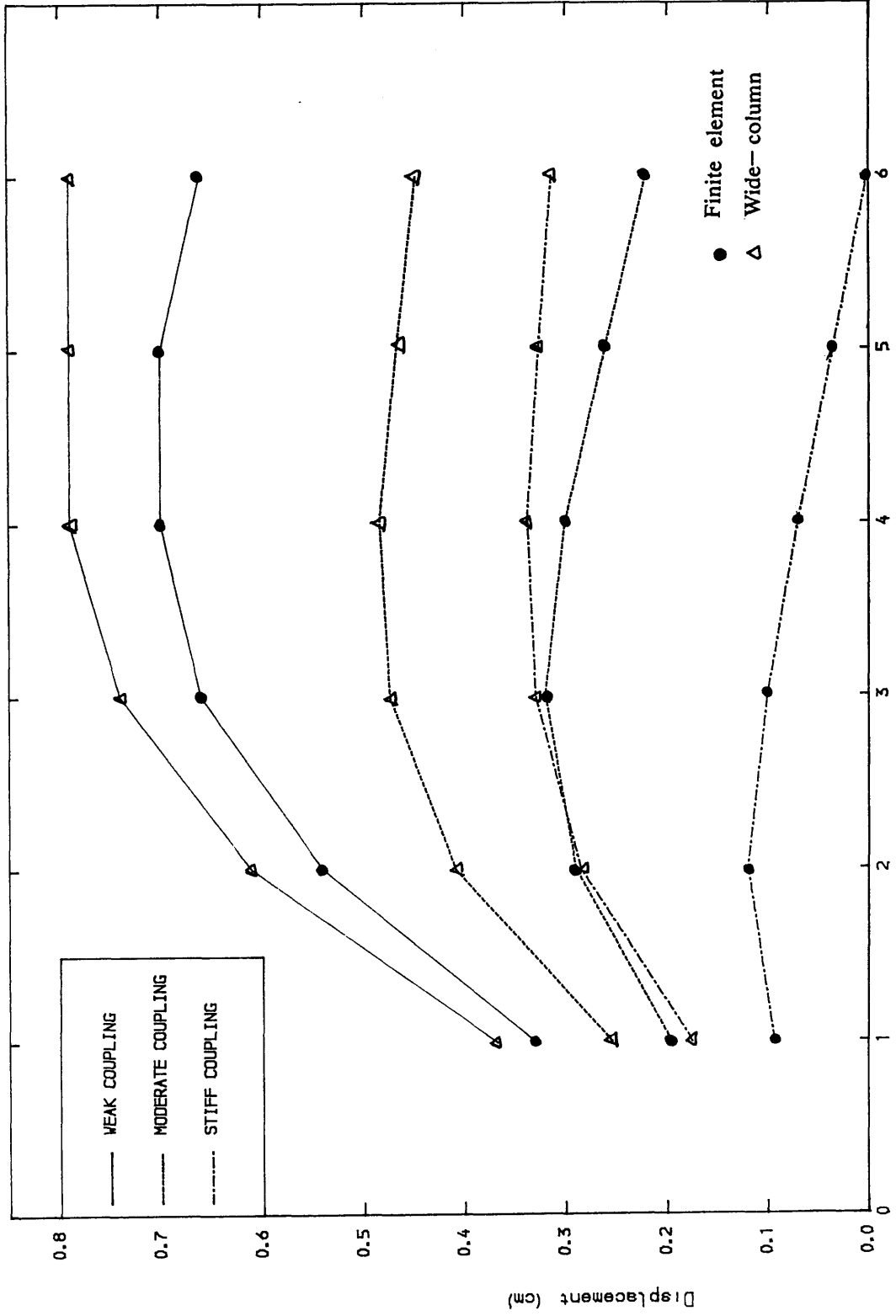
Beam

FIG (2-22) RELATIVE VERTICAL DISPLACEMENT IN LINTEL BEAMS
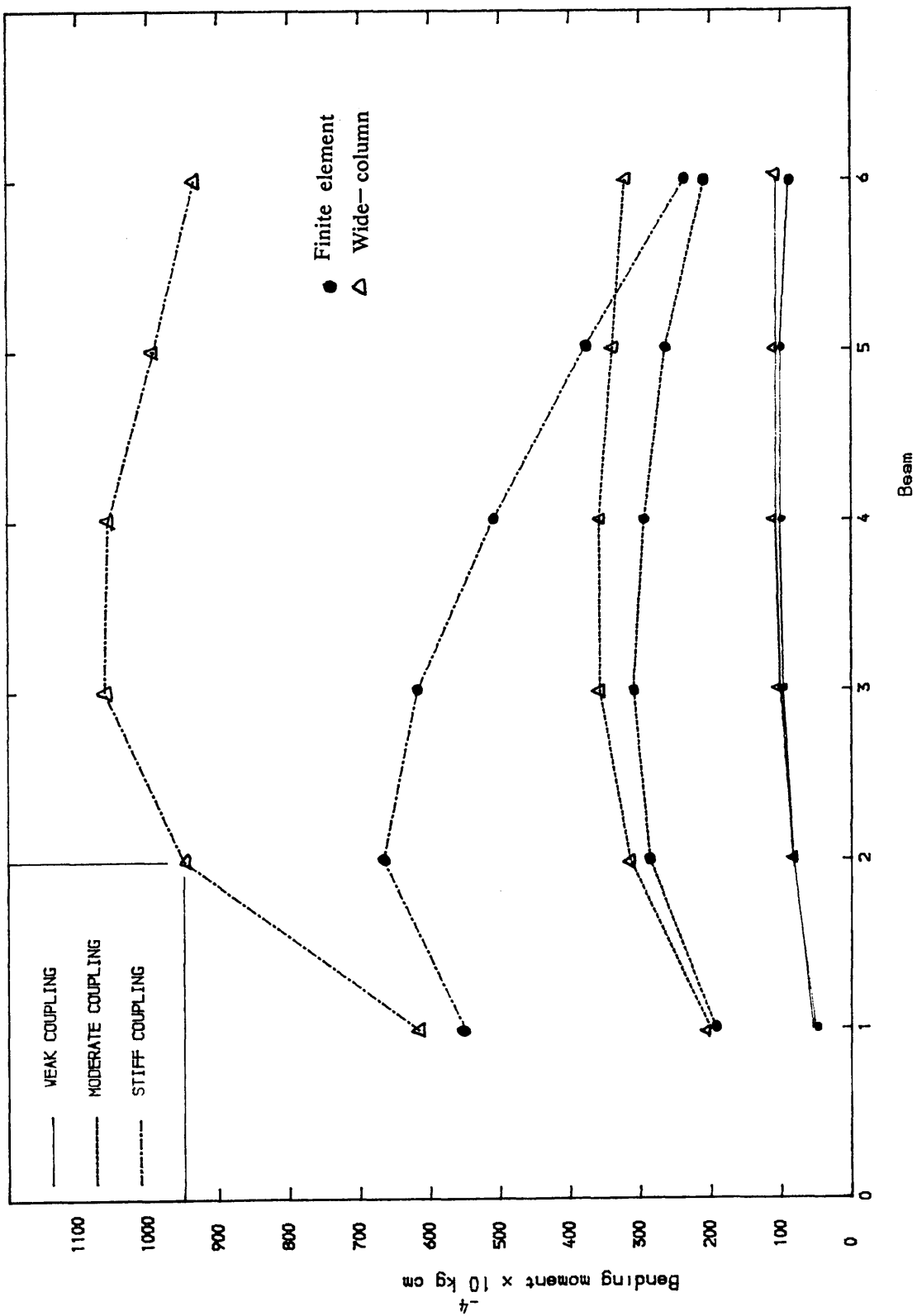
FIG (2-23) *BENDING MOMENTS IN LINTEL BEAMS (Finite element/Wide column analogy).*
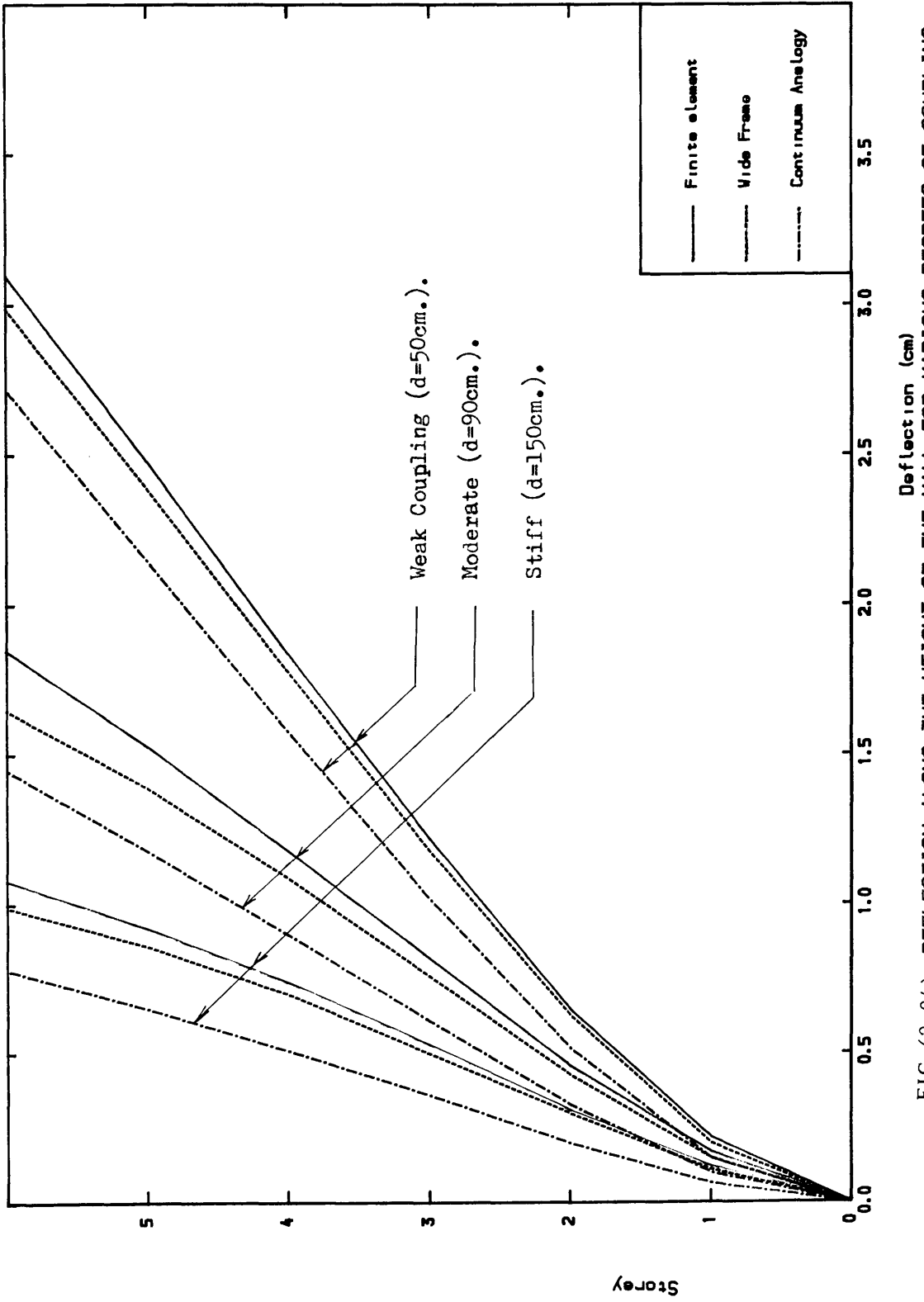
FIG (2-24) DEFLECTION ALONG THE HEIGHT OF THE WALL FOR VARIOUS DEGREES OF COUPLING.

REFERENCES (2)

AKIN, J.E.

Application and implementation of finite element methods.

Academic Press Inc., 1982.

AL-MAHAIDI, R.S. and NILSON, A.H.

Coupled shear wall analysis by lagrange multipliers.

A.S.C.E, Vol. 101, Nov. 1975.

BATHE, K. J.

Finite element procedures in engineering analysis

Prentice—Hall, Englewood Cliffs, 1981.

BECK, H.

Contribution to the analysis of coupled shear walls.

ACI Journal, Vol. 59, 1962, pp. 1055—1070

BHATT, P.

Effect of beam—shear wall junction deformations on the flexibility of the connecting beams.

Build. Sci., Vol. 8, pp. 149—151, 1973.

BREBBIA, C. A. and CONNOR, J. J.

Fundamentals of finite element techniques for structural engineers.

Wiley, New York, 1974.

DESAI, C. S.

Elementary finite element method

Prentice—hall, Englewood Cliffs, 1979.

CHAN, H.C. and CHEUNG, Y. K.

Analysis of shear walls using higher order finite elements.

Building and Environment, Vol. 14, pp. 217—224, 1979.

CHITTY, L.

On the cantilever composed of a series of parallel beams interconnected by cross bars.

Phil. Mag., 1947.

COOK, R. D.

Concepts and applications of finite element analysis.

Second edition, Wiley, New York, 1981.

COULL. A. and PURI, R.D.

Analysis of coupled shear walls of variable cross section.

Build. Sci., Vol. 2, 1968, pp. 313−320.

COULL, A. and SUBEDI, N.K.

Coupled shear walls with two and three bands of openings.

Build. Sci., Vol. 7, pp. 81−86, 1972.

ELKHOLY, I.A.S. and ROBINSON, H.

Analysis of multibay coupled shear walls.

Build. Sci., Vol. 8, pp. 153−157, 1973.

ELKHOLY, I.A.S. and ROBINSON, H.

An inelastic analysis of coupled shear walls.

Build. Sci., Vol. 9, pp. 1−8, 1974.

GALLAGHER, G. H.

Finie element analysis fundamentals.

Prentice−Hall, Englewood Cliffs, 1975.

GIRIJAVALLABHAN, C.V.

Analysis of shear walls by finite element method.

Proceedings, Symposium on application of finite elements in civil engineering, Vanderbilt University, Nov. 1969, pp. 631−641.

GIRIJAVALLABHAN, G. C.

Analysis of shear walls with openings.

Jnl. Str. Div., ASCE, Vol. 95, pp. 2093−2103, 1969.

GLUCK, J.

Elastoplastic analysis of coupled shear walls.

Journal of Engineering Structural Division, ASCE, Vol 99, No. ST8, pp. 1743−

GREEN, N. B.

Bracing walls for multistory buildings.

ACI Journal, pp. 233–   , 1953.

HINTON, E. SCOTT, F. C. and RICKETTS, R. E.

Local least square stress smoothing for parabolic isoparametric elements.

Int. Jnl. Num Methods in Eng., Vol 9, pp. 235–256, 1975.

HUSSEIN, W.A.

Analysis of multibay shear wall structure by the shear connection method.

Build. Sci., Vol. 7, pp. 69–73, 1972.

JEYACHANDRABOSE, C. and KIRKHOPE, J.

Least square smoothing for the eight node serependity plane
stress element.

Int. Jnl. Num. Methods in Eng., pp. 1164–1166, 1983.

LEW, I.P. and NAROV, F.

Three dimensional equivalent frame analysis of shear walls.

Concrete International, Oct. 1983, pp. 25–30.

LIM, P.T.K et al.

Finite element analysis of curved box girder bridges.

Developments in bridge design and construction, Crosby Lockwood,

Rockey, K.C. at al. Eds, London 1971.

MacLEOD, I.A.

Lateral stiffness of shear walls with openings.

Tall Buildings, Pergamon Press, Oxford 1967, pp. 223–244.

MacLEOD, I.A.

New rectangular finite element for shear wall analysis.

Journal of Structural Division, ASCE, Vol. 95,

No. ST3, 1969, pp. 399–409.

MacLEOD, I.A.

Structural analysis of wall systems.

The Structural Engineer, No. 11, Vol. 55, Nov. 1977, pp. 487–

MICHAEL, D.

The effect of local wall deformations on the elastic interaction
of cross walls coupled by beams.
Tall Buildings, Pergamon Press, Oxford 1967, pp. 253—270.

OAKBERG, R.G. and WEAVER, W.Jr.

Analysis of frames with shear walls by finite elements.
*Proceeding, Symposium on application of finite elements
in civil engineering, Vanderbilt University, Nov. 1969, pp. 567—607.*

PAULAY, T.

An elastoplastic analysis of coupled shear walls.
ACI Journal, Vol. 67, Nov. 1970, pp. 915—922.

PAULAY, T.

Coupling beams of reinforced concrete shear walls.
*Journal of Structural Division, ASCE, Vol. 97,
No. ST3, 1971, pp. 843—*

ROSMAN, R.

Approximate analysis of shear walls subject to lateral loads.
ACI Journal, Vol. 61, No. 6, 1964, pp. 717—733.

SHWAIGHOFER, J. and MICROYS, H. F.

Analysis of shear walls using standard computer programs.
ACI Journal, pp. 1005—1007, 1969.

SISODIYA, R.G. and CHEUNG, Y.K.

A higher order in—plane parallelogram element and its application
to skewed girder bridges.
Developments in bridge design and construction, Crosby Lockwood,
Rockey, K.C. at al. Eds, London 1971, pp. 304—317.

UNGUREAUNU, N.

A new structural model for shear walls analysis.
*International symposium on earthquake structural engineering,
St. Louis, Missouri, USA, August 1976, pp. 1277—1291.*

WEAVER, W.Jr. LEE, D.G. and DERBALIAN, G.

Finite element for shear walls in multistory frames.
Journal of Structural Division, ASCE, Vol. 107,
No. ST7, July. 1981, pp. 1365—1369.

WINOKUR, A. and GLUCK, J.

Ultimate strength analysis of coupled shear walls.
ACI Journal,Vol. 65, Dec. 1968, pp. 1029—1036.

ZIENKIEWICZ, O. C.

The finite element method.
Third edition, McGraw—Hill, 1977.

ZIENKIEWICZ, O. C. and PHILLIPS, D. V.

An automatic mesh generation scheme for plane and curved surfaces
by isoparametric coordinates.
Int. Jnl. Num. Methods in Eng., Vol. 3, pp. 519—528, 1971.

CHAPTER 3

NUMERICAL MODELLING OF CONCRETE AND STEEL

3-1 INTRODUCTION :

Analysis of the complete response of structural systems of steel and concrete requires consideration of a number of nonlinear effects. The most important of these effects include tensile cracking and compressive crushing of concrete, nonlinear material properties, concrete steel bond, aggregate interlock and reinforcement dowel action. The finite element method offers a convenient and adaptable means whereby such complex systems may be analysed. The basic information required is the multidimensional stress—strain relations describing adequately the characteristics of reinforced concrete materials. These are called the constitutive laws and may be viewed as the simplified mathemetical descriptions of the behaviour of the constituent materials approximating closely the real behaviour. They are based on experimental data, and allow formulation for concrete relations between any applied multiaxial stress state and the strains or distortions resulting from it. Various approaches have been suggested and several proposals have been made for the description of an ultimate strength surface for concrete. A first important consideration is that the constitutive properties of concrete have not yet been universally defined and there is no generally accepted material law which fully describes the concrete behaviour in combined stress conditions, Buyukozturk et al. 1985. In addition to the disagreement on the theory upon which the constitutive model is to be built, elasticity, plasticity or endochronic, a large scatter of results has been observed on past test studies on the response of concrete to multiaxial stress states. The scatter can be attributed to two principal factors: variations of the materials tested and variation in the test method and loading systems.

In the following, the mathematical modelling for each of the constituents, steel

and concrete, are described separately.

3-2 MECHANICAL BEHAVIOUR OF CONCRETE :

The purpose of this section is to summarize some of the key facets of the experimental behaviour of plain concrete under uniaxial and biaxial states of stress. These experimental test data are essential in the development of constitutive models for concrete and provide data for the determination of the various parameters which appear in the mathematical model to be presented later in this chapter.

3-2-1 UNIAXIAL COMPRESSIVE STRESS-STRAIN RESPONSE :

Consideration of uniaxial stress-strain response of plain concrete under short term loading is a useful starting point for a discussion of more complex conditions. Typical curves for concrete subjected to monotonic uniaxial compressive stress versus axial, lateral and volumetric strains are shown in Fig (3-1). In Fig (3-2) different uniaxial stress-strain curves are given for concretes with various compressive strengths f_c'. The development of microcracking is closely related to the characteristics of stress-strain relations, Hsu et al. 1963 and Chen and Yamaguchi 1985. The main experimental observations can be summarized as follows: (a) concrete has a nearly linear elastic behaviour up to about 30% of its maximum compressive strength f_c'. Although some bond cracks at the mortar-coarse aggregate interfaces already exist, they are quite stable and have little tendency to propagate. (b) For stresses above 0.3 f_c', concrete begins to soften as further bond microcracks form. (c) Beyond 0.75 f_c', these microcracks propagate and extend through the cement mortar and the stress-strain curve bends sharply until it approaches the peak stress f_c', beyond which a crushing failure is observed at some ultimate strain in the range 0.003-0.004 approximately, when the

crack system eventually becomes unstable causing failure. The exact point of complete breakdown is highly variable and depends on the relative stiffness of the specimen and the testing system.(d) The shape of the stress—strain curve is similar for low, normal and high strength concretes, and all peak points are located close to a strain value of 0.002. (e) Beyond the peak point f_c' higher strength concrete exhibits a more sharply descending branch and behaves in a brittle manner.

Numerous mathematical expressions based on the above experimental data have been used to predict uniaxial compressive stress—strain response using curve—fitting techniques. An excellent and comprehensive summary of these efforts has been presented by Popovics 1970. Carreira and Chu 1985 proposed a complete stress—strain relationship of plain concrete in compression for both the ascending and descending branches of the stress—strain diagram. Wan 1988 proposes an equation to represent the uniaxial compressive stress—strain relation of concrete as a generalized form of Popovics 1970 and Saenz 1964. It consists of two parameters, to control the ascending and descending behaviour.

3—2—2 UNIAXIAL TENSILE STRESS—STRAIN RESPONSE :

The tensile strength of plain concrete, generally 5—10% of the compressive strength of concrete can be determined by several testing methods. These methods may be broadly classified into three types: direct, flexure and indirect as indicated in Fig (3—3). When tested under strain control using direct tensile tests in a stiff testing apparatus, the uniaxial stress—strain response of plain concrete is approximately linear up to about 80% of the peak stress and some softening is apparent thereafter, Fig (3—4). The drawbacks of the direct pull tests are the difficulties of holding the specimens so as to eliminate eccentricity of the line of action of the load, and the development of secondary stress concentration induced by the holding devices. Consequently, the direct tension tests are infrequently used,

instead, flexure and indirect tests are more appropriate. Of all the indirect methods introduced in recent years, the splitting tests are the most common ones. An apparaisal of the splitting tests on cylinders, widely used, has been given by Wright 1955, and splitting tests on cubes has been described by Nilssons 1961. In the split cylinder test, a concrete cylinder is laid horizontally between the loading platens of a testing machine and compressed along the line of a diameter until the specimen splits along a vertical diameter plane as indicated in Fig (3−3). An elastic analytical study using finite elements for various splitting tests has been reported by Davies and Bose 1968, and a more refined treatment of this problem has been given by Chen and Chen 1976, Chen and Chang 1978. The tensile strength in flexure is known as the modulus of rupture and is obtained by testing a plain concrete beam under symmetrical two point loading applied at one third span points.

The tensile strength of concrete evaluated by means of flexure tests conducted on plain concrete beams tends in general to be higher than the tensile strength of a split cylinder, which in turn tends to be higher than tensile strength obtained from a direct tension test Chen 1970.

From the above discussion, it can be appreciated that the effective tensile strength of concrete may be difficult to determine, despite its wide use as a criterion for the onset of cracking and its importance in most constitutive models. Balakrishnan and Murray 1988 found that the tensile strength of concrete influences the failure mode and failure load of shear critical beams. With the presence of reinforcing steel the prediction of stress levels to cause cracking and crack directions becomes considerably more uncertain.

3- 2- 3 BIAXIAL BEHAVIOUR :

Biaxial stress states are typical of the structural action in many important classes of structures such as beams, panels, slabs and shells, and involve a range of admissible stress somewhat lower than triaxial ones. In modelling these structures, test results for concrete under biaxial loading are sufficient.

In recent years, a large amount of research has been done on the mechanical properties of concrete in biaxial states of stress, and have shown that under different combinations of biaxial loading, the strength and stress- strain response of concrete are somewhat different to those observed under uniaxial conditions. In contrast, the procedures used in design are based primarily on material properties obtained from uniaxial strength tests.

Most experimental investigations of the strength of concrete under biaxial states of stress, not yet incorporated into design procedures, generally agree with the shape of failure envelopes shown in Fig (3- 5). Severe deviations in the region near equal biaxial compression stress state can be observed. These deviations are due mainly to factors such as testing machine characteristics and variations of the materials tested. Because no systematic study of the importance of these two factors could be found in the litterature, an international cooperative study, Gerstle et al. 1980, was undertaken by main research laboratories active in multiaxial concrete testing. All participants used specimens of the same concrete cast and cured in one laboratory. The differences among tests methods are predominantly a function of the specimen boundary conditions as determined by different loading systems used: dry steel platens, lubricated steel platens, brush bearing platens and fluid cushion among others. It has been found, Gerstle et al. 1980, that the scatter of results in all test series disminished considerably with absence of constraints on the specimen boundaries. The boundary constraints inhibit transverse specimen deformations, and therefore result in erroneous material properties. Unconstrained specimen boundaries

are necessary to obtain moduli for prediction response to general stress states.

In this numerical study the experimental findings and failure envelope of Kupfer, Hisdorf and Rush 1969 have been used to simulate the behaviour of concrete. These tests were conducted on square thin concrete panels 20x20x5 cm subjected to inplane loading. The ratio of the stresses was held constant throughout loading (proportional loading). This appears to be more suitable to determine the biaxial strength of concrete over the entire range of biaxial stress combinations, as compared to previous experiments conducted on cylinders and cubic specimens, neither of which falls under the category of plane stress. To eliminate the effects of boundary restraints, brush bearing platens flexible enough to follow the concrete deformations without appreciable restraint were used. Fig (3—6) illustrates the experimental failure strength envelope for three types of concrete subjected to proportional biaxial loading. Three possible biaxial states are distinguished namely; biaxial compression, combined compression and tension, and biaxial tension. Under the conditions of biaxial compression, the ultimate compressive strength of concrete is greater than uniaxial compression due to confinement effects. A maximum strength increase of approximately 25% is achieved at stress ratio $\sigma_1/\sigma_2 = 0.5$. This increase is reduced to about 15% at an equal biaxial compression state $\sigma_1/\sigma_2 = 1.0$.

Under the combination of tension and compression, concrete exhibits a noticeably reduced strength. The compressive strength decreases almost linearly as the applied tensile stress is increased.

Under biaxial tension, concrete exhibits a nearly constant tensile strength which is almost the same as that of its uniaxial tensile strength.
The strength relations for three concretes under biaxial stress states are given by the interaction curves in Fig.(3—6), have been approximated by the following expressions in terms of principal stresses which are plotted in Fig.(3—6):

Compression— Compression:

$$(\sigma_1/f_c' + \sigma_2/f_c')^2 + \sigma_1/f_c' + 3.65\,\sigma_2/f_c' = 0 \qquad \text{............ (3—1)}$$

Compression— Tension:

$$\sigma_2/f_t = 1 + 0.8\,\sigma_1/f_c' \qquad \text{............ (3—2)}$$

Tension— Tension:

$$\sigma_2 = f_t = 0.64\,\sqrt[3]{f_c'^2} \qquad \text{............ (3—3)}$$

3— 3 CONSTITUTIVE MODELLING OF CONCRETE :

Constitutive laws for reinforced concrete are the simple analytical formulations to represent numerically the complicated stress— strain behaviour of concrete. A large number of numerical models and techniques for the analysis of reinforced concrete structures has been developed and the literature abounds with their implementation and application ASCE 1982, Chen 1982, CEB 1983, Bangash 1989. At present, most of the constitutive models can be classified into one of the following models, ASCE 1982.

        (a) Elasticity based models (Linear/Nonlinear)

        (b) Plasticity based models

        (c) Plastic— Fracture type models.

        (d) Endochronic models.

In the following, the various constitutive models above are described. The

analytical model used in this study is then presented to simulate analytically the experimental behaviour of concrete under any combination of biaxial stress conditions.

3-3-1 ELASTICITY BASED MODELS (Linear/Nonlinear)

A recent state of the art report summary of finite element analysis of reinforced concrete structures ASCE 1982 shows that, in spite of the general recognition of the nonlinear material behaviour of concrete, most analyses use a linear elasticity approach for modelling the material response in pre— and post—peak stress range. This may be attributed to the difficulties encountered in assessing various parameters involved with complex material models and in their computer implementation. Significant realism in predictions can be achieved using a nonlinear stress—strain relationship. In general, two different approaches are employed in the formulation of nonlinear elasticity based stress—strain laws:

(a) Finite (or total) material behaviour characterization in variable secant moduli form, known as *hyperelastic* type of formulation.

(b) Incremental (or differential) material descriptions of the *hypoelastic* type using variable tangent moduli.

This means that the stress—strain relationships can be expressed as either:

$$\{ \sigma \} = [D] \{ \epsilon \} \qquad \ldots\ldots\ldots (3-4)$$

or

$$\{ d\sigma \} = [D] \{ d\epsilon \} \qquad \ldots\ldots\ldots (3-5)$$

in the *hyperelastic* and *hypoelastic* formulations respectively.

Where $[D]$ represents either the secant or tangential constitutive matrix; $\{ \sigma \}$ and $\{ \epsilon \}$ are the total stress and strain vectors; and $\{ d\sigma \}$ and $\{ d\epsilon \}$ are the

stress and strain increment vectors.

In the *hyperelastic formulations*, the current state of stress is assumed to be uniquely defined as a function of the current state of strain, that is the material response at any instant is a function only of the current state of stress and not of the load history. These models simulate the response of concrete sustaining monotonic or proportional loading with reasonable accuracy, but they fail to predict inelastic deformations when the material experiences unloading. One such approach is the nonlinear deformation model obtained by Kupfer and Gerstle 1973 through the decomposition of the stress and strain into a hydrostatic and deviatoric portions.Based on monotonic biaxial tests, closed form expressions for the secant shear modulus G_s and bulk modulus K_s were derived by curve fitting the experimental data. Kotsovos and Newman 1978, based on their own tests, developed a hyperelastic model in a similar approach to Kupfer and Gerstle 1973. Mathematical expressions were obtained for the variation of the bulk and shear moduli in the form of those obtained by Kupfer and Gerstle 1973, but included a correction function that takes into account volume changes that occur under deviatoric stress. Romstad et al. 1974 rather than utilizing continuous curves, defined a number of damage regions in which the material moduli are altered to match the softening due to increasing stresses. Within each region the modulus of elasticity and Poisson's ratio are kept constant.

In the *hypoelastic formulation* the material response at any instant is a function of the current state of strain, and of the stress path followed to reach that state. Due to their path dependant behaviour characteristic, incremental hypoelastic models provide a more realistic description of concrete behaviour under non—monotonic and non—proportional loading regimes than the hyperelastic models. Various special simplified forms of the hypoelastic formulation have been developed and used extensively in the finite element application to concrete structures. In the simplest approach of formulating such models, the constitutive relations are

restricted to be incrementally isotropic, Bathe and Ramaswamy 1979, Gerstle 1981 or orthotropic Darwin and Pecknold 1977 and Liu et al. 1972..

In this study a concrete model based on the orthotropic hyperelastic formulation is used with the principal directions of orthotropy coinciding with the principal stress directions.

3-3-2 PLASTICITY BASED MODELS :

The theory of plasticity was initially developed for metals and has been used extensively to describe the behaviour of reinforced concrete structures. In general, models based on the theory of plasticity describe concrete as an elastic— perfectly plastic material or account for some hardening as an elasto— plastic hardening material.

The construction of the stress— strain matrix in elastoplasticity can be detailed by specifying a yield function, a flow rule (associated or non— associated) and a hardening rule (isotropic, kinematic or mixed). The yield condition specifies the state of multiaxial stress corresponding to the start of plastic flow. It is assumed that yielding occurs only if the stress $\{ \sigma \}$ satisfy the general yield criterion of the form:

$$F (\{ \sigma \}, k) = 0 \qquad \text{....... (3-6)}$$

where k is a hardening parameter.

During an infinitesimal increment of stress, changes of strain are assumed to be divisible into elastic recoverable and plastic irrecoverable components, thus:

$$\{ d\epsilon \} = \{ d\epsilon_p \} + \{ d\epsilon_e \} \qquad \text{......... (3-7)}$$

A flow rule is assumed which determines the direction of plastic strain increments

$\{ d\epsilon_p \}$ subsequent to yielding with a plastic potential function Q ($\{ \sigma \}$, k) as follows:

$$\{ d\epsilon_p \} = \lambda \left[\frac{\partial Q}{\partial \sigma} \right] \qquad \ldots\ldots\ldots \text{(3-8)}$$

where λ is a proportionality constant.

The elastic strain and stress increments are related by the elasticity matrix [D]

$$\{ d\epsilon_e \} = [D]^{-1} \{ d\sigma \} \qquad \ldots\ldots\ldots \text{(3-9)}$$

Substituting (3-9) and (3-8) into (3-7), the total incremental strains are written as:

$$\{ d\epsilon \} = [D]^{-1} \{ d\sigma \} + \lambda \left[\frac{\partial Q}{\partial \sigma} \right] \qquad \ldots\ldots\ldots \text{(3-10)}$$

When plastic yield is occuring, the stresses are on the yield surface given by (3-6), differentiating this we can write the consistency condition as:

$$dF = \left[\frac{\partial F}{\partial \sigma} \right]^T \{ d\sigma \} - A \lambda = 0 \qquad \ldots\ldots \text{(3-11)}$$

in which we make the substitution:

$$A = - \frac{\partial F}{\partial k} dk \frac{1}{\lambda} \qquad \ldots\ldots \text{(3-12)}$$

Premultiplying both sides of Eq (3-10) by $\{ \partial F/\partial \sigma \}^T [D]$ and eliminating $\{ \partial F/\partial \sigma \}^T \{ d\sigma \}$ using Eq (3-11) we obtain the plastic multiplier λ to be :

$$\lambda = \frac{\left[\dfrac{\partial F}{\partial \sigma} \right]^T [D] \{ d\epsilon \}}{\left[\dfrac{\partial F}{\partial \sigma} \right]^T [D] \left[\dfrac{\partial Q}{\partial \sigma} \right]} \qquad \ldots\ldots \text{(3-13)}$$

and substituting for λ from (3–13) into (3–10) gives

$$[d\sigma] = [D] - \frac{[D]\left\{\frac{\partial Q}{\partial \sigma}\right\}\left\{\frac{\partial F}{\partial \sigma}\right\}^T[D]}{A + \left\{\frac{\partial F}{\partial \sigma}\right\}^T[D]\left\{\frac{\partial Q}{\partial \sigma}\right\}} \{ d\epsilon \}$$

or $\qquad [d\sigma] = [D_{ep}] \{ d\epsilon \}$ .... (3–14)

where $[D_{ep}]$ is the incremental elasto–plastic constitutive matrix.

Although the assumptions regarding loading function and normality rule need further experimental confirmation, the appeal of this formulation to concrete is due to the fact that it extends to concrete a well established mathematical theory.

The theory of plasticity with an associated flow rule ($F = Q$) has been used extensively in early studies to describe the behaviour of concrete. Cervenka and Gerstle 1972 used Von Mises criterion to study reinforced concrete panels; Suidan and Shnobrish 1973 used the same criterion for beams; Hand et al. 1973 for plates and shells.

In the field of concrete research as related to the theory of plasticity, attempts have been made to alter some of the classical failure theories such as Von Mises in order to overcome some disadvantages or otherwise improve their agreement with the observed behaviour of concrete. New failure theories were therefore developed with specific application to concrete such as the Buyukozturk 1977 generalized Mohr Coulomb theory based on the biaxial experimental data of Kupfer et al 1969 and Liu et al 1972(a). However, the need for a non– associated flow rule ($F \neq Q$), ie formulation of the plastic potential function Q, has been demonstrated by Vermeer and de Borst 1984. Therefore, the application of non– associated flow rule has been introduced by Han and Chen 1986, Hu and

Schnobrish 1989 which has succeeded in controling the major deviations observed in the volumetric strains using the associated flow rule, however much more computational effort is required.

3–3–3 PLASTIC– FRACTURING MODELS :

In a recent study Andenaes et al. 1977 on the post– fracture behaviour of concrete under biaxial compression has indicated that the normality flow rule used for plastic flow of concrete is not strictly observed in the case of fractured concrete. This has led to constitutive models based on the plastic– fracturing theory. In contrast to plastic phenomena characterized in terms of loading surfaces that depend on stresses, $\{ \sigma \}$, the fracturing phenomena are better described in terms of loading surfaces that depend on strains, $\{ \epsilon \}$, rather than stresses, $\{ \sigma \}$ Thus, the plastic– fracturing theory requires two loading surfaces, Bazant and Kim 1979 :

$$F \ (\ \{ \ \sigma \ \}, \ H \ ) = 0$$
$$\Phi \ (\ \{ \ \epsilon \ \}, \ H') = 0 \qquad \ldots\ldots\ldots\ldots (3–15)$$

where, H and H', are some hardening and fracturing parameters, respectively. The functions F and Φ are chosen to depend only on the first and second invariants and take into account both plastic and fracturing deformations. In this theory the incremental stress– strain relations take the form :

$$\{ d\sigma \} = [\ D \ ] \ \{ d\epsilon \} \qquad \ldots\ldots\ldots (3–16)$$

where

$$[\ D \ ] = [\ D^{el}] - [\ D^{pl}] - [\ D^{fr}] \qquad \ldots\ldots\ldots (3–17)$$

in which, $[\ D^{el}]$ is the elastic stiffness matrix, and $[\ D^{pl}]$ and $[\ D^{fr}]$, introduce

the decrease of the stiffness [D] due to plastic strain increments and fracturing stress decrements respectively. [D] is the concrete material stiffness, non symmetric and generally not orthotropic.

The theory combines plastic strain increments and fracturing stress decrements, which reflect micro—cracking and accounts for internal friction, inelastic dilatancy due to microcracking, strain softening, degradation of elastic moduli, etc. The model requires six inelastic material parameters obtained by Bazant and Kim by computer analysis and fitting a large set of various types of test data for concrete as available in the literature. Inelastic analysis of reinforced concrete shear walls using the plastic—fracturing theory proposed by Bazant and Kim 1979 has been verified by Hiroshi and Setsuro 1985. Analytical predictions were in good agreement with experimental results, but under repeated reversal loading the analytical hysteresis loops were smaller than the experimental ones.

3— 3— 4 ENDOCHRONIC BASED MODELS :

All the models considered so far, elasticty, plasticity and plastic—fracturing are incrementally linear. The endochronic based models are incrementally nonlinear and the material behaviour is defined in terms of several internal states parameters. The central key in the endochronic theory is that the stress state is considered to be function of the strain rate and the strain history, defined with respect to an internal time measure, which is an internal state variable of the material. This intrinsic time is a non—decreasing scalar variable used to measure the extent of the irreversible damage of the internal structure of the concrete material when subjected to deformation histories. The most extensive developments along these lines for concrete, have been carried out by Bazant and Bhat 1976 who extended the theory, originally developed for metals by Valanis 1971, to concrete. This extension comprises several important nonlinear effects expressed analytically with

an extension set of functions which fit experimentally observed behaviour of plain concrete; inelastic volume dilatancy, strain softening range, strain rate effects, etc. Further refinements of the theory were devised by Bazant 1978 and Bazant and Shieh 1980. It should be mentioned, that this increase of scope is achieved at the expense of greater complexity and a large number of material parameters. This formulation with some adapatations was applied by Al— Manaseer 1983 to predict the nonlinear behaviour of beams. In general this type of formulation appears to have remarkable potential for special practical applications. However, further research is needed particularly in order to simplify and reduce the number of material constants without sacrifying accuracy.

3— 4 CRACKED CONCRETE MODELS:

In contrast to the observed ductility of concrete under biaxial compression states, concrete is a highly brittle material in biaxial tension in which a cracking type of failure occurs in the early stages of loading long before either concrete or steel start yielding. Consequently, the formation of cracks is undoubtedly one of the most important nonlinear phenomena which govern the behaviour of concrete. Consequently, any numerical procedure which is used for the analysis of concrete structures should embody a sound numerical approach which models the formation, closing and re— opening of cracks, and post— cracking phenomena.

In the following the crack formation model along with the subsequent post— cracking phenonmena used in this study are described.

In the finite element analysis of concrete structures, three different approaches have been employed for crack modelling:

      (1) Discrete cracking models.

      (2) Smeared cracking models.

      (3) Fracture cracking models.

Depending on the purpose of analysis a particular cracking model may be selected from these alternatives.

3-4-1 Discrete cracking models :

The discrete cracking model which is the earliest finite element model of reinforced concrete to include the effect of cracking, was introduced by Ngo and Scordelis 1967 when analysing beams with predefined located cracks. Nilson 1968 modified this approach to allow the finite element model to generate the location of cracks. With this reperesentation adjacent elements are disconnected by separation of common nodal points when the average stress exceeds the tensile strength of concrete, Fig (3-7a). Further improvements were due to Al-Mahaidi 1979 who refined the method of representing cracks by defining either two or four nodes at a single point tied together by stiff linkage elements until cracking occurs in one or two directions respectively, Fig (3-7b). The approach suffers from two drawbacks. First, it implies a continuous change in nodal connectivity, which does not fit the nature of the finite element method which works in terms of unknown displacements. Secondly, the crack is constrained to follow a predefined path along the element edges. The drawbacks are considered to be serious and attempts to eliminate them have been reported. Prominent among these are the introduction of graphics-aided algorithms of automatic mesh redefinition by Ingraffea and Saouma 1985 and techniques which permit discrete cracks to extend through finite elements , Blauwendraad 1985, so that cracks are no longer forced to align with the original interelement boundaries. The lack of generality in possible crack direction and the continuously changing topology of the finite element mesh, seem to limit the scope of this concept to very special research applications.

3— 4— 2 Smeared cracking model :

In the smeared crack system, first introduced by Rashid 1968, the cracked concrete is asumed to remain a continuum and implies an infinite number of parallel fissures across that part of the cracked finite element Fig (3— 8). The formation of cracks is simulated more easily by representing cracked concrete as an orthotropic material and phenomena which act subsequent to cracking such as aggregate interlock, dowel action and tension stiffening can be appropriately simulated. However, the smeared crack strategy has not escaped criticism, the prime objection voiced against it be: ʒ that it would tend to spread crack formation over the entire structure so that it would be incapable of predicting major dominant shear cracks as local fracture. The arguments change when we consider distributed fracture. Examples are the diffuse crack patterns in large scale shear walls or panels due to the presence of densely distributed reinforcement. Such cases provide a true physical basis for smeared concepts, since the scale of the representative continuum is very large compared to the crack spacing. With increased activity in concrete modelling by finite elements, questions were raised regarding the correctness of the simple concrete smeared crack models. The major point that was raised related to the dependance of the solution to the grid size used. In fact Bazant and Cedolin 1979 had expressed a concern that solutions using this technique would not converge with grid refinement if only a limiting tensile strength criterion is used to estabilish crack formation. They recommended a criterion based on the critical strain energy release rate. A modification of the strength based criterion, wherein strain softening is considered and its modulus is adjusted with respect to the element size, was found to yield mesh independent results, Rots et al. 1985. This led to the incorporation of the fracture mechanics concepts and significant strides have been made by several investigators.

Smeared crack concepts can be categorized into fixed and rotating smeared crack models. With a fixed concept, the crack direction is fixed during the entire computational process with double orthogonal cracks, Grayson and Stevens 1979, or non-orthogonal multi-directional cracks, De Borst and Nauta 1985. However, it has been demonstrated experimentally, Vecchio and Collins 1982, that crack directions may change throughout loading especially for panels not equally reinforced or for those panels with skew reinforcement. Research efforts have resulted in several constitutive relationships accounting for the variation of crack directions, Cope et al. 1980, Gupta and Akbar 1984,1985, Milford and Schnobrich 1984, and Crisfield and Wills 1989. An excellent overview of these different crack concepts has been produced by Rots and Blauwendraad 1989.

3-4-3 Fracture mechanics :

The fracture mechanics model is an area which is being very actively studied in solving various types of cracking problems in metals and ceramics. In its current state of development, the practical applicability of fracture mechanics to reinforced concrete materials is still under active investigation by several researchers, Bazant and Cedolin 1980.

In this study the smeared crack concept is used to model the crack formation. It is assumed that the response of concrete under tensile stress is assumed to be linear elastic behaviour until the fracture surface is reached.
Both the maximum principal stress and maximum principal strain failure criteria have been commonly used to predict the stress or strain levels at which concrete tensile cracking occurs. Phillips 1972 considered both criteria and found that the maximum principal stress failure criterion gave the better correlation with test results and that the strain criterion can produce stiffer predictions. Consequently, in

this study, the maximum principal tensile stress failure criterion is used to predict tensile crack development.

3— 5 PRESENT MODEL FOR CONCRETE :

The use of the theory of plasticity with a yield function and its flow rule to derive the elesto— plastic constitutive relationship for concrete rests primarily on the assumption that concrete undergoes plastic yielding in a similar manner to that of ductile metals. The nonlinear stress— strain response of concrete is due mainly to cracking and bond failure between the aggregate and mortar. The cumulative effects of these brittle failures is the main factor causing nonlinearities. This behaviour is certainly different from that of ductile metals, the yielding of which is caused by actual plastic flow.

The endochronic theory and the plastic— fracturing theory are certainly more accurate but require several material parameters and extensive computational effort. The use of such models for analysis of large structural systems, such as coupled shear walls, is not recommended from an efficient computing effort viewpoint. However, an international competition putting into practice these different theories has been organised by Collins and Vecchio 1985. It has been found that there is no correlation between the complexity of the analytical models and the accuracy of the resulting predictions. Very simple models can produce predictions that are just as good or just as bad as those arrived at by very complex models, such as the endochronic theory.

The model used in this study is computationally simple but capable of simulating the dominant nonlinear behaviour of reinforced concrete. The assumptions adopted in the model are based on the experimental phenomenological observations and include the simulation of tensile cracking and post— cracking phenomena such as friction at crack interfaces, dowel action in bars crossing

cracks, tension stiffening due to bond, nonlinear multiaxial compression behaviour of concrete and yielding of reinforcement.

3-5-1 CONCRETE IN COMPRESSION :

Under biaxial compression state of stress, concrete can be either elastic, non-elastic or crushed. No experimental test is available to accurately define these states and therefore, assumptions have to be made.

In this study the experimental results of Kupfer et al. 1969 shown in Fig (3-6) are modified as shown in Fig (3-9). An initial elasticity-limit loading surface is assumed by scaling the ultimate failure envelope so that two zones, elastic and non-elastic, are defined, Fig (3-9). Concrete is assumed to be elastic isotropic if the state of stress $\{ \sigma \}$ is on or below the initial elasticity limit loading surface defined by:

$$(\sigma_1/kf_c' + \sigma_2/kf_c')^2 + \sigma_1/kf_c' + 3.65 \, \sigma_2/kf_c' \leqslant 0 \qquad \ldots\ldots \text{(3-18)}$$

where $k < 1$ is the scaling factor of the ultimate surface ($k = 0.3$ is adopted). Concrete is assumed to be inelastic if the condition above is not satisfied, and an orthotropic biaxial model is used. Test data from experimentally loaded biaxial specimens appear to support the use of orthotropic material models. Support for this supposition is found in the experimental results of Kupfer et al. 1973 as reported by Link 1976. From comparison of Young moduli, E_1 and E_2 and Poisson's ratios ν_1 and ν_2, in the principal directions, Link concluded that there was noteworthy effects of stress related anisotropy in the compression-compression states for strains beyond 80% of the breaking strain. However, in compression-tension stress states he concluded that stress related anisotropy is significant. This finding has been confirmed by Maekawa and Okamura 1983, who

have reported results of a carefully conducted and detailed study of biaxially loaded concrete in the compression— tension zones.

The material stiffness matrix that relates the strain vector $\{ \epsilon \}$ to any biaxial offending compressive stress $\{ \sigma \}$, is altered according to the state of the material, elastic, non— elastic or crushed as described below.

3— 5— 1— 1 Elastic concrete :

Prior to nonlinear behaviour or crushing, concrete is assumed to be elastic, homogeneous and isotropic material, and the stresses and strains relate in the following manner if Eq. (3— 18) is fulfilled:

$$
\begin{bmatrix} \sigma_x \\ \sigma_y \\ \tau_{xy} \end{bmatrix} = \frac{E_c}{(1-\nu^2)} \begin{bmatrix} 1 & \nu & 0 \\ \nu & 1 & 0 \\ 0 & 0 & (1-\nu)/2 \end{bmatrix} \begin{bmatrix} \epsilon_x \\ \epsilon_y \\ \gamma_{xy} \end{bmatrix} \qquad \ldots \ldots (3\text{-}19)
$$

This can be written in the principal stress directions as:

$$
\sigma = \frac{E_c \ \epsilon}{1 - \nu \alpha} \qquad \ldots \ldots (3\text{-}20)
$$

which expresses the stress, σ, in one of the principal directions considered, in terms of the corresponding strain ϵ in the same direction, and the principal stress ratio α taking into account the biaxial confinement effects. These parameters are defined as:

E_c The initial uniaxial modulus of elasticity.

α The stress ratio between the stress in the perpendicular direction to that in the direction considered.

ν Poisson's ratio of concrete.

3- 5- 1- 2 Inelastic concrete :

Prior to crushing, nonlinear behaviour of concrete is assumed to occur if the state of stress is above the initial elasticity limit surface but below or on the ultimate failure envelope. This is expressed as:

$$(\sigma_1/kf_c' + \sigma_2/kf_c')^2 + \sigma_1/kf_c' + 3.65\ \sigma_2/kf_c' > 0$$
$$(\sigma_1/f_c' + \sigma_2/f_c')^2 + \sigma_1/f_c' + 3.65\ \sigma_2/f_c' \leqslant 0 \qquad \ldots\ldots(3-21)$$

The concrete is then assumed to be orthotropic with the axes of orthotropy coinciding with the principal stress directions.

To account for the nonlinear stress- strain relationship of concrete in the principal stress directions, Eq. (3- 20) for elastic concrete is modified as proposed by Saenz 1964 but accounting for biaxial compression effects in a similar manner to that proposed by Liu et al. 1972b in the form:

$$\sigma = \frac{A + B\ E_c\ \epsilon}{(1-\nu\alpha)(1 + C\ \epsilon + D\ \epsilon^2)} \qquad \ldots\ldots\ldots\ldots (3-22)$$

in which A, B, C and D are parameters which depend upon the shape of the stress- strain curve. Fundamentally, an expression describing the stress- strain relationship for concrete must fulfill the following conditions:

(a) At the initiation of loading, that is for no strain, the stress must be equal to zero and the initial slope defines the initial modulus of elasticity. This can be expressed as follows:

$$\sigma = 0\ ;\ d\sigma/d\epsilon = E_c/(1-\nu\alpha) \qquad \text{at } \epsilon = 0 \qquad \ldots(3-23)$$

(b) When the concrete reaches its peak stress σ_p the strain at this point is ϵ_p and the stress—strain curve becomes horizontal ie:

$$\sigma = \sigma_p \ ; \ d\sigma/d\epsilon = 0 \quad \text{at } \epsilon = \epsilon_p \qquad \cdots\cdots\cdots (3-24)$$

Applying the boundary conditions (3—23) and (3—24) provide four conditions to define the unknown parameters A, B, C and D of Eq. (3—22) which are then uniquely defined as:

$$A = 0$$

$$B = 1$$

$$C = E_c/[\ \sigma_p(1-\nu\alpha) \ ] - 2/\epsilon_p$$

$$D = 1/\epsilon_p^2$$

Re—introducing these constants to Eq. (3—22), then it becomes:

$$\sigma = \cfrac{E_c \ \epsilon}{(1-\nu\alpha)\left[1+\left(\cfrac{1}{1-\nu\alpha} \ \cfrac{E}{E_s} - 2\right)\left(\cfrac{\epsilon}{\epsilon_p}\right) + \left(\cfrac{\epsilon}{\epsilon_p}\right)^2\right]} \qquad \cdots\cdots\cdots (3-25)$$

where E_s is the secant modulus of elasticity at peak stress, ie $E_s = \sigma_p/\epsilon_p$. Using Eq. (3—25), the material stiffness in each principal direction is evaluated solely by the principal strain ϵ in the same direction and the principal stress ratio α accounting for biaxial effects. If the principal axes of orthotropy are assumed to coincide with the principal stress directions, the incremental stress—strain relationships take the form:

$$\begin{Bmatrix} d\sigma_1 \\ d\sigma_2 \\ d\tau_{12} \end{Bmatrix} = \frac{1}{(1-\nu_1\nu_2)} \begin{bmatrix} E_1 & \nu_2 E_1 & 0 \\ \nu_1 E_2 & E_2 & 0 \\ 0 & 0 & (1-\nu_1\nu_2)G \end{bmatrix} \begin{Bmatrix} d\epsilon_1 \\ d\epsilon_2 \\ d\gamma_{12} \end{Bmatrix} \quad \ldots \ldots \quad (3\text{-}26)$$

where $\nu_1 E_2 = \nu_2 E_1$ and subscripts 1 and 2 denote the current principal stress axes. The material moduli E_1, E_2, G, ν_1 and ν_2 are stress and strain dependant. In this study two modifications to Eq. (3–26) are now made. First, a more convenient expression results if an equivalent Poisson's ratio, ν, is defined as:

$$\nu^2 = \nu_1 \nu_2 \qquad \ldots \ldots \ldots \quad (3\text{-}27)$$

Second, since no information is available on shear modulus G, the assumption is made that it is independant of axis orientation, Darwin and Pecknold 1977. This leads to the relation:

$$(1-\nu^2)\, G = 1/4\, (E_1 + E_2 - 2\nu\sqrt{E_1 E_2}) \qquad \ldots \ldots \ldots \quad (3\text{-}28)$$

Equation (3–26) then takes the form:

$$\begin{Bmatrix} d\sigma_1 \\ d\sigma_2 \\ d\tau_{12} \end{Bmatrix} = \frac{1}{(1-\nu^2)} \begin{bmatrix} E_1 & \nu\sqrt{E_1 E_2} & 0 \\ \nu\sqrt{E_1 E_2} & E_2 & 0 \\ 0 & 0 & 1/4(E_1+E_2-2\nu\sqrt{E_1 E_2}) \end{bmatrix} \begin{Bmatrix} d\epsilon_1 \\ d\epsilon_2 \\ d\gamma_{12} \end{Bmatrix} \quad (3\text{-}29)$$

The determination of the load dependant properties E_1, E_2, ν occuring in Eq. (3–29), which completely characterize the stress–strain law, is now described.

The values of Young's moduli E_1 and E_2 for a given principal stress ratio are found as the slopes of the stress–strain curve given by Eq. (3–25) which is valid up to the peak strain ϵ_p. Beyond this peak secant Young's moduli are used, ie:

$$E_i = d\sigma/d\epsilon \qquad \epsilon \leqslant \epsilon_p$$

$$E_i = \sigma_p/\epsilon \qquad \epsilon_u \geqslant \epsilon > \epsilon_p \qquad\qquad \ldots\ldots\ldots (3\text{-}30)$$

where ϵ_u is the ultimate strain. It may be noted that little is known regarding the shape of the descending branch of the stress—strain curve in biaxial states of stress. The descending branch is particularly dependant upon the rate of straining and the technique of loading, Tasuji et al. 1978,1979.

In several simple experimental tests reported in CEB 1983b, it has been observed that the ratios of lateral strain to principal compressive strain remains constant until approximately 80% of the maximum compressive stress, f_c', at which stress the apparent Poisson's ratio begins to increase (critical stress in Fig (3—1)). This is confirmed by the experimental observations, Kupfer et al. 1969, which require treating a variable Poisson's ratio, Fig (3.10). This is in agreement with most engineering materials as they become incompressible, $\nu = 0.5$, when approaching failure. A secant value, ν_s, of poisson ratio may be more appropriate to use when the material dilates under compaction.

In this study a variable Poisson's ratio is computed in each principal direction. The analytical model simulating the experimental behaviour Fig (3.10), and similar to that reported by Ottosen 1979, is an ellipse as shown in Fig (3.11):

$$\nu_s = \nu \qquad\qquad \text{for } r = \sigma/f_c' \leqslant r_a$$

$$\ldots\ldots (3\text{-}31)$$

$$\nu_s = \nu_f - (\nu_f - \nu_i)\sqrt{1 - \left(\frac{r - r_a}{1 - r_a}\right)^2} \qquad \text{for } r > r_a$$

in which $\nu_i = 0.2$ is the initial Poisson's ratio, $\nu_f = 0.36$ the secant value of Poisson's ratio at failure, $r_a = 0.8$ and r is the ratio of the actual stress to the corresponding value of that stress at failure $r = \sigma/f_c'$.

Eqs. (3—30) and (3—31) fully define the incremental stress—strain relation (3—29).

In the event where the state of stress violates the ultimate failure envelope the total stresses are brought back to the ultimate failure surface until the crushing type of failure defined below occurs. The procedure is to scale the total stresses by a factor m < 1 so that the stresses m $\{ \sigma \}$ remain on the ultimate surface and the excessive stress $(1 - m)$ $\{ \sigma \}$ is released as residual stresses. This scaling, ensuring the non-violation of the ultimate experimental strength envelope, is chosen because the criterion of crushing is in the strain space, whereas in the stress space the violation of the failure envelope is not assumed as a condition of crushing.

3-5-1-3 Crushed concrete :

Crushing failure is the complete loss of strength of the material in all directions. The lack of available experimental data on concrete ultimate deformation capacity under multiaxial stress states has resulted in the appropriate strain criterion being adopted by simply converting the ultimate failure envelope described in the stress space directly into strains. thus:

$$(\epsilon_1/\epsilon_u + \epsilon_2/\epsilon_u)2 + \epsilon_1/\epsilon_u + 3.65 \ \epsilon_2/\epsilon_u = 0 \qquad \ldots\ldots\ldots\ldots (3-32)$$

where ϵ_1 and ϵ_2 are the total principal strains and ϵ_u is an ultimate total strain extrapolated from uniaxial test results $(\epsilon_u = 0.0035)$.

The crushing type of failure is therefore assumed to be a strain controlled phenomenon. When ϵ_u reaches the value specified as ultimate strain (0.0035), the material is assumed to lose all its characteristics of strength and rigidity in all directions. This is accomplished by simply setting the constitutive material stiffness matrix [D] to a null matrix at any integration point where crushing failure occurs and this will be maintained during all subsequent loading stages.

3—5—2 CONCRETE IN TENSION :

3—5—2—1 Singly cracked concrete :

If the maximum principal tensile stress exceeds the tensile capacity of concrete, cracking will occur along a plane normal to the direction of the offending principal stress, Fig (3—8). Once a crack has formed, it is assumed that tensile stresses cannot be supported across the crack and the stiffness of the material is reduced significantly in this direction. However, material parallel to the crack is still capable of carrying stress prevailing parallel to the crack, and some shear force can be transferred along the rough surfaces of a crack. Accordingly the material stiffness of concrete now takes the form:

$$[\ D']_{cr} = \begin{bmatrix} E_c & 0 & 0 \\ 0 & 0 & 0 \\ 0 & 0 & \beta G \end{bmatrix} \qquad \ldots\ldots\ldots (3\text{-}33)$$

where the modulus of elasticity E_c is set to zero in the principal direction normal to the crack. Further a reduced shear modulus $\beta G < G$ is assumed on the cracked plane to account for aggregate interlock and dowel action. Since cracks form at different angles, the material stiffness matrix $[\ D']_{cr}$ expressed in the local coordinates system (n,t) is transformed to the global coordinates system (x,y). If the angle between the crack direction and the global x—axis is θ_{cr}, then the local material stiffness $[\ D']_{cr}$ is transformed to the global coordinate system as:

$$[\ D\ ]_{cr} = [\ T\ ]^T [\ D']_{cr} [\ T\ ] \qquad \ldots\ldots\ldots (3\text{-}34)$$

where the standard strain transformation matrix $[\ T\ ]$ is:

$$[T] = \begin{bmatrix} C^2 & S^2 & CS \\ S^2 & C^2 & -CS \\ -2CS & 2CS & C^2 - S^2 \end{bmatrix} \qquad \dots\dots\dots \quad (3\text{-}35)$$

where $C = \cos \theta_{cr}$, $S = \sin \theta_{cr}$ and θ_{cr} the orientation of the crack given by:

$$\text{Tan } 2\theta_{cr} = 2\tau_{xy}/(\sigma_x - \sigma_y)$$

however, the angle θ_{cr} given by the equation above will lie between $-45°$ and $+45°$. The actual crack direction is determined from a Mohr's circle.

3-5-2-2 Doubly cracked concrete :

The presence of shear stresses along the current first crack at the moment of its formation will cause subsequent cracking and effectively produce changes in the crack orientation. In fact, retaining a reduced shear retention factor $\beta => \tau_{xy} \neq 0$ implies that the primary crack directions do not coincide with the principal plane and consequently the second cracks may not be necessarily orthogonal to the previous crack. This has been confirmed by experimental results of Vecchio and Collins 1982 where changes in crack orientations has been observed especially for panels not equally reinforced or for those panels with skew reinforcement.

In this study, the direction of the first crack θ_{cr} is fixed in the analysis for further loading and a second crack is allowed to occur in the orthogonal direction when the stress state produces a principal stress which exceeds the tensile strength of concrete. Therefore, two smeared cracks in two orthogonal directions may develop in a previously singly cracked concrete, or previously uncracked concrete if both principal stresses are tensile and exceed the tensile strength of concrete. In this case, the material stiffness matrix is given by:

$$[\ D'\ ]_{cr}\ =\ \begin{bmatrix} 0 & 0 & 0 \\ 0 & 0 & 0 \\ 0 & 0 & \beta'G \end{bmatrix} \qquad \ldots \ldots \ (3\text{-}36)$$

where $\beta'= 0.5\beta$ is the shear retention factor for doubly cracked points, assumed to be half the shear retention for singly cracked gauss points.

3-5-3 TENSION STIFFENING :

As the concrete reaches its tensile strength, primary cracks form. At the primary cracks, the concrete stress drops to zero and steel carries the full load as indicated diagramatically in Fig (3-12). However, between cracks, load is shared between steel and concrete due mainly to bond. The ability of intact concrete between each pair of adjacent tensile cracks to assist tensile steel in carrying the total internal tensile load is called tension stiffening. The stiffening is the additional contribution of cracked concrete to the overall stiffness of the system. This partial tensile strength or tension stiffening will decrease gradually as more cracks develop and breakdown of the bond between steel and concrete occurs.

Early investigators assumed that crack formation was a brittle and instantaneous process and tension stiffening was neglected, inducing large tensile stresses released from the cracked zones. Usually, a large number of equilibrium iterations is needed to redistribute the sudden release of the tensile crack stresses. The use of tension stiffening is not only more realistic, but tensile forces released from cracked zones are gradually redistributed into the structure.

Currently, the tension stiffening can be modelled in two ways. In one case, the tension portion of the concrete stress-strain curve has been given a descending branch beyond the cracking point as introduced by Scanlon and Murray 1974 and Lin and Scordelis 1975. The second method is an increase in the steel stiffness to

account for concrete adhering to the bar, Gilbert and Warner 1978. Currently, the descending branch is the most commonly used and can take various forms, Fig(3—13), as adopted by various investigators, Cope and Edwards 1985.

Tension softening which many researchers are now investigating is different than tension stiffening even if it manifests itself as a softening phenomenon. Tension softening is a local material softening observed during strain controlled experiments and is a property of plain concrete. Tension stiffening is a global property of reinforced concrete. It is a consequence of the presence of steel within concrete and the fact that average material properties are used over a finite domain to estabilish the stiffness characteristics of that domain. The tension softening of concrete and the tension stiffening of intact concrete between cracks have been superimposed by Balakrishnan and Murray 1988a to obtain an average homogenized tensile stress— strain relationship.

A model similar to the one proposed by Cope et al. 1980 and Al—manaseer and Phillips 1987 is used in this study. The model Fig (3—13b) assumes that:

$$\sigma = \frac{\alpha_2 \, f_t{}' \, (\alpha_1 - \dfrac{\epsilon}{\epsilon_{cr}})}{\alpha_1 - 1} \qquad \text{for} \quad \alpha_1 \epsilon_{cr} > \epsilon \geqslant \epsilon_{cr}$$

$$.... \quad (3-36)$$

$$\sigma = 0 \qquad \text{for} \; \epsilon \geqslant \alpha_1 \epsilon_{cr}$$

where $f_t{}'$ is the tensile strength of concrete, ϵ_{cr} the cracking strain. ϵ, σ, strain and stress normal to the crack direction, and α_1, α_2 are quasi—material model constants. In this model, the initial crack opening is accompanied by a sudden partial release of the stress components normal to the crack, after which, stress is released linearly with increasing tensile strain, until strain $\epsilon = \alpha_1 \, \epsilon_{cr}$ is reached, at which point it is assumed that total bond failure has occured and there can be

no tensile stress normal to the crack.

Different values of α_1 have been used in the literature; Lin and Scordelis 1975 adopted a value of about 6, Gilbert and Warner 1978 used 10 while Cope et al. 1980 set $\alpha_1 \epsilon_{cr}$ to 1.5 ϵ_u which is equivalent to $\alpha_1 = 20$, ϵ_u being the compressive crushing strain. There is, however little experimental evidence from which definitive values of α_1 can be determined. The precise properties required to accurately simulate tension stiffening are dependant upon crack spacing, reinforcement ratios and interface bond transfer. The state of the art is deficient in determining these properties in a definite manner, Balakrishnan and Murray 1988. It should be noted that because the model contains continuity of displacements between concrete and reinforcing steel, i.e, full bond is assumed and hence the introduction of tension stiffening will cause the steel stresses to be underestimated.

3-5-4 SHEAR ACROSS CRACKS AND SHEAR RETENTION FACTOR :

Aggregate interlock, Fig (3.14a), and dowel action,Fig (3.14b), are the main mechanisms of load transfer along reinforced concrete crack interfaces, Vintzeleou et al. 1986 and Soroushian et al. 1988. The roughness of the crack surface leads to aggregate interlock. Dowel action occurs in steel bars crossing cracks as they tend to counteract the crack width increasing during sliding shear movement, Johnston and Zia 1971.

It is well known that shear stresses transferred across interfaces in concrete, such as crack interfaces, have a significant influence on the behaviour of concrete structures, and many investigations on this subject have been carried out, Hofbeck et al. 1969, Dulaczka 1972, Paulay and Loeber 1974 and Millard and Johnson 1985. Experimental results have shown that aggregate interlock resists more shear than dowel action, because large amounts of slip are required to develop significant dowel action.The mechanism of shear transfer has gradually become clear from

many experimental studies. Based on those experimental studies, various analytical models of shear transfer have been developed, Fardis and Buyukozturk 1979. The final objective of these models seems to determine a constitutive equation which can be implemented in a structural analysis computer program.

To account for shear transfer across the cracks in finite element numerical analysis, the shear retention factor, β , was first introduced by Phillips 1972, Suidan and Shnobrish 1973, Hand et al. 1973 and Yuguzugullu and Schnobrish 1973. This parameter is defined as an assumed numerical factor $0 \leqslant \beta \leqslant 1$ to account for the reduction in shear modulus after the development of a crack. Values greater than zero were found necessary to prevent numerical difficulties. Currently, two main approaches are the most commonly used; the constant shear retention factor method, where β is chosen rather arbitrarily and kept constant, Phillips and Zienkiewicz 1972, Suidan and Shnobrish 1973, Hand et al. 1973, and the variable shear retention factor, where β is assumed to vary as a function of the strain normal to the crack or as a function of the average crack width Cedolin and Deipoli 1977; Al Mahaidi 1979; Agrawal et al. 1981; Cope and Rao 1983; Damjanic 1985 and Cervera et al. 1987, see Fig.(3.15). In reality aggregate shape and size, reinforcement ratio and bar size also influence the shear stiffness. Considering various structures, very little influence on the failure loads was found by Hand et al. 1973 and by Lin and Scordelis 1975 when β was varied between 0.2—1.0 and 0—1.0, respectively. Only a minor influence on deflections and cracking was observed by Yuguzugulu and Shnobrish 1973 when β varies between 0—1.0. On the other hand, Cedolin and Deipoli 1977, analysing a beam failing in shear, observed an extreme sensitivity of the β values on the calculated failure loads. Recently Perdikaris and White 1985 have presented an engineering model for shear transfer based on an extensive experimental study. The measured effective transfer shear modulus in the panels subjected to biaxial tension and monotonic shear remained approximately constant at about 0.05—0.07G (β= 0.05—0.07). It

appears that the shear retention factor, β, is subject to much dispute. In this study, a first simplified approach involves the assumption that the shear stiffness depends only on the crack opening which is determined by the external forces which cause cracking. In connection with a smeared crack representation the fictitious strain normal to the crack , representing the crack width, is used to compute the shear stiffness. Therefore a reduced shear modulus βG is a function of the maximum tensile strain ever reached normal to the crack, which is shown in Fig $(3-15c)$ and defined by

$$
\begin{cases}
\beta = \dfrac{(\beta_1 - \beta_2)}{(\beta_3 - 1)} \left(\beta_3 - \dfrac{\epsilon}{\epsilon_{cr}}\right) + \beta_2 & \text{for } \beta_3 \, \epsilon_{cr} > \epsilon > \epsilon_{cr} \\
\beta = \beta_2 & \text{for } \epsilon > \beta_3 \epsilon_{cr}
\end{cases}
\qquad \ldots\ldots(3\text{-}37)
$$

here β_1, β_2 and β_3 are quasi–material model constants. When β_1 is set equal to β_2, the model reduces to the constant shear retention factor method.

3-6 CONSTITUTIVE MODELLING OF STEEL BARS :

In contrast to concrete behaviour, the behaviour of reinforcing steel bars is comparatively well understood, if not completely, at least under monotonic loading. As steel reinforcement bars are comparatively thin, they are assumed capable of transmitting axial loads only along their direction.

The constitutive model used in this study is based on experimental test results. Typical stress-strain curves for steel bars used in reinforced concrete construction were obtained from steel bars loaded monotonically in tension. The curves exhibit an initial elastic portion, a yield plateau at which the strain increases with little or no increase in stress, a strain hardening range in which strss again increases with strain, and finally a range in which the stress drops off until fracture occurs. Yielding is accompanied by a slight abrupt decrease in stress and the stress-strain diagram has the shape appearing in Fig (3-16). The stresses are referred to as the upper and lower yield strengths. The lower yield strength is usually considered to be the true characteristic of the material and is referred to simply as the yield strength.

The length of the yield plateau is generally a function of the strength of the steel. High strength, high carbon steels have a much shorter yield plateau than lower strength, low carbon steel. In addition, high strength steels have a smaller ductility before fracture than low strength steel.

In finite element analysis, it is necessary to idealize the experimental shape of the stress-strain curve. Fig (3-17) shows four different idealizations in common use for reinforcing steel behaviour. To be used it is necessary to determine experimentally, the stress and the corresponding strain at the onset of yield, the elastic modulus as well as the hardening modulus, and the ultimate strain before fracture.

In the present study, the three first idealizations of Fig (3—17) are incorporated in the finite element program simulating the behaviour of reinforcing steel, these are secant uniaxial stress—strain models, identical in tension and compression :

(a) Elastic—perfectly plastic model Fig (3.17a):

$$0 \leqslant \epsilon_i \leqslant \epsilon_y \quad => \quad E_i = E_s$$
$$\epsilon_u \geqslant \epsilon_i \geqslant \epsilon_y \quad => \quad E_i = E_s \, \epsilon_y / \epsilon_i \qquad \qquad \qquad \ldots\ldots\ldots(3-38)$$
$$\epsilon_i \geqslant \epsilon_u \quad => \quad E_i = 0$$

(b) Bilinear model Fig (3.17b):

$$0 \leqslant \epsilon_i \leqslant \epsilon_y \quad => \quad E_i = E_s$$
$$\epsilon_u \geqslant \epsilon_i \geqslant \epsilon_y \quad => \quad E_i = E_s \, \epsilon_y / \epsilon_i + H \, (\, 1 \, - \, \epsilon_y / \epsilon_i \,) \quad \ldots..(3-39)$$
$$\epsilon_i \geqslant \epsilon_u \quad => \quad E_i = 0$$

(c) Trilinear model Fig (3.17c):

$$0 \leqslant \epsilon_i \leqslant \epsilon_y \quad => \quad E_i = E_s$$
$$\epsilon_0 \geqslant \epsilon_i \geqslant \epsilon_y \quad => \quad E_i = E_s \, \epsilon_y / \epsilon_i \qquad \qquad \qquad \ldots\ldots(3-40)$$
$$\epsilon_u \geqslant \epsilon_i > \epsilon_u \quad => \quad E_i = E_s \, \epsilon_y / \epsilon_i + H \, (\, 1 \, - \, \epsilon_0 / \epsilon_i \,)$$
$$\epsilon_i \geqslant \epsilon_u \quad => \quad E_i = 0$$

The elastic—perfectly plastic model is quite adequate for mild low yield strength steel having large yield plateau. On the other hand, for high yield steel, the strain hardening effect may be important in absence of the yield plateau, in which case the bilinear model is more suitable.

3-7 FINITE ELEMENT REPRESENTATION OF STEEL BARS :

The modelling of reinforcing steel for finite element analysis of reinforced concrete structures has been attempted at least by one of the following three alternative representations

       (a) Discrete representation.

       (b) Embedded representation.

       (c) Smeared representation.

3-7-1 Discrete:
In a discrete representation of the reinforcement the actual bars are replaced by one dimensional finite elements Fig (3.18c). The reinforcing bars may be considered to be pin connected one dimensional members directly attached to the nodes of concrete, Cedolin et al. 1977, Grayson and Stevens 1979. Alternatively, beam elements capable of resisting axial forces, shear and bending, may be used. The use of beam elements, with three degrees of freedom per node, to represent steel depends on the choice of concrete element and may be suitable and necessary in the case of heavy bars for which bending has a significant effect. In either case, linkage elements can be used to represent the steel-concrete interaction accounting for possible relative displacement of the reinforcement relative to the surrounding concrete.

3-7-2 Embedded:
For an embedded representation, Fig (3.18b), a steel bar is considered to be an axial member built into the concrete element so that its displacements are consistent with those of the element, implying perfect bond to be assumed. This representation introduced by Phillips 1973 and Phillips and Zienkiewicz 1976, has been widely used in connection with higher order isoparametric elements.

Balakrishnan and Murray 1987 presented an embedded formulation with bond—slip effects, but extra degrees of freedom in the global stiffness matrix associated with slip between concrete and steel increase the computational cost.

Early embedded reinforcement models, when applied to problems with curved or draped reinforcement impose significant constraints on the selection of the overall mesh, due to the fact that the reinforcement must be aligned with one of the local isoparametric element coordinate axes. More recently, embedded representations that allow a generally oriented and curved embedded reinforcement have been developed Chang et al. 1987, Elwi and Hrudey 1989 and Phillips and Wu 1990. Allwood and Bajarwan 1989 described generally orientated bars with respect to concrete elements including the effects of bond—slip and avoided any additional increase in the number of equations to be solved using an iterative procedure. Phillips and Wu 1990 presented an orientated embedded formulation with bond—slip in a similar approach to Balakrishnan and Murray 1987. However, the extra degrees of freedom associated with bond—slip are condensed out so that there is no increase in the global stiffness matrix.

With these formulations, the geometry of the finite element mesh can be constructed independently of the reinforcement layout. Every bar can be modelled in its correct position and bond—slip between reinforcement and concrete dealt with.

3—7—3 Smeared: For a smeared or distributed representation, Fig (18—a), the steel is assumed to be distributed over the concrete element. The smeared steel is assumed to have unidirectional stiffness corresponding to the direction of its physical layout which can have any particular orientation angle. Again perfect bond must be assumed. Generally, in a shearwall a large number of reinforcing bars are placed. Due to this feature, it is rather difficult to model each reinforcing bar individually and to represent bond by link elements. Consequently, in many cases,

the behaviour of a shearwall is studied using a distributed representation of the reinforcement.

In the present study, the smeared approach for representing steel has been adopted, due primarily to heavy reinforcement for which an embedded or discrete models requires not only a large machine computational effort, but input data for individual bars which is not practical. In addition, the use of discrete bar models dictates the concrete mesh leading very slender (high aspect ratio) concrete elements if the bar spacing is close. Nevertheless, smeared steel representations have been successfully applied to study various structures; beams; Frantzeskakis et al. 1989, slabs   , panels; Agrawal et al. 1981, shells;   Akram— Younis 1988 and shear walls; Santha kumar 1979.

In the present smeared approach used in this study, and referring to Fig(3-18), the stress— strain relations for steel reinforcement in its local directions is:

$$
\begin{Bmatrix} \sigma_x' \\ \sigma_y' \\ \tau_{xy}' \end{Bmatrix} - [D_s'] \begin{Bmatrix} \epsilon_x' \\ \epsilon_y' \\ \gamma_{xy}' \end{Bmatrix} \qquad \dots\dots\dots\dots(3\text{-}41)
$$

where $[D_s]$ is the elasticity matrix of steel and is given by:

$$
[D_s'] = \begin{bmatrix} \rho_x' E_s & 0 & 0 \\ 0 & \rho_y' E_s & 0 \\ 0 & 0 & 0 \end{bmatrix} \qquad \dots\dots\dots (3\text{-}42)
$$

in which ρ_x', ρ_y' are the steel percentages in the local directions x', y' respectively, E_s being the instantaneous modulus of elasticity of steel as updated using the constitutive model presented in section (3— 6). With the steel disposed at

an angle θ_S measured counterclockwise from the x-axis, the local steel stiffness matrix is transformed to the global cartesian space (Oxy) from the local one (Ox'y') using the standard strain transformation matrix, thus:

$$[\ D_s \ ] = [\ T_\epsilon \ ]^T [\ D_s' \ ] [\ T_\epsilon \ ] \qquad \ldots\ldots\ldots (3-43)$$

where, $[\ T_\epsilon \ ]$ is the same standard transformation matrix of Eq(3-35) used for cracks, but with $c = \cos(\theta_S)$, $s = \sin(\theta_S)$ and θ_S being the steel angle.

3-8 CONCRETE STEEL INTERACTION :

The load carrying behaviour of reinforced concrete is influenced by the interaction between plain concrete and the reinforcement. Stress transfer between these two materials in the longitudinal direction of the bars is called bond. The mechanism of bond can be conceived as being comprised of three components: Chemical adhesion, Friction and Mechanical interlock between steel and concrete. The effect of bond becomes evident when cracking of concrete occurs. After cracking, the tensile stresses normal to the crack initially transmitted by concrete, are to a large extent transferred from concrete to reinforcement by bond mechanisms.

If bond slip is to be taken into account, special interface elements must be used for the connection of the reinforcement elements to the concrete elements. three types of bond elements which have been developed will be described briefly below.

The simplest type of these elements is the bond-link element developed by Ngo and Scordelis 1967. The linkage element has no physical dimensions. It connects two nodes with identical coordinates and can be conceptually thought of as two orthogonal springs. A nonlinear bond-slip relationship, obtained from pull out

tests, is assigned to the spring parallel to the bar, and a very high stiffness is given to the spring perpendicular to the bar to prevent separation between the bar and the concrete, Fig(3-19 a).

A second way of modelling bond in finite element calculations is through the employment of contact elements developed by Schaffer 1975. It connects the nodes of a steel element with the nodes of an adjacent concrete element. The contact element has a finite dimension and double nodes, the number of which is such that the order of the contact element should be compatible with the order of the concrete and reinforcement elements, Fig(3-19b).

A third group of bond elements is called bond zone elements differs significantly from the two type of elements desribed previously. This element was developed by De Groot et al. 1981 who made a special approach by combining reinforcement steel and adjacent concrete into a so—called bond zone element with finite thickness. The element stiffness matrix for the bond zone element is described comprehensively by De Groot et al. 1981. A good review of these models has been given by Keuser and Melhorn 1987.

The use of bond elements involves additional effort and is normally used to analyse detail problems such as corbels and end anchorage zones. For the entire structure, complete compatibility is usually assumed, and the effect of bond can be modelled in an indirect way by tension stiffening.

As mentioned in (3—7—3), using a smeared approach representation of steel implies perfect bond between reinforcement and concrete. Assuming a perfect bond the composite material stiffness is

$$[\text{D}] = [\text{D}_c] + [\text{D}_s]$$

The composite material stiffness matrix is used in Eq. (2—30) to compute the element stiffness of a reinforced concrete element. For embedded and discrete formulations the composite stiffness is performed separately.
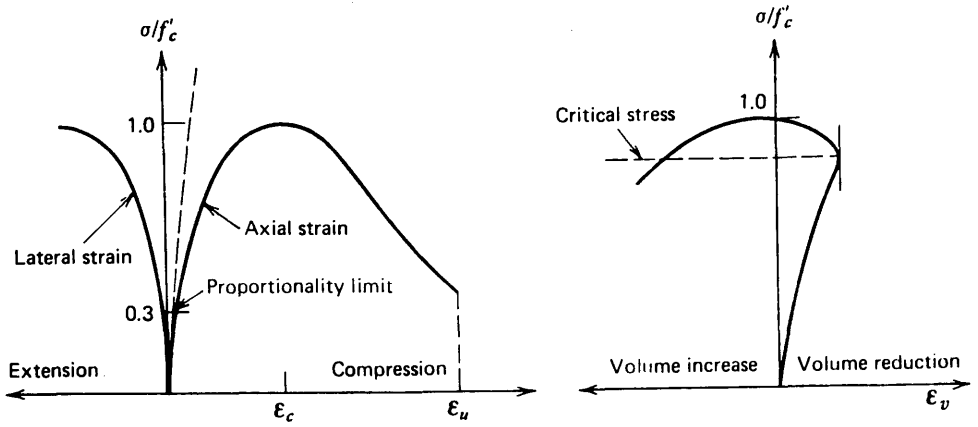
Fig (3−1) UNIAXIAL COMPRESSIVE STRESS/AXIAL,LATERAL AND
VOLUMETRIC STRAIN RELATIONSHIPS.
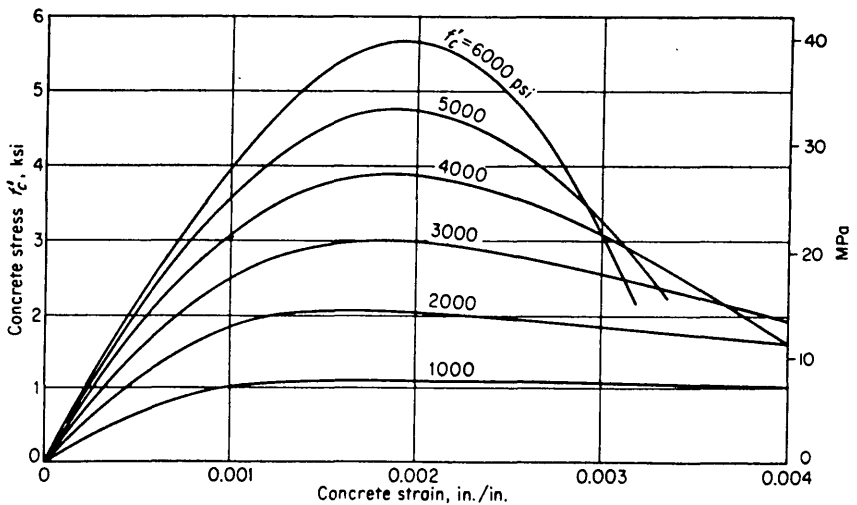
Fig (3-2) TYPICAL CONCRETE STRESS-STRAIN CURVES IN
COMPRESSION.
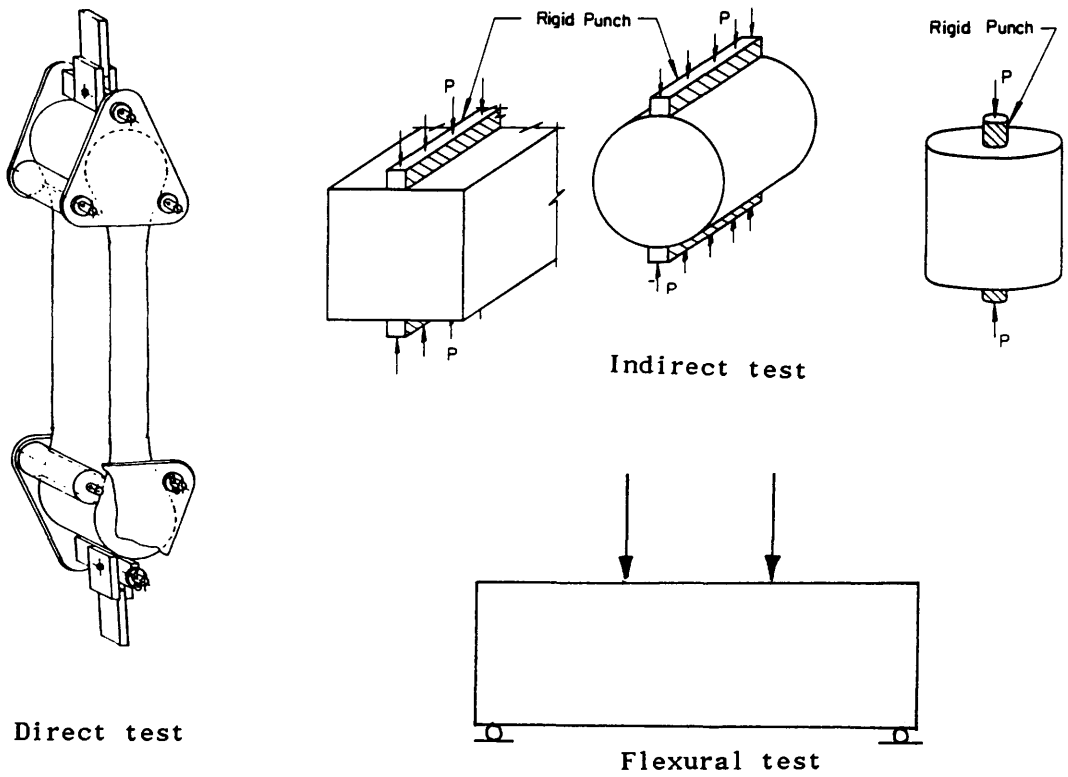
Fig (3-3) DIRECT, INDIRECT AND FLEXURAL TESTS FOR TENSILE STRENGTH.

Curve	Aggregate		Age
No.	Type	Size	(months)
1	Granite	3/8-3/16"	2
2	Gravel	3/8-3/16"	2
3	Gravel	3/16-B.S.7	3
4	Gravel	3/8-3/16"	2
5	Gravel	3/8-3/16"	1
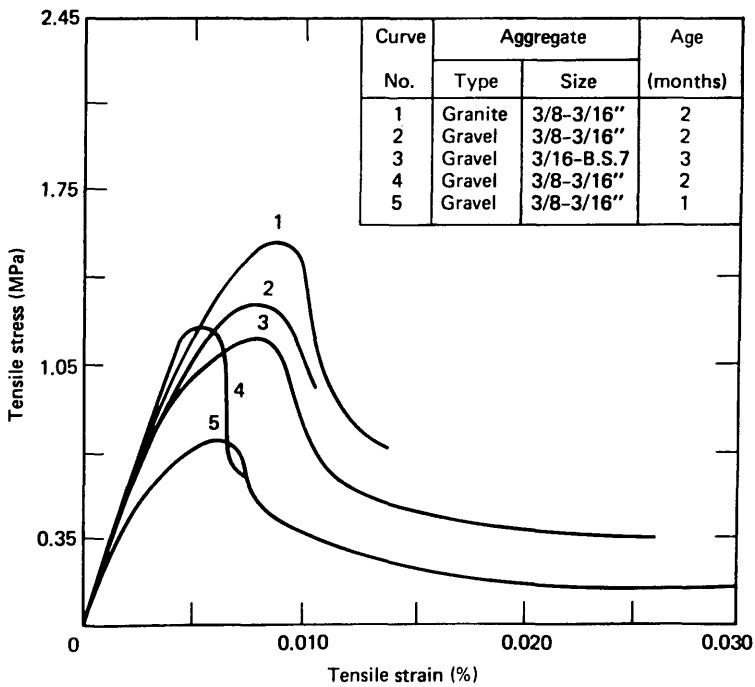
Fig (3-4) TYPICAL TENSILE STRESS-STRAIN CURVES FOR CONCRE
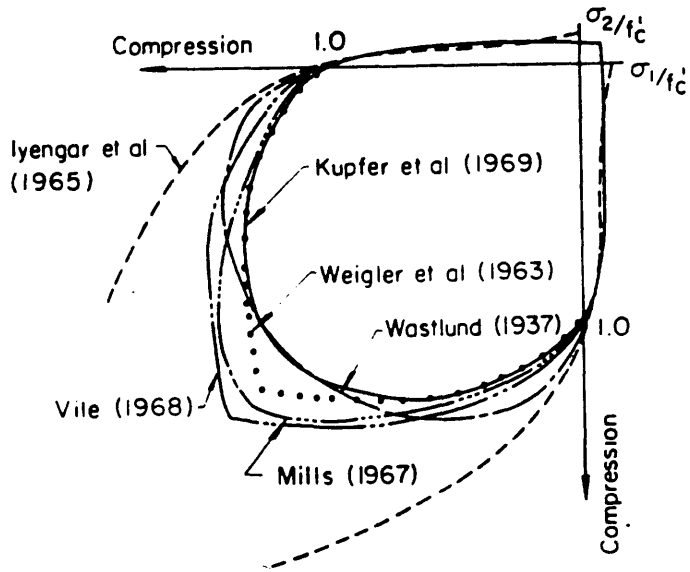
Fig (3-5) BIAXIAL STRENGTH OF CONCRETE.
(Review of previous tests)
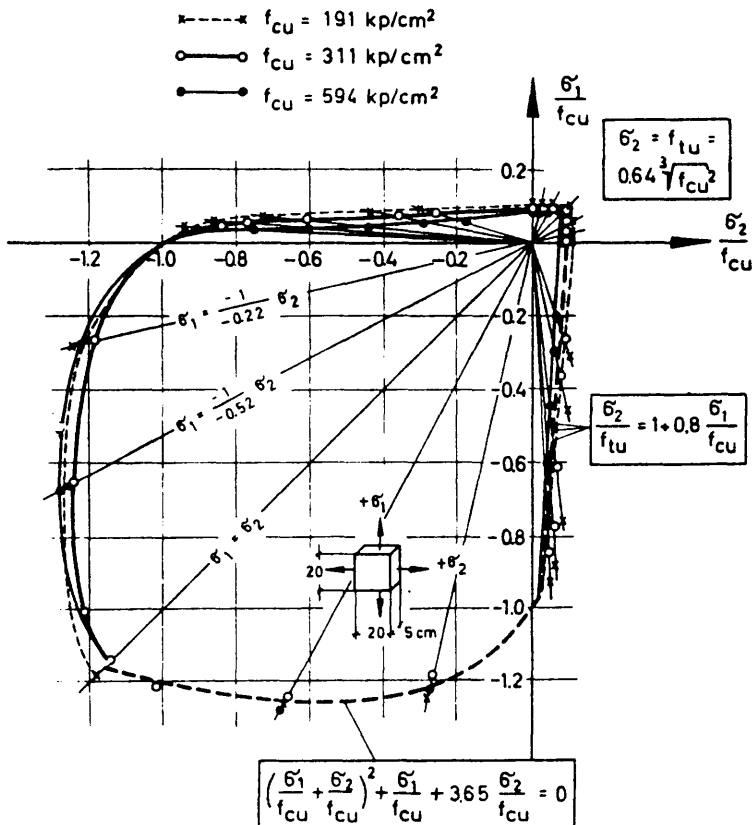
Fig (3-6) BIAXIAL STRENGTH OF CONCRETE USING
BRUSH BEARING PLATENS. (Kupfer et al. 1969)

(a) One-directional Cracking   (b) Two-directional Cracking   (c) Diagonal Cracking
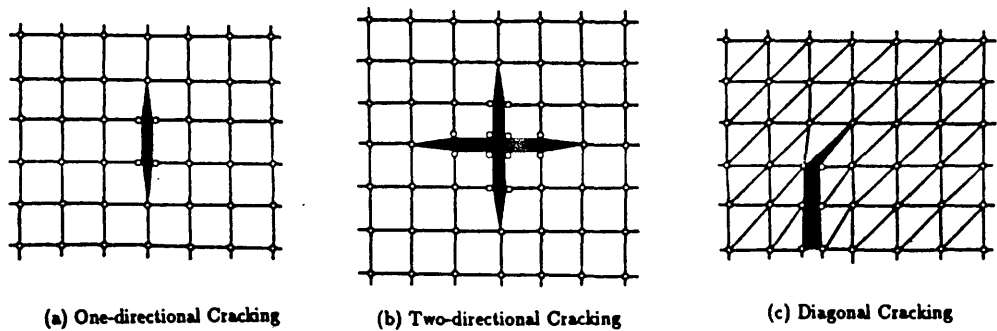
Fig (3-7) DISCRETE CRACKING REPRESENTATIONS.
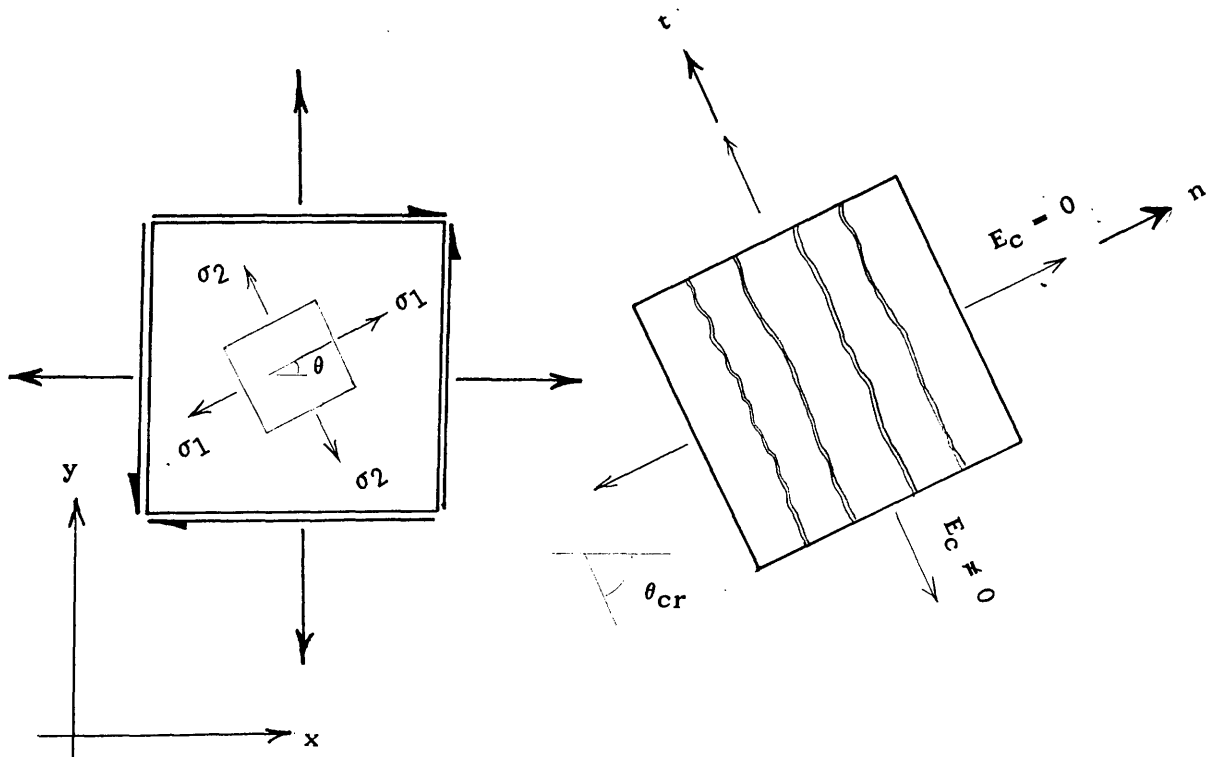
Fig (3-8) SMEARED CRACKING REPRESENTATIONS.

(1) Elastic limit surface

(2) Ultimate surface
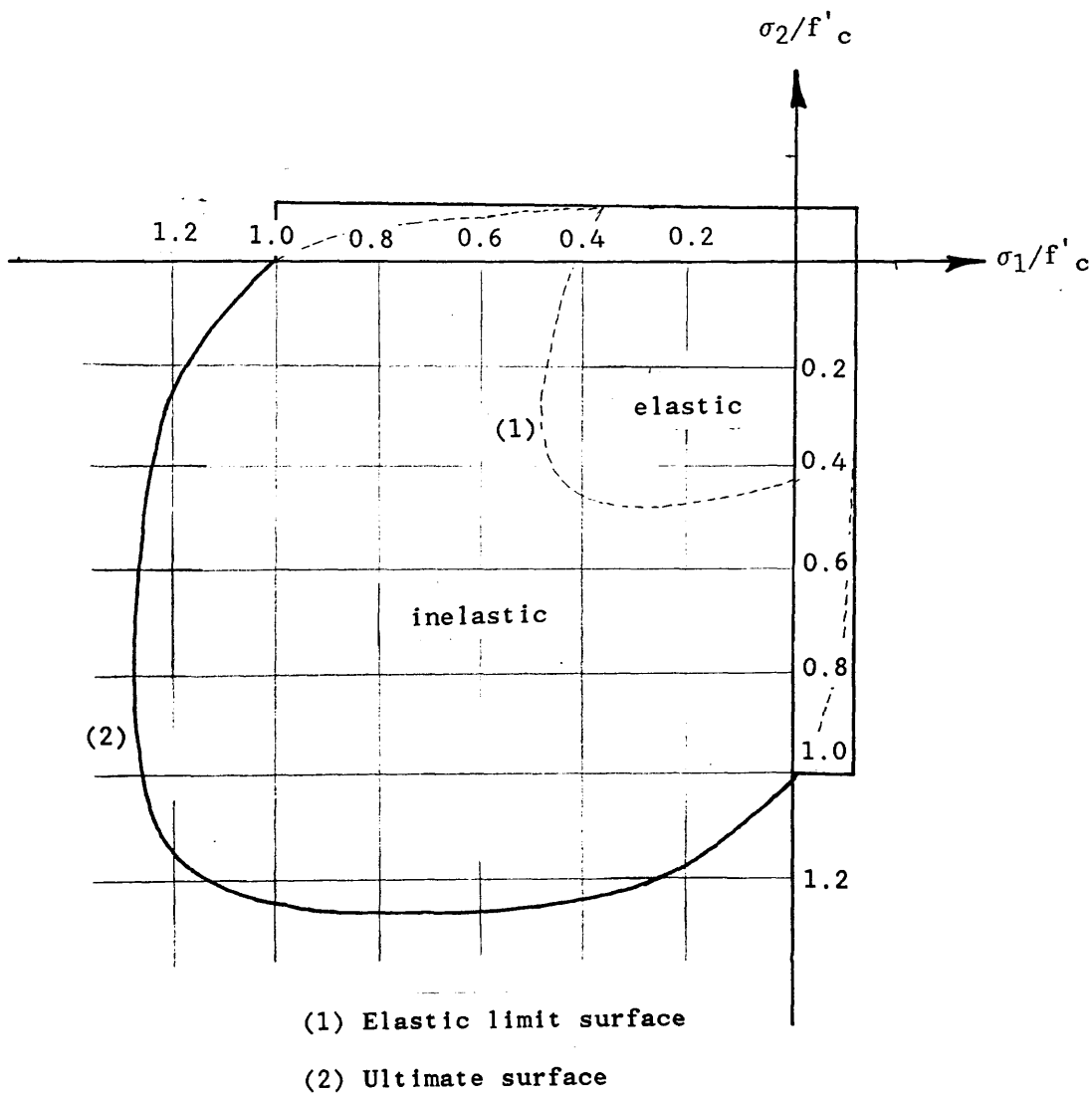
FIG (3-9) ADOPTED BIAXIAL STRENGTH OF CONCRETE
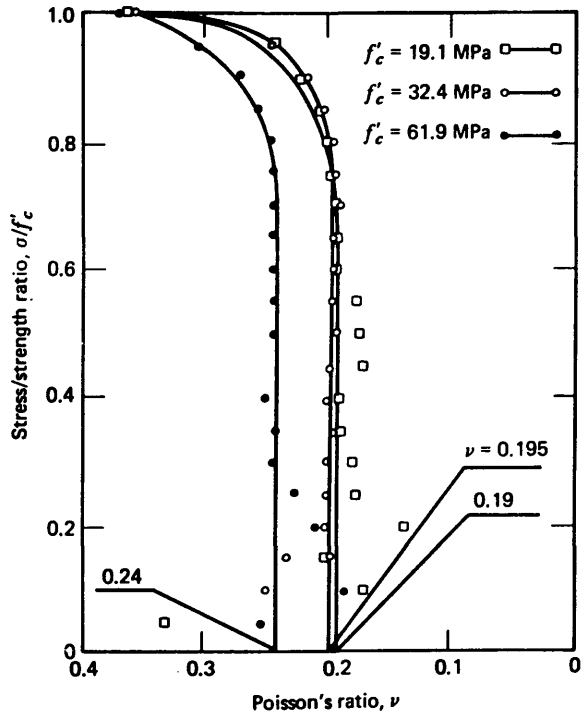
Fig (3-10) RELATION BETWEEN STRESS/STRENGTH RATIO
AND POISSON'S RATIO.
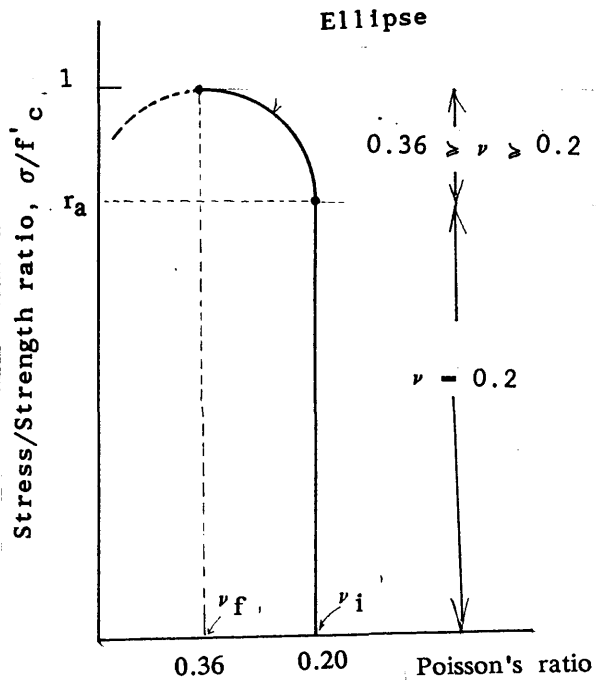
Fig (3-11) ADOPTED VARIATION OF POISSON'S RATIO.
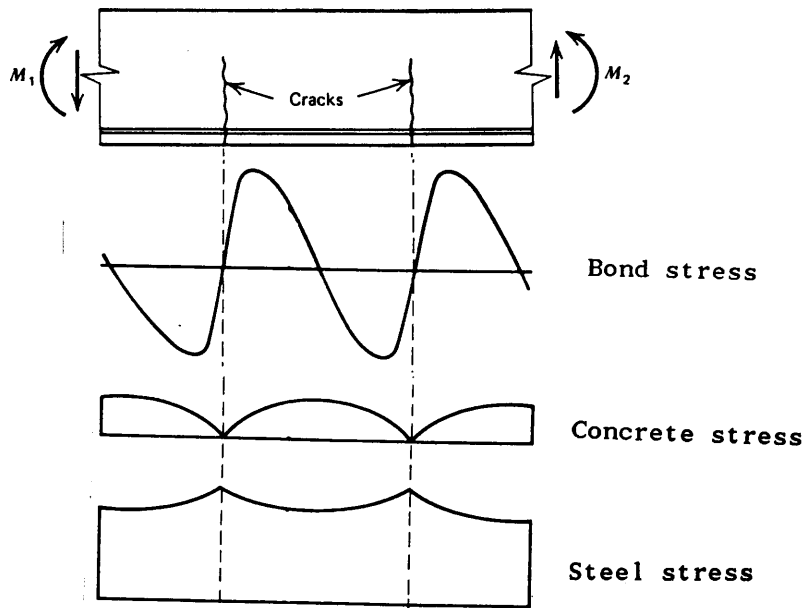
Fig (3-12) EFFECT OF BOND BETWEEN CRACKS.
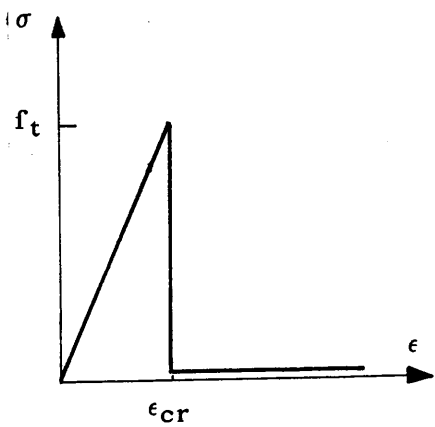
(a) No tension stiffening
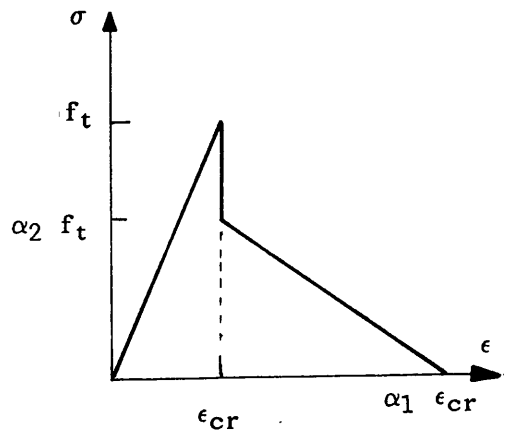
(b) Discontinuous response after cracking
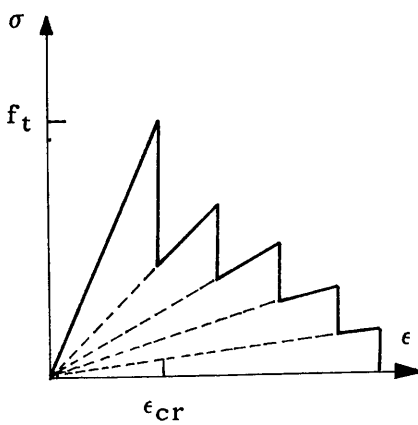
(c) Stepped response after cracking
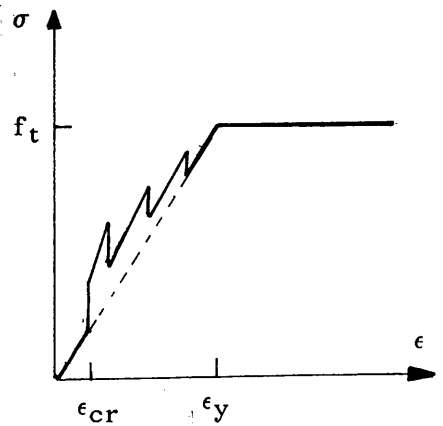
(d) Modified steel tension stress-strain

Fig (3-13) TENSION STIFFENING MODELS.
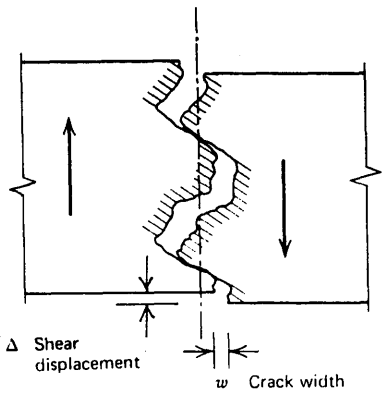
(a) Aggregate interlock along
a cracked plane.
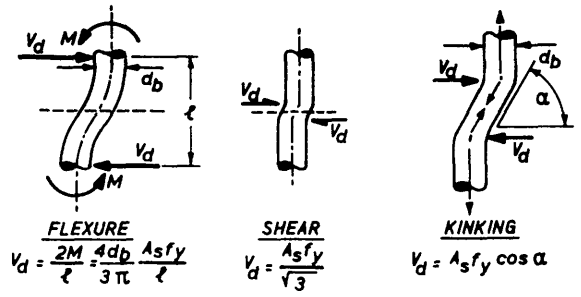
(b) Dowel action mechanisms
across a crack interface.

Fig (3-14) MECHANISMS OF SHEAR TRANSFER.
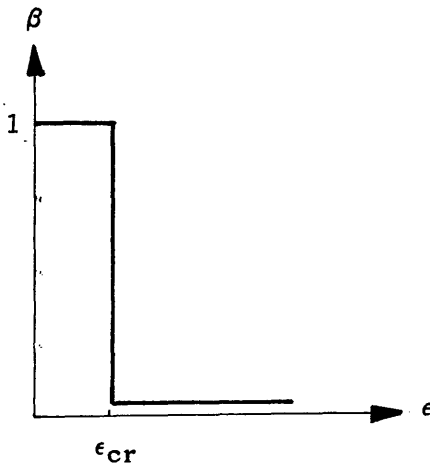
(a) No shear retention
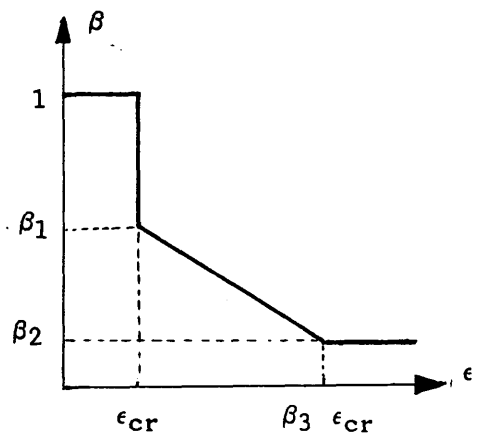
(c) Linear shear retention
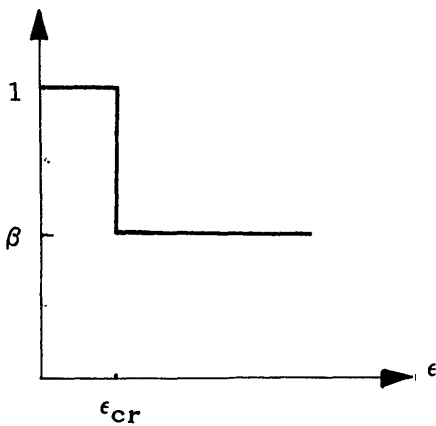
(b) Constant shear retention
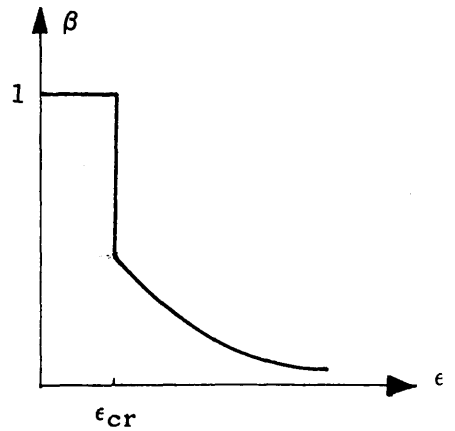
(d) Hyperbolic shear retention

Fig (3-15) NUMERICAL MODELLING OF THE SHEAR RETENTION.
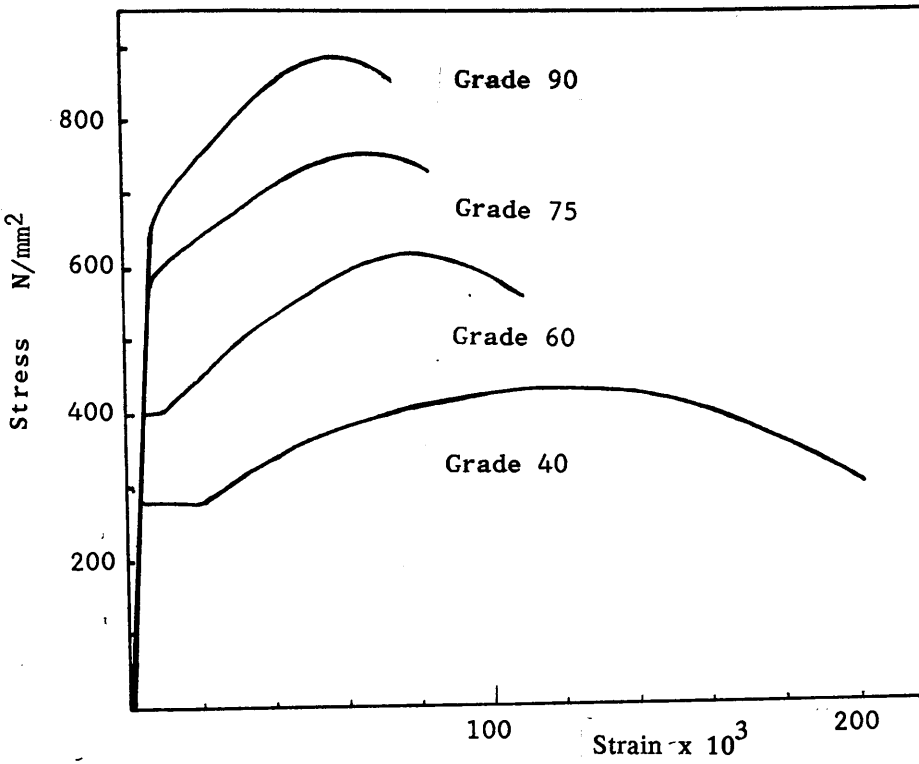
Fig (3-16) TYPICAL STRESS-STRAIN CURVES FOR
NON-TENSIONED REINFORCING BARS.
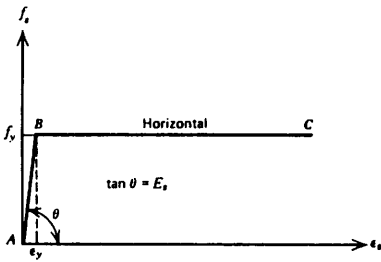
(a) Elastic perfectly plastic
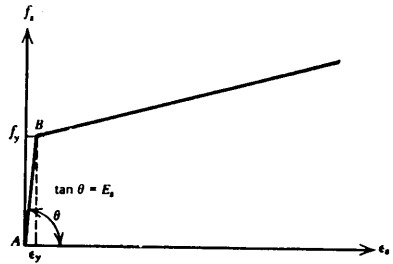
(b) Bilinear approximation
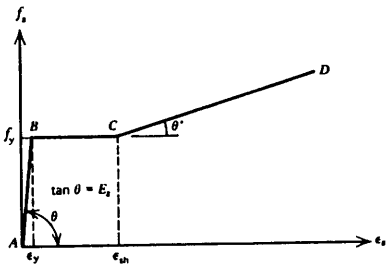
(c) trilinear approximation
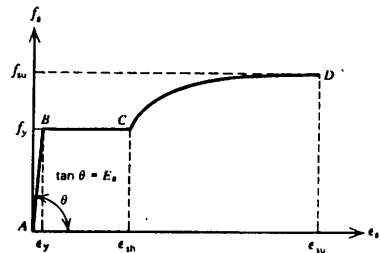
(d) Complete curve

Fig (3-17) IDEALIZATION OF THE STRESS-STRAIN CURVE
FOR STEEL IN TENSION OR COMPRESSION.
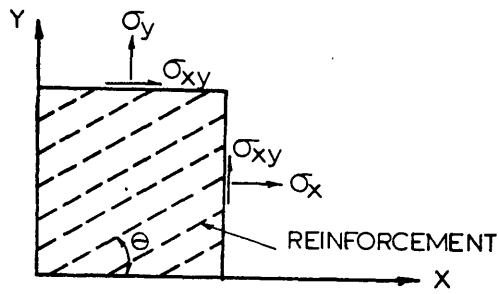
(a) DISTRIBUTED
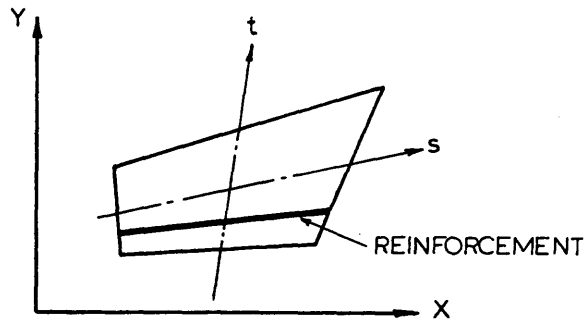
(b) EMBEDDED
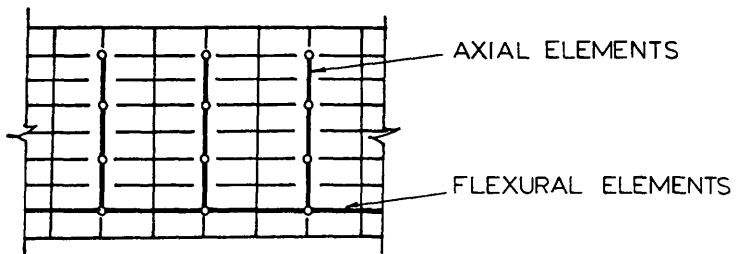
(c) DISCRETE

Fig (3-18) FINITE ELEMENT REPRESENTATIONS OF STEEL.
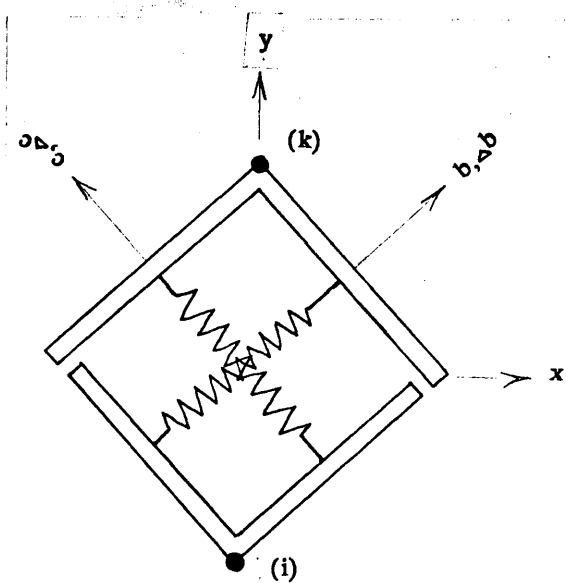
(a) BOND-LINK ELEMENT
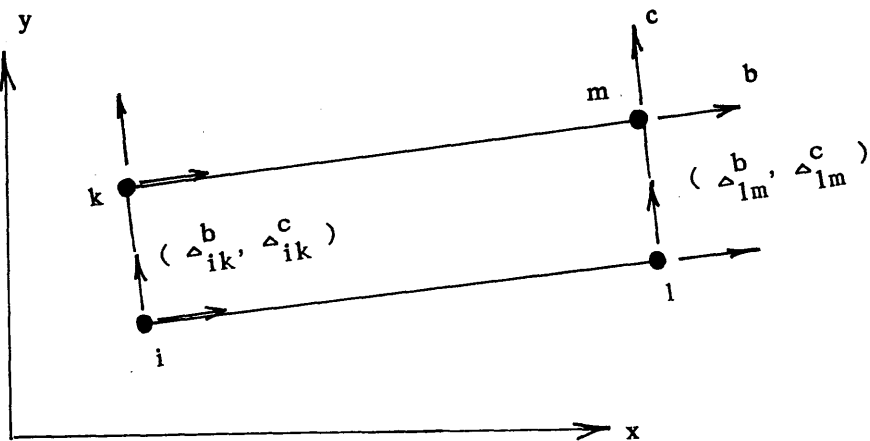
(b) LINEAR CONTACT ELEMENT
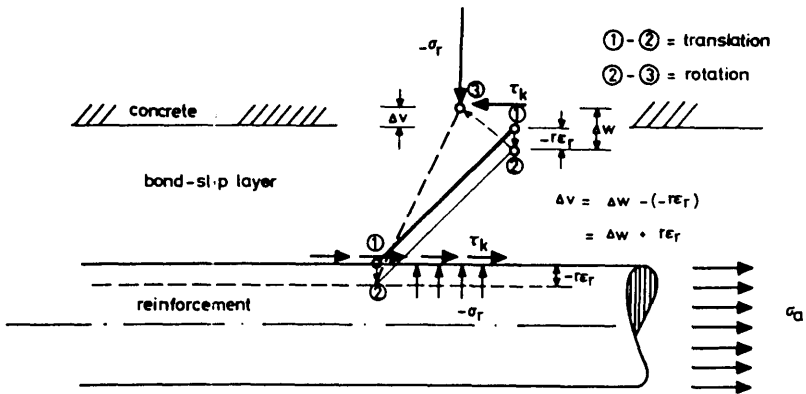
(c) BOND-ZONE ELEMENT

Fig (3-19) NUMERICAL MODELLING OF CONCRETE-STEEL INTERACTION

REFERENCES (3)

AHMAD, M. and BANGASH, Y.

A three dimensional bond analysis using finite elements.

Computers and structures, Vol. 25, pp.281−296, 1987.

AKRAM− YOUNIS, T.

Ultimate load analysis of reinforced concrete stiffened shells and folded slabs used in architectural structures.

Ph.D Thesis, University of Wales, 1988.

ALLWOOD, R.J. and BAJARWAN, A.A.

A new method for modelling reinforcement and bond in finite element analysis of reinforced concrete.

Int.Jnl.Num.Meth.Eng, Vol 28, pp.833− 844, 1989.

AL− MAHAIDI

Nonlinear finite element analysis of concrete deep members.

Research Report No. 79− 1, Cornell University, January 1979.

AL− MANASEER, A.A.

A nonlinear finite element study of reinforced concrete beams.

Ph.D. Thesis, University of Glasgow, Glasgow, Scotland 1983.

AL− MANASEER, A.A. and PHILLIPS, D.V.

Numerical study of some post− cracking material parameters affecting nonlinear solutions in reinforced concrete deep beams.

Can.Jnl.Civ.Eng., Vol. 14, pp. 655− 666, 1987.

ANDENAES, E. , GERSTLE, K. and KO, H.Y.

Response of mortar and concrete to biaxial compression.

J. Eng. Mech. Div, ASCE, Vol. 103(4), pp 515− 525, 1977.

ARNESEN, A. ,SORENSEN, S.I. and BERGAN, P.G.

Nonlinear analysis of reinforced concrete.

Computers and structures, *Vol. 12, pp.571−579, 1980.*

A.S.C.E   Commitee on concrete and masonry structures.

A state of the art report on finite element analysis of reinforced concrete structures

A.S.C.E (1981).

BALAKRISHNAN, S. and MURRAY, D.W.

Concrete constitutive model for NLFE analysis of structures

Journal of structural engineering, ASCE, Vol.114, No.7, July 1988, pp. 1449−1487.

BALAKRISHNAN, S. and MURRAY, D.W.

Prediction of R/C panel and deep beam behaviour by NLFEA.

Journal of structural engineering, ASCE, 1988.

BANGASH, M.Y.H

CONCRETE and concrete structures:

Numerical modelling and applications.

Elsevier Applied Sciences 1989.

BATHE, K.J. and RAMASWAMY

On three—dimensional nonlinear analysis of concrete

structures.

J. Nuclear Eng. and Design, Vol. 52, 1979, pp 385—409.

BAZANT, Z.P. and BHAT, P.D.

Endochronic theory of inelasticity and failure of concrete.

ASCE Journal of engineering mechanics division, Vol. 102,

No. EM4, Aug. 1976, pp. 701—722.

BAZANT, Z.P.

Endochronic inelasticity and incremental plasticity.

International Journal of Solids and Structures, Vol. 14,

No. 9, Sep. 1978, pp. 691—714.

BAZANT, Z.P. and KIM, S.S.

Plastic—Fracturing theory of concrete.

Journal of the Engineering Mechanics Division, ASCE, Vol. 105,

No. EM3, June 1979, pp. 407—428.

BAZANT, Z.P. and SHIEH, C.L.

Hysteretic fracturing endochronic theory for concrete.

Journal of the Engineering Mechanics Division, ASCE, Vol. 106,

No. EM5, Oct. 1980, pp. 929—950.

BAZANT, Z.P. and CEDOLIN, L.

Fracture mechanics of reinforced concrete.

Journal of the Engineering Mechanics Division, ASCE, Vol. 106, No. EM6, Dec. 1980, pp. 1287−1306.

BAZANT, Z.P and CEDOLIN, L.

Blunt crack band propagation in finite element analysis.

J.Eng.Mech.Div.,ASCE, Vol.105(2), 1979,p297− 315.

BLAAUWENDAARD, J.

Realisations and restrictions− Applications of numerical models to concrete structures.

Proc. US−JAPAN Seminar, ASCE 1985,p 557− 578.

BRESLER, B. and PISTER, K.S.

Strength of concrete under combined stresses.

ACI Journal, Vol. 30, No. 3, Sep. 1958, pp. 321−345.

BUYUKOZTURK, O.

Nonlinear analysis of reinforced concrete structures.

Computers and Structures, Vol. 7, pp.149−156, 1977.

BUYUKOZTURK, O. and SHAREEF, S.S.

Constitutive modeling of concrete in finite element analysis.

Computers and Structures, Vol. 21, No. 3, pp.581−610, 1985.

CEDOLIN, L., CRUTZEN, Y.R.J. and POLI, S.D.

Triaxial stress− strain relationship for concrete.

Journal of the Engineering Mechanics Division, ASCE, Vol. 103, No. EM3, June 1977, pp. 423−439.

CEDOLIN, L. and DEIPOLI, S.

Finite element studies of shear critical R/C beams.

Journal of the Engineering Mechanics Division, ASCE, Vol. 103, No. EM6, June 1977, pp. 395−410.

CEDOLIN, L. and MULAS, M.J.

Biaxial stress— strain relation for concrete.

Journal of the Engineering Mechanics Division, ASCE, Vol. 110, No. EM2, Feb. 1984, pp. 187—206.

CERVENKA, V. and GERSTLE, K.H.

Inelastic analysis of reinforced concrete panels.

IABSE, Vol. 32—II, 1972, pp. 26—39.

CERVERA, M., HINTON, E. and HASSAN, O.

Nonlinear analysis of R/C plate and shell structures using 20 noded isoparametric brick elements.

Computers and Structures, Vol. 25, No. 6, pp 845—869, 1987.

CHANG, T.Y., TANIGUCHI,H and CHEN, W.F.

Nonlinear finite element analysis of reinforced concrete panels.

Jnl. Str. Eng, ASCE, VOL 113, No. 1, pp. 122—140, 1987.

CHEN, A.C.T. and CHEN, W.F.

Constitutive relations for concrete.

Journal of the Engineering Mechanics Division, ASCE, Vol. 101, No. EM4, Aug. 1975, pp. 465—481.

CHEN, A.C.T. and CHEN, W.F.

Constitutive equations and punch indentation of concrete.

Journal of the Engineering Mechanics Division, ASCE, Vol. 101, No. EM6, Dec. 1975, pp. 889—906.

CHEN, A.C.T. and CHEN, W.F.

Nonlinear analysis of concrete splitting tests.

Computers and Structures, Vol. 6, pp. 451—457, 1976.

CHEN, W.F. and CHANG, T.Y.P.

Plasticity solutions for concrete splitting tests.

Journal of the Engineering Mechanics Division, ASCE, Vol. 104, No. EM3, June 1978, pp. 691—704.

CHEN, W.F.

Constitutive equations for concrete.

Introductory Report, IABSE Colloquium on plasticity in reinforced concrete, Copenhagen, Denmark, May 21—23 1979, pp.11—34.

CHEN, W.F and SALEEB A.F.

Constitutive equations for engineering materials.
John Wiley & Sons, 1982.

CHEN, W.F. and SUZUKI, H.

Constitutive models for concrete.
Computers and Structures, Vol. 12, pp 23—32, 1980.

CHEN, W.F. and TING, E.C.

Constitutive models for concrete structures.
Journal of the Engineering Mechanics Division, ASCE, Vol. 106, No. EM1, Feb. 1980, pp. 1—19.

CHEN, W.F.

Plasticity in reinforced concrete.
McGraw—Hill Book Company, New—York, 1982.

CHEN, W.F. and YAMAGUCHG

Finite element analysis of reinforced concrete structures.
Proceedings of the seminar sponsored by the Japan society for the promotion of science, Tokyo, Japan, May 21—24, 1985, pp. 48—71, Eds. Mayer, C. and Okamura, H.

COLLINS, M.P., VECCHIO, F.J.

An international competition to predict the response of reinforced concrete panels.
Canadian Journal of Civil Engineering, Vol.12, 1985, pp. 624— 644.

COMITE EURO— INTERNATIONAL DU BETON.

Application of the finite element method to two— dimensional reinforced concrete structures.
Bulletin d'information No. 159, Oct. 1983.

COMITE EURO-INTERNATIONAL DU BETON.
>   Concrete under multiaxial states of stress,
>   Constitutive equations for practical design.
>   *Bulletin d'information No. 156, Oct. 1983.*

COPE, R.J., RAO, P.V., CLARK, L.A. and NORRIS, P.
>   Modelling of reinforced concrete behaviour for finite
>   element analysis of bridge slabs.
>   *Numerical methods for nonlinear problems, Vol. 1, 1981,*
>   *pp. 457-470, Edt. Taylor, c. et al., Pineridge Press, Swansea.*

COPE, R.J. and EDWARDS, K.R.
>   Nonlinear finite element analysis of eccentrically
>   stiffened bridge decks.
>   *FEICOM-1985, Bombay, India, Dec. 2-6 1985, pp. 435-448.*

COON, M.D. and EVANS, R.J.
>   Incremental constitutive laws and their associated failure
>   criteria with application to plain concrete.
>   *International Journal of Solids and Structures, Vol. 8, 1972,*
>   *pp. 1169-1183.*

COWAN, H.C.
>   The strength of plain, reinforced and prestressed concrete
>   under the action of combined stresses.
>   *Magazine of Concrete Research, Vol. 5, No. 14, Dec. 1953, pp.75-86*

DAMJANIC, F.
>   A finite element formulation for analaysis of RC structures.
>   *FEICOM-1985, Bombay, India, Dec. 2-6 1985, pp. 413-422.*

DARWIN, D. and PECKNOLD, D.A.
>   Nonlinear biaxial stress-strain law for concrete.
>   *Journal of the Enginnering Mechanics Division, ASCE, Vol. 103,*
>   *No. EM2, Apr. 1977, pp. 229-241.*

DARWIN, D. and PECKNOLD, D.A.

Analysis of cyclic loading of plane R/C structures.

Computers and Structures, Vol. 7, pp. 137–147, 1977.

DAVIES, J.D and BOSE, D.K.

Stress distribution in splitting tests.

ACI Journal, Vol. 65, No. 8, pp. 662–669,1968.

DE–BORST, R. and NAUTA, P.

Non orthogonal cracks in a smeared finite element model.

Eng. Comput., Vol. 2, March 1985, pp. 35–46.

De GROOT, A.K ,KUSTERS, G.M.A and MONNIER, T.

Numerical modeling of bond slip behaviour.

HERON, Delft University, Vol.26, No.1b, 1981.

DULACSKA, H.

Dowel action of reinforcement crossing cracks in concrete.

ACI Journal, Dec. 1972, p 754–757.

ELWI, A.A. and MURRAY, D.W.

A 3–D hypoelastic concrete constitutive relationship.

Journal of the Engineering Mechanics Division, ASCE, Vol. 105, No. EM4, Aug. 1979, pp. 623–641.

ELWI, A.E. and HRUDEY, T.M.

Finite element model for curved embedded reinforcement.

Jnl. Eng. Mechanics, Vol. 115, No. 4, 1989, pp. 740–754.

EPSTEIN, M. and MURRAY, D.W.

A biaxial law for concrete incorporated in BOSOR5 code.

Computers and Structures, Vol. 9, No. 1, July 1978, pp. 57–63.

FARDIS, M.N., BUYUKOZTURK,O.

Shear transfer model for reinforced concrete.

Jnl of the Eng. Mec. Div., ASCE, Vol. 105, 1979, pp. 255–275.

FARDIS, M.N., ALIBE, B. and TASSOULAS, J.L.

Monotonic and cyclic constitutive law for concrete.

Journal of the Engineering Mechanics Division, ASCE, Vol. 109, No. EM2, April 1983, pp. 516−536.

GEDLING, J.S., MISTRY, N.S. and WELCH, A.K.

Evaluation of material models for reinforced concrete structures.

Computers and Structures, Vol. 24, No. 2, pp. 225−232, 1986.

GERSTLE, K.H. et al.

Behaviour of concrete under multiiaxial stress state.

Journal of the Engineering Mechanics Division, ASCE, Vol. 106, No. EM6, Dec. 1980, pp. 1383−1403.

GERSTLE, K.H.

Simple formulation of biaxial concrete behaviour.

ACI Journal, Vol. 78, Jan. 1981, pp. 62−68.

GILBERT, R.I and WARNER, R.F.

Tension stiffening in reinforced concrete slabs.

journal of Engineering Structural Division, ASCE, Vol. 104, No. ST2, 1978, pp. 1885−1900.

GUPTA, A.K. and AKBAR, A.

Cracking in reinforced concrete analysis.

Journal of Engineering Structural Division, ASCE, Vol. 110, No. ST8, Aug. 1984, pp. 1735−1746.

GUPTA, A.K. and AKBAR, H.

Analysis of RC concrete membrane shells.

FEICOM−85, Bombay, India, Dec. 2−6 1985, pp.423−434.

GRAYSON, R. and STEVENS, L.K.

Nonlinear analysis of structural systems of steel and concrete.

Proceedings of the third International conference in Australia on finite element methods, July 1979, pp.179−196.

HAN, D.J and CHEN, W.F.
Constitutive modeling in analysis of concrete structures.
J. Eng. Mech. Div, ASCE, Vol.112, 1986.

HAND, F.R., PECKNOLD, D.A. and SCHNOBRISH, W.C.
Nonlinear layered analysis of RC plates and shells.
Journal of Engineering Structural Division, ASCE, Vol. 99,
No. ST1, July 1973, pp. 1491−1505.

HIROSHI, Y and SETSURO, N.
Analysis of reinforced concrete walls by plastic− fracturing theory.
US− JAPAN Proceedings, 1985, pp. 204− 213.

HOFBECK, J.A., IBRAHIM, I.O. and MATOCK, A.H.
Shear transfer in reinforced concrete.
ACI Journal, Feb. 1969, pp. 119−128.

HSU, T.C.C., SLATE, F.O., STURMAN, G.M. and WINTER.G.
Microcracking of plain concrete and the shape of the
stress− strain curve.
ACI Journal, Vol. 60, No. 14, Feb. 1963, pp. 209−224.

HU, H.T and SCHNOBRISH, W.C.
Constitutive modeling of concrete by using nonassociated
plasticity.
J. Mat. in Civ. Eng, ASCE, Vol.1, No. 4, 1989.

INGRAEFFA, A.R and SAOUMA, V.
Numerical modeling of discrete cracks propagation in
reinforced and plain concrete.
Fracture Mechanics of Concrete, Sih,G.C and di Tomasso,A eds.
Martinus Nijhoff Publishers, p 171− 225, 1985.

JOHNSTON, D.W and ZIA, P.
Analysis of Dowel action.
ASCE, Vol. 97, No. ST5, 1971, pp. 1611− 1630.

KARSAN, E.D. and JIRSA, J.O.

Behavior of concrete under compressive loadings.

Journal of the Structural Division, ASCE, Vol. 95,

No. ST12, Dec. 1969, pp. 2543—2563.

KEUSER, M. and MEHLHORN, G.

Finite element models for bond problems.

Journal of Structural Engineering, ASCE, Vol. 113,

No. 10, Oct. 1987, pp. 2160—2173.

KOTSOVOS, M.D. and NEWMAN, J.B.

Behaviour of concrete under multiaxial stresses.

ACI Journal, Vol. 74, No. 9, Sep. 1977, pp. 443—446.

KOTSOVOS, M.D. and NEWMAN, J.B.

Generalized stress— strain relations for concrete.

Journal of the Engineering Mechanics Division, Vol. 104,

No. EM4, Aug. 1978, pp. 845—856.

KOTSOVOS, M.D. and NEWMAN, J.B.

A mathematical description of the deformational behavior of

concrete under complex loading.

Magazine of Concrete Research, Vol. 31, No. 107, June 1979,

pp.77—90.

KOTSOVOS, M.D.

A mathematical description of the strength properties of

concrete under generalized stress.

Magazine of Concrete Research, Vol. 31, No. 108, Sep. 1979,

pp. 151—158.

KOTSOVOS, M.D. and NEWMAN, J.B.

A mathematical description of deformational behavior of

concrete under generalized stress beyond ultimate strength.

ACI Journal, Vol. 77, No. 5, Sep. 1980, pp. 340—346.

KOTSOVOS, M.D. and PAVLOVIC, M.N.

Nonlinear finite element modelling of concrete structures,

Basic analysis, Phenomenological insight and Design implications.

Eng. Comput., Vol. 3, Sep. 1986, pp. 243−250.

KUPFER, H.B., HILSDORF, H.K. and RUSH, H.

Behaviour of concrete under biaxial stresses.

ACI Journal, Vol. 66, No. 8, Aug. 1969, pp. 656−666.

KUPFER, H.B. and GERSTLE, K.H.

Behaviour of concrete under biaxial stresses.

Journal of the Engineering Mechanics Division, Vol. 99,

No. EM4, Aug. 1973, pp. 853−866.

LADE, P.V.

Three parameter failure criterion for concrete.

Journal of the Engineering Mechanics Division, ASCE, Vol. 108,

No. EM5, pp. 850−863.

LIN, C.S. and SCORDELIS, A.C.

Nonlinear analysis of RC shells of general form.

Journal of the Structural Division, ASCE, Vol. 101,

No. ST3, March 1975, pp. 523−538.

LIU, T.C.Y., NILSON, A.H. and SLATE, F.O.

Stress−strain response and fracture of concrete in

uniaxial and biaxial compression.

ACI Journal, Vol. 69, No. 5, May 1972, pp. 291−295.

LIU, T.C.Y, NILSON, A.H. and SLATE, F.O.

Biaxial stress−strain relations for concrete.

Journal of the Engineering Structuarl Division, ASCE, Vol. 98,

No. ST5, May 1972, pp. 1025−1034.

MAEKAWA, K. and OKAMURA, H.

The deformational behaviour and constitutive equation of concrete

using the elasto—plastic and fracture model.

Jnl. of the faculty of Engineering, No. 2, Uni. of Tokyo, 1983.

MILLARD,S.G and JOHNSON, R.P.

Shear transfer in cracked reinforced concrete.

Magazine of Concrete Research, Vol.37, No.130, p3—15, 1985.

MILLS, L.L. and ZIMMERMAN, R.M.

Compressive strength of plain concrete under multiaxial

loading conditions.

ACI Journal, Vol. 67, Oct. 1970, pp. 802—807.

MURRAY, D.W. et al.

Concrete plasticity theory for biaxial stress analysis.

Journal of the Engineering Mechanics Division, ASCE, Vol. 105,

No. EM6, Dec. 1979, pp. 989—1006.

NEVILLE, A.M.

Properties of concrete.

Pitman, London, 1977.

NILSON, A.H.

nonlinear analysis of reinforced concrete by finite element method.

ACI Journal, Vol. 65, No. 9, Sep. 1968, pp. 757—766.

NILSSON, S.

The tensile strength of concrete determined by spliting tests on cubes.

RILEM Bullletin, New Series, No. 11, June 1961, pp.63—67.

NGO, D. and SCORDELIS, A.C.

Finite element analysis of reinforced concrete beams.

ACI Journal, Vol. 64, No. 3, March 1967, pp. 152—163.

OTTOSEN, N.S.

A failure criterion for concrete.

Journal of the Engineering Mechanics Division, ASCE, Vol. 103,

No. EM4, Aug. 1977, pp. 527—535.

OTTOSEN, N.S.

Constitutive model for short term loading of concrete.

Journal of the Engineering Mechanics Division, ASCE, Vol. 105,

No. EM1, Feb. 1979, pp. 127–141.

OTTOSEN, N.S.

Evaluation of concrete cylinder tests using finite elements.

Journal of the Engineering Mechanics Division, ASCE, Vol. 110,

No. EM3, March 1984, pp. 465–481.

OWEN, D.R.J. and HINTON, E.

Finite element in plasticity — Theory and Practice.

Pineridge Press, Swansea, U.K. 1980.

PAULAY, T. and LOEBER, P.J.

Shear transfer by aggregate interlock.

Shear in Reinforced Concrete, SP 42, ACI, Detroit, Michigan 1974.

PHILLIPS D.V.

Nonlinear analysis of structural concrete by

finite element method.

Ph.D. Thesis, University of Wales, Swansea, U.K, 1972.

PHILLIPS, D.V. and ZIENKIEWICZ, O.C.

Finite element nonlinear analysis of concrete structures.

Proc. Instn. Civ. Eng. Part 2, Vol. 61, March 1976, pp.59–88.

PHILLIPS, D.V. and WU, Z.P.

An orientated embedded bar formulation with bond—slip.

Proceedings of the International Conference on Numerical Methods

in Engineering, Theory and applications.

NUMETA 1990, pp. 320–328, Swansea 7–11 Jan. 1990.

POPOVICS, S.A.

A review of stress—strain relationships for concrete.

ACI Journal, Vol. 67, No. 3, 1970, pp. 243–248.

RASHID, Y.R.

Analysis of prestressed concrete pressure vessels.

Nuclear Engineering and Design, Vol. 7, No.4, April 1968, pp.334–344.

ROMSTAD, K.M., TAYLOR, M.A. and HERMANN, L.R.

Numerical biaxial Characterization for concrete.

Journal of the Engineering Mechanics Division, ASCE, Vol. 100,

No. EM5, Oct. 1974, pp. 935–948.

ROTS,J.G., NAUTA, P., KUSTERS, G.M.A, BLAUWENDRAAD, J.

> Smeared crack approach and fracture localization in concrete.
>
> HERON Journal, Delft University, Vol. 30, No. 1, 1985, pp. 1—47.

ROTS, J.G., and BLAUWENDRAAD, J.

> Crack models for concrete: Discrete or Smeared ?
>
> Fixed, Multidirectional or Rotating ?
>
> HERON Journal, Delft University, Vol. 34, No. 1, 1989, pp. 1—59.

SAENZ, I.P.

> Discussion of 'Equation of the stress—strain curve of concrete'
>
> by Desayi, P. and Krishnan, S.
>
> *ACI Journal, Vol. 61, No. 9, Sep. 1964, pp. 1129—1235.*

SANTHA KUMAR, A.R.

> Nonlinear finite element analysis of RC coupled shear walls.
>
> *Proceedings of the third international conference in Australia on finite element methods, July 1979, pp. 283—297.*

SARNE, Y.

> Material nonlinear time dependant theree dimensional finite element analysis of reinforced concrete and prestressed concrete structures.
>
> *Thesis presented to the Massachusetts Institute of Technology, Cambridge, Mass. 1974, in partial fulfillment of the requirements for the degree of Doctor of Philosophy.*

SCANLON , A. and MURRAY, D.W.

> Time dependant reinforced concrete slab deflections.
>
> *ASCE, Vol. 100, No. ST9, 1974, pp. 1911—1924.*

SCHNOBRICH, W.C.

> Behavior of reinforced concrete structures predicted by the finite element method.
>
> *Computers and Structures, Vol. 7, pp. 365—376, 1977.*

SCHNOBRICH, W.C.

The role of finite element analysis of reinforced concrete structures.
Finite element analysis of reinforced concrete structures,
Proceedings of the seminar sponsored by the Japan society for
promotion of science, Tokyo, Japan, May 21—24 1985,
Edts. Mayer, C. and Okamura, H.

SCHNOBRICH, W.C. and HU, H.T.

Use of finite element techniques to predict nonlinear behaviour of
reinforced concrete structures.
FEICOM—85, Bombay, India, Dec. 2—6 1985, pp. 395—412.

SOROUSHIAN, P., OBASEKI, K. and CHOI, K.B.

Analysis of aggregate interlock behaviour at cracks in
reinforced concrete.
Magazine of Concrete Research, Vol.40, No.142, Mar. 1988, pp. 43—49.

SUIDAN, M and SHNOBRISH, W.C.

Finite element analysis of reinforced concrete.
ASCE, Vol. 99, ST10, 1973, pp. 2109—2122.

SUZUKI, H. and CHEN, W.F.

Elastoplastic fracture analysis of concrete structures.
Computers and Structures, Vol. 16, No. 6, pp. 697—705, 1983.

TASUJI, M.E., SLATE, F.O. and NILSON, A.H.

Stress strain response and fracture of concrete in biaxial loading.
ACI Journal, Vol. 75, No. 7, July 1978, pp. 306—312.

TASUJI, M.E., NILSON, A.H. and SLATE, F.O.

Biaxial stress— strain relationships for concrete.
Magazine of Concrete Research, Vol.131, No.109, Dec.1979, pp.217—224

VALANIS, K.C.

A theory of viscoplasticity without yield surface.
Archives of Mechanics, Warsaw, Vol. 23, 1971, pp 517—551.

VALLIAPAN, S. and DOOLAN, T.F.

Nonlinear stress analysis of reinforced concrete.

ASCE, Vol. 98, No. ST4, 1972, pp. 885—898.

VERMEER, P.A and De BORST, R.

Non associated plasticity for soils, concrete and rock.

HERON, Delft University, vol.29, No.3, pp 1—64, 1984.

WAN, T.T.

Uniaxial compression stress—strain relations of concrete.

ASCE, Vol.114,pp 2133—2136, 1988.

WRIGHT, P.J.F.

Comments on an indirect tensile test on concrete cylinders.

Magazine of Concrete Research, Vol. 7, No. 20, July 1955, pp.87—96.

YUGUZUGULLU, O., SCHNOBRISH, W.C.

A numerical procedure for the determination of the behaviour
of shear wall frame system.

ACI Journal, Vol. 70, No. 7, 1873, pp. 474—479.

CHAPTER 4

SOLUTION TECHNIQUES FOR NONLINEAR PROBLEMS

4-1 INTRODUCTION :

For linear elastic problems the set of equilibrium equations is linear and can be solved by efficient direct equation solvers using Gauss elimination, Cholesky, frontal methods, or some iterative methods like Gauss— Seidel or Jordan methods.

However, concrete is not an elastic material and reinforced concrete structures do not behave linearly even at low load levels due primarily to early cracking. As a consequence, in many cases including coupled shear— walls, linear elastic analysis leads to results which are far from the real behaviour of the structure and can be on the unsafe side. In fact an ultimate limit state analysis based on linear elastic structural behaviour is a conventional (but apparently contradictory) procedure, while acting forces are computed on the basis of linear constitutive relationships, the nonlinear nature of these relationships are considered in computing design ultimate resisting moments.

In general, most problems in solid mechanics are nonlinear and therefore, require nonlinear analysis if realistic results are to be obtained. In the displacement method of finite element, nonlinearities occur in three different forms:

(a) Material nonlinearity.

(b) Geometric nonlinearity.

(c) Material and Geometric nonlinearity.

Material nonlinearity encompasses problems in which stress— strain relations are not linear. For reinforced concrete they can vary from short term nonlinear

relationships such as yielding of steel and concrete, cracking..etc, to time dependant effects such as creep and shrinkage.

Although linear stress—strain equations are assumed to hold in the second category, problems involving geometric nonlinearity arise from both nonlinear strain—displacement relations, and finite changes in geometry. Equilibrium equations based on the original geometry are no longer valid due to large displacements and need to be modified to take into account the new geometry. Also, higher order derivatives terms must be included in the strain—displacement relations Eq (2—8).

The third and most general category of nonlinear problems involves nonlinear material constitutive behaviour as well as geometric nonlinearity involving large strains and displacements.

In this investigation only material nonlinearity caused by short term nonlinear behaviour of concrete and steel is considered. These include yielding or crushing of concrete under high compressive stresses, tensile cracking, aggregate interlock, dowel action, yielding of steel,..etc. The mathematical model and the constitutive laws defining the stress—strain relations for both steel and concrete have been presented in Chapter (3). In this chapter the basic formulation of the nonlinear problem and the numerical techniques used in this study to solve it are given.

4—2 BASIC FORMULATION OF THE PROBLEM :

For problems where only the material behaviour is nonlinear the relationship between stress and strain is assumed to be of the form :

$$F \ (\ \sigma \ , \ \epsilon \ ) \ = \ 0 \qquad\qquad .... \ (4-1)$$

Finite element discretization eventually results in a set of simultaneous expressions expressed by:

$$[\ K_S(\sigma, \epsilon) \ ] \ \{ \ \delta \ \} = \{ \ F \ \} \qquad \dots\dots(4\text{-}2)$$

in which the external nodal forces $\{ \ F \ \}$ are related to the nodal degrees of freedom $\{ \ \delta \ \}$ through the structural stiffness $[\ K_S \ ]$, which in turn, is a function of the material nonlinearities for a given state of stress.

Equations $(4-2)$ are initially formed at the element level, so that before solution of Eq $(4-2)$ can proceed, the element stiffness relations are added into the global structural system through appropriate assembly of element stiffnesses and load vector. An advantage of finite element analysis is that the stiffness matrix of the element assemblage is not only symmetric and positive definite but is also banded. Taking advantage of the banded symmetric nature of the global structural stiffness matrix of the sysytem $[\ K_S \ ]$, it is necessary to store only the symmetric half-bandwidth of the stiffness matrix minimizing considerably the cost of analysis and storage requirements. In fact, this leads to high speed access to stored data and back-up storage is avoided, while operations necessary for the equation solution are performed only on the nonzero coefficients clustered around the diagonal of the stiffness matrix. However this banded property depends on the nodal point numbering of the finite element mesh, and care must be taken to obtain an effective nodal point numbering. There are different schemes to store the semi-band stiffness coefficients. These may be stored in a matrix form or as a one dimensional array or skyline.

The need to solve large systems of equations has led to two well estabilished approaches, the banded and frontal methods. The frontal method was developed to accommodate large matrices with relatively small core requirements on medium size computers, whereas banded solution methods rely mainly on the availability of large size computers. The first approach makes use of large storage disks and can be said to be I/O (input/output) intensive. The second approach makes use of a

fast CPU to work within a large core or more likely a large virtual memory, and can be said to be CPU intensive. It should be noted that the performance of frontal procedures is highly dependant upon the ordering of elements to minimize the wavefront. This is contrary to bandwidth solvers where ordering of nodes is crucial to obtaining the smallest possible bandwidth. For structural problems of simple regular geometry efficient numbering of elements or nodes is straightforward, whereas for complex geometries, algorithms have been developed to reduce the bandwidth, Collins 1973 and Puttonen 1983 or the wavefront, Razzaque 1980 and Pina 1981.

The fundamental feature of the frontal or wavefront method is that the entire stiffness matrix is never formed but the assembly process alternates with the solution. The frontal algorithm requires little main storage but demands appreciable book— keeping and data transfers to and from disk storage as needed. Now that virtual operating systems are widespread and large enough, there is an argument that all this complicated programming is not really necessary. The suitability of the wavefront scheme over other procedures depends on the problem size and also on the system hardware. For very large problems or when using a hardware with little main storage such as PC computers, the frontal procedure is certainly an efficient alternative.

In this study, the global stiffness matrix is stored in a semiband matrix form, and Choleski decomposition is used to solve the nonlinear structural equilibrium equations (4— 2) which are restated as:

$$[L] [U] \{ \delta \} = \{ F \} \qquad \dots\dots\dots\dots\dots (4\text{-}3)$$

A condition for the nonlinear solution of Eq (4— 3) to be reliable and accurate is that the basic laws of continuum mechanics must be obeyed, ie;

(a) equilibrium, (b) compatibility and (c) the constitutive relations of the material.

Displacement compatibility is automatically satisfied in the displacement finite element technique. Therefore it becomes only necessary to enforce that the nonlinear constitutive relations of steel and concrete are correctly satisfied whilst at the same time preserving equilibrium of the structure. The non—violation of the constitutive laws of the materials can be satisfied using the mathematical model presented in Chapter (3) simulating the observed experimental behaviour of reinforced concrete. For equilibrium conditions, due to material degradation (cracking and crushing) and consequently the release of residual stresses that the material cannot support the equilibrium equations (4—2) are not satisfied, the lack of equilibrium would give rise to residual forces $\{ \Psi \}$ expressed through:

$$\{ \Psi \} = \{ F \} - \sum \int [B]^T \{ \sigma \} \, dv \qquad \dots \dots \dots (4-4)$$

in which the residual forces $\{ \Psi \}$ result from the lack of equilibrium between the external applied forces $\{ F \}$ and the developed internal forces $\{ F_{int} \}$.

In the following sections the numerical techniques that attempt to meet the equilibrium requirements are presented.

4—3 NUMERICAL TECHNIQUES FOR NONLINEAR ANALYSIS :

In recent years, significant activities have been undertaken to improve the efficiency, stability and range of applications of solution schemes in handling nonlinear finite element problems. For these problems, there is no general method of solution and only some of the widely used methods will be discussed here. Mondkar et al. 1978, Bergan et al. 1978, Crisfield 1980, 1982 and Gadala et al. 1984 provide more comprehensive information on different solution algorithms.

The commonly used solution methods for nonlinear problems may be broadly classed into the following categories:

  (a) Incremental methods (step— wise)

  (b) Iterative methods (Newton— Raphson)

  (c) Incremental— Iterative procedures (Mixed)

  (d) Accelerated methods.

  (e) Arc— length methods.

A crucial factor in the development of finite element computer programs for nonlinear analysis is the proper selection of solution algorithms. As opposed to linear problems, it is difficult to develop one single method of general validity that can be used in a routine manner. Some of the solution procedures mentioned above are either suitable for certain classes of nonlinear problems, or certain requirements must be satisfied to ensure convergence to the correct solution. For these reasons, a computer program for nonlinear analysis should possess several alternative algorithms for the solution of nonlinear systems at user will. This has been adopted in this study, and in the following sections the numerical procedure that has been implemented in the computer program and the other techniques mentioned above are now described for completeness.

4-3-1 INCREMENTAL METHOD:

The incremental solution is carried out by applying the total external loading as a sequence of sufficiently small increments so that the structure can be assumed to respond linearly within each increment. In this way the incremental or step-wise procedure approximates a nonlinear problem as a series of linear problems. The structural response due to each load increment is obtained as an increment of displacements. These displacement increments are accumulated to assess the overall response at any stage of the loading, and this is repeated until the total load has been reached.

At each load step the stiffness matrix is recomputed tracing the damage due to fracture, crushing or cracking, and the nonlinearities induced in the constituent materials.

The incremental procedure is schematically indicated in Fig (4-1) for a one dimensional situation. The recurrence relation at any general i^{th} load step may be given in the following algorithm:

$$[K_s]_i \{ \Delta\delta \}_i = \{ \Delta F \}_i \qquad \text{....... (4-5)}$$

$$\{ \delta \}_i = \{ \delta \}_{i-1} + \{ \Delta\delta \}_i$$

$$\{ F \}_i = \{ F \}_{i-1} + \{ \Delta F \}_i$$

where $\{ \Delta\delta \}_i$ and $\{ \Delta F \}_i$ are the displacement and load increments respectively, $[K_s]_i$ is the tangent stiffness matrix of the structure at the position defined by the total accumulated displacements and loads respectively. The incremental displacement vector $\{ \Delta\delta \}_i$ is obtained by solving the set of simultaneous equations (4-5), and the corresponding increments in strains and stresses are then determined.

The computation involves one solution per load increment and since no iteration is

made to restore equilibrium and account for force redistribution, the scheme is characterized by the continuous accumulation of errors inducing the drifting of the solution from the true equilibrium path unless very fine force increments sizes are used which can be computationally inefficient.

4-3-2 ITERATIVE PROCEDURES :

With an iterative solution scheme, the total load is applied in one increment and the solution is obtained by successive iterations. At each iteration stresses are evaluated according to the material constitutive laws. These stresses are then used to compute the equivalent internal nodal forces which may not be in equilibrium with the externally applied loads. The residual forces between the external and internal forces are in fact a portion of the total applied load that cannot be resisted by the structure due to its nonlinear behaviour. These unbalanced nodal forces are calculated and reapplied over the structure by the next iteration giving additional corrective displacements, and hence new stresses, which result in a new set of internal equivalent nodal forces. This process is repeated until equilibrium between the external applied load and the internal forces is approximated to some acceptable degree.

4-3-3 INCREMENTAL-ITERATIVE PROCEDURE :

The main disadvantage of the incremental procedure is the lack of equilibrium and the indeterminate drifting of the solution from the true equilibrium curve Fig (4-1). Although equilibrium conditions hold in the iterative scheme, no information can be obtained at intermediate load levels if needed. To overcome these shortcomings, efficient procedures can be obtained by combining both incremental and iterative solution methods. The resulting method is widely used and is known

as the mixed or incremental—iterative method. Using such a technique, the complete response of a structure is obtained. Valuable information is available during step loading to assist the process by which the structure fails while equilibrium is automaticallly satisfied through successive iterations at each load step. This is schematically represented in Fig (4—2) and Fig (4—3) in which the loading is increased from $\{ F \}_{i-1}$ to $\{ F \}_i = \{ F \}_{i-1} + \{ \Delta F \}$. An estimation of the displacements $\{ \Delta\delta \}$ due to $\{ \Delta F \}$ is given by:

$$\{ \Delta\delta \} = [K_s]^{-1} \{ \Delta F \}$$
$$\{ \delta \}_i = \{ \delta \}_{i-1} + \{ \Delta\delta \} \qquad \ldots(4-6)$$

in which $\{ \delta \}_{i-1}$ is the vector of displacements at the end of the previous increment, $[K_s]$ is the structural stiffness matrix.

Using the total nodal displacements, strains and hence stresses for any point within an element can be determined. These stresses are then converted to principal stresses and compared against the material stress—strain curves to check for cracking, crushing and yielding as presented in chapter 3. Should any of these stress occur the stresses are brought down to the required level so that the constitutive laws are not violated. The equivalent nodal forces, $\{ f_{int} \}$, required to equilibrate these stresses are then determined for each element

$$\{ f_{int} \} = \int [B]^T \{ \sigma \} \, dv \qquad \ldots (4-7)$$

where $\{ \sigma \}$ is the vector of stresses.

The equivalent nodal loads for all elements in Eq. (4—7) are appropriately assembled to give a total nodal internal force vector $\{ F_{int} \}$ for the structure

$$\{ F_{int} \} = \sum \int [B]^T \{ \sigma \} \, dv \qquad \ldots (4-8)$$

The global internal forces $\{ F_{int} \}$ are then substracted from the external applied

loads $\{ F \}_i$ to give a vector of internal residual forces $\{ \Psi \}_i$.

$$\{ \Psi \}_i = \{ F \}_i - \{ F_{int} \} \qquad \text{.... (4-9)}$$

If the internal stresses and the external loads were in equilibrium, $\{ \Psi \}_i = 0$. Generally this is not true, so $\{ \Psi \}_i$ has to be redistributed over the structure and the process is repeated. If it converges, then the terms in $\{ \Psi \}_i$ become negligible and the applied load is incremented with a new load step. The same analysis is then repeated until a load level is reached at which, the residual forces $\{ \Psi \}_i$ can not be removed at which stage collapse is assumed to have occurred.

The global stiffness matrix $[K_s]$ can take various forms and various mixed procedures can be built accordingly; Three iterative procedures are examined here: Newton-Raphson (N-R), modified Newton-Raphson (mN-R) and quasi Newton method (q-N).

Newton-Raphson involves reforming and factoring the coefficient matrix $[K_s]$ for each iteration at each increment, a computationally expensive process. However, the reformed matrix, reflecting material properties from the latest approximation to the solution, in general produces a better approximation in the next iteration Fig (4-2).

In the modified Newton-Raphson procedure the coefficient matrix is not reformed during all iterations Fig (4-3). Typically it is formed and factored at the beginning of each increment but other strategies may require a reform after a given number of preselected iterations.

Quasi-Newton methods have been used more recently to solve nonlinear systems. These methods involve modifications of the inverse of the coefficient matrix at each iteration. The modifications are cheaper to accomplish than a full reform and refactor of the matrix and yet convey enough information about the structural properties to reduce the number of iterations and ensure convergence.

(i) Newton—Raphson methods : The Newton—Raphson method is based on the tangential stiffness matrix at the current stress level. This requires formation and factorization of the stiffness corresponding to the current deformation state at each iteration cycle (i), Fig (4—2). At each iteration [K_s] is updated and expressed in terms of the current approximation of the dispalcements. The updated solution is calculated as follows:

At the first iteration 1 of increment step (i)

$$\{ \Delta\delta \}_i^1 = [K_s (\sigma, \epsilon)]_{i-1}^{-1} \{ \Delta F \}_i$$

$$\{ \delta \}_i = \{ \delta \}_{i-1} + \{ \Delta\delta \}_i^1$$

and at iteration (j>1) of increment (i)

$$\{ \Delta\delta \}_i^j = [K_s (\sigma, \epsilon)]_{i,j}^{-1} \{ \Psi \}_j$$

$$\{ \delta \}_i = \{ \delta \}_i + \{ \Delta\delta \}_i^j \qquad \ldots (4\text{-}10)$$

thus each solution increment is tangential to the curve at the last iteration as depicted in Fig (4—2). It can have a fast convergence rate but suffers from a number of drawbacks. In particular, the cost per iteration can become excessive for large systems with a large number of degrees of freedom, since the global stiffness [K_s] has to be both reformed and refactorized at each iteration.

(ii) Modified Newton—Raphson methods: For modified Newton—Raphson iterations, the tangent stiffness matrix [K_s] can be based on the initial elastic stiffness of the structure and remains constant throughout the analysis Fig (4—3), known as the constant stiffness method. In this case the tangent stiffness matrix is formed and factored only once and the update to the solution is calculated as:

At the first iteration 1 of increment step (i)

$$\{ \Delta\delta \}_i^1 = [K_s]^{-1} \{ \Delta F \}_i$$

$$\{ \delta \}_i = \{ \delta \}_{i-1} + \{ \Delta\delta \}_i^1$$

and at iteration (j>1) of increment (i)

$$\{ \Delta\delta \}_i^j = [K_s]^{-1} \{ \Psi \}_j$$

$$\{ \delta \}_i = \{ \delta \}_i + \{ \Delta\delta \}_i^j \qquad \dots(4\text{-}11)$$

For the iterations the initial stiffness is used and it is only necessary to calculate the out of balance loads and backsubstitute. As the coefficient matrix is not updated based on the information from the latest iteration, it generally entails slow convergence. To improve the rate of convergence the stiffness matrix $[K_s]$ is updated at the beginning of each load step or at a number of predetermined iterations in the analysis.

(iii) Quasi−Newton methods: Quasi−Newton methods aim to update the stiffness matrix or its inverse without actually reforming and refactoring the matrix. The global stiffness matrix is updated for every iteration based not on the actual mechanical damage in the structure but on the convergence behaviour in previous iterations. In practice this modification is performed on the inverse matrix and can be accomplished by vector multiplication, leading usually to the destruction of the banded symmetry nature of the stiffness matrix. This drawback is very significant for large problems, only Davidon and BFGS updates preserve symmetry. For each iteration quasi−Newton methods require fewer operations to update the coefficient matrix than the Newton−Raphson method. The BFGS matrix update, discovered in the same year 1970 by Broyden, Fletcher, Goldfarb and Shanoo updates the

coefficient matrix in a way that preserves both symmetry and positive definite property from one iteration to the next, as presented by Mathies et al. 1979.

4-3-4 ACCELERATION METHODS :

Developments in numerical analysis and applied mathematics can be used to further improve the efficiency of the various incremental- iterative procedures at low additional cost. Recently, a number of techniques have been introduced in order to accelerate the rate of convergence of Newton- Raphson solution procedures for nonlinear structural analysis, such as the accelerated method proposed by Crisfield 1980.

Early accelerators such as the modified Aitken- δ^2 method discussed by Boyle and Jennings (1973) has been tested by Cope and Rao (1980) who found that generally the procedure does not speed up convergence. On the other hand, Chow and Kay 1984 have shown that significant savings in solution time has been achieved and that the method is effective in accelerating the rate of convergence. Cope and Rao (1980)found that the α- constant stiffness method due to Nayak and Zienkiewicz 1972 as implemented proved to be unstable. More recently, Araujo 1989 presented extrapolation formulas for an improved estimate of the incremental displacements in order to accelerate the convergence of the modified Newton- Raphson method when analysing reinforced concrete structures.

4-4 Arc length methods:

The method was originally proposed by Wempner (1971) and Riks (1972) and, as modified by Crisfield (1981) and Ramm (1981), can be easily introduced into a standard finite element computer program . The basic idea in all arc- length methods is to modify the load level at each iteration, rather than holding the

applied load level constant during a load step, so that the solution follows some specified path until convergence is attained. It follows that the load level is unknown, and therefore an additional equation is needed in order to solve the equilibrium equations. This is achieved by forcing the load to follow a specified constraint surface, Fig (4−4). The constraint surface can take various forms as indicated in Fig (4−4); Hyperlinear Wempner 1971 and Riks 1979; Spherical Crisfield 1981 and elliptic Padovan et al. 1982. Bellini and Chulya 1987 reviewed and compared various existing arc−length algorithms for the automatic incremental solution of nonlinear finite element equations and proposed an improved algorithm based on essential ideas from Bathe and Dvorkin 1983. These strategies have significantly extended the range of Newton−Raphson schemes to trace equilibrium paths beyond turning points (snap−back/snap−through). However, several difficulties are present and prominent; among these are the extra storage requirement and adjustment of size, shape and orientation of the constraint surface, so as to enhance numerical robustness.

4−5 CONVERGENCE CRITERIA :

Since in a numerical process, equilibrium conditions are unlikely to be satisfied exactly, criteria to terminate iterations have to be established for objective analysis. The main purpose of a reliable convergence criterion is to monitor the gradual elimination of the out of balance residual forces until the desired accuracy has been achieved. The accuracy is the error or convergence tolerance specified and accepted by the analyst. Although fine tolerances are desirable, specifications have to take into account the cost of computing necessary for a particular degree of accuracy, and should be commensurate with the physical uncertainties already involved in the description of a structure. To check the decay of residual forces for every degree of freedom is computationally a formidable task and sometimes

impossible. Therefore, some overall checks based on the computed quantities must be considered. Three types of convergence criteria have been widely used for nonlinear structural analysis, namely;

(a) <u>Force convergence criterion :</u>

$$\frac{\|\ \psi\ \|_{i,j}}{\|\ \Delta F\ \|_{i,j}} \times 100 \leqslant FTOL$$

where the notation represents the euclidian norm at iteration i of increment j, and FTOL is the pre-set force convergence tolerance.

(b) <u>Displacement convergence criterion :</u>

$$\frac{\|\ \Delta\delta\ \|_{i,j}}{\|\ \delta\ \|_{i,j}} \times 100 \leqslant DTOL$$

where DTOL is the displacement convergence tolerance.

(c) <u>Energy convergence criterion :</u>

$$\frac{|\ \Psi\ .\ \Delta\delta\ |}{|\ \Delta F\ .\ \Delta\delta\ |} \times 100 \leqslant ETOL$$

where ETOL is the energy convergence tolerance.

Convergence criteria are used also as means of detecting the collapse of the analysed structure as the magnitude of the successively iterative displacements increases continually at the post failure stage.

In this investigation the energy convergence criterion is used to check for equilibrium. The force or displacement convergence criteria can not be used due to the different displacements units of the finite element used. The analysis is terminated and collapse is assumed to have occured if, either the energy convergence criterion is not satisfied and was unrealisically high, or the number of iterations within an increment exceeded a preselected value. A value of 150 iterations was adopted.

In this study the incremental—iterative procedures and its variants have been adopted, in which the global stiffness matrix is:

(a) — Held constant throughout the analysis

(b) — Updated at every iteration

(c) — Updated only at the second iteration of every increment

(d) — Updated at some preselected iterations 1,2,5,10,...

The first alternative is used for very large problems such as coupled shear walls to be presented in Chapter 6, and the third alternative is used for relatively smaller problems involving beams and panels to be studied in the next section.
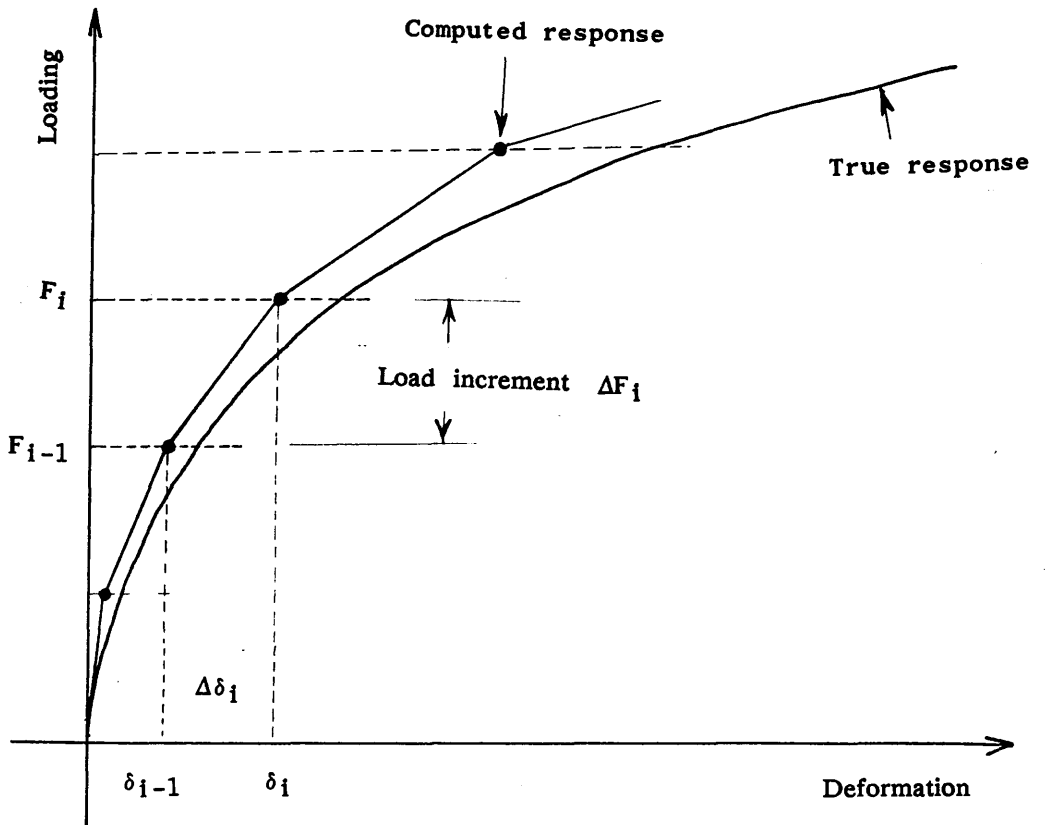
Fig (4-1) INCREMENTAL METHOD WITHOUT
EQUILIBRIUM ITERATIONS.
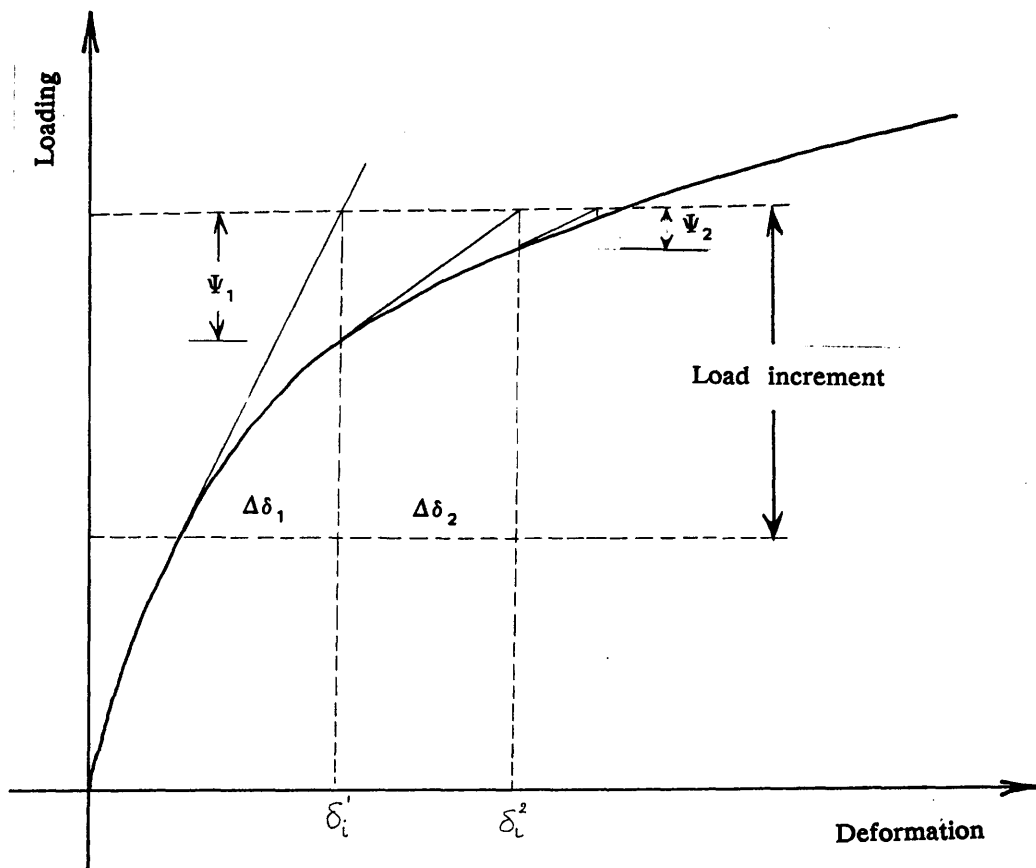
Fig (4-2) NEWTON-RAPHSON METHOD.
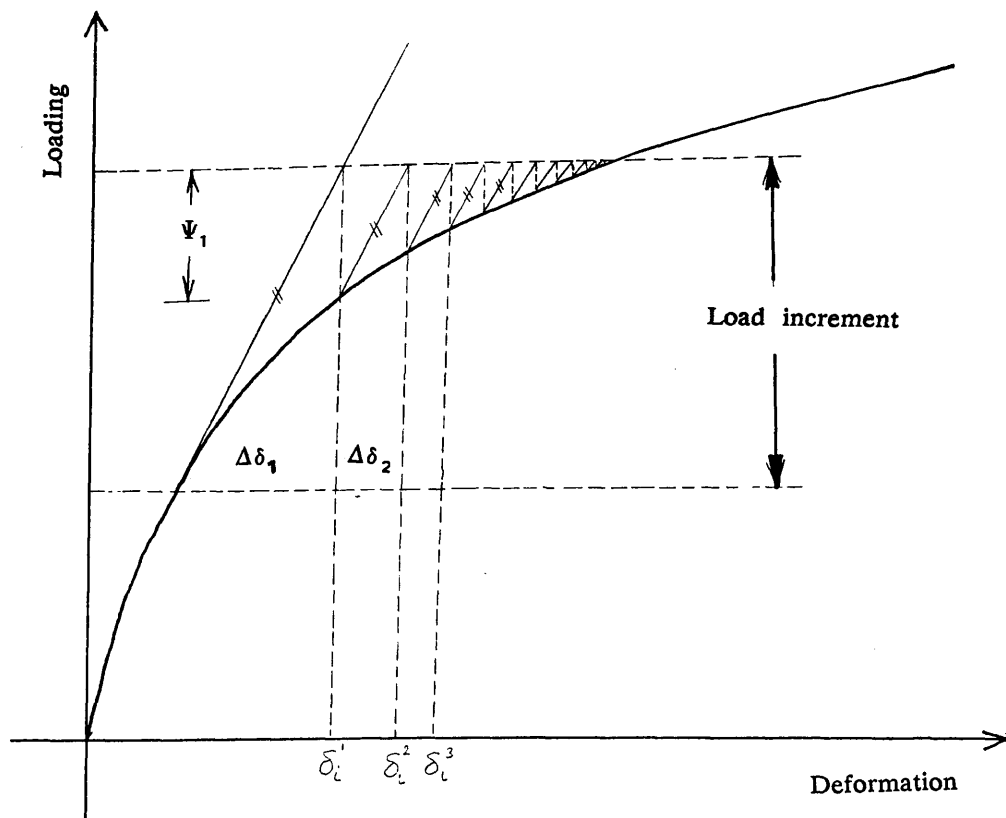
Fig (4-3) MODIFIED NEWTON-RAPHSON METHOD.
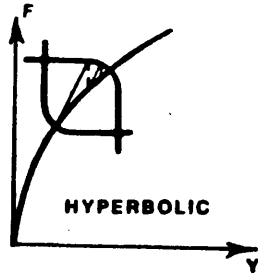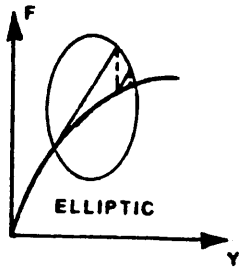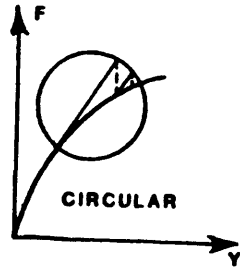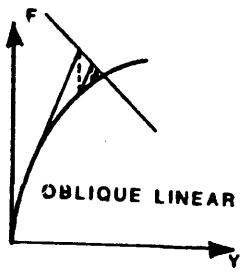
(a) Various constraint surfaces in force-deflection space
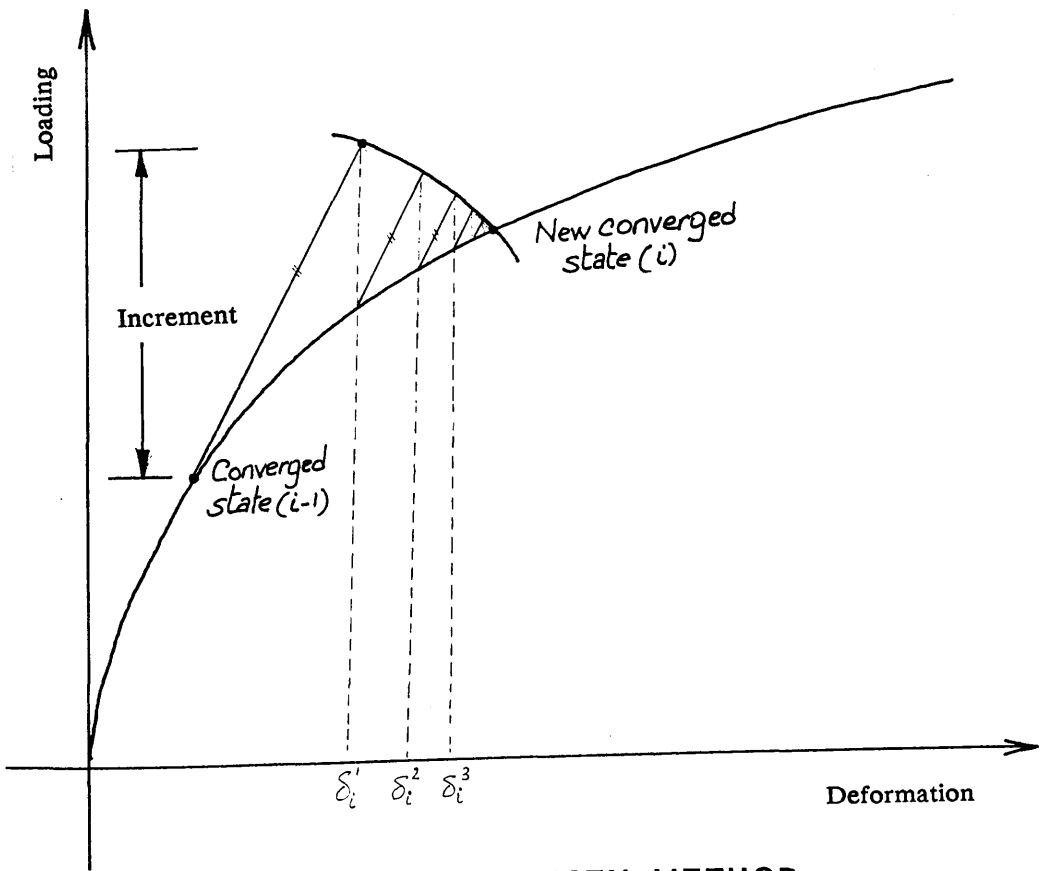
FIG (4-4) ARC LENGTH METHOD

REFERENCES (4)

ARAUJO, J.M.

    Optimization of Newton—Raphson methods in reinforced

    concrete nonlinear analysis. Comp.& Str., Vol. 33, pp. 735—741, 1989.

ATTARD, M.M. and SOMERVAILLE, I.J.

Nonlinear analysis of thin walled open beams.

Computers and Structures, Vol. 25, No. 3, pp. 437—443, 1987.

BATHE, K.J. and DVORKIN, E.N.

    On the automatic solution of nonlinear finite element equations.

    Computers and Structures, Vol. 17, No. 5—6, pp. 871—879, 1983.

BELLINI, P.X. and CHULYA, A.

    An improved automatic incremental algorithm for the efficient

    solution of nonlinear finite element equations.

    Computers and Structures, Vol. 26, No 1—2, pp.99—110, 1987.

BERGAN, P.G.

    Solution algorithms for nonlinear structural problems.

    Computers and Structures, Vol. 12, pp. 497—509, 1980.

BERGAN, P.G., HOLAND, I. and SOREIDE, T.H.

    Use of current stiffness parameter in solution of nonlinear problems.

    Energy methods in finite element analysis,

    Edts. Glowinski, R., Rodin, E.Y. and Zienkiewicz, o.c. John Wiley and Sons.

BERGAN, P.G.

    Automated incremental—iterative solution schemes.

    Numerical methods for nonlinear problems, Vol.1,

    Proceedings of the International conference, Swansea, Sep. 2—5 1980,

    Pineridge Press, Swansea.

BERGAN, P.G., et al.

    Solution techniques for nonlinear finite element problems.

    Int. Jnl. of Num. Methods in Eng., Vol. 12, pp. 1677—1696, 1978.

BOYLE, E.F. and JENNINGS, A.

Accelerating the convergence of elasto- plastic stress analysis.

Int. Jnl. of Num. Meth. in Eng., Vol. 7, pp. 232—235, 1973.

CHOW, Y.K. and KAY, S.

On the AITKEN acceleration method for nonlinear problems.

Computers and Structures, Vol. 19, No. 5—6, pp. 757—761, 1984.

COLLINS, R.J.

Bandwidth reduction by automatic renumbering.

Int. Jnl. Num. Meth. Eng., Vol. 6, 1973.

COPE, R.J.   RAO, P.V. and EDWARDS, K.R.

Nonlinear finite element analysis techniques for concrete slabs.

Numerical methods for nonlinear problems, pp. 445— 456,

Swansea, 2— 5 september 1980.

CRISFIELD, M.A.

Incremental/Iterative solution procedures for nonlinear
structural analysis.

Numerical methods for nonlinear problems, Vol. 1,

Proceedings of the International conference, Swansea, Sep. 2—5 1980,

Edts. Taylor, C., Hinton, E. and Owen, D.R.J.,

Pineridge Press, Swansea.

CRISFIELD, M.A.

The automatic nonlinear analysis of stiffened plates and
shallow shells using finite elements.

Proc. Instn. of Civ. Eng., Part 2, Dec. 1980, Vol. 69, pp. 891—909.

CRISFIELD. M.A.

A fast incremental/Iterative solution procedure that handles
snap through.

Computers and Structures, Vol. 13, pp. 56—62, 1981.

CRISFIELD, M.A.

Solution procedures for nonlinear structural analysis.

Recent advances in nonlinear computational mechanics,
Edts. Hinton, E. et al., Pineridge Press, Swansea, U.K., 1982
PP. 1—39.

CRISFIELD, M.A.

An arc— length method including line searches and accelerations.
Int. Jnl. of Num. Meth. in Eng., Vol.19, pp. 1269—1289, 1983.

CRISFIELD, M.A.

Accelerating and damping the modified Newton— Raphson method.
Computers and Structures, Vol. 18, No. 3, pp. 395—407, 1984.

GADALA, M.S. and ORAVAS, G.A.

Numerical solution of nonlinear problems of continua,
Survey of formulation methods and solution techniques.
Computers and Structures, Vol. 19, No. 5—6, pp. 865—877, 1984.

MATTHIES, C. and CONNOR, J.

The solution of nonlinear finite element equations.
Int. Jnl. of Num. Meth. in Eng., Vol. 14, pp. 1613—1626, 1979.

MONDKAR, D.P. and POWELL, G.H.

Evaluation of solution schemes for nonlinear structures.
Computers and Structures,

NAYAK, G.C. and ZIENKIEWICZ, O.C.

Note on the ALPHA— constant stiffness method for the analysis
of nonlinear problems.
Int. Jnl. of Num. Meth. in Eng., Vol. 4, pp. 579—582, 1972.

ODEN, J.T.

Numerical formulations of nonlinear elasticity problems.
Jnl. Eng. Str. Div., ASCE, Vol. 93, pp. 235—255, 1967

PADOVAN, J. and LACKNEY, J.

On the development of hierarchical solution strategies for
nonlinear finite element formulations.

Computers and Structures, Vol. 19, No. 4, pp.535—544, 1984.

PADOVAN, J. and MOSCARELLO, R.
Locally bound constrained Newton— Raphson solution algorithms.
Computers and Structures, Vol. 23, No. 2, pp. 181—197, 1986.

PINA, H.L.G.
An algorithm for frontwidth reduction.
Int. Jnl. Num. Meth. Eng., Vol. 17, 1981.

PUTTONEN, J.
Simple and effective bandwidth reduction algorithm.
Int. Jnl. Num. Meth. Eng., Vol. 19, 1983.

RAMM, E.
Strategies for tracing nonlinear response near limit points.
Nonlinear finite element analysis in structural mechanics,
Proceedings of the Europe—U.S. Workshop, 28—31 July 1980,
Edts. Wunderlish, W., Stein, E. and Bathe, K.J.
Springler—Verlag, New—York, 1981, pp. 63—89.

RAZZAQUE, A.
Automatic reduction of frontwidth for finite element analysis.
Int. Jnl. Num. Meth. Eng., Vol. 15, 1980.

RIKS, E.
The application of Newton's method to the problem of elastic stability.
Jnl. Appl. Mech, Vol. 39, pp. 1060—1066, 1972.

WEMPNER, G.A.
Discrete approximations related to nonlinear theories of solids.
Int. Jnl. Solids. Struct., Vol. 7, pp. 1581—1599, 1971.

ZIENKIEWICZ, O.C., VALLIAPAN, S. and KING, I.P.
Elasto— plastic solution of engineering problems,
Initial stress finite element approach.
Int. Jnl. of Num. Meth. in Eng., Vol. 1, pp.75—100, 1969.

CHAPTER 5

VALIDATION OF THE NUMERICAL MODEL

In the previous sections the theoretical aspects of the computational method adopted in the present nonlinear analysis of reinforced concrete have been described. In this section, some practical applications of the proposed model are presented and comparisons with experimental and other numerical results are given. The main purpose is to verify the applicability and the accuracy of the numerical model against various carefully conducted experimental tests involving different members exhibiting various modes of failure. This was found necessary before a complete nonlinear study of reinforced concrete coupled shear walls is performed as reported in the next chapter.

The load deformation responses of reinforced concrete panels and beams (shallow, moderate and deep) including ultimate load, cracking patterns and directions at various stages of loading are investigated. The numerical model has been tested against the following experimental results :

(1)— Cervenka's shear panel W2.

(2)— Gijsbers and Smit beam.

(3)— Wallraven moderately deep beam.

(4)— Maier and Thuerlimann shear wall panels.

    — Flanged panels (S1,S2),

    — Panels without flanges (S4,S9 and S10).

(5)— Bresler's shallow beam.

(6)— Bresler and Scordelis beam OA1

(7)— Bresler and Scordelis beam OA2

(8)— Bresler and Scordelis beam OA3

(9)– Khaskeli continuous deep beam

(10)– Vecchio and Collins panels

   – Panel 25 (plane stress)

   – Panel 27 (pure shear)

(11)– Murazumi et al. shear walls with large openings.

Most of the reinforced concrete structures considered above to check the validity of the numerical model failed in shear mode. It is well known that reinforced concrete structures failing in flexure are somewhat easier to predict the behaviour. The stiffness matrix is updated at the second iteration of every increment and a constant shear retention factor $\beta = 0.5$ has been adopted unless otherwise stated.

5-1 CERVENKA'S Shear panel W2 :

The first example deals with a reinforced concrete shear panel W2 tested by Cervenka and Gerstle 1972. The test panel is orthogonally reinforced concrete square plate 30X30in., 3 inches in thickness, reinforced as indicated in Fig (5-1). The horizontal reinforcement was varied, so that a larger percentage was placed in the bottom six inches of the panel than was placed in the top twenty four inches. The shear panel, shown in Fig (5-1), was cast in two combined panels to form one beam-like specimen to simplify the testing procedure. This arrangement enabled testing of the beam as a simply supported beam with midpoint load. The concentrated reactions at the supports and the load point are transmitted to the panels by three vertical ribs as shown in Fig(5-1). These ribs help to maintatin the lateral stability of the specimen during testing. The test specimen W2 tested by Cervenka and Gerstle 1972 is analysed by the finite element program developed in this study. The finite element idealization of the panel is shown in Fig (5-2). A total of 224 nodes and 195 elements involving 3x3 gauss integration order to integrate the element stiffness and to monitor the state of the material were used to discretize half of the panel taking accont of symmetry.

Comparison between the numerical and experimental load displacement response as obtained by Cervenka and Gerstle and the numerical prediction in this study is shown in Fig (5-3). The effect of using various shear retention factors (β= 0.3,0.5,0.7) simulating smooth to rough crack interface can be seen to have little influence on the ultimate load. The ability of the proposed model to duplicate experimental crack pattern is demonstrated in Fig (5-4) for three different load levels. The comparison is reasonable for 14.0 Kips and quite good for 24.0 Kips, where predicted crack locations and crack directions reveals a good agreement with the experimental results The analytical solution indicates the presence of cracks in

the centre thickened rib. Whether or not these cracks were present in specimen W2 cannot be ascertained. The experimental crack pattern also indicates that local crushing of concrete in the compressive zone of the specimen occured. This type of behaviour is also indicated by the analytical solutions where high compressive stresses $(0.85 \, f_c')$ developed but no actual crushing occured.

It may be concluded that the analytical solution gave a reasonable duplication of the experimental behaviour of this test specimen in terms of load−deflection up to failure, and crack direction and location at different stages of loading.

Reinforcement: #3 4 × 4 mesh
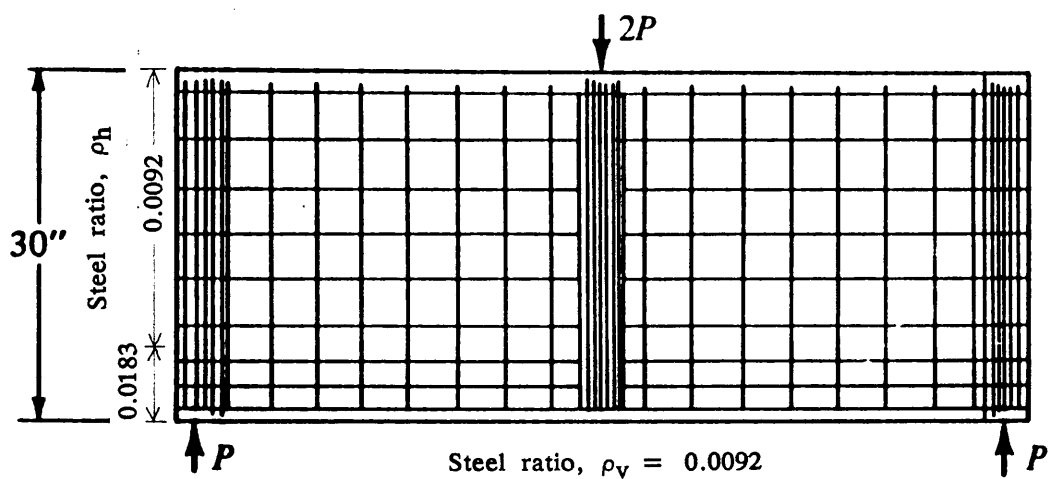
Elevation
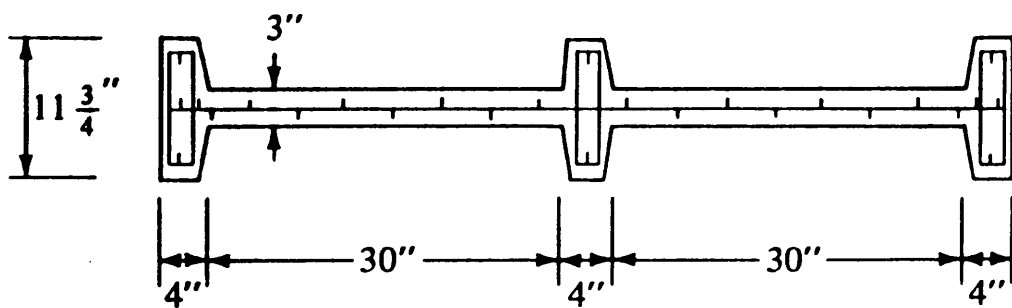
Section

Concrete: $f'_c = 3880$ lb/in^2 $f'_t = 529$ lb/in^2 $E_c = 2.9 \times 10^6$ lb/in^2

Steel: $f_y = 51,200$ lb/in^2 $E_s = 27.3 \times 10^6$ lb/in^2

FIG (5-1) Dimensions, reinforcement and loading for Cervenka's panel W2.
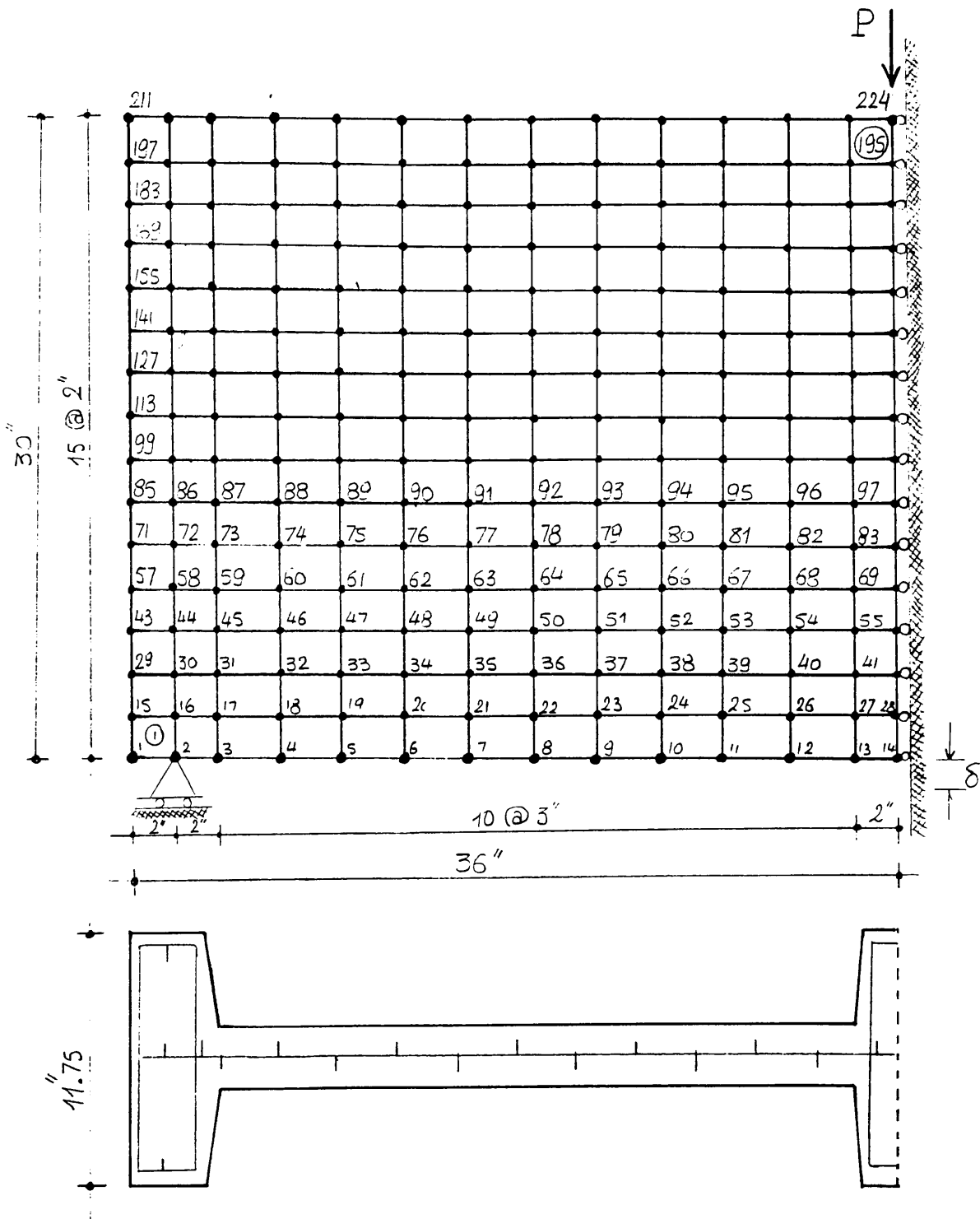
Fig (5—2) Finite element discretization of Cervenka's panel W2.
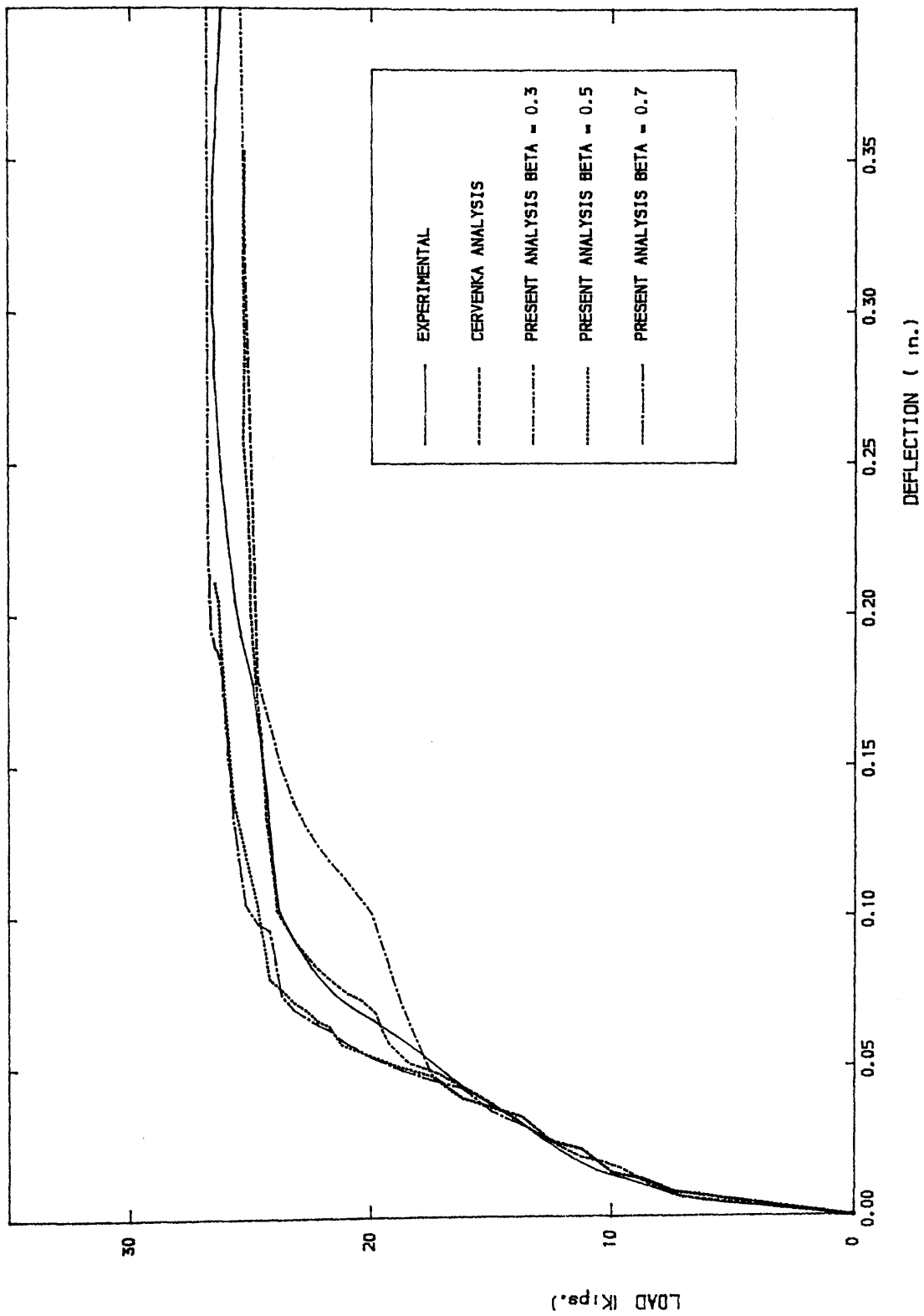
Fig (5-3) Load deflection for Cervenka's RC panel.

P = 14.0 Kips

P = 24.0 Kips

P = 25.5 Kips
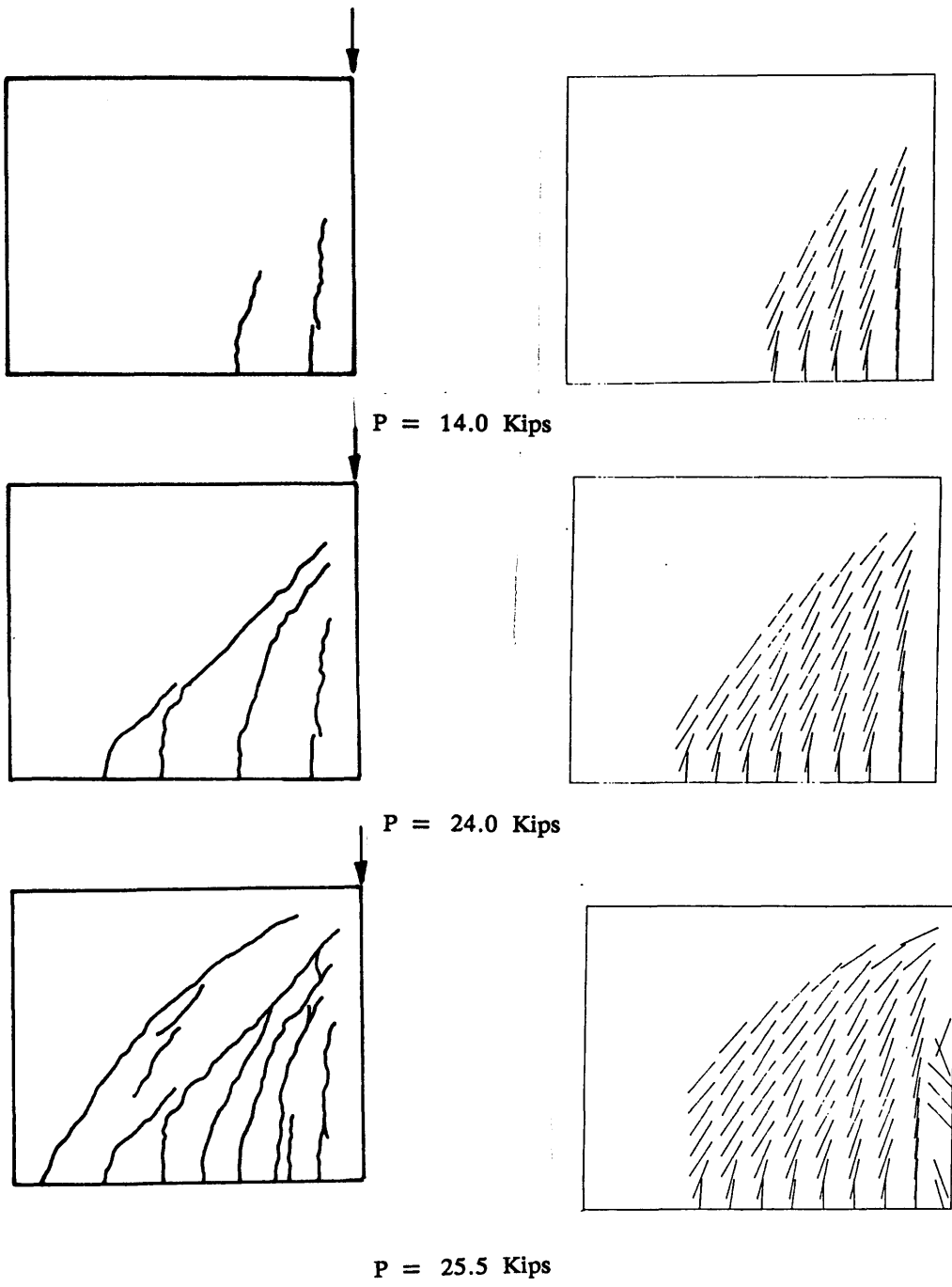
Fig (5-4) Comparison of numerical and experimental crack patterns for panel W2.

5— 2 Gijsbers and Smit beam failing in diagonal tension:

Here, a beam which was selected from an experimental programme carried out by Gijsbers & Smit 1977 has been nmerically modelled. The testing programme was original in the sense that the beams were subjected to a uniformly distributed load, while the majority of tests reported in literature has concentrated on single or multiple point loading systems. The distributed load means that both the experiment and the numerical modelling predictions have to be performed under load control.

As shown in Fig (5— 5), the actual beam was relatively small compared with the large supporting end blocks that had been added in order to introduce the desired moment/shear ratios. By varying the sizes a,e and L the moment/shear ratio as well as the slenderness of the beam could be varied. In this way a wide range of shear failure mechanisms had been investigated. This included diagonal tension failure and shear— compression failure, one of which will be considered here.

The beam to be studied contained compressive as well as tensile reinforcement, but no stirrups. The bending moment at midspan amounts to three times the bending moment at the clamped end. The material data and the beam are shown in Fig (5— 5). The finite element mesh used for this beam is shown in Fig (5— 6). The calculated load deflection at midspan are compared to the experimental results of Gijsbers and Smit 1977 and the numerical prediction of Rots et al. 1985 in Fig (5— 7). Two sets of numerical results, one using a moderate shear retention factor $\beta = 0.5$ and the other using a high shear retention factor $\beta = 0.7$ are used. A good agreement with the experimental results is observed at failure. The numerical results seem to give stiffer behaviour than the observed experimental test in the early stages of loading. The experiment was characterised by the abrupt loss of stiffness in the final stage which was due to the sudden development of a diagonal tension crack.

At first sight, the numerical analysis appears to be capable of reproducing this

complex type of shear failure. Closer examination of the   load displacement curve reveals a noteworthy irregularity, namely an important decrease of stiffness at a loading level of about 70 kN/m. It is instructive to plot the crack patterns just before this irregularity (q= 69kN/m) and just beyond it (q= 75kN/m). This is done in Fig (5– 8) & Fig (5,9). Note that these two loading levels roughly coincide with impending experimental failure and experimental failure respectively. The diagram reveals that it is not only the experiment but also the numerical analysis leads to a dominant crack developing solely within such a limiting loading interval. Although the type of failure mechanism and failure load are reproduced quite well, it is rather disappointing that the numerical load deflection response is significantly stiffer than the experimental over a wide range of loading. This stiffer response in the elastic range of loading may be attributed to the material properties such as Young's modulus or the finite element needs further refinement.
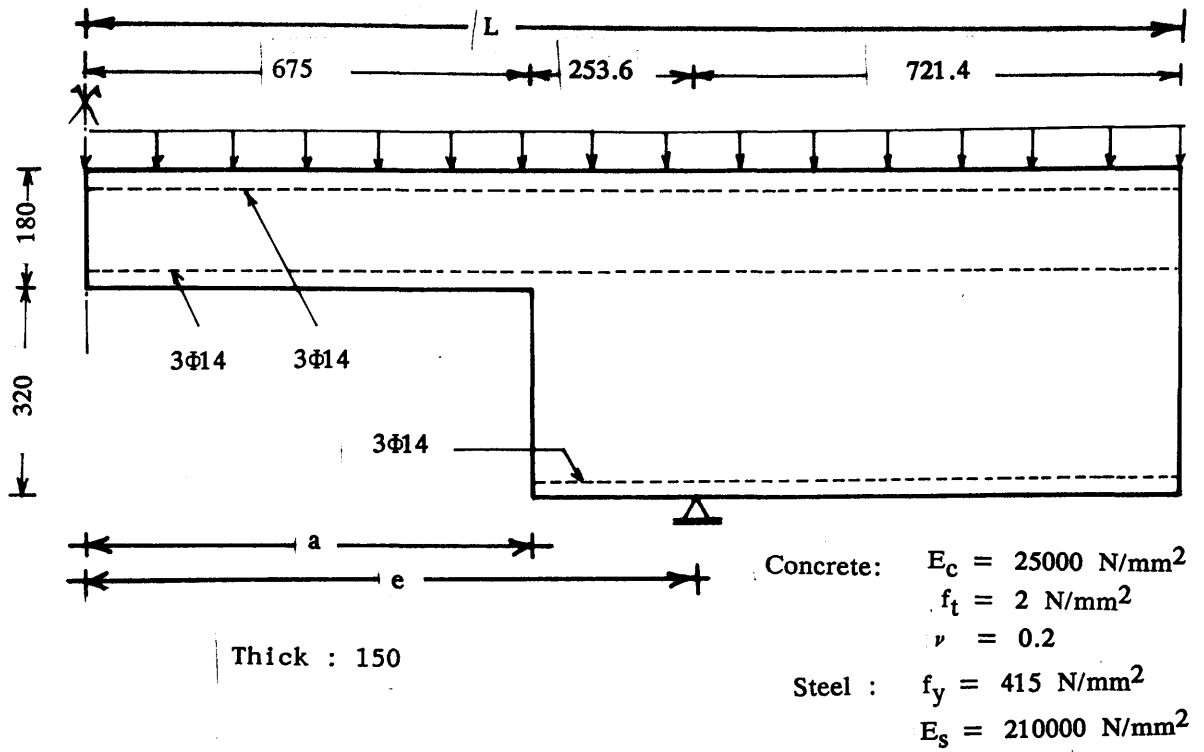
Fig (5-5) Reinforced concrete beam (Gijsbers and Smit 1977).
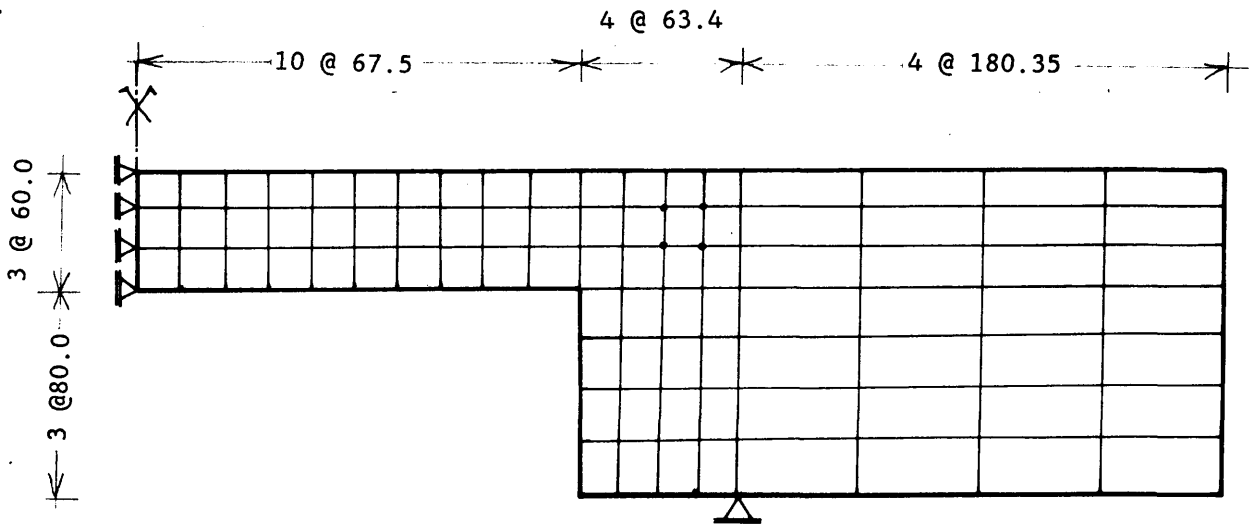
Fig (5-6) Finite element idealization for reinforced beam.

FIG (5-7) NUMERICAL AND EXPERIMENTAL LOAD DEFLECTION CURVE

Legend:

——	EXPERIMENTAL Gijsbeq
——	Rots et al. 1985
—·—·—	BETA = 0.5
········	BETA =0.7

DEFLECTION AT MIDSPAN (mm)

LOAD q (Kn/m)
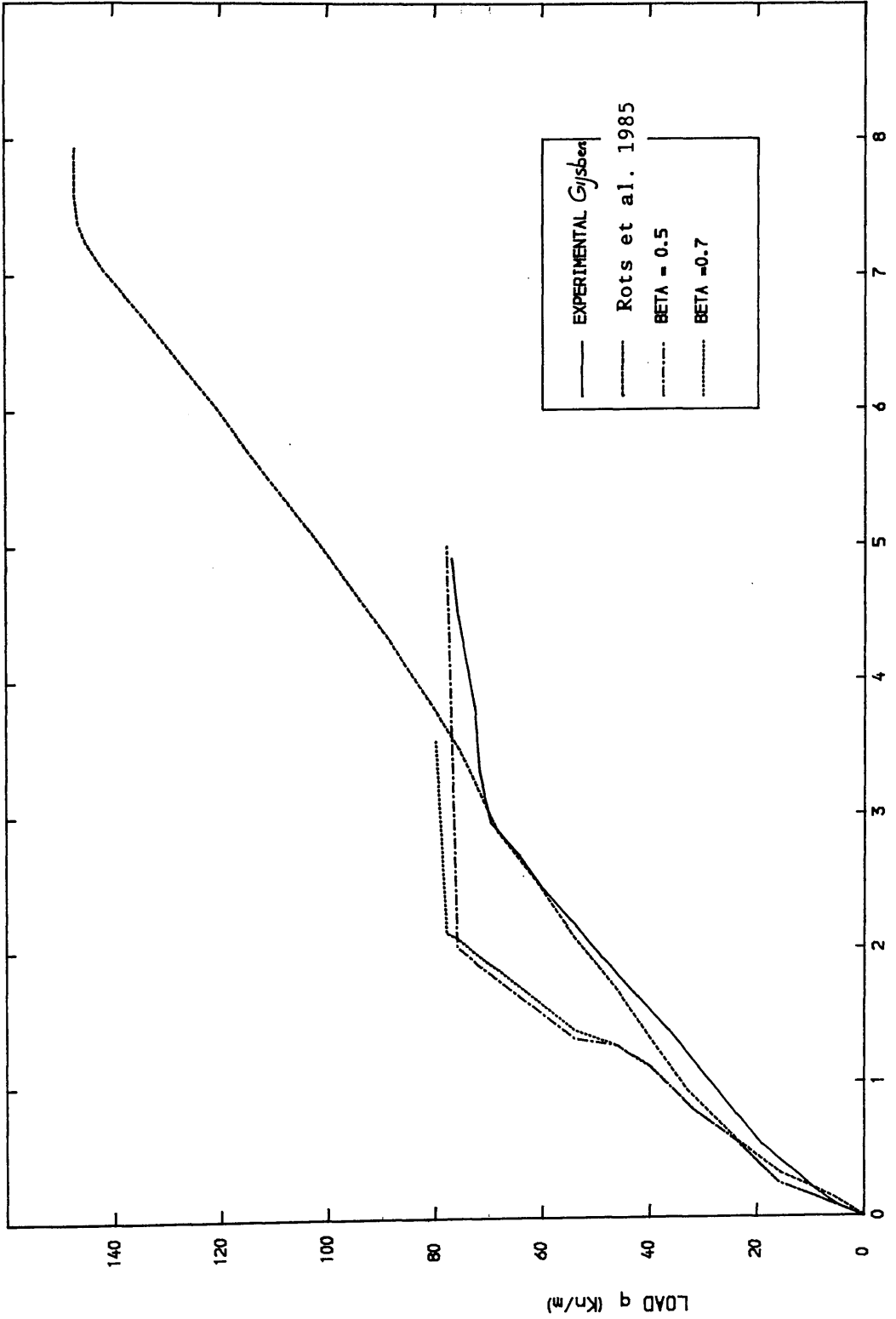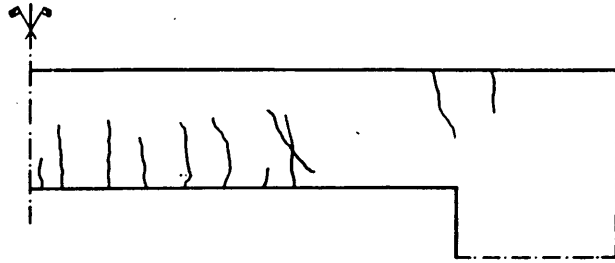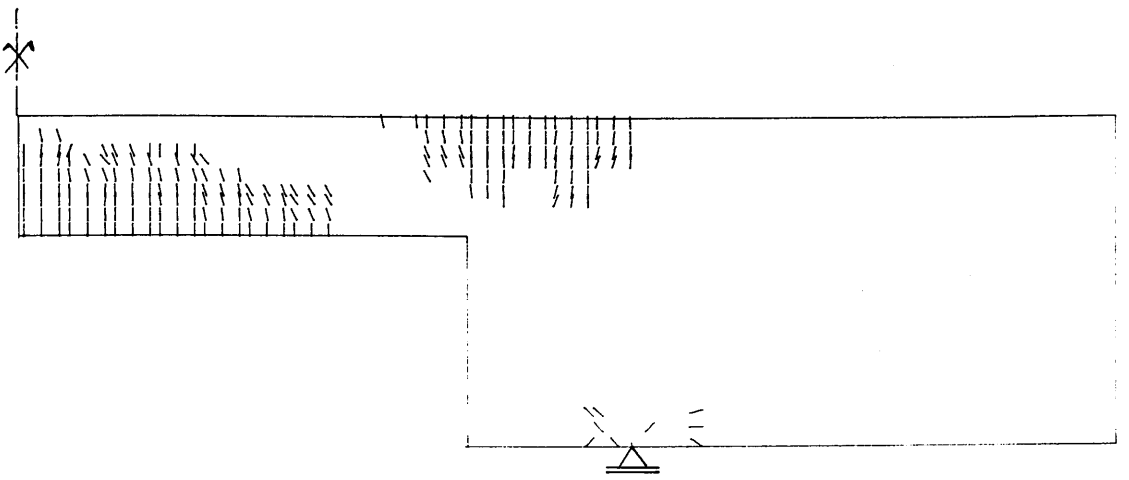
Fig (5-8) Crack pattern at impending failure (q=69kN/m).
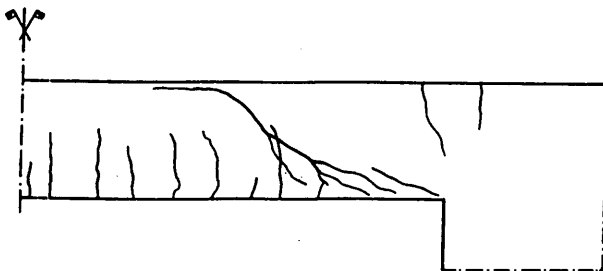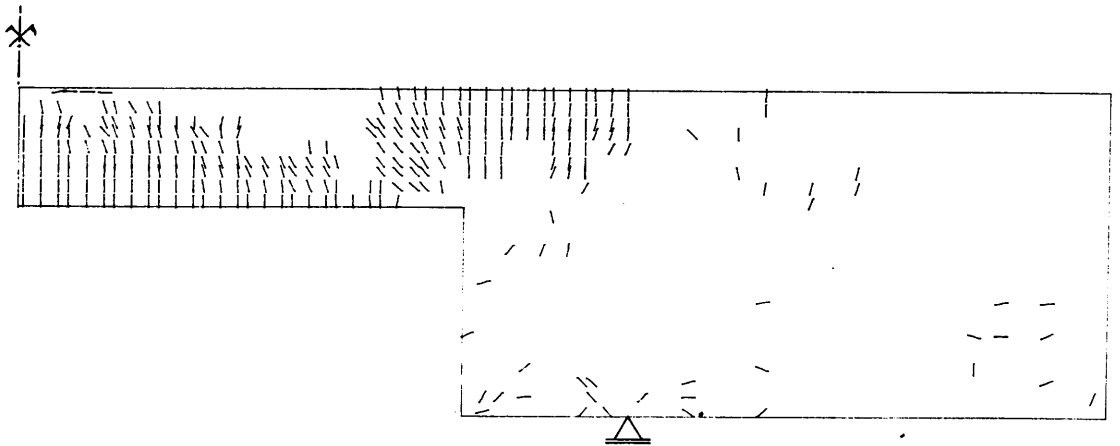
Fig (5-9) Crack pattern at failure (q=75kN/m).

5-3 WALLRAVEN'S moderately deep beam :

The moderately deep beam of Fig (5-10) has been considered. This beam failing in shear has been tested experimentally by Wallraven 1977 and has been analysed by DE Borst 1986 using the DIANA finite element program.

The beam had a thickness of 200mm and had no shear reinforcement as shown in Fig (5-10). The material properties of concrete and longitudinal reinforcement at the bottom of the beam are summarized below:

Concrete: Steel :

E_c = 28000 N/mm^2 E_s = 210000 N/mm^2

f_c = 40 N/mm^2 f_y = 440 N/mm^2

f_t = 2.5 N/mm^2

ν = 0.20

In the experiment, it was observed that shear failure occured due to diagonal cracks. Prior to the development of diagonal cracks, vertical cracks had arisen predominantly in the constant moment zone. In the numerical analysis the observed vertical cracks due to bending arise first. On subsequent loading the principal stresses rotate due to high shear stresses and new non-vertical cracks form.

The present study tests the possible impact of the values of the shear retention factor β on the computational results. Numerical results have been carried out for 3 different values of the shear retention factor, namely $\beta=0.3$, $\beta=0.5$ and $\beta=0.7$ simulating smooth to rough crack surfaces. In all analyses vertical cracks due to bending arise first. On subsequent loading the stresses rotate and new, non-vertical cracks due to shear form in the region between the point load and the supports Figs (5-11),(5-12). In Fig (5-13) no marked difference exists between the numerical results for the different values of the shear retention factor β on the load displacement curve which is in good agreement with the experimental results.
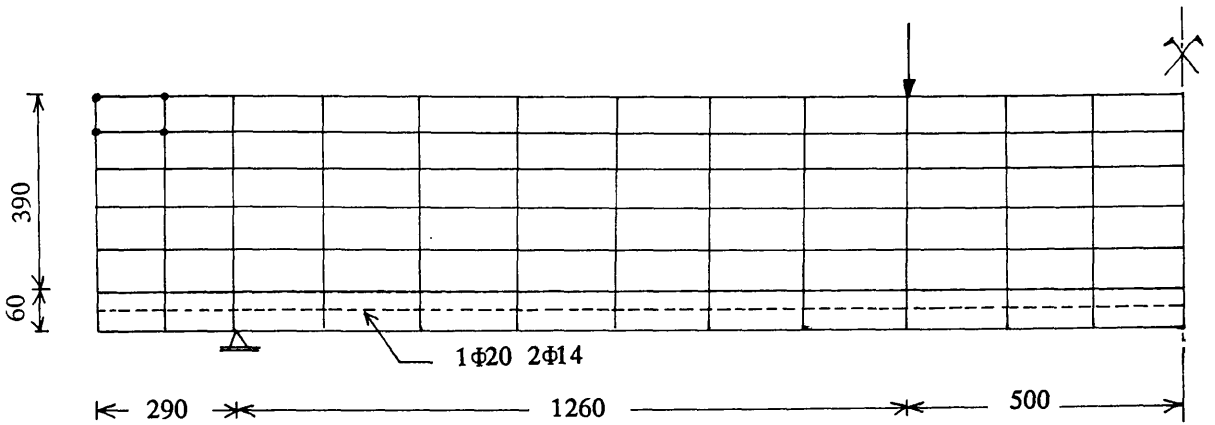
Fig (5-10) Finite element mesh for moderately deep beam.
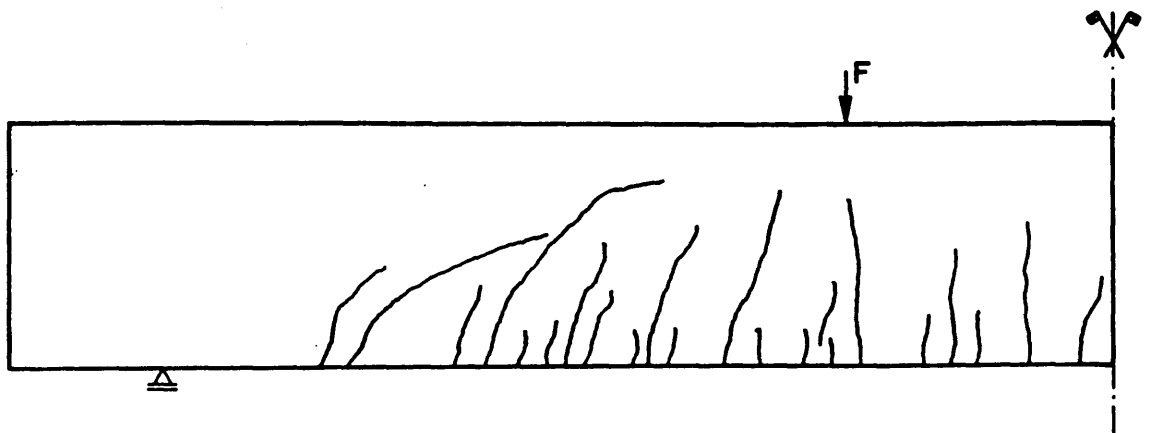
Fig (5-11) Experimentally recorded crack pattern at
impending failure.
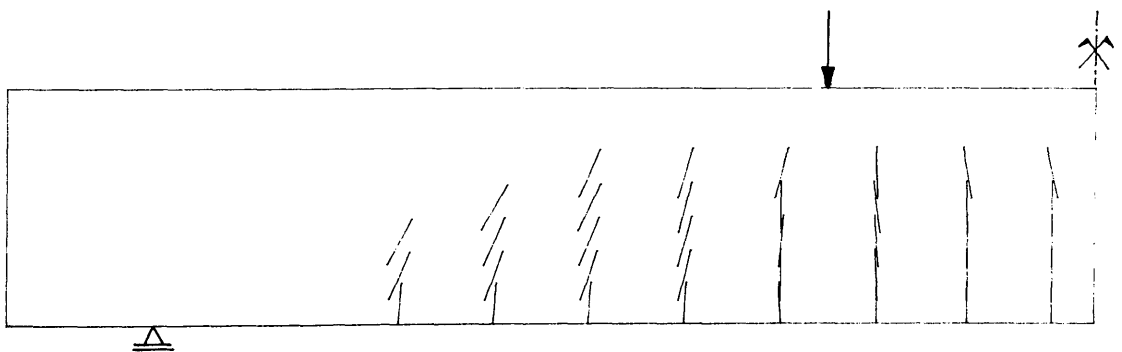
Fig (5-12) Predicted crack pattern at impending failure
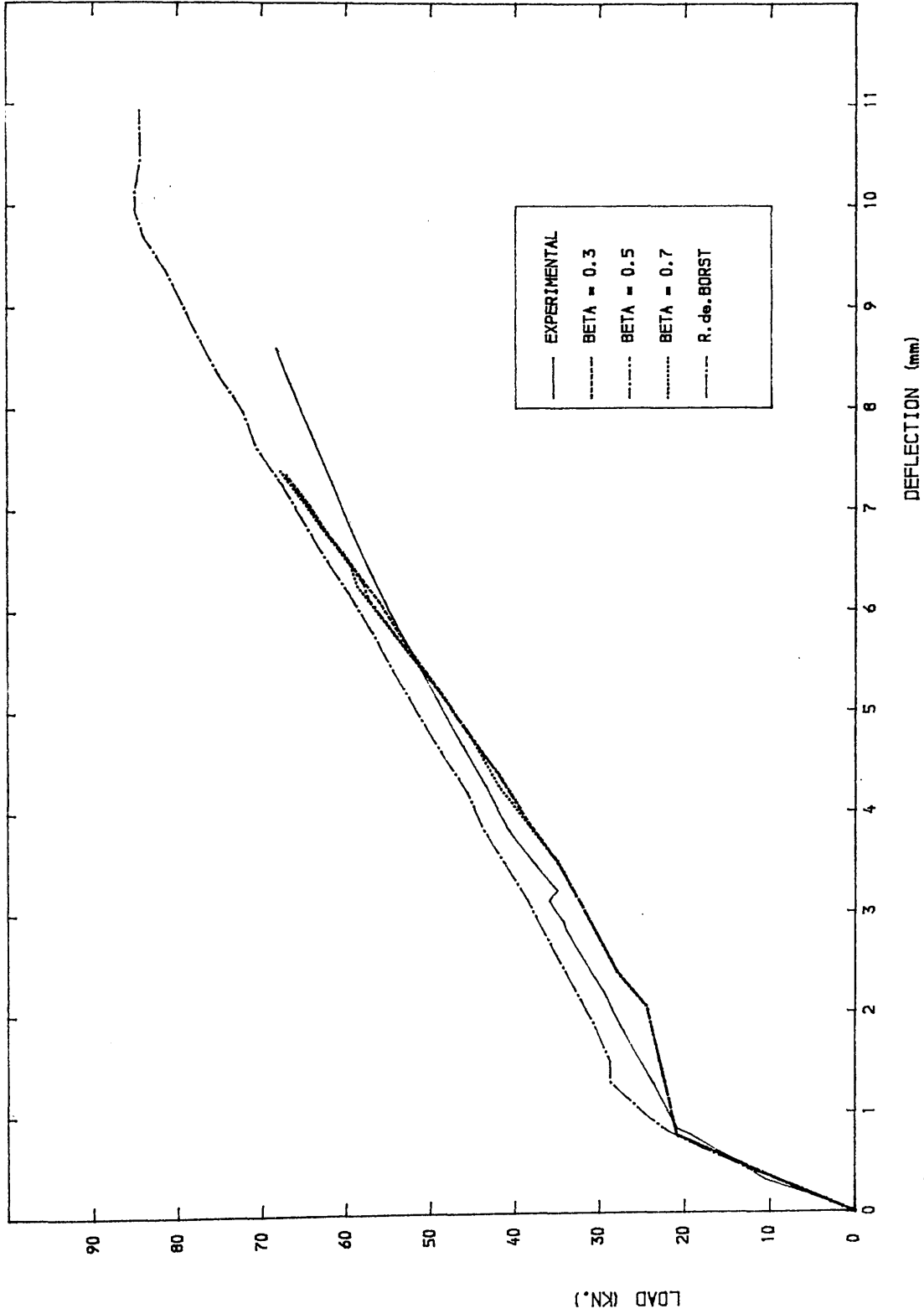
Fig (5-13) LOAD DEFLECTION FOR WALLRAVEN MODERATELY DEEP BEAM

5-4 MAIER and THUERLIMANN shear wall panels :

Maier and Thuerlimann 1986 studied experimentally the failure behaviour of shear wall panels. The study described below concerns numerical analysis of several of these panels, by means of the finite element program developed. The major objective is to show to which extent the failure behaviour can be simulated.

Five of the ten shear wall panels tested by Maier and Thuerlimann 1986 are analysed. These panels are of two different forms, flanged (panels S1,S2) and unflanged (panels S4,S9 and S10) as shown in Fig (5-14). The panels were supported on a rigid block base and loaded through a top slab Fig (5-15). The loads include vertical forces F_v and a horizontal force F_h. F_v was first applied under load control before F_h was applied by monotonic displacement control. Reinforcement was provided in both vertical and horizontal directions. Fig (5-14) summarizes the amount of reinforcement and the values of the average vertical stress σ_y caused by F_v. All the panels were essentially isotropically reinforced except panel S9 where only vertical reinforcement was present. The initial vertical compressive stress was rather low, except for panel S2 which was initially compressed to 0.3 f'_c. The material properties of concrete which varied slightly for different cases are summarized below:

	PANELS S1,S2 (With flanges)	PANELS S4,S9 & S10 (No flanges)
CONCRETE :		
Young's modulus	E_c = 34000.0	28000.0 MPa
Cylinder strength	f'_c = 35.0	30.0 MPa
Tensile stress	f_t = 3.2	3.0 MPa
STEEL :		
Young's modulus	E_s = 198000.0	198000.0 MPa
Yield stress	f_y = 495-575 MPa	

The panels were assumed to be in a state of plane stress, so the web and the flanges were modelled with plane stress elements of different thickness. The finite element mesh used for the analysis is shown in Fig (5–15).

The results of analysis are now discussed and compared to the experimental observations of Maier et al. and numerical predictions of Wang et al. 1990.

Panels S4 and S10 without flanges and isotropically reinforced:

These two panels were both isotropically reinforced and only different in that panel S10 had extra reinforcement in the tension side. Figs.(5–16),(5,17) show the calculated load displacement responses. Good agreement to the experiment was achieved for both panels. Typical crack results for panel S10 are presented in Fig (5–18) showing a good fit to the test results at three different stages of loading.

Panel S9 without vertical reinforcement:

This is an extreme situation of orthotropy with only vertical reinforcement. It is found to be difficult to simulate accurately the load displacement response, Fig(5–19). The predicted response agreed reasonably well with the experimental response in the early stages of loading but deviates much at failure. High distortions of the finite element grid at failure is shown in Fig (5–20). The predicted and experimental crack pattern at failure are shown in Fig (5–21). Although the horizontal flexural cracks in the right flange and the diagonal cracks in the panel are reproduced well, the analytical model predicted cracks in the left flange not observed during the experiment where a major diagonal crack was observed at failure.

Panels S1 and S2 with flanges:

The calculated load displacement responses and the maximum loads are in satisfactory agreement with the test for both panels as shown in

Figs.(5— 22),(5— 23). Similarly to the panels without flanges, yielding of the reinforcement can be observed at high load stages. The deformed finite element mesh for panel S2 at failure is shown in Fig(5— 24), where slight lateral displacement of nodes 15— 21 is slightly different due to cracking. Experimental and predicted crack patterns at failure for panel S2 are compared in Fig (5— 25).

Panels without flanges   Panels with flanges
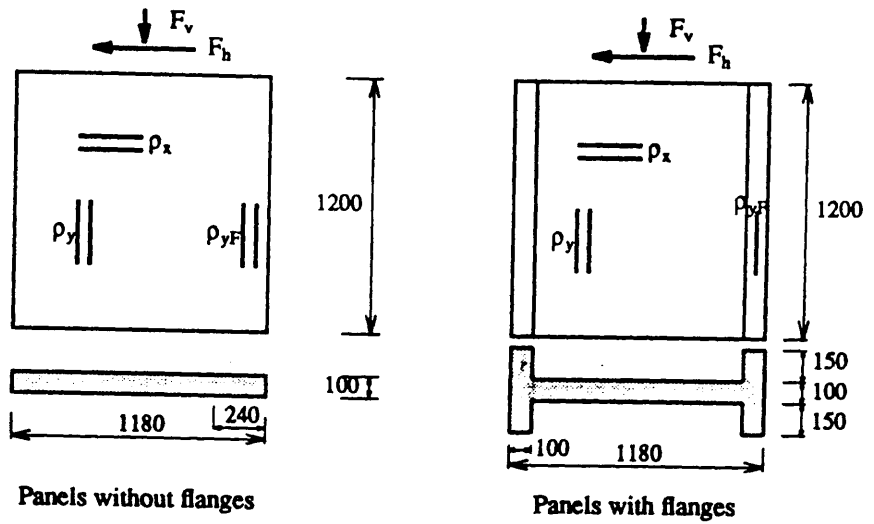
Panels	Geometry	ρ_x 10^{-3}	ρ_y 10^{-3}	ρ_{yf} 10^{-3}	σ_y N/mm^2
S1	With flanges	10.3	11.6	11.6	-2.43
S2	With flanges	10.3	11.6	11.6	-9.29
S4	No flanges	10.3	10.5	10.5	-2.22
S9	No flanges	0.0	9.9	9.9	-2.20
S10	No flanges	9.8	10.0	57.1	-2.22

Reinforcement ratio and initial vertical stress

Fig (5-14) Geometry of the panels (dimensions in mm).
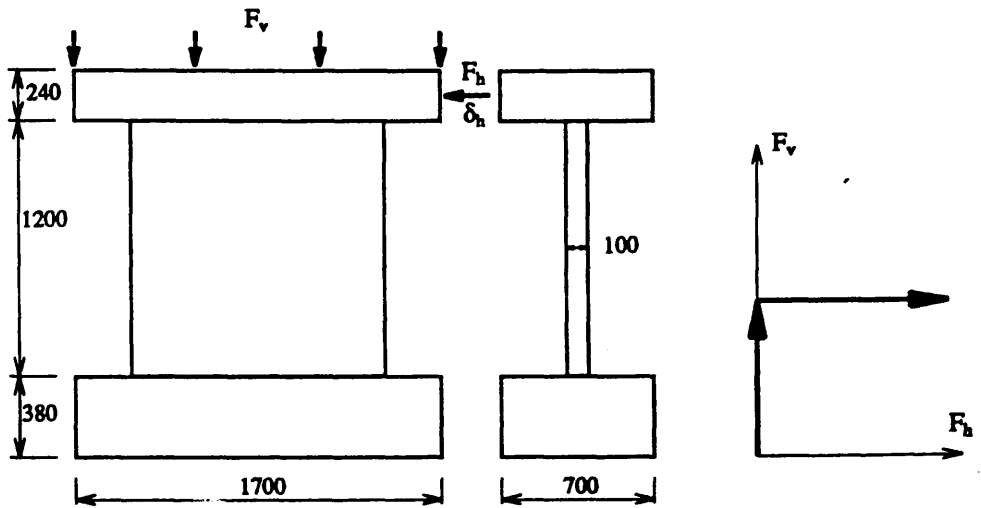
(a) Test set-up and loading path

Panels (S1, S2)

Panels (S4, S9 and S10)
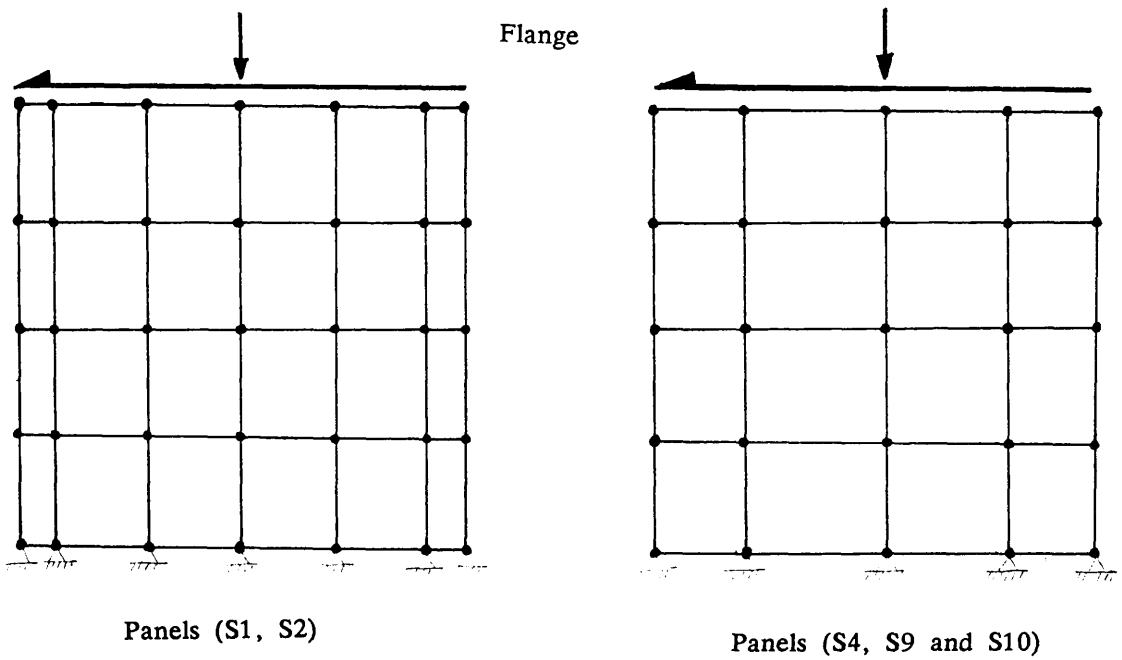
(b) Finite element discretization

FIG (5-15) TEST SET UP AND NUMERICAL MODEL
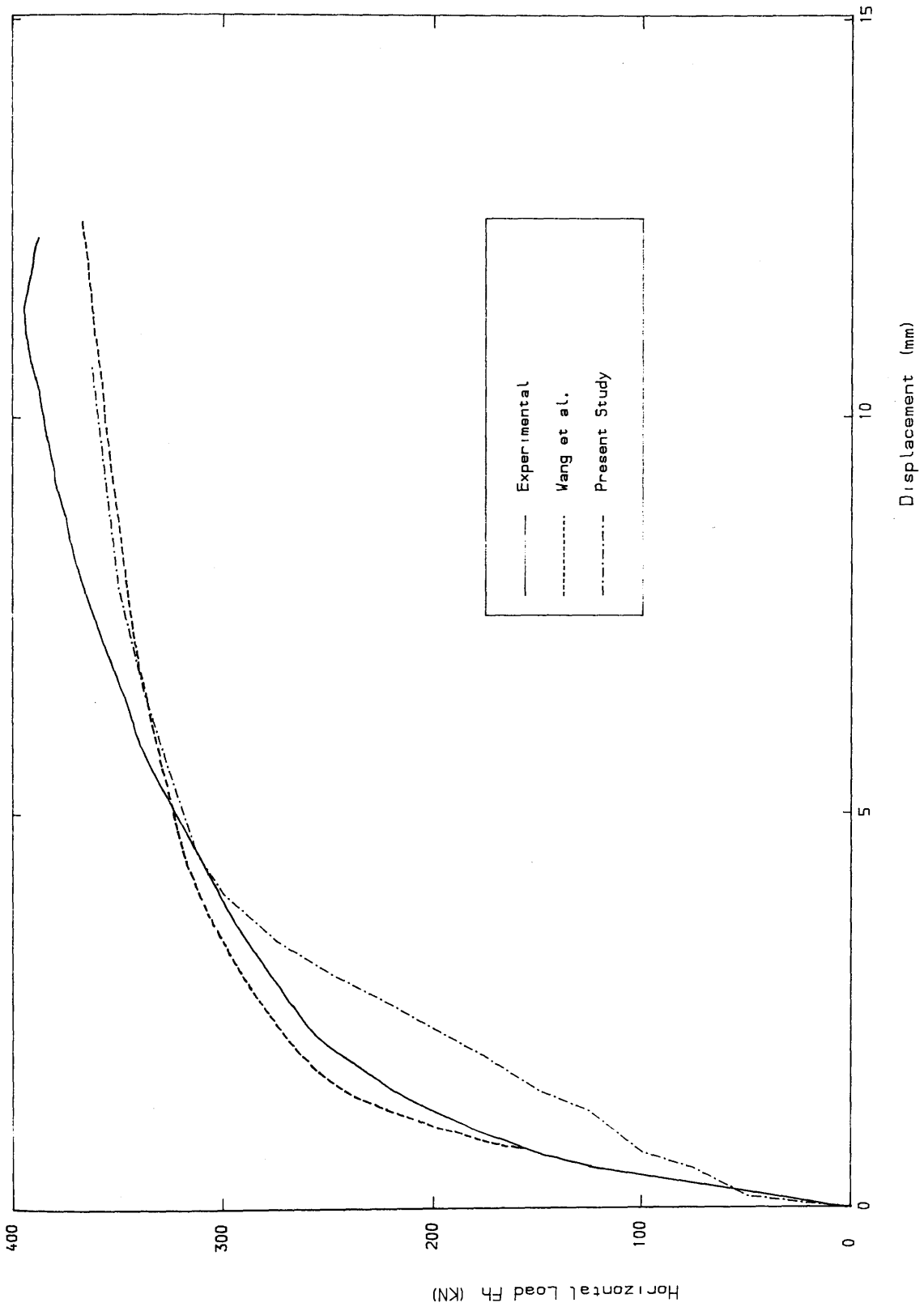
Fig (5-16) Load displacement response for panel (S4).
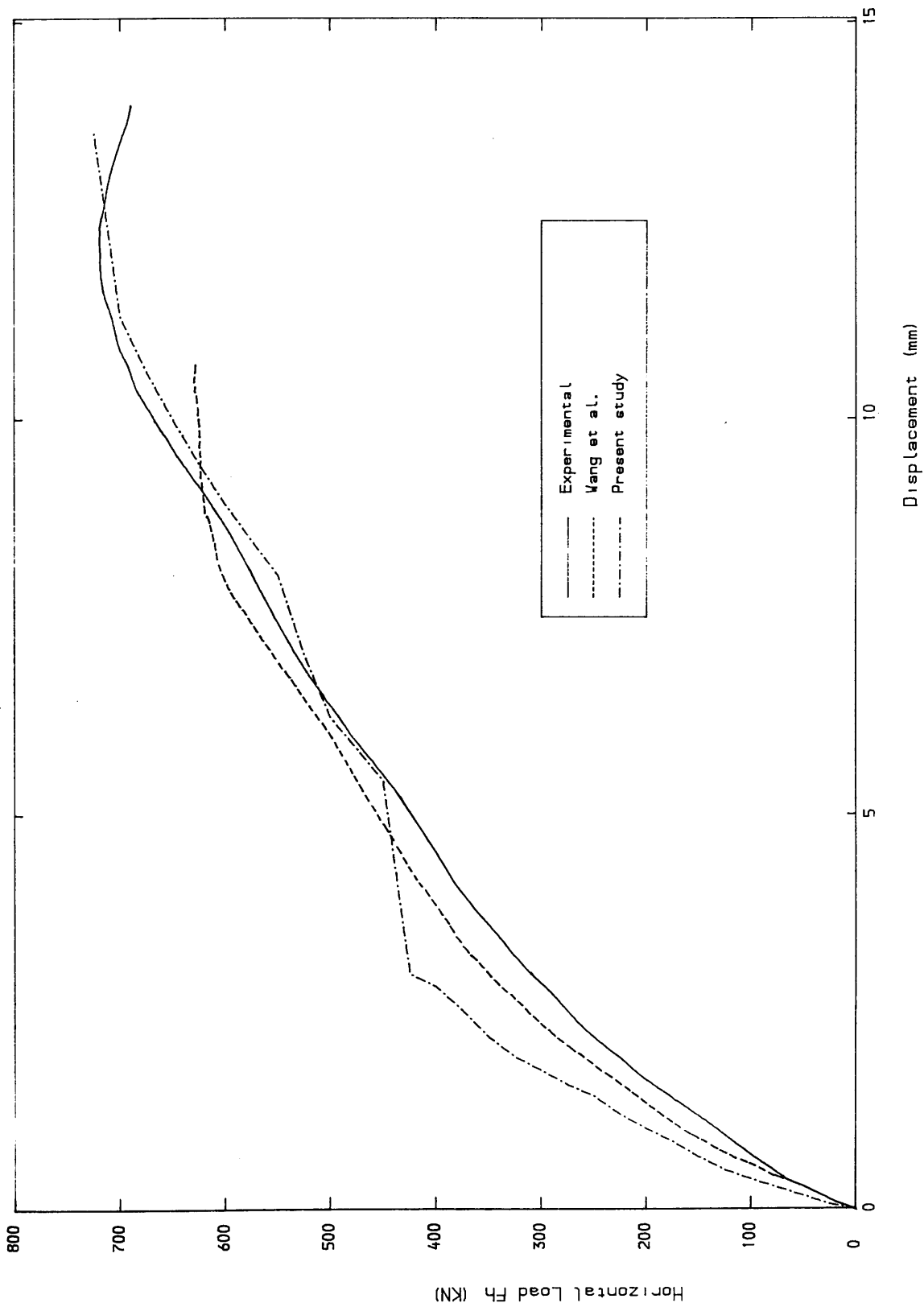
Fig (5-17) Load displacement response for panel (S10).
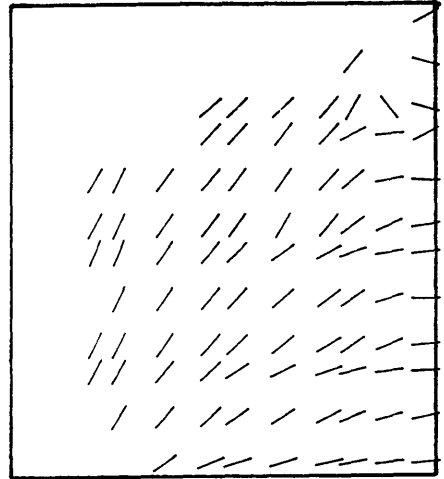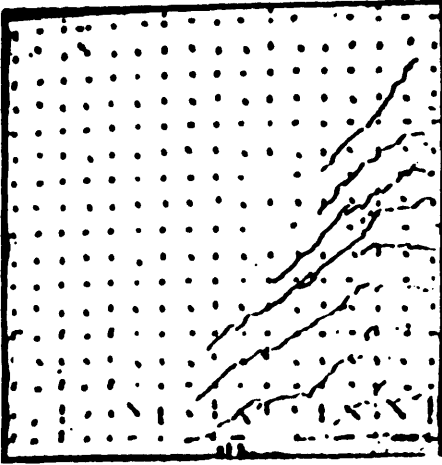
$\delta_h = 2.7$ mm
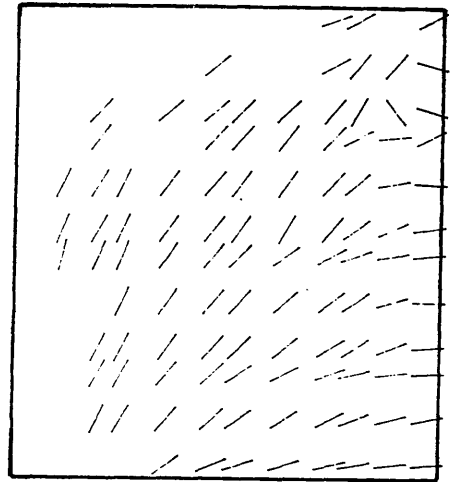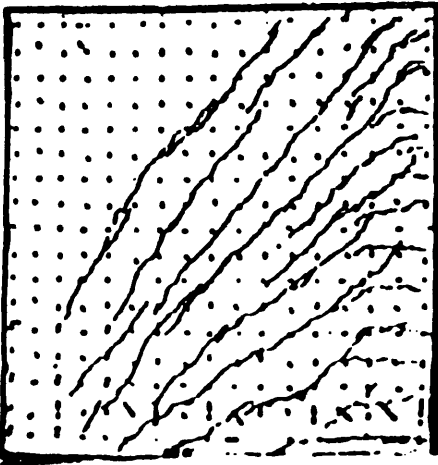
$\delta_h = 5.5$ mm
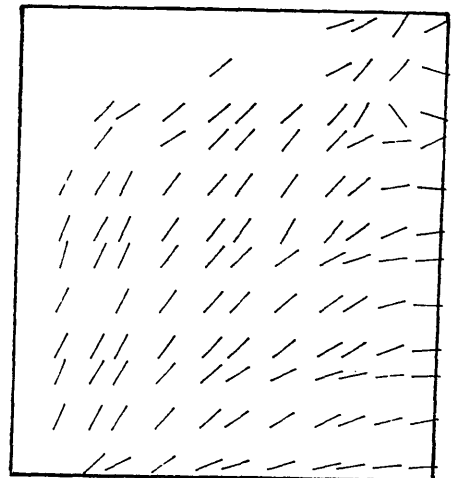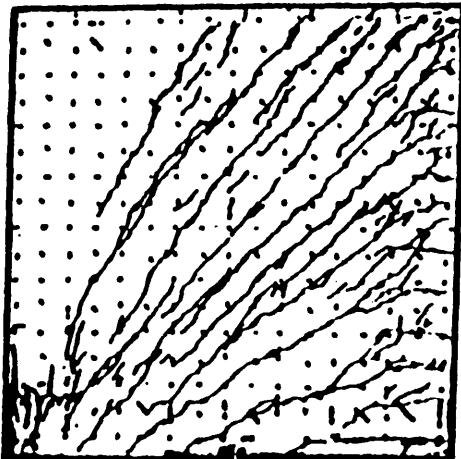
$\delta_h = 12.5$ mm

Fig (5-18) Crack development of panel (S10).
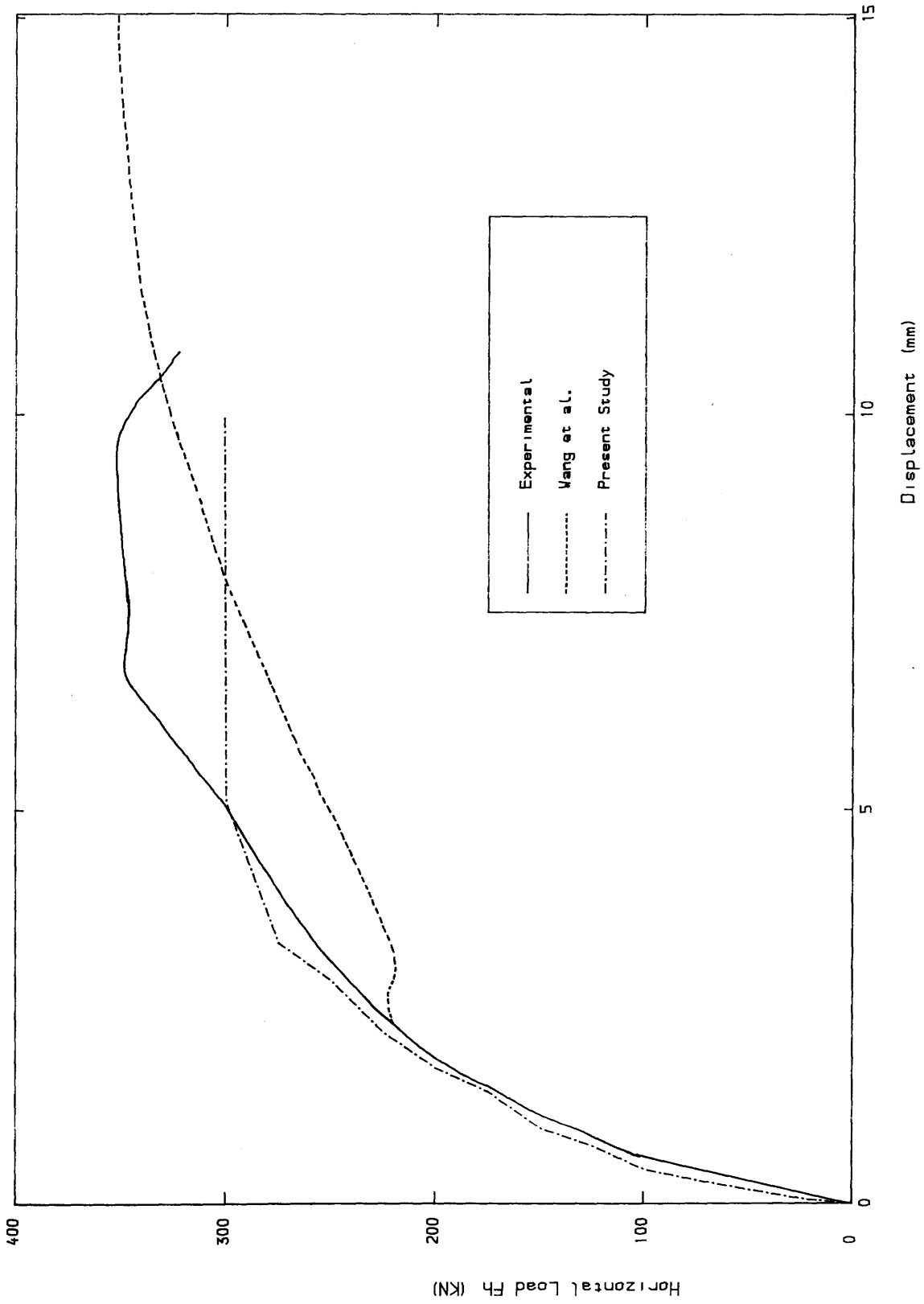
Fig (5-19) Load displacement response for panel (S9).
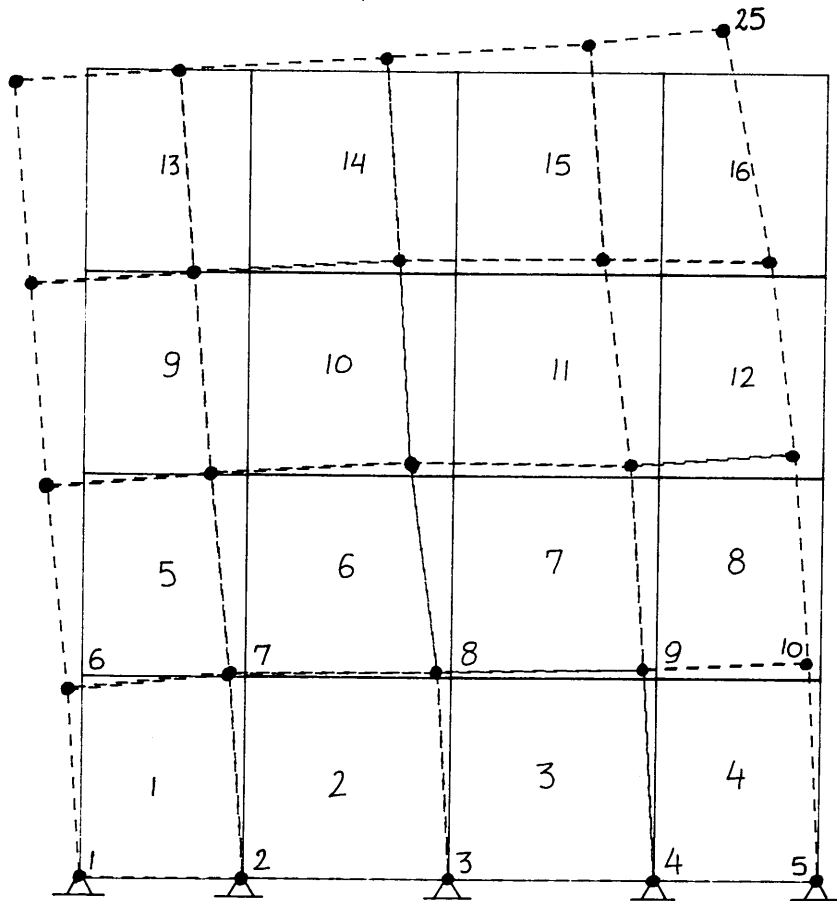
Fig (5-20) Finite element mesh at failure of panel (S9).
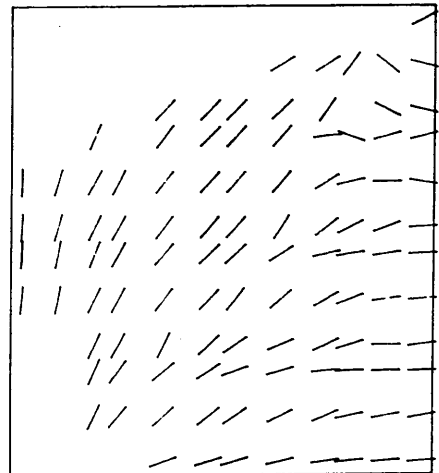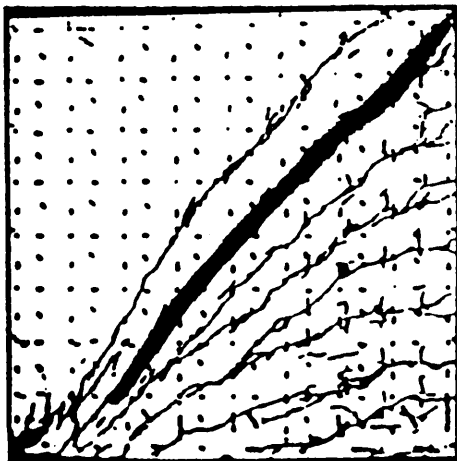
Fig (5-21) Predicted and experimental crack pattern
for panel (S9).
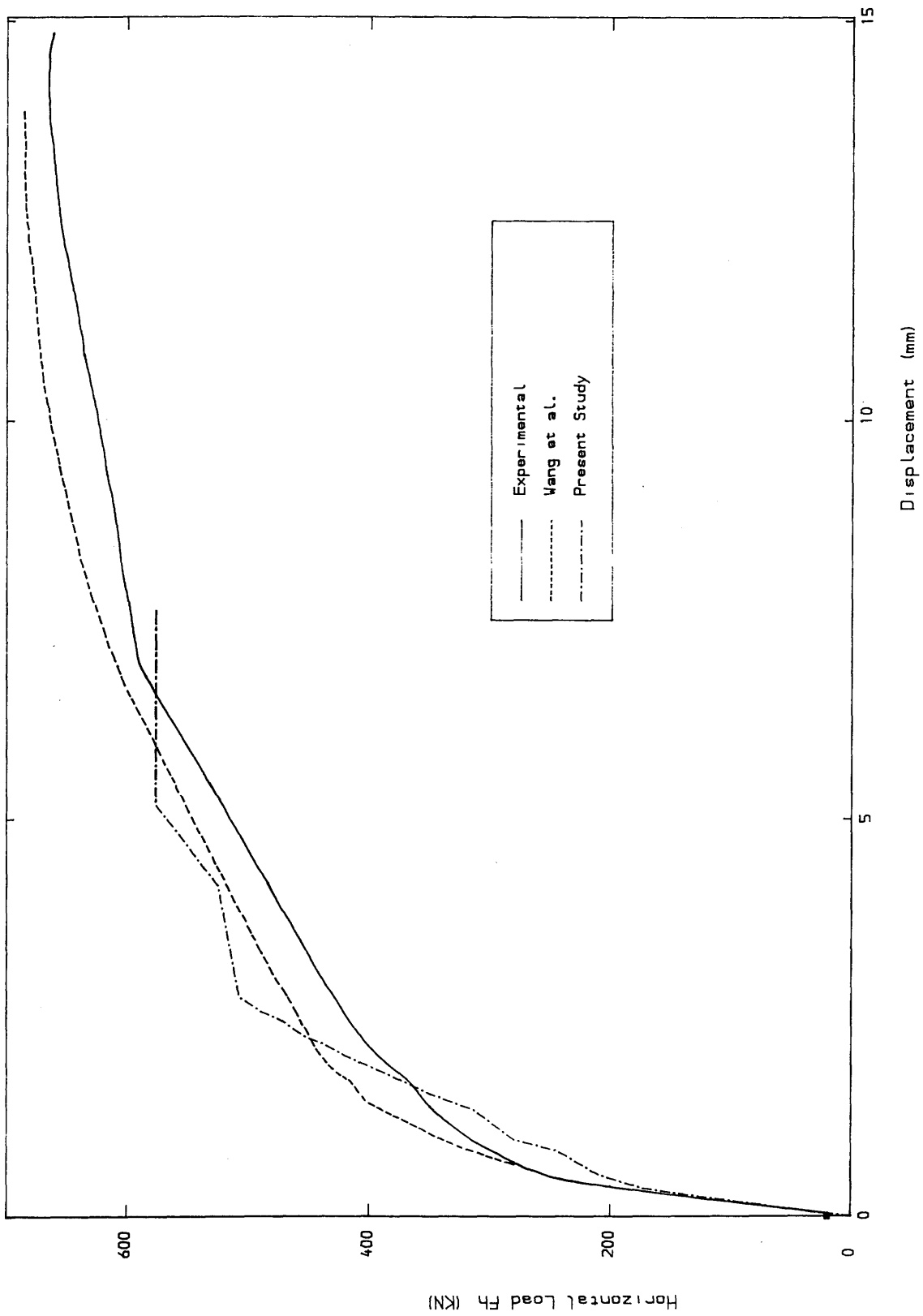
Fig (5-22) Load displacement response for panel (S1).
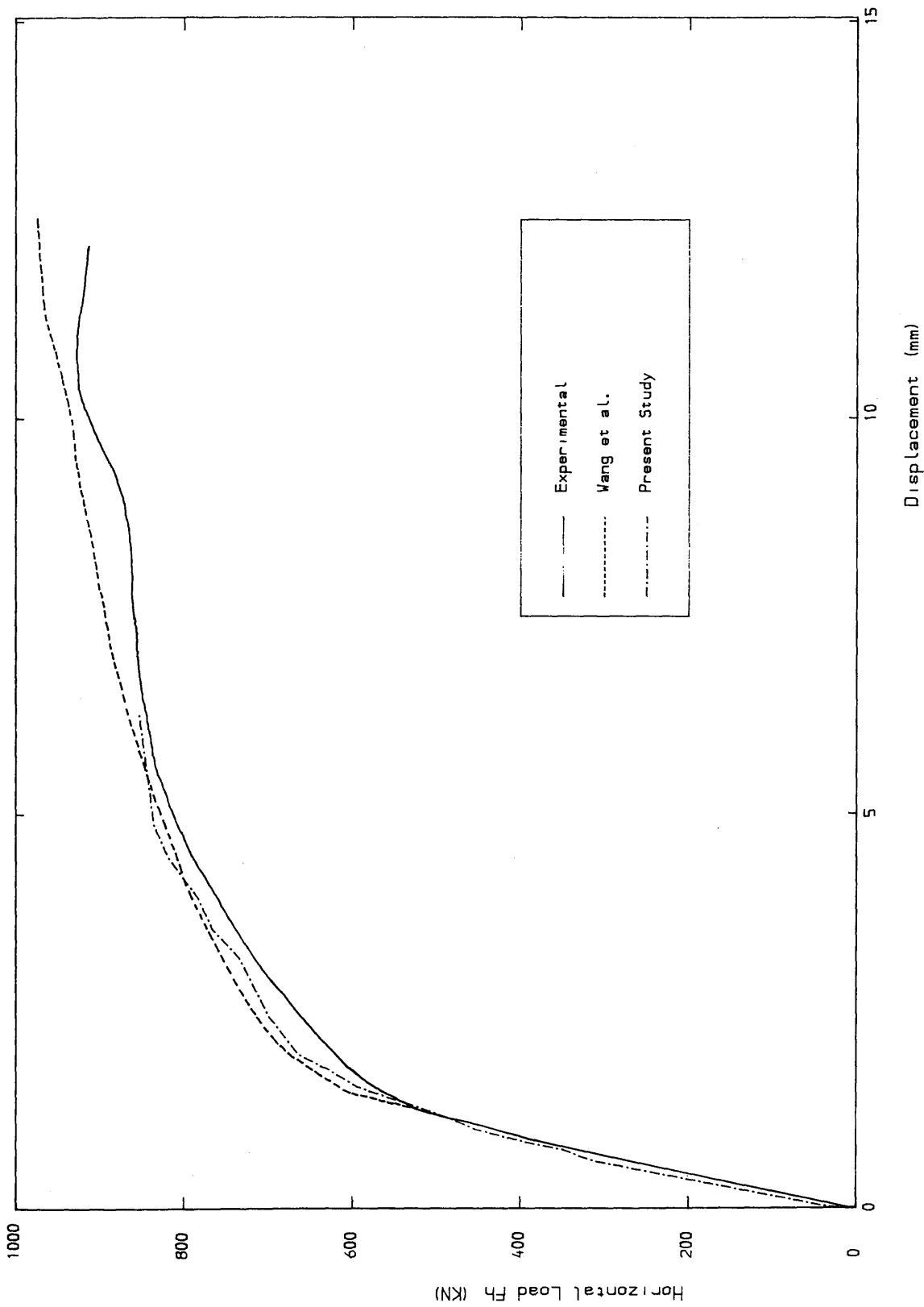
Fig (5-23) Load displacement response for panel (S2).
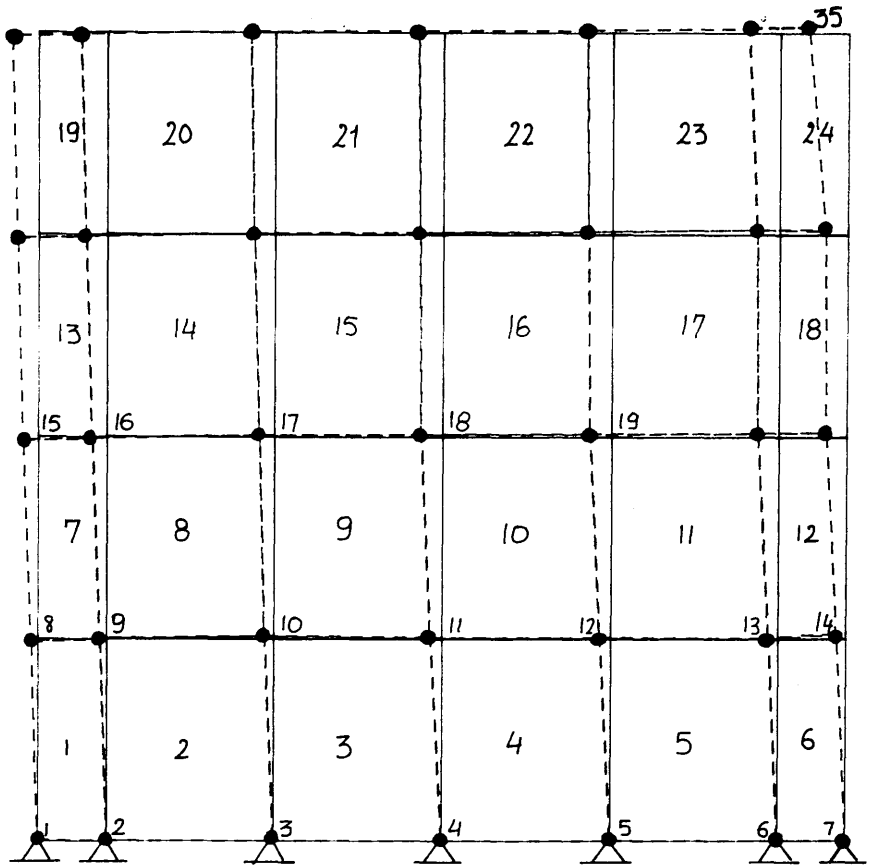
Fig (5-24) Finite element mesh at failure of panel (S2).
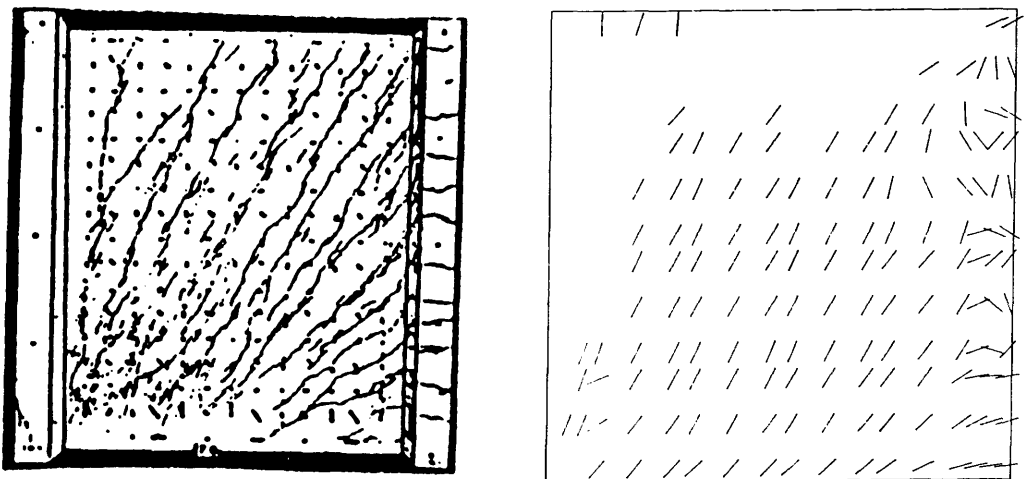
Fig (5-25) Predicted and experimental crack pattern for panel (S2).

5—5 BRESLER'S shallow beam:

The ability of the proposed model to simulate the behaviour of a simple type of structure is demonstrated with the simply supported, reinforced concrete beam tested by Scordelis & Bresler (1964) is shown in Fig (5—26). This beam has a span of 12ft. with cross sectional dimensions 21.75x9.0in. It has no web reinforcement and the longitudinal reinforcement consists of four bars with a total area of $4in^2$.

The beam is subjected to a central concentrated load and the experimentally determined failure load by crushing of concrete is 58Kips.

The experimental results are considered to be very reliable so the beam has almost become a benchmark for testing analytical and numerical formulations. The analytical model, shown in Fig(5—26), takes advantage of symmetry so that only one half of the beam is considered. 27 elements are used each with a 3 by 3 grid of integration points. The single row of steel is modelled by placing smeared longitudinal steel in the bottom row of elements.

The material constants used in the analysis are:

<u>Concrete:</u>

E_c — 3300 Kips/in^2

f_c = 3.16 Kips/in^2

f_t = 0.33 Kips/in^2

ν = 0.20

<u>Steel :</u>

E_s — 27800 Kips/in^2

f_y = 60 Kips/in^2

H = 0

<u>Comparison with test results :</u>

In Fig (5—27) the experimental load deflection curve at the midspan section of the beam is compared with the curves using the present numerical model for

various shear retention factors. Fig (5—27) also contains the numerical results of Hinton et al. in which they treated the concrete and steel as hardening—plastic materials and used a grid of 10 three dimensional elements disposed in two layers through the thickness. It can be seen that numerical solutions compare favourably with the experimental load deflection curve.

Crack patterns for different load intensities are plotted in Fig (5—28) and they can be compared with the experimental crack pattern at failure.

Three other beams shown in Fig (5—29) which have been tested by Bresler and Scordelis will be analysed in this investigation.

5—6 Bresler Scordelis beam OA1:

The finite element mesh layout for the Bresler Scordelis beam OA1 with shear span to depth ratio of 3.97, is shown in Fig (5—30a). The load deflection curve predicted by the finite element method is compared to the experimental curve in Fig (5—31). A comparison shows a good agreement between the numerical and experimental curves up to failure load. The experimental crack pattern at failure load of 75.0 Kip is shown in Fig (5—32d). The analytical crack patterns obtained in this study is shown in Fig(5—32a—c) for different load levels up to failure. Fig (5—32a) corresponds to the onset of cracking at a load level of 24.0 kip, where flexural vertical cracks are evident. Fig (5—32b) corresponds to a load level of 42.0 Kip where inclined shear cracks start to develop, and Fig (5—32c) shows the crack pattern at numerical failure load of 72.0 Kip.

The maximum tensile stress in steel at failure was 48 Ksi well below the yield strength of 80.5 Ksi. Thus the numerical failure is directly attributable to the loss of shear stiffness.

5-7 Bresler Scordelis beam OA2:

The load deflection curve for this beam with a shear span to depth ratio of 4.90 is shown in Fig (5-33). The finite element prediction is again in good agreement with test results. Crack pattern at three different load levels are shown in Fig (5-34a-c), corresponding to the onset of cracking at 24.0 Kip, inclined shear cracks at 49.5 Kip and at failure load of 84.9 Kip.The failure mode can be identified by comparing the cracking pattern at failure, Fig(5-34). The horizontal cracking near the point load and the inclined shear cracks, clearly indicates the failure mode as diagonal tension. The analytical crack pattern at failure compares favorably with that obtained from the experiment shown in Fig (5-34c).

5-8 Bresler Scordelis beam OA3:

This beam with a shear span to depth ratio of 6.94 is reported to have failed in the diagonal tension mode. The load deflection relationship observed during the experiment is compared to the finite element prediction in Fig (5-35). The prediction is not particularly good at failure. The load deflection graph shows parallel behaviour, however the numerical model underestimates the failure load by 15%. The crack pattern observed in the experiment compares favourably with that predicted by the analysis shown in Fig (5-36). Compared to beam OA2, there is less penetration of cracking into the compressive zone.
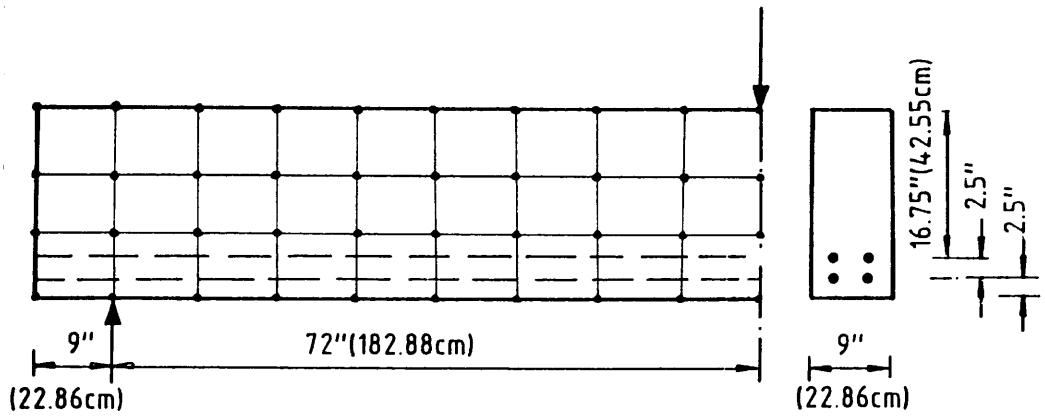
Fig (5-26) Bresler-Scordelis shallow beam.
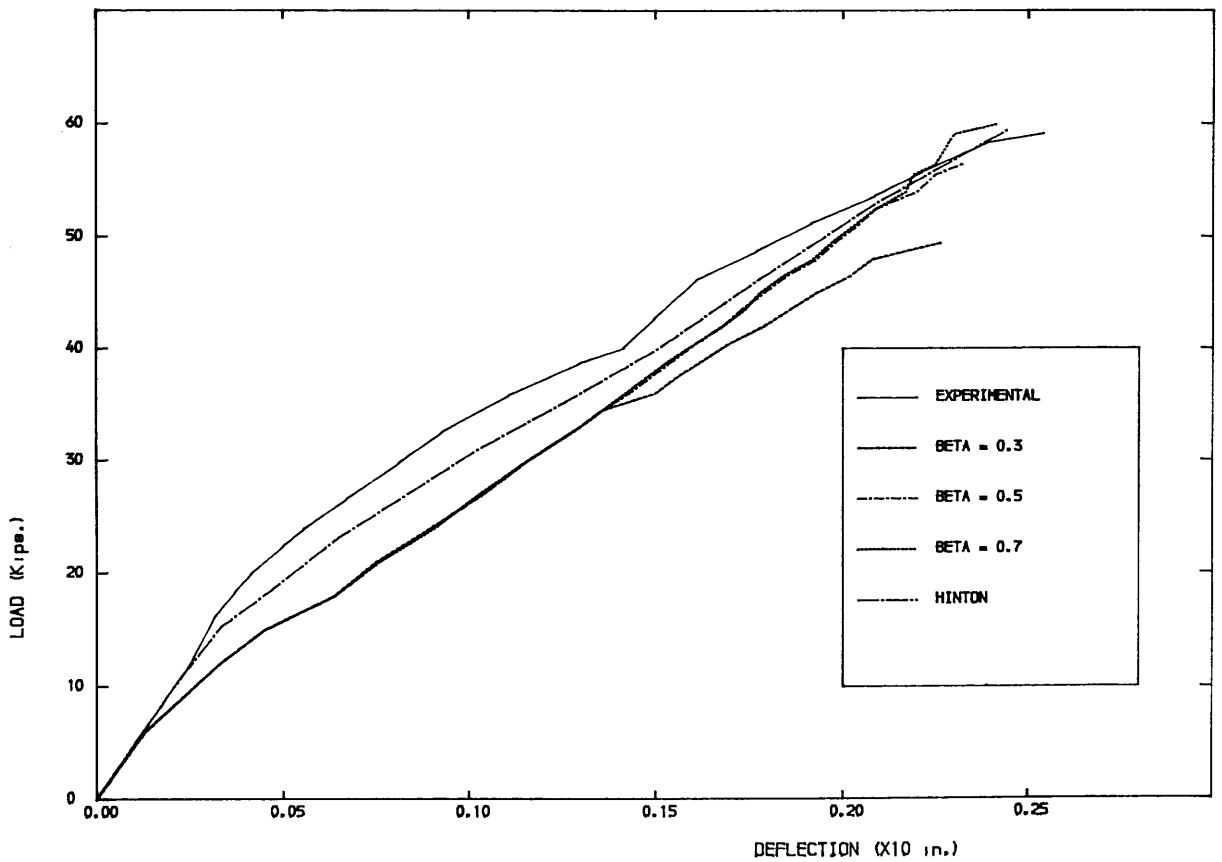
Fig (5-27) Load deflection for Bresler RC beam.
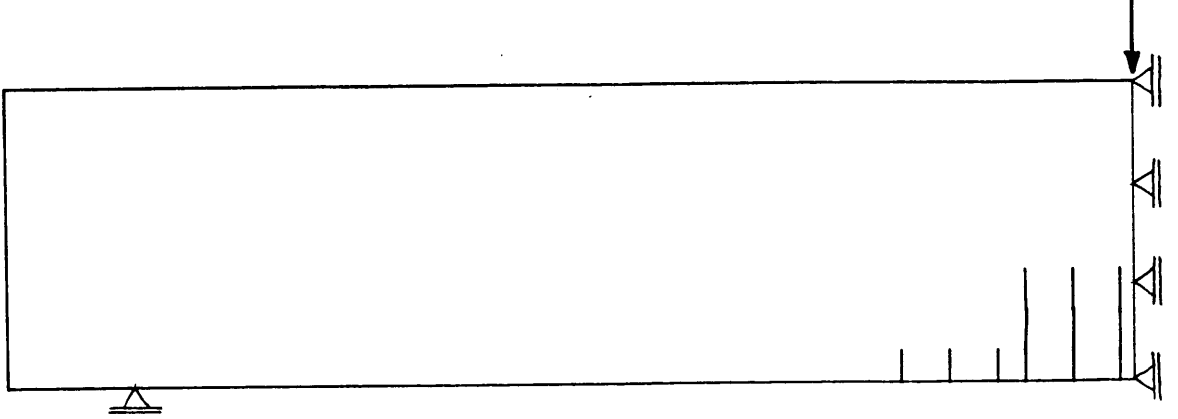
Onset of cracking P = 7 Kip.
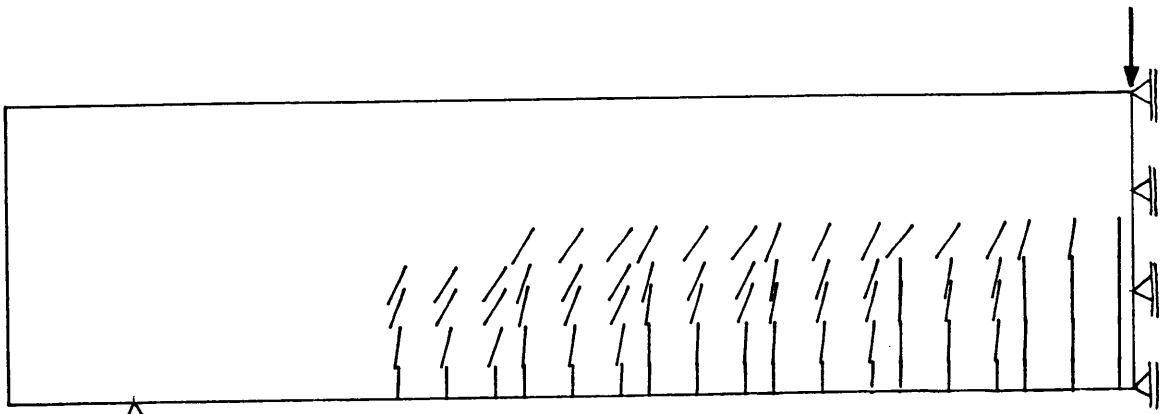
Crack pattern at P = 40 Kip.
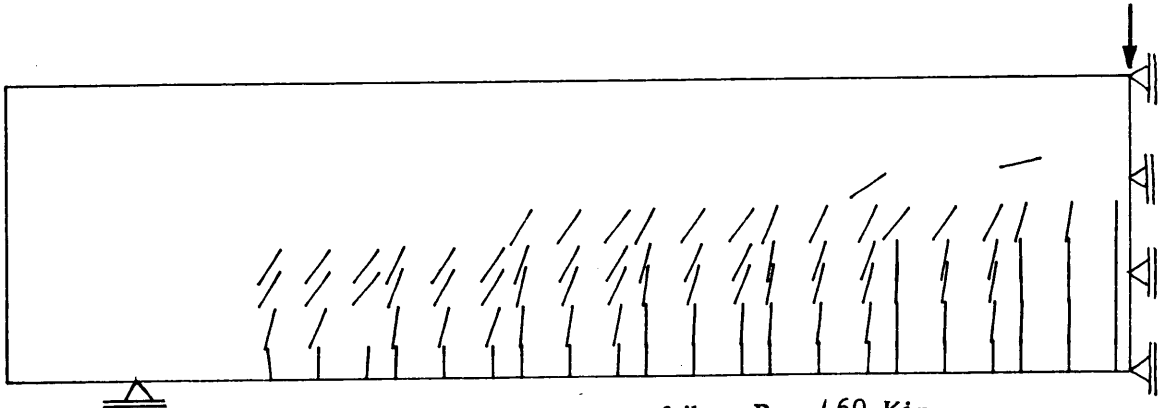
Crack pattern at failure P = 160 Kip.
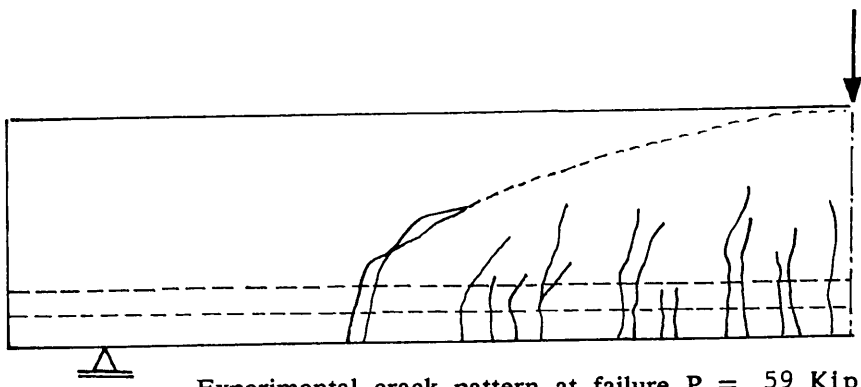
Experimental crack pattern at failure P = 59 Kip.

Fig (5-28) Crack pattern for Bresler shallow beam.
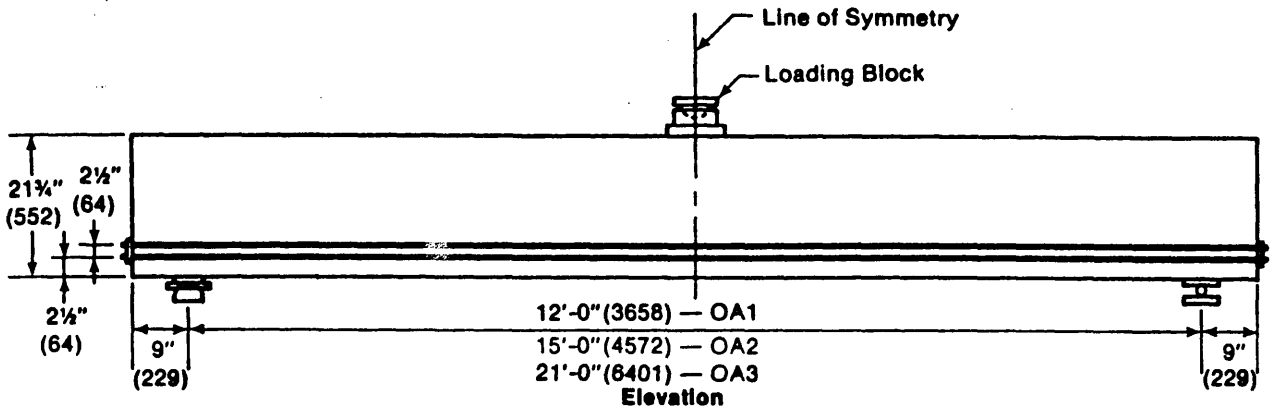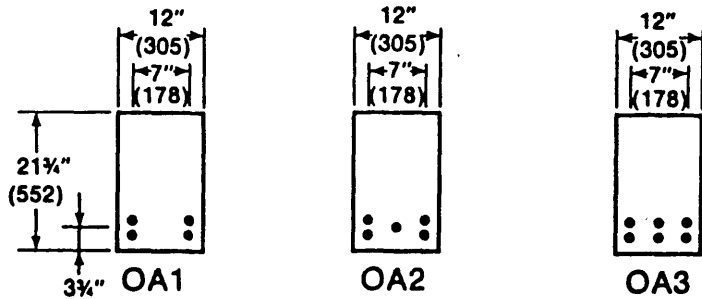
Fig (5-29) Bresler-Scordelis reinforced concrete beams.
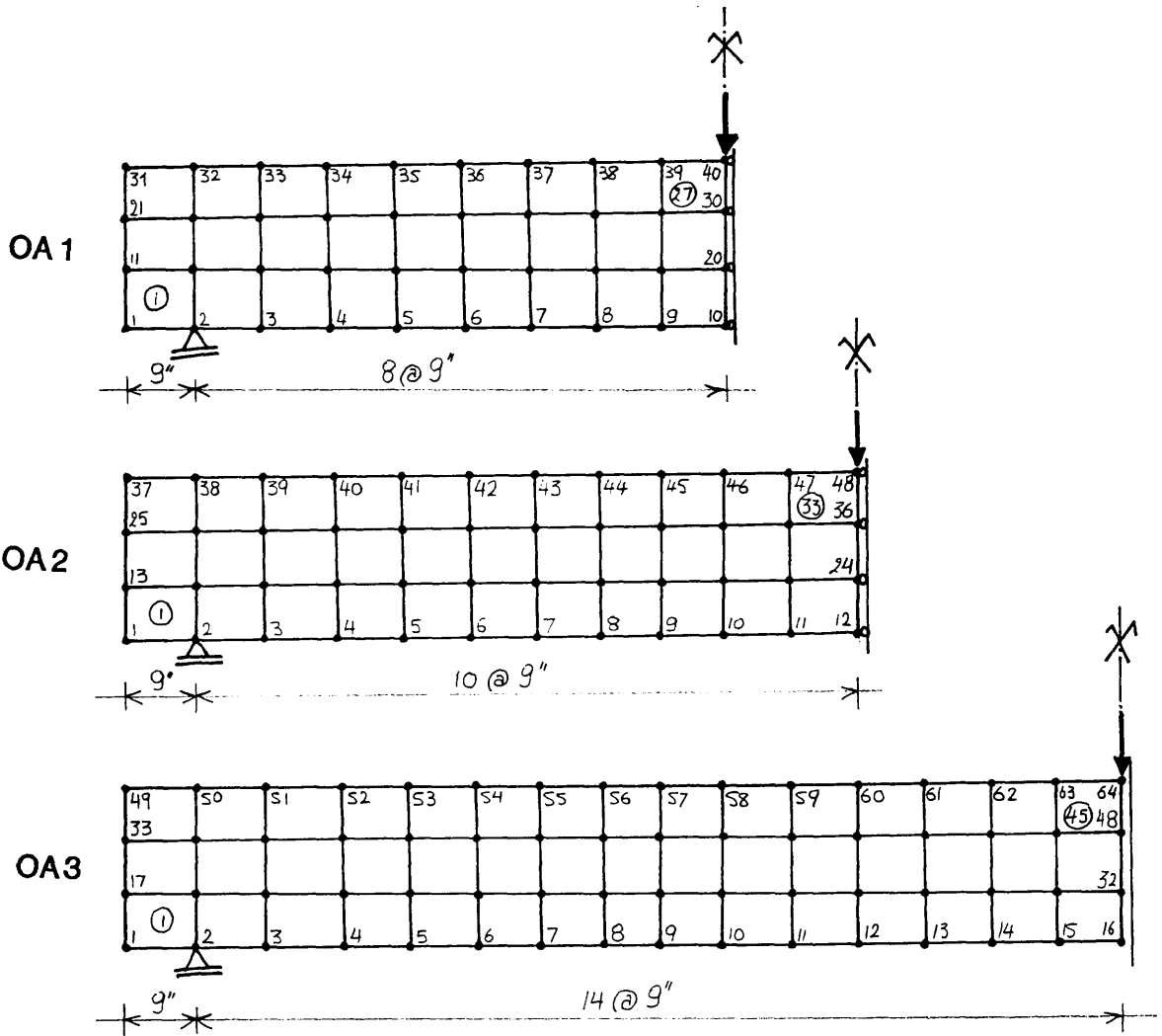
Fig (5-30) Finite element grids for Bresler-Scordelis beams.
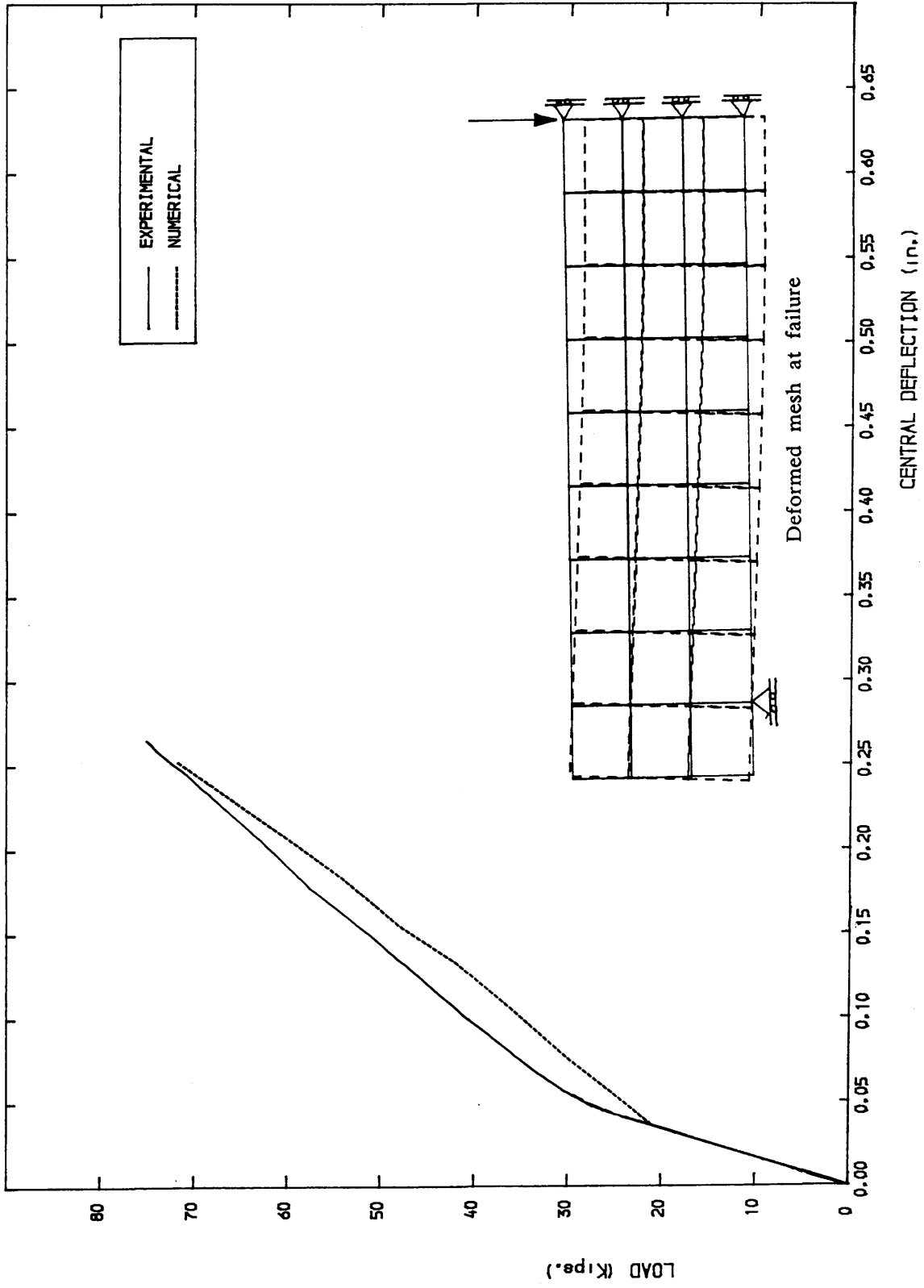
Fig (5-31) Load deflection for Bresler-Scordelis beam OA1.
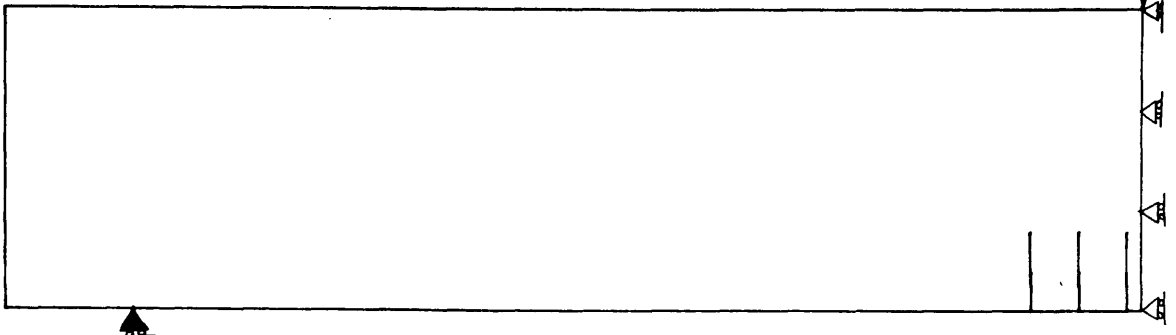
Onset of cracking P = 24.0 Kip.
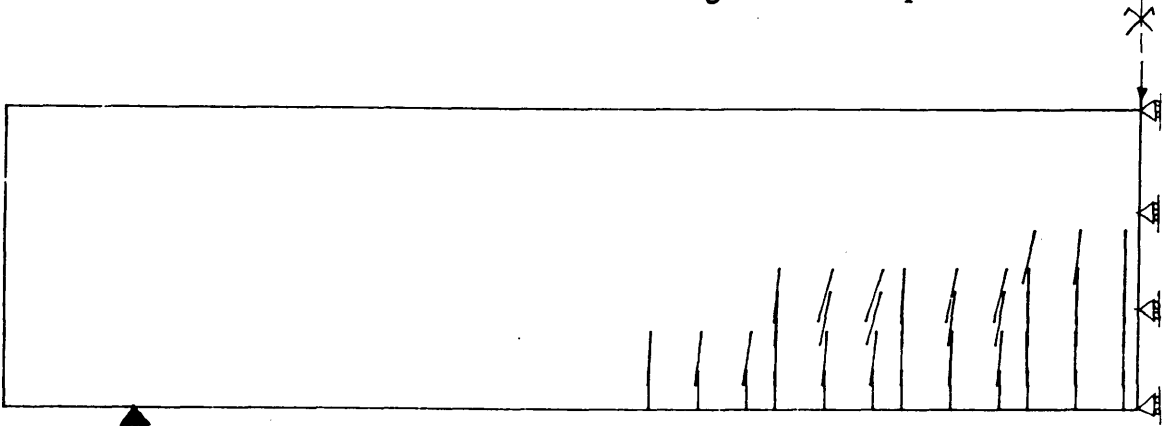
Crack pattern at P = 42.0 Kip.
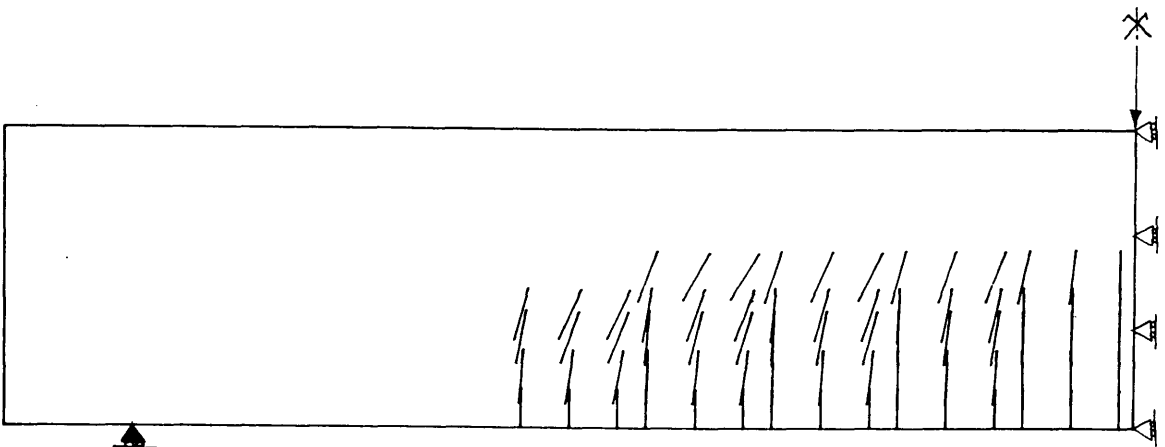
Numerical crack pattern at failure P = 72.0 Kip.
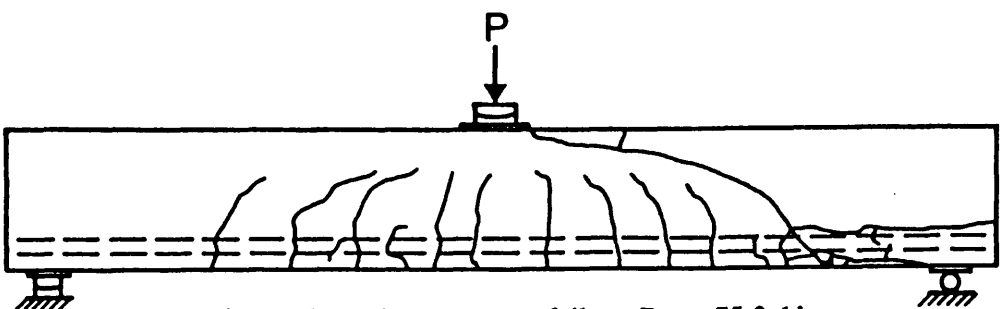
Experimental crack pattern at failure P = 75.0 kip.

Fig (5-32) Crack pattern for Bresler-Scordelis beam OA 1.

EXPERIMENTAL

NUMERICAL

Deformed mesh at failure

CENTRAL DEFLECTION (in.)

LOAD (kips,)
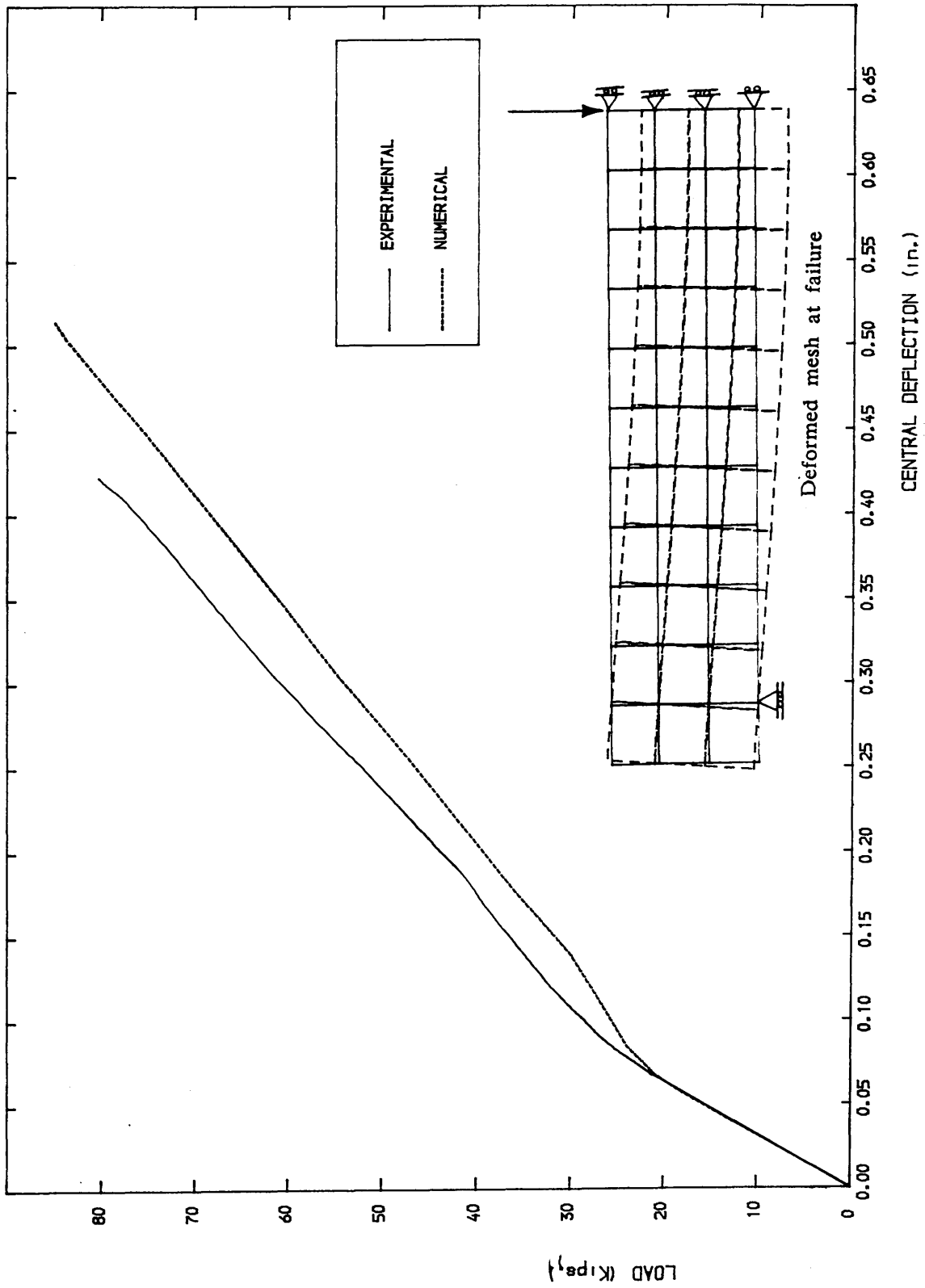
Fig (5-33) Load deflection for Bresler-Scordelis beam OA2.
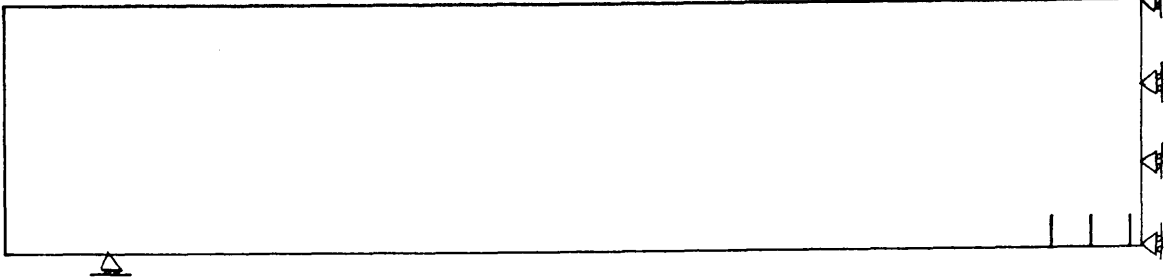
Onset of cracking P = 21.0 Kip.
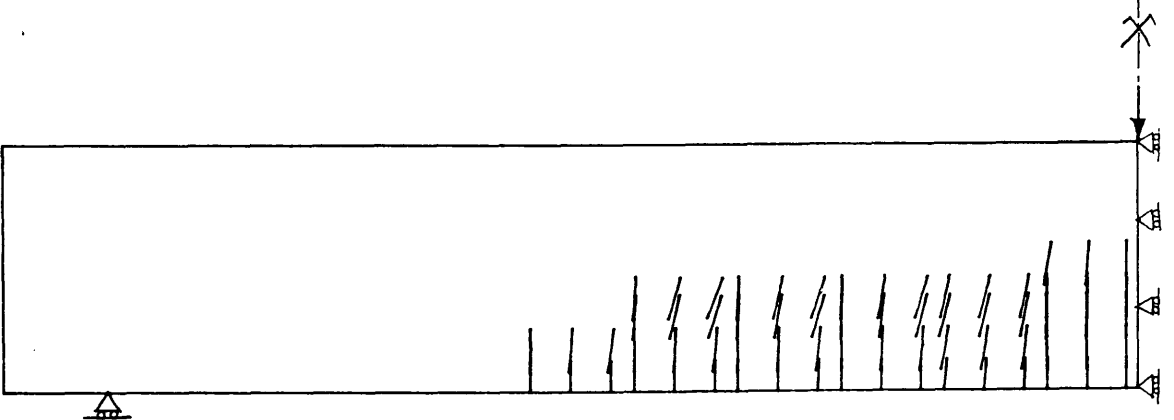
Crack pattern at P = 49.5 Kip.
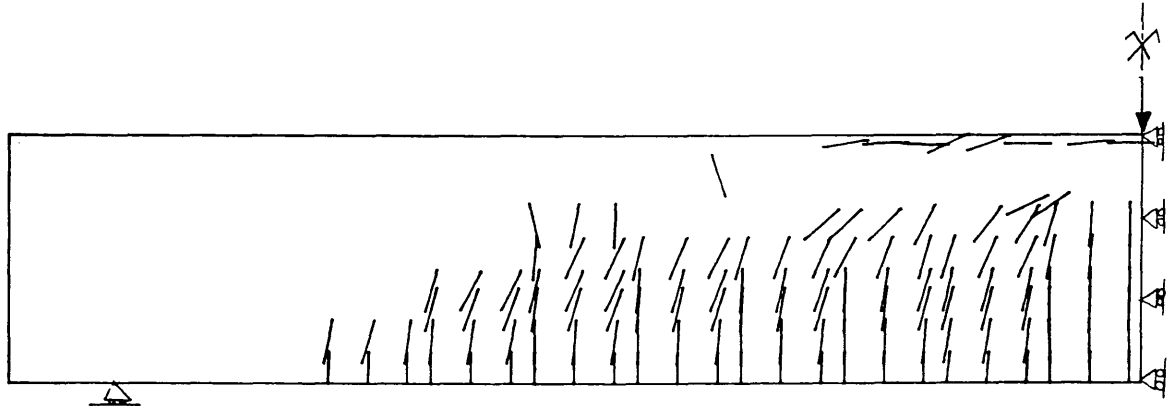
Numerical crack pattern at failure P = 84.9 Kip.

P
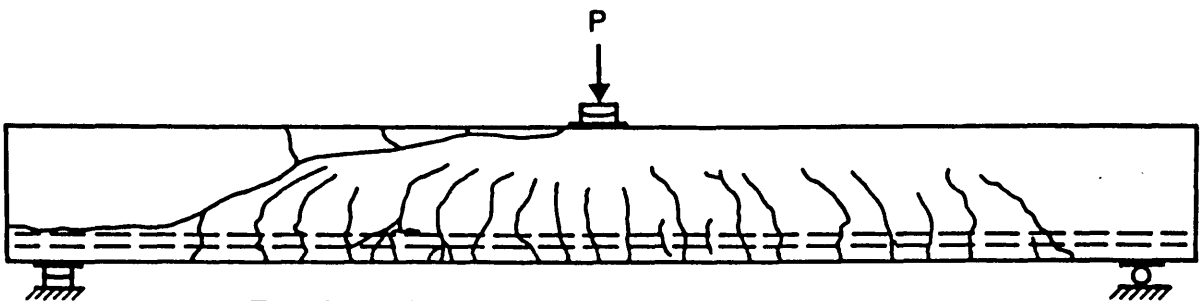
Experimental crack pattern at failure P = 80.0 Kip.

Fig (5-34) Crack pattern for Bresler-Scordelis beam OA2.
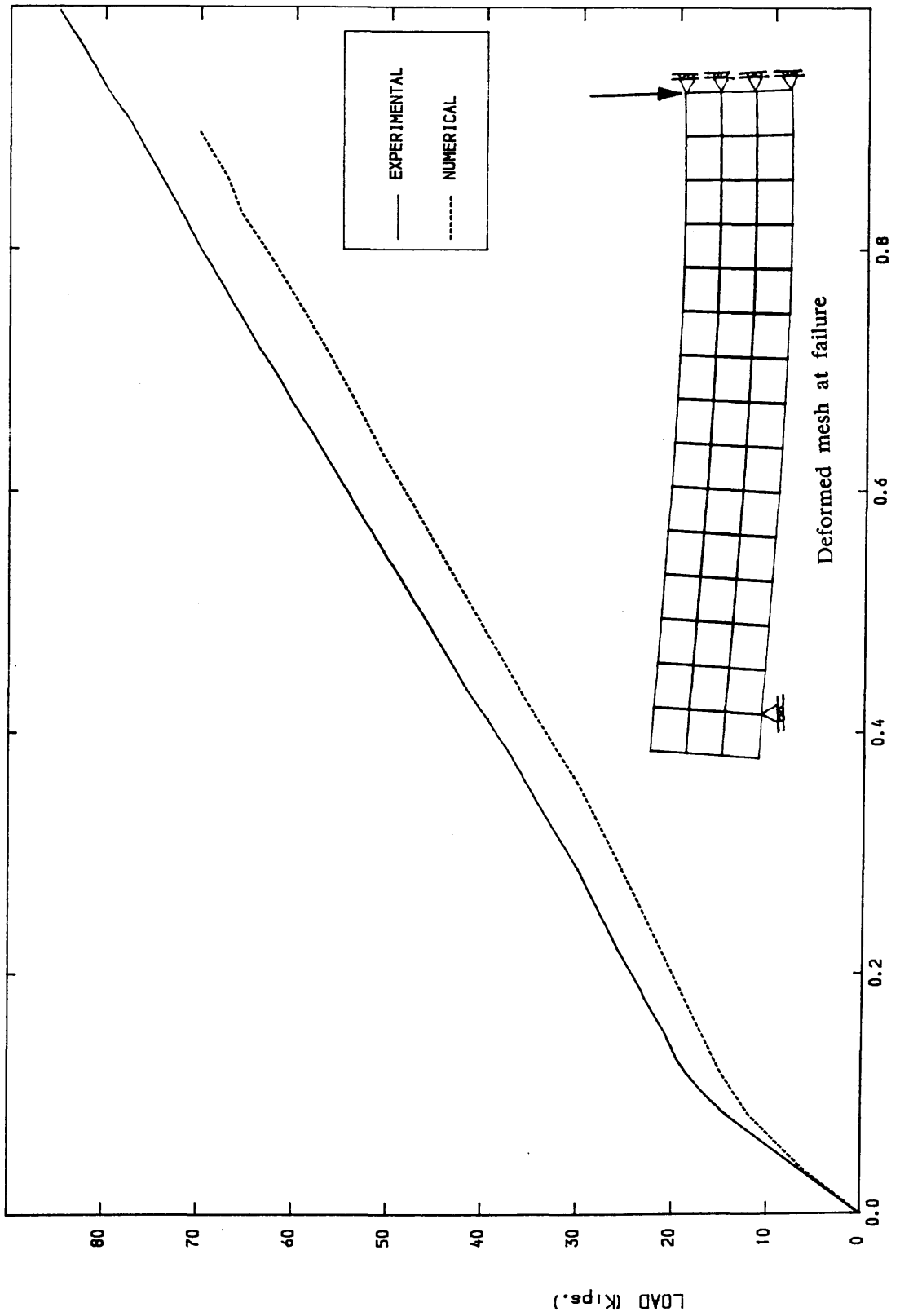
Fig (5-35) Load deflection for Bresler-Scordelis beam OA3.
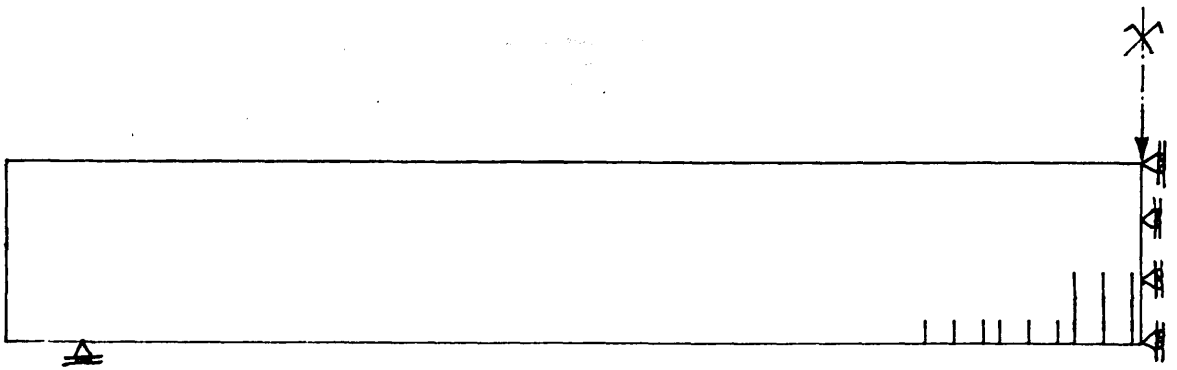
Onset of cracking P = 15.0 Kip.
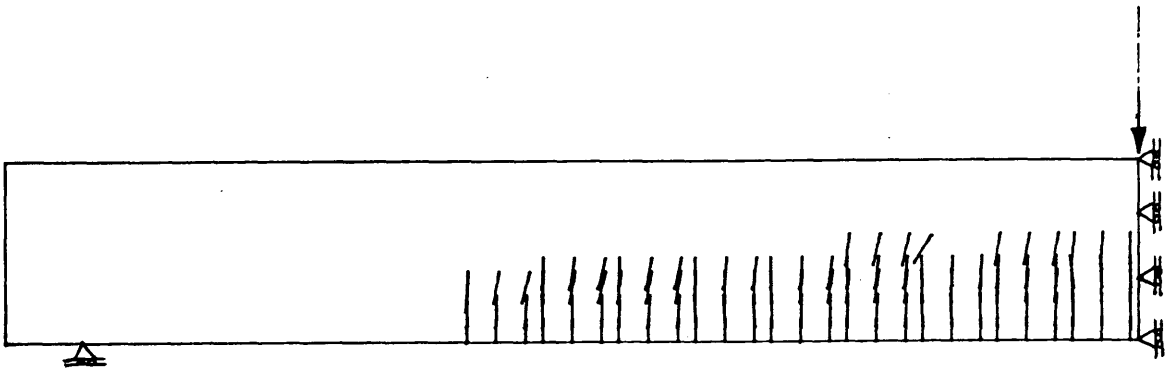
Crack pattern at P = 42.0 Kip.
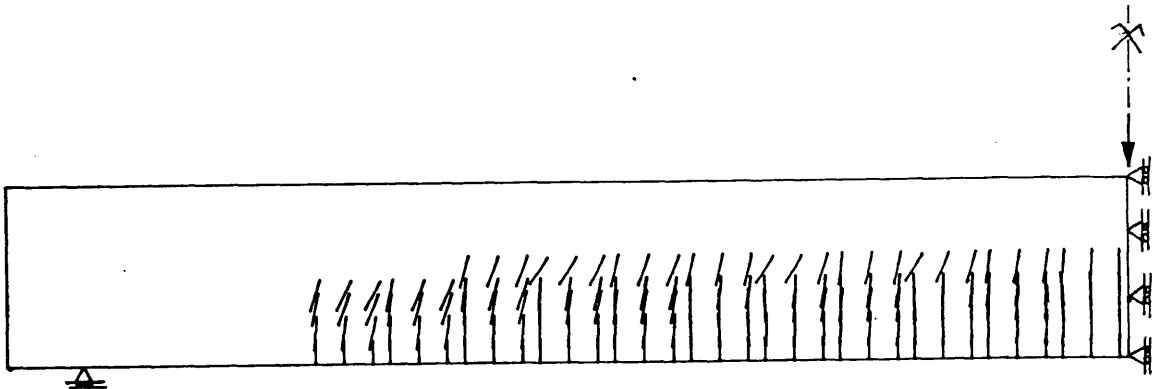
Numerical crack pattern at failure P = 70.5 Kip.

P
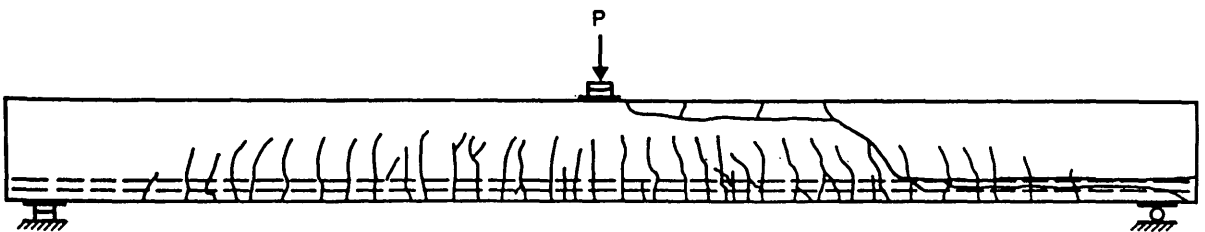
Experimental crack pattern at failure P = 85.0 kip.

Fig (5-36) Crack pattern for Bresler-Scordelis beam OA3.

5-9 KHASKHELI Deep beam :

A two-span continuous deep beam shown in Fig (5-37) is analysed. This beam has been tested experimentally by Khaskheli 1987. The geometry and loading of this beam are shown in Fig (5-37). The beam was designed to carry a total ultimate load of 850 kN as two concentrated loads acting at the centres of each span. The beam failed in shear at a load of 1333 kN. The overall depth and length of the beam were 900mm and 2000mm respectively with a thickness of 100mm. The span between the centres of support bearings was 960mm. The measured material properties used in the analysis are as follows:

Concrete	Steel	
$f_c' = 63$ N/mm^2	$\Phi 6$	$\Phi 8$
$f_t = 3.22$ N/mm^2	$f_y = 513$ N/mm^2	$f_y = 501$ N/mm^2
$E_c = 19.5$ N/mm^2	$E_s = 200$ N/mm^2	$E_s = 195$ N/mm^2

Taking advantage of symmetry, only one span of the beam is considered and idealized as shown in Fig (5-38). The predicted load-deflection relationships are compared with the experimental results in Fig (5-39) where good agreement is evident. The deformed finite element mesh at failure is plotted in Fig (5-40) and Fig (5-41) shows the crack pattern at failure.
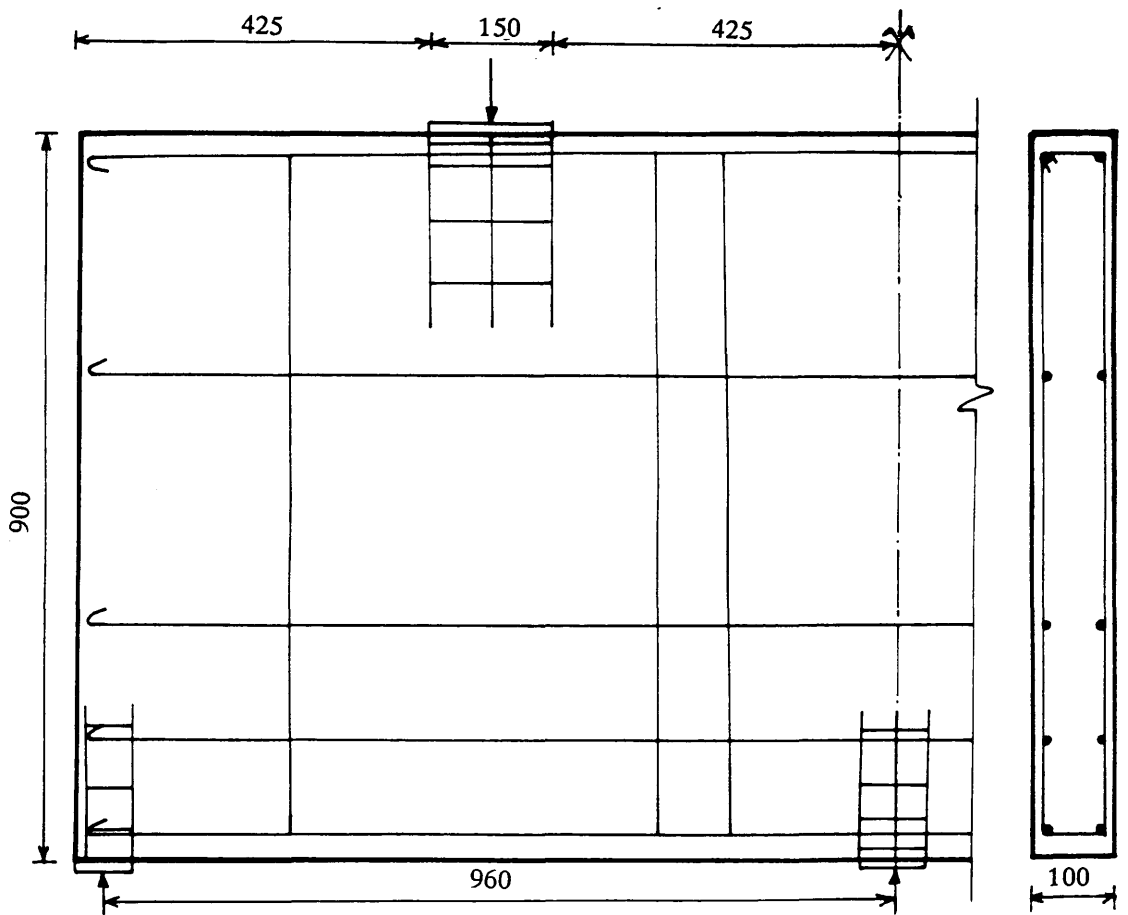
Fig (5-37) Khaskheli continuous deep beam.
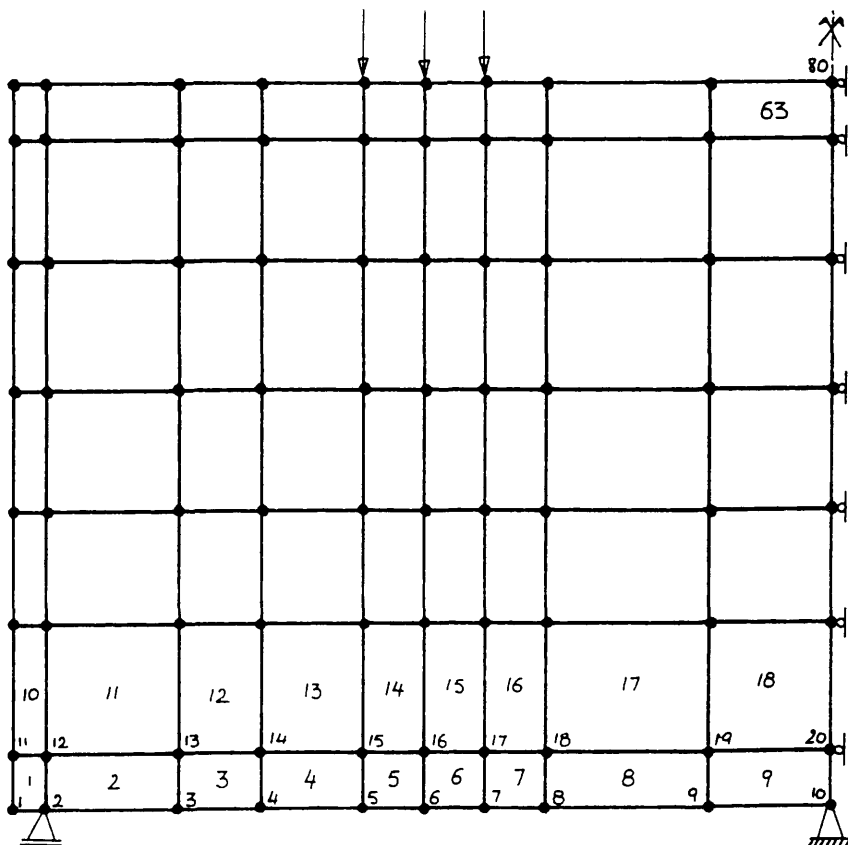
Fig (5-38) Finite element idealization of deep beam.
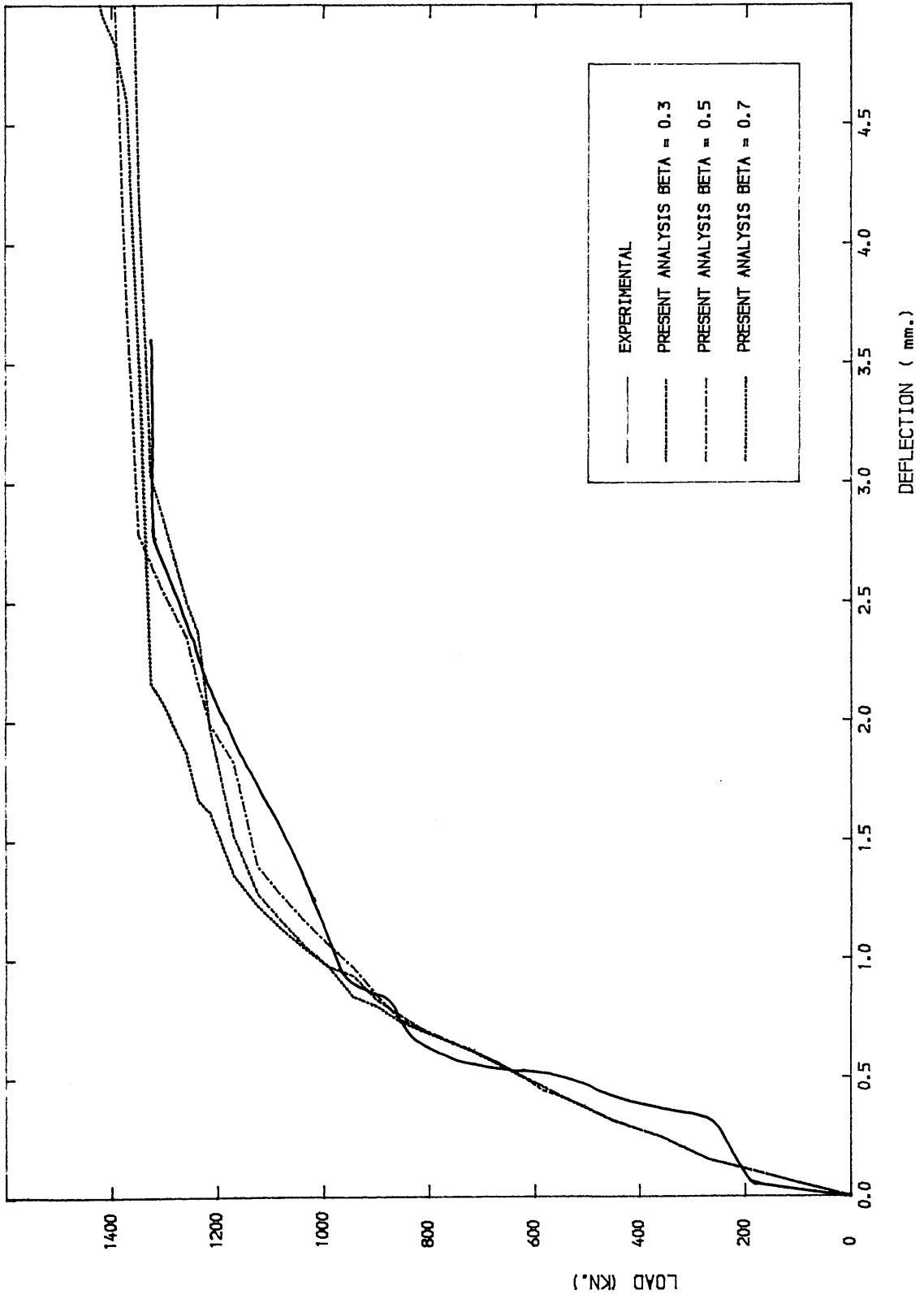
Fig (5-39) Load deflection for Khaskheli RC deep beam.
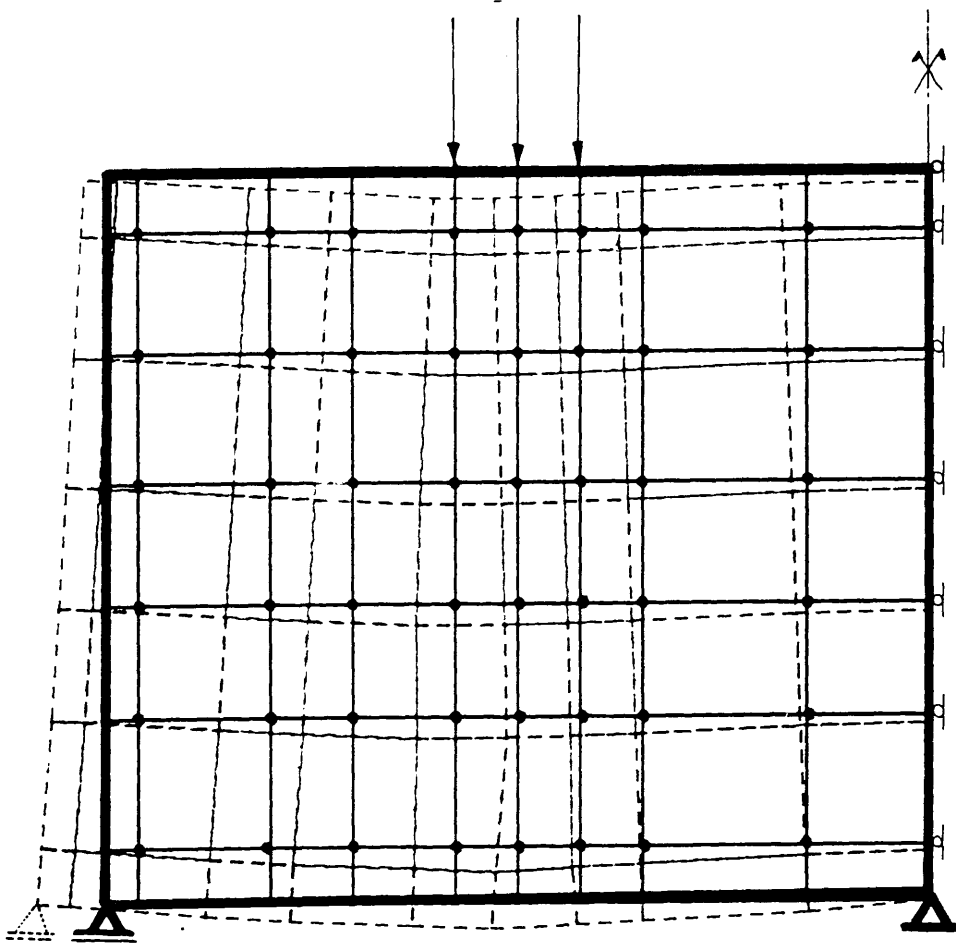
Fia (5-40) Deformed finite element mesh at failure.
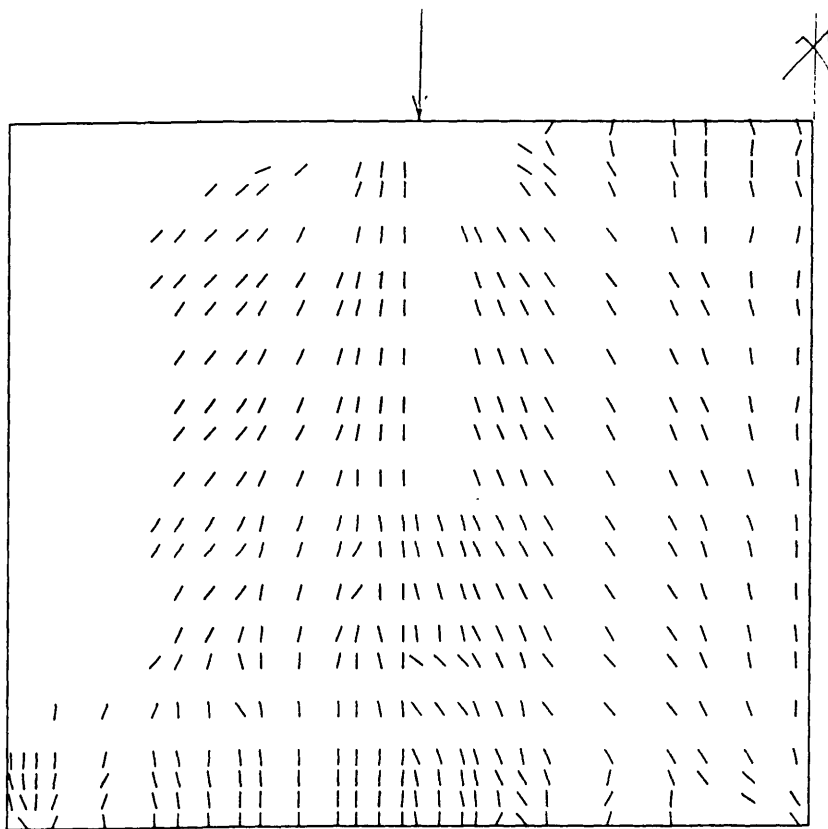
Fig (5-41) Crack pattern for Khaskheli RC deep beam.

5-10 VECCHIO AND COLLINS PANELS:

Vecchio and Collins 1982, conducted an excellent study on the behaviour of reinforced concrete panels under shear and normal stresses. In their experimental programme they tested 30 specimens of dimensions 890x890x70mm on a special testing rig shown in Fig (5-42) which allowed any plane stress state to be created in the panels. In all cases the reinforcement was arranged parallel to the panel sides, but with different ratios and amounts for different specimens. To date, there is no acceptable theory capable of predicting the full load-deformation response of such elements. This was made evident in a recent international competition, Vecchio et al. 1985, in which 43 leading researchers from 13 different countries attempted to predict the load-deformation response of 4 of the 30 reinforced concrete panels. It should be emphasized that the 4 panels were deliberately chosen so that in none of the panels was the load capacity governed by yielding of steel. The predictions were strongly dependent on the assumed stress-strain characteristics of concrete.

Of the whole series, only two specimens will be considered here, namely panels (27) and (25) shown in Fig (5-43). Both have equal reinforcing ratios of 0.01785 in the x and y directions. Panel 27 was loaded in pure shear, while panel 25 was subjected to a combination of shear and biaxial compression as shown in Fig (5-43). Both panels were loaded proportionally, the material properties used for the numerical analysis being as follows:

	PANEL 27	PANEL 25
CONCRETE :		
Young's modulus	$E_c = 20000$	20000 N/mm^2
Poisson ratio	$\nu = 0.15$	0.15
Compressive strength	$f_c' = 20.5$	19.3 N/mm^2
Tensile stress	$f_t = 2.4$	2.0 N/mm^2
STEEL :		
Young's modulus	$E_s = 200000$	200000 N/mm^2
Yield stress	$f_y = 442.0$	442.0 N/mm^2

The tests are designed so that the response of the panels is mainly dependent on the concrete behaviour. Both panels failed due to crushing of cracked concrete. These examples are included here because they are a demanding test on the computational material model. The intention was, given that panel 27 loaded in pure shear fails by concrete crushing, it might be expected on the basis of a simplistic Mohr's circle type analysis that panel 25, which is loaded by shear plus biaxial compression, might fail earlier. The finite element discretization of the two panels is given in Fig (5— 42).

Results from the numerical analyses are shown in Fig (5— 44) and (5— 45) compared to those obtained experimentally by Vecchio and Collins 1982 and numerically by Hinton et al. 1987. It is interesting to observe how the additional biaxial compression in panel 25 influences the failure load in comparison with panel 27. Satisfactory agreement between the experimental failure results and the numerical prediction is obtained for panel 27 as compared to the much poorer predictions in the case of panel 25. It should be admitted that this may be partly due to limitations in the relatively simple numerical model and difficulty of the problem at hand. However, Panel 25 was reported by Vecchio and Collins to be poorly cast as it contained voids.
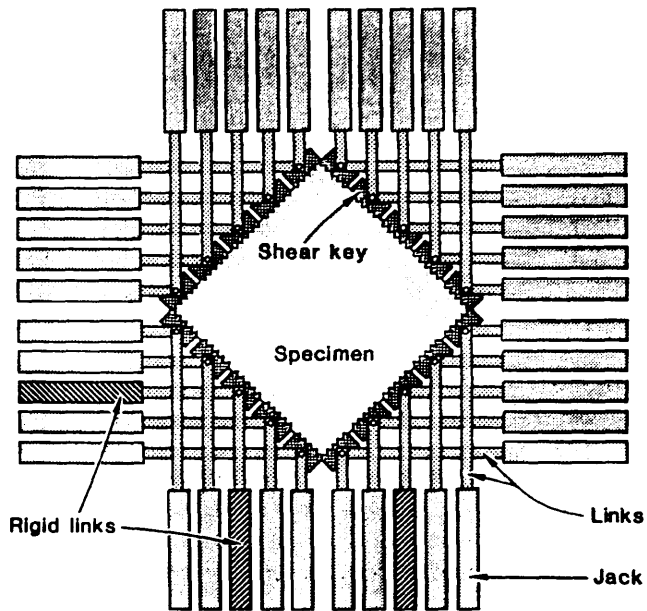
Fig (5-42) Jack and link assembly used to apply shear and
normal stresses.

Steel ratio: $\rho_x = \rho_y = 0.01785$
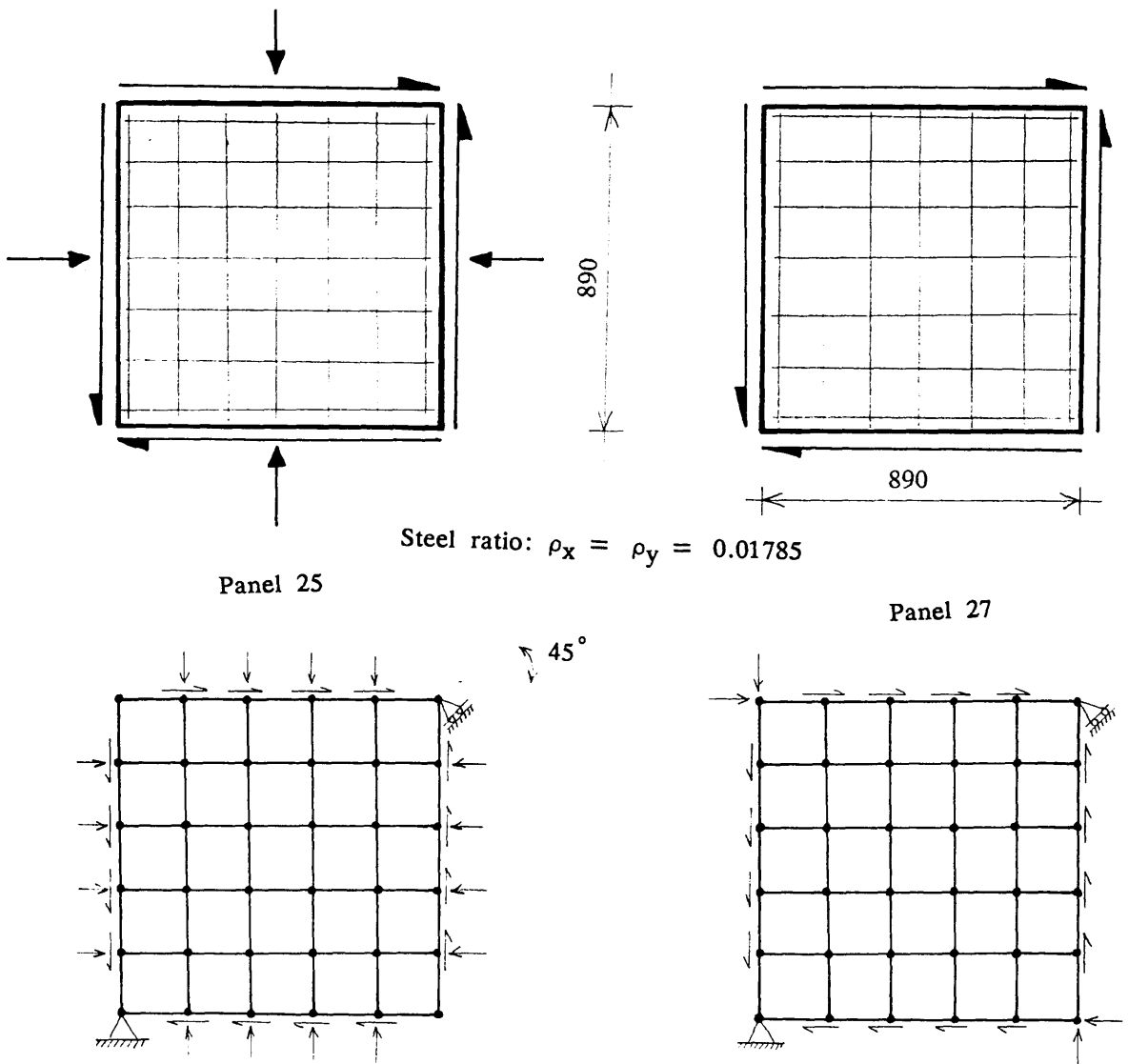
Panel 25

Panel 27

Fig (5-43) Finite element of Vecchio and Collins panels.
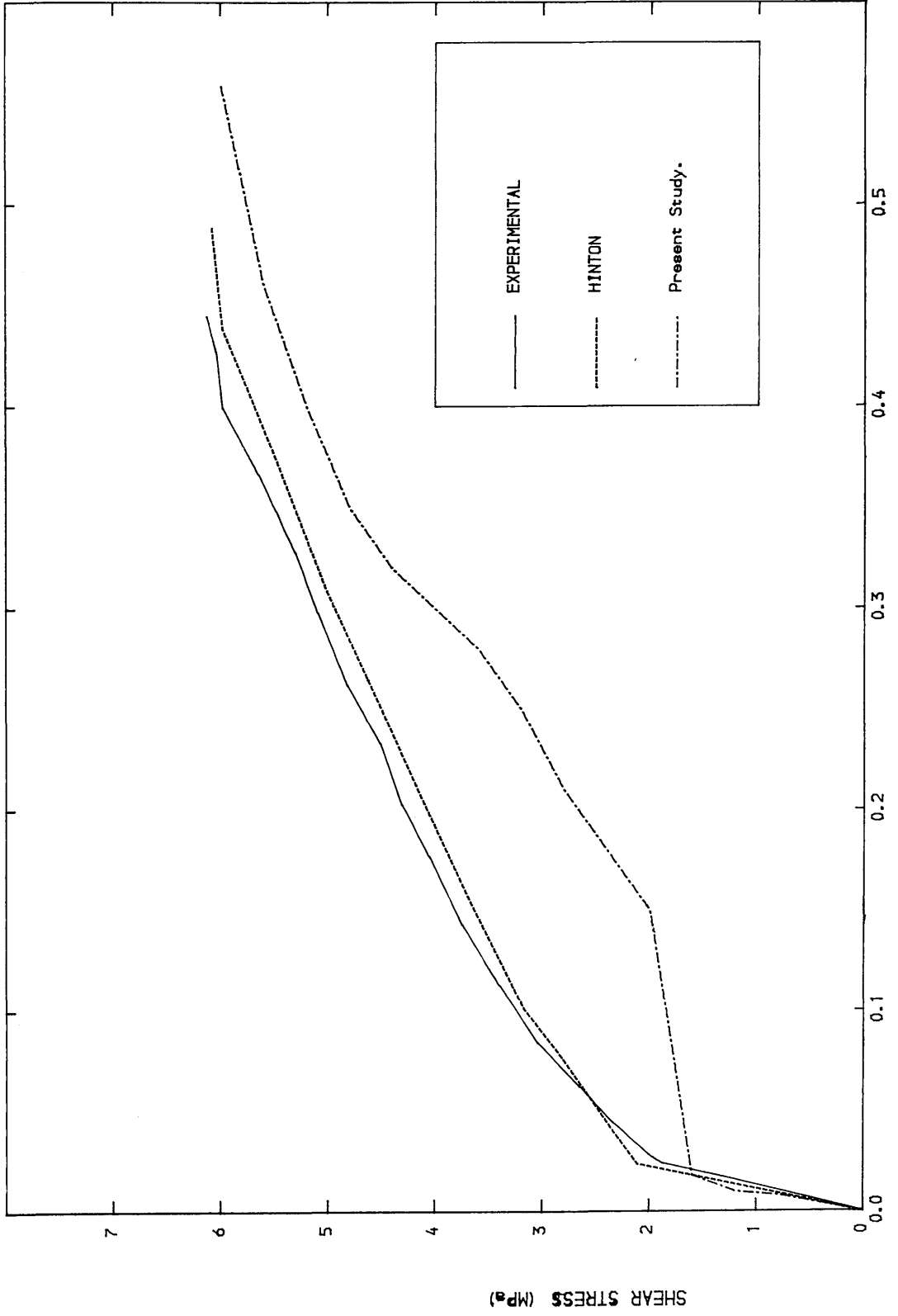
SHEAR STRAIN (X10-2)

Fig (5-44) Shear stress-strain of Vecchio panel 27.

SHEAR STRESS (MPa)

EXPERIMENTAL

HINTON

Present Study.

SHEAR STRAIN (X10-2)

SHEAR STRESS (MPa)

EXPERIMENTAL

Present Study.

HINTON
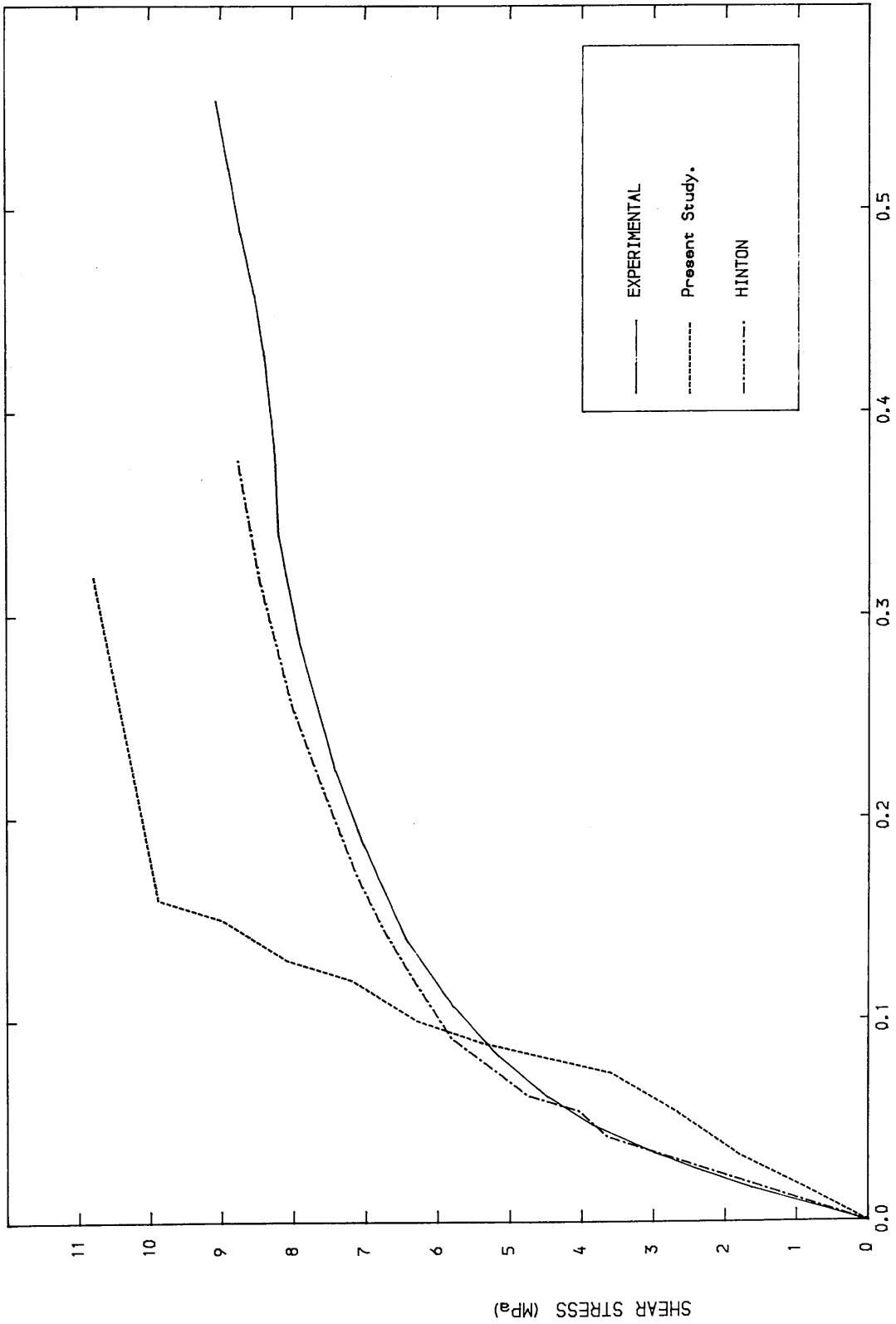
Fig (5-45) Shear stress-strain of Vecchio panel 25.

5-11 ANALYSIS OF SHEAR WALLS WITH LARGE OPENINGS :

Two shear walls with large openings subjected to lateral loads and analysed by Murazimi et al. 1981 using ADINA are considered. Fig (5-46) shows the geometry of the structure analysed. The shear walls are enclosed in concrete rigid frames. The width and depth of the columns are 60x60cm, and those of the beam are 35x70cm. The thickness and reinforcement ratio of the wall were 15cm and 0.316% respectively. The finite elment mesh chosen to discretize the shear wall is shown in Fig (5-47). The material properties used in the numerical analysis are:

<u>Concrete</u>

$f_c' = 210$ kg/cm^2

$f_t = 21$ kg/cm^2

$E_c = 210000$ kg/cm^2

$\nu = 0.17$

<u>Steel</u>

$f_y = 3000$ kg/cm^2

$E_s = 2100000$ kg/cm^2

Two cases are analysed :

(1) The shear wall with two openings, subjected to uniformly distributed horizontal loads applied at the top of the upper beam (Case B1).

(2) The same shear wall described above, subjected to the same amount of lateral load applied in the opposite direction   (Case B2).

The relationships between lateral loads and displacements are shown in Figs (5-48),(5-50), about which the following comments may be made.

(a) The stiffness in the elastic region and the cracking load are almost the same, regardless of the direction of applied lateral loads.

(b) The load displacement curves for cases B1 and B2 showed different behaviours in nonelastic regions beyond cracking loads and have different failure loads.

Therefore it may be concluded that the stiffness against lateral loads in the two directions are different.

Crack patterns for both cases are shown in Figs (5— 49),(5— 51). In both cases, the first cracks were observed near the corner of openings, and then cracked areas gradually extended all over the walls.

The major conclusions from this chapter is that the finite element method can be used to predict the behaviour of reinforced concrete members subjected to in plane forces if proper care is taken in modelling the material behaviour. The load deflection response, crack pattern, failure load and failure mode can be predicted with an accuracy that is acceptable for engineering purposes.

The simple strength criterion with a smeared crack model is adequate to study global behaviour as demonstrated by the various reinforced concrete elements studied. Reasonable crack patterns were obtained for the sample problems discussed despite the apparent wide diffusion. A constant shear retention factor $\beta = 0.5$ was found to lead satisfactory results and therefore has been adopted in this study. The present model can be used with confidence to predict the nonlinear behaviour of reinforced concrete coupled shearwalls for which very few experimental tests exist and this is presented in the next chapter.
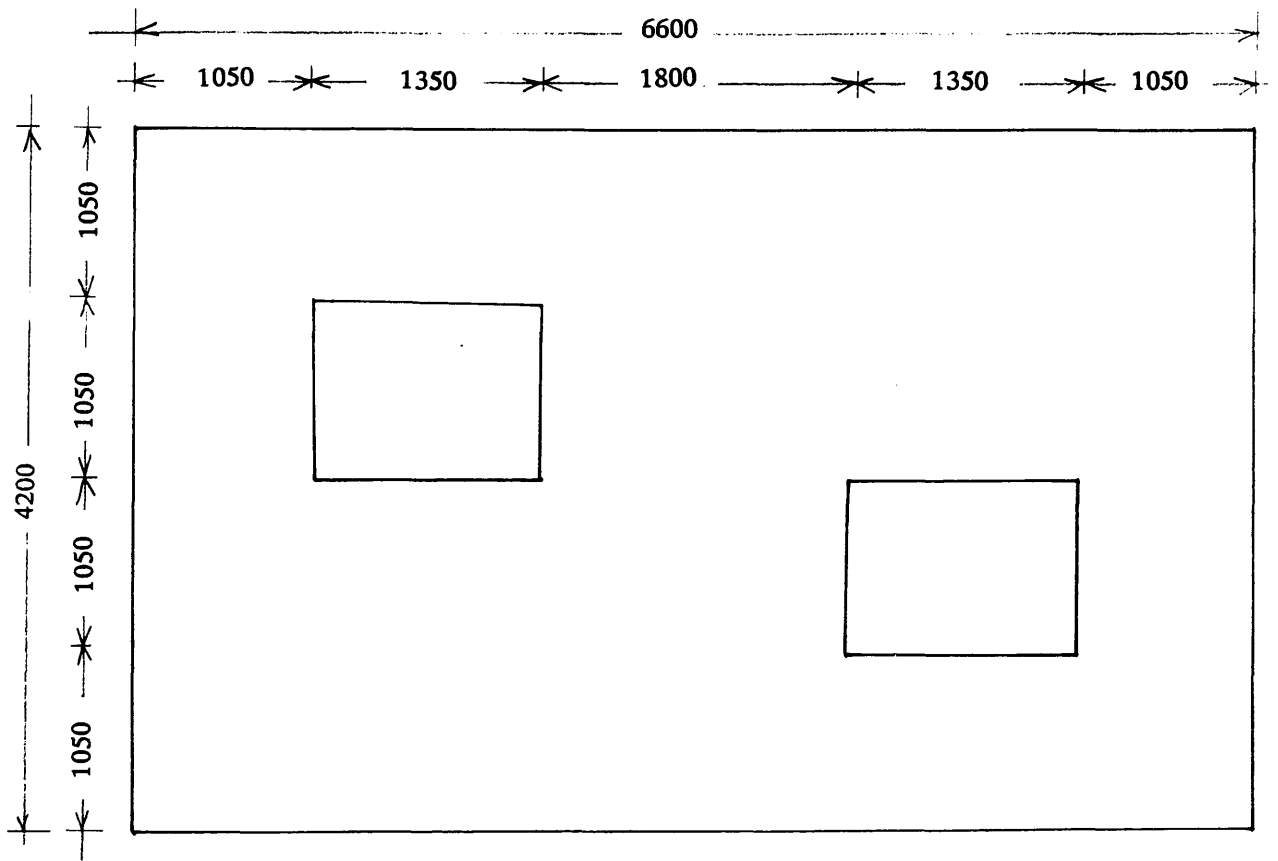
Fig (5-46) Shear wall with two openings.
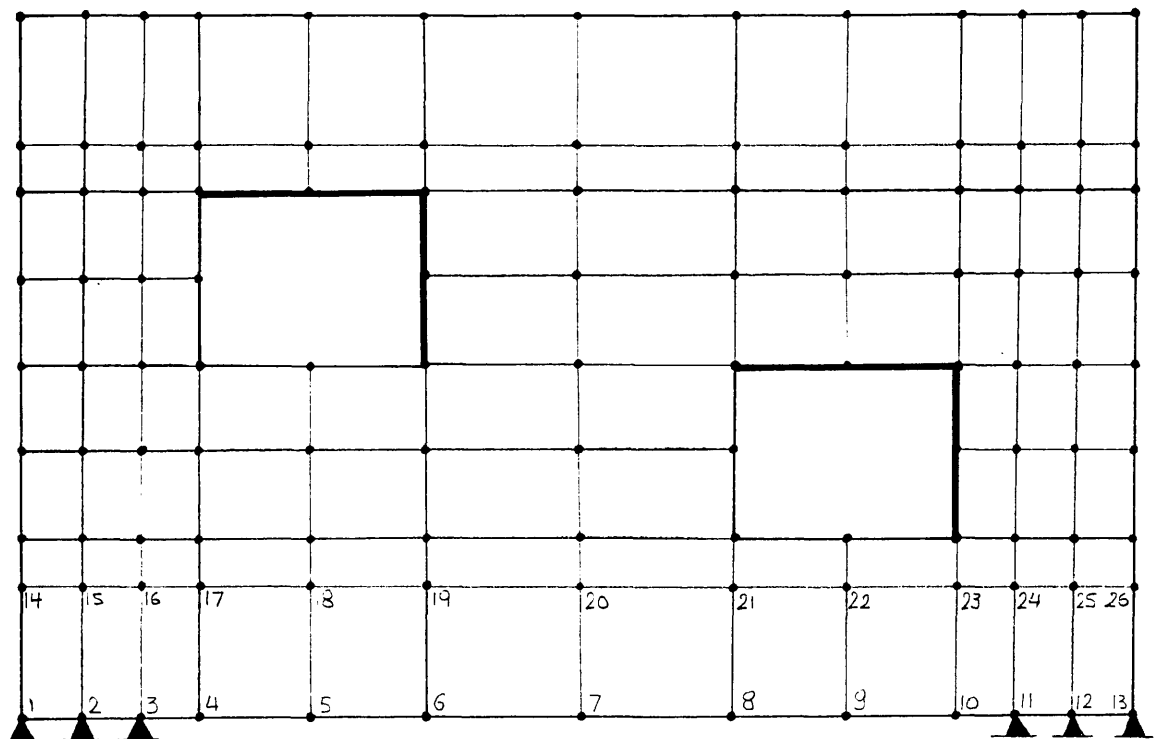
Fig (5-47) Finite element model of the shear wall.
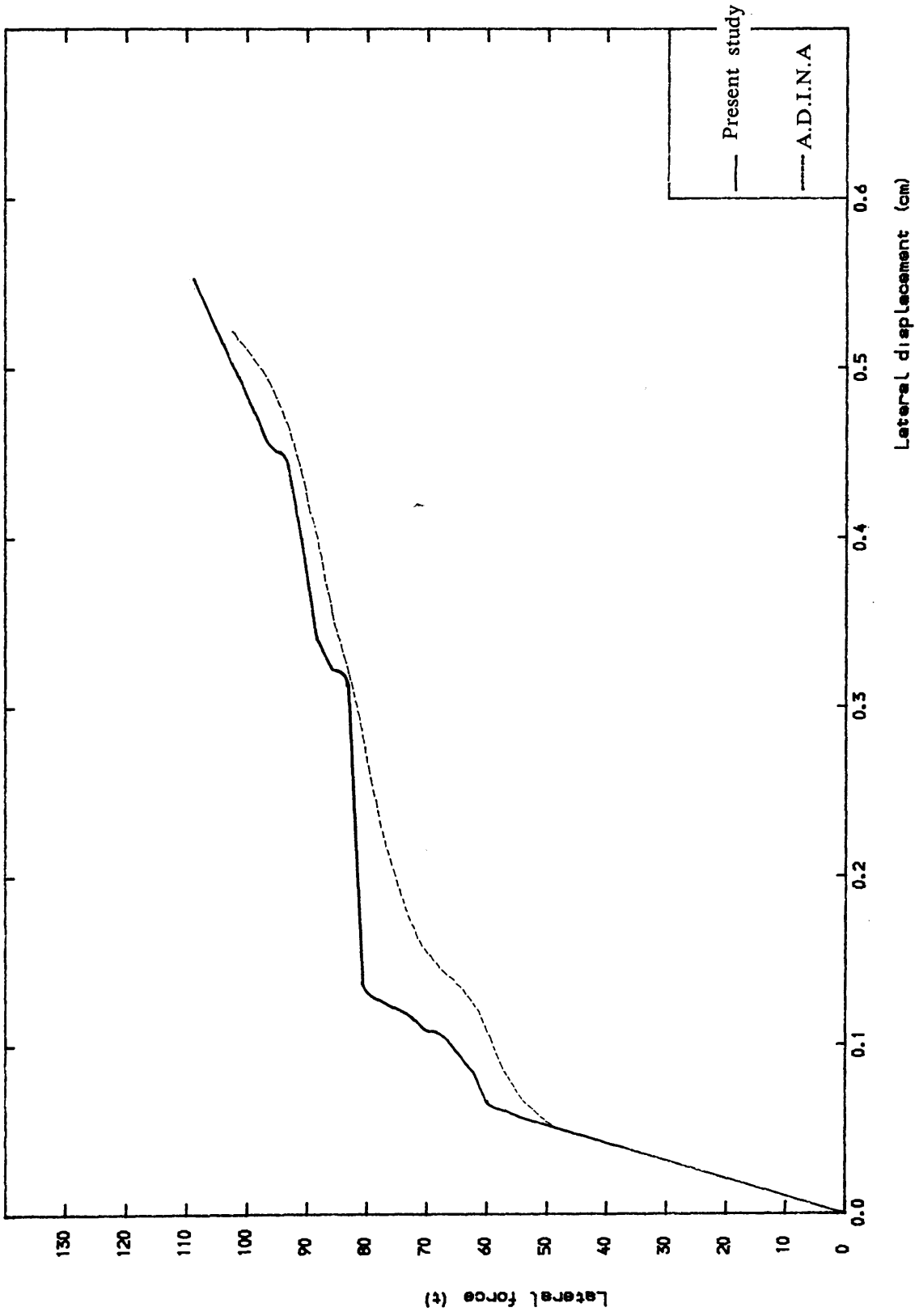
Fig (5-48) Lateral force-lateral displacement response for wall B1.

P = 54.6 t

P = 59.8 t

P = 62.4 t

Fig (5-49) Development of cracks for panel (B1).

P = 72.8 t

P = 85.8 t

P = 104.0 t
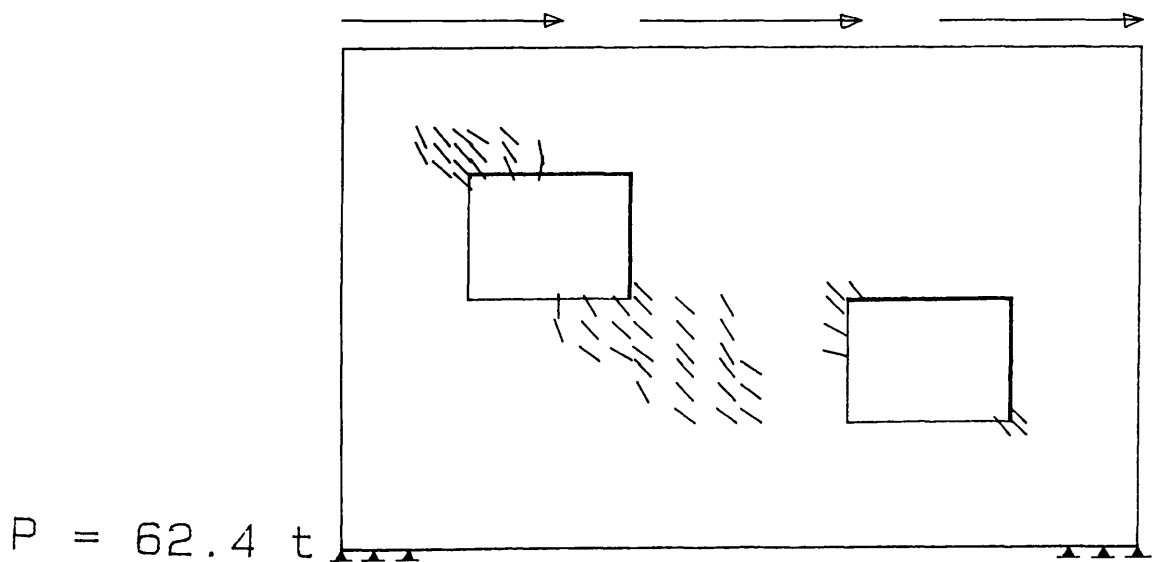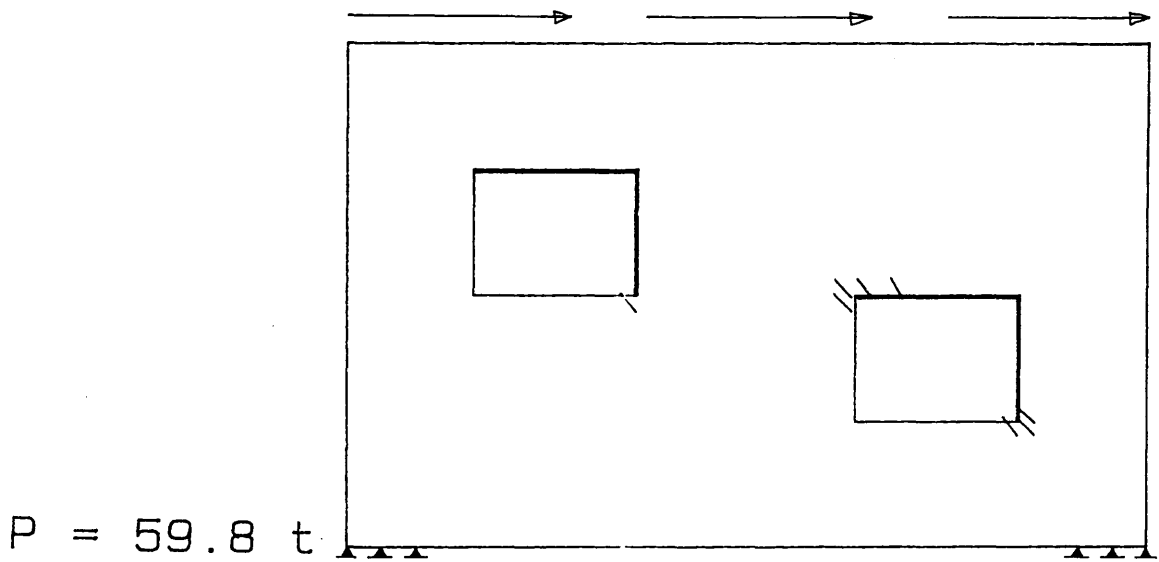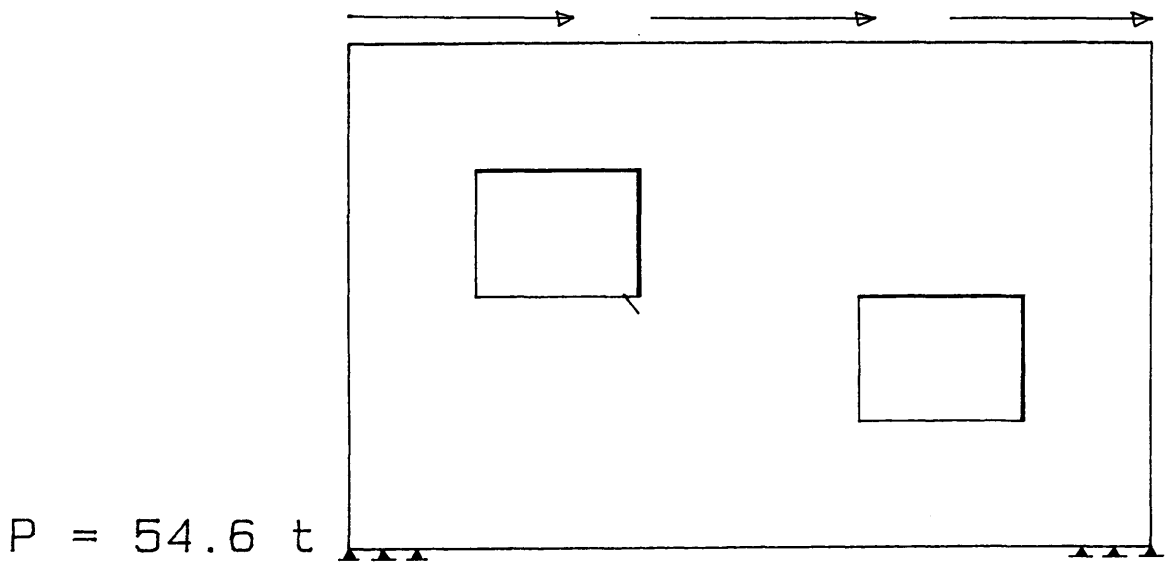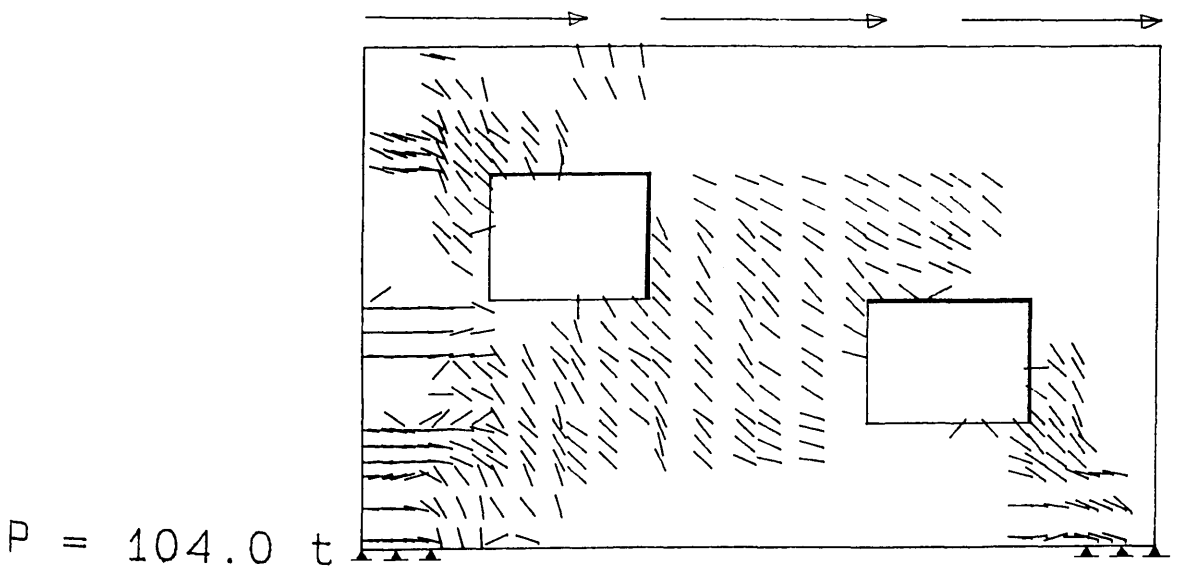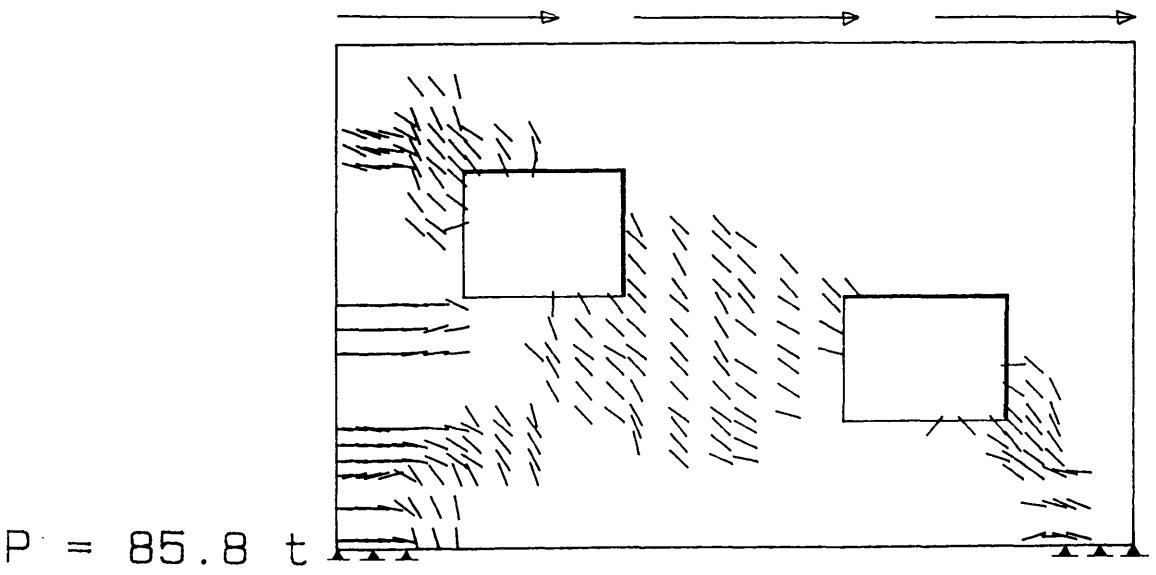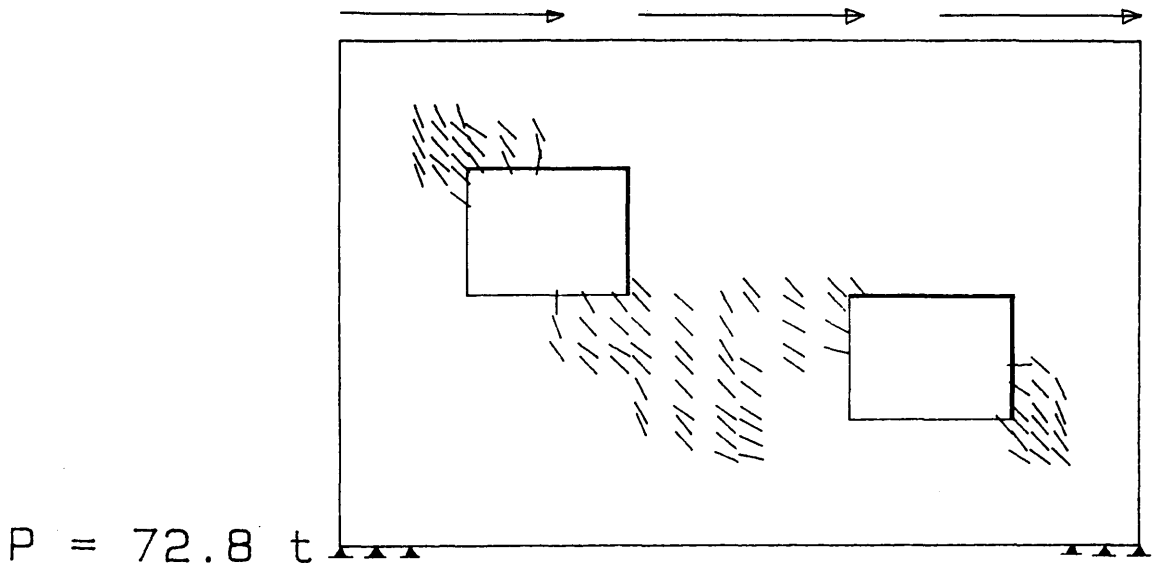
Fig (5-49) Development of cracks for panel (B1) (Continued).
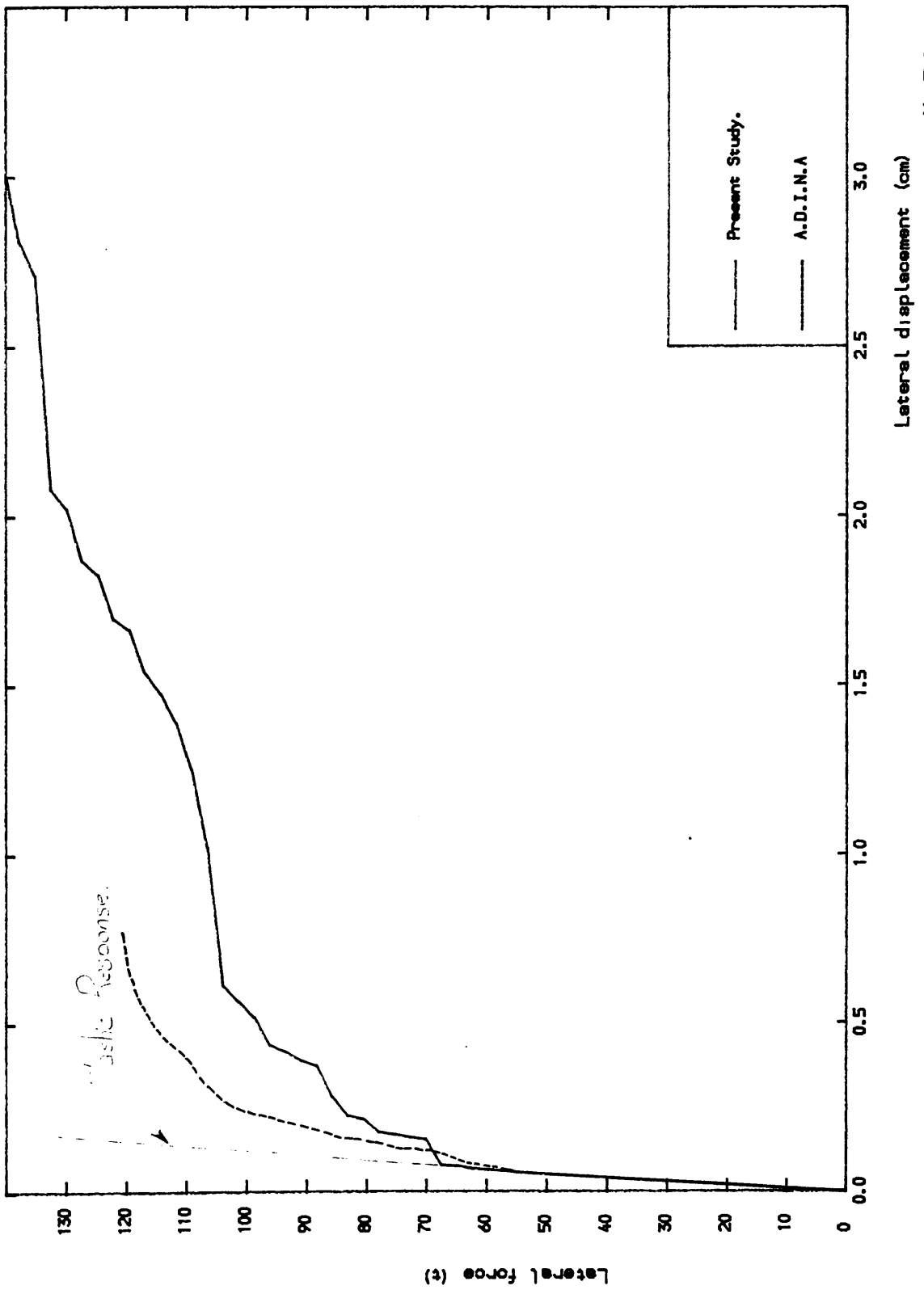
Fig (5-50) Lateral force-lateral displacement response for wall B2.

P = 52.0 t
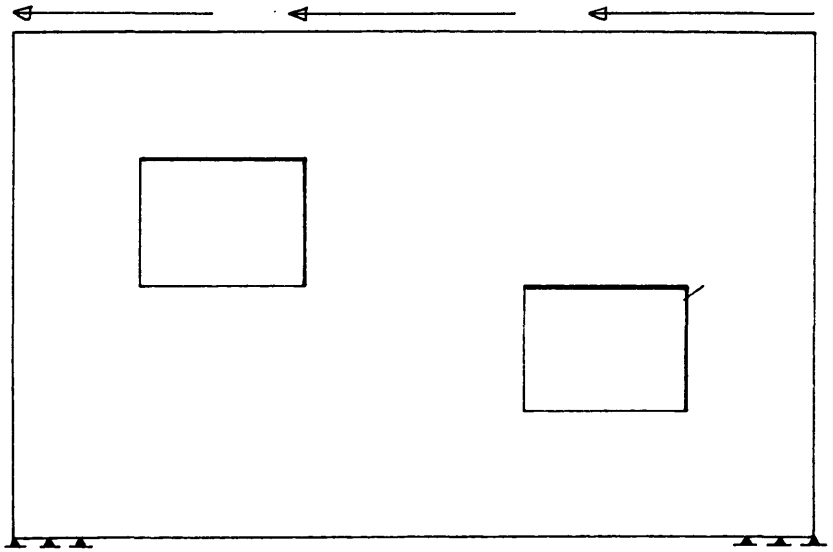
P = 65.0 t
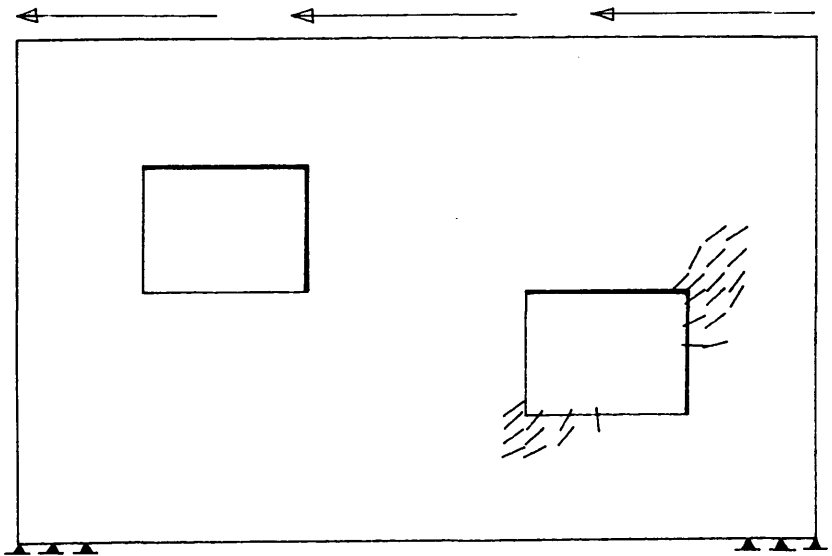
P = 78 t
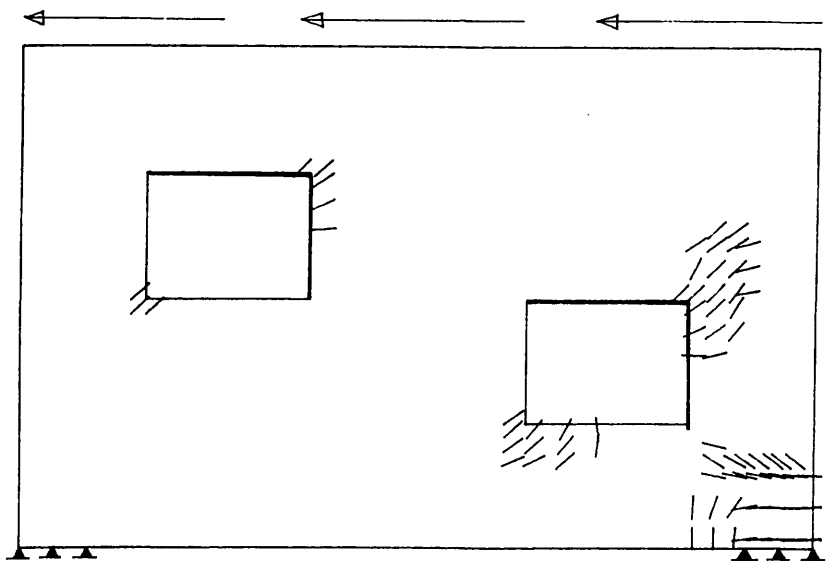
Fig (5-51) Development of cracks for panel (B2)

P´ = 91.0 t
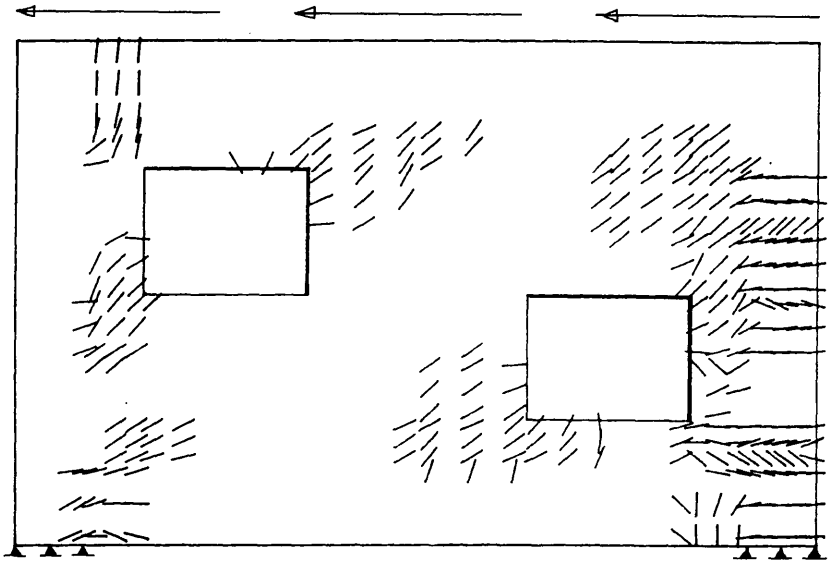
P= 117 t
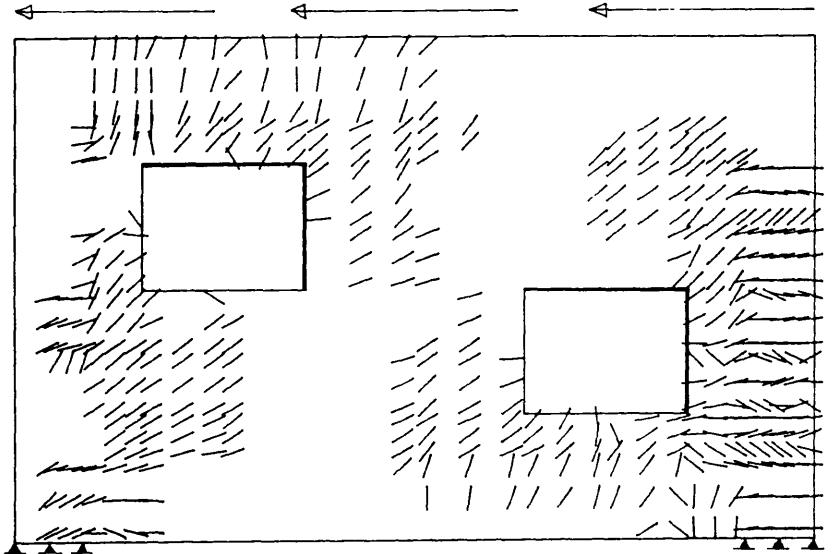
P = 130 t
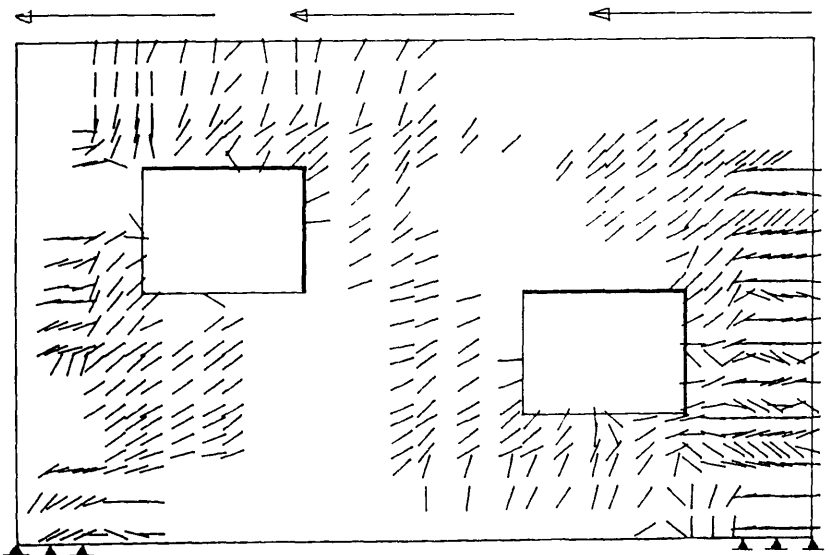
Fig (5-51) Development of cracks for panel (B2) (continued).

REFERENCES (5)

BRESLER, B. and SCORDELIS, A. C.

Shear strength of reinforced concrete beams

ACI, Vol. 60, pp. 51—75, 1963.

CERVENKA, V. and GERSTLE, K. H.

Inelatic analysis of reinforced concrete panels, part 2,

Experimental verification and application.

IABSE publications, Vol. 32—II, pp. 25—39, 1972.

CERVERA, M. HINTON, E. and HASSAN, O.

Nonlinear analysis of reinforced concrete plate and shell structures

using 20 noded isoparametric brick element.

Computers and Structures, Vol. 25, pp. 845—869, 1987.

DE BORST, R.

Computational aspects of smeared crack analysis, in

Computational modelling of reinforced concrete structures,

(Eds. Hinton, E. and Owen, R.), Chapter 2, pp. 44—83, 1986.

GIJSBER, F.B.J. and SMIT, C.L.

Resultaten van de eerste serie dwarskrachtproeven

Report No. BI—77, Institute TNO for building materials and

building structures, Rijswijk, 1977.

MAIER, J. and THUERLIMANN, B.

Bruchversuche en stahlbetonsceiben,

Institute for baustatic und konstruction, Delft university, 1986.

MURAZUMI, Y. et al.

Application of ADINA to nonlinear analysis of reinforced concrete

shear walls with openings.

Computers and Structures, Vol. 13, pp.727—736, 1981.

ROTS, J. G. et al.
> Smeared crack approach and crack localization in concrete
> *HERON, Vol. 30, No. 1, pp. 1986.*

VECCHIO, F. and COLLINS, M. P.
> The response of reinforced concrete to inplane shear and normal stresses
> Publ. No. 82−03, Dept. Civ. Eng., Toronto University, 1982.

WALRAVEN, J. C.
> The influence of depth on the shear strength of lightweight
> concrete beams without shear reinforcement.
> Report 5−78−4, Stevin lab., Delft Univ., Delft, 1978.

WANG, Q.B. et al.
> Failure of reinforced concrete panels.
> How accurate the models must be ?
> *Computer Aided Analysis and Design of concrete structures,*
> *Proc. 2nd Int. Conf, Austria 1990, pp.*

CHAPTER 6

APPLICATIONS TO COUPLED SHEAR WALLS

6-1 INTRODUCTION :

This study has been undertaken with the objective of developing a computational model of reinforced concrete for the nonlinear analysis of large scale reinforced concrete structures, specifically coupled shear walls.

In the previous sections the theoretical aspects of the computational method adopted in the present nonlinear analysis of reinforced concrete structures have been described. Also some practical applications of the model have been presented and comparisons with experimental and other numerical solutions to test the applicability and the accuracy. The comparisons of numerical predictions and experimental tests show satisfactory agreement illustrating its computational efficiency for practical use in modelling reinforced concrete in the research situation. Therefore the numerical model can be confidently applied to reinforced concrete coupled shear walls.

In this section numerical predictions of the fundamental behaviour of reinforced concrete coupled shear walls up to failure is performed. Typical coupled shear walls are investigated varying the degree of coupling and position of the openings as shown in Fig (6-1). First, a symmetric six story reinforced concrete coupled shear wall Fig (6-1a) is analysed by varying the stiffness of the connecting lintel beams. By varying the positions of the openings a staggered Fig (6-1c) and an unsymmetric Fig (6-1b) shear wall are considered. The effect of an additional stiffening beam at midheight Fig (6-1d) and at the top are also considered. To the author's knowledge, previous investigations of the degree of coupling on the behaviour of coupled shear walls available in the literature assumed either ideal elastic behaviour or elasto-plastic behaviour. The effects of cracking

and nonlinear behaviour of concrete and steel were not considered in a parametric study. The reinforcement distributed vertically and horizontally with ratio ($\rho_x = \rho_y = 2\%$) and the material properties of concrete and steel are as follows:

<u>Concrete</u>   <u>Steel</u>

$f'_c = 25$ N/mm^2 $f_y = 420$ N/mm^2

$f_t = 2.5$ N/mm^2 $E_s = 210000$ N/mm^2

$E_c = 14000$ N/mm^2 $\epsilon_y = 0.002$

$\nu = 0.2$

Finally, comparisons are made with the recent experimental work of Subedi 1990, on two microconcrete coupled shear walls.

6—2 EFFECT OF THE DEGREE OF COUPLING :

6—2—1 WALL WITH WEAK COUPLING (d = 50 cm) :

The finite element discretization shown in Fig (6—2) consists of 718 nodes and 600 elements with a total number of 5400 integration and sampling points to monitor cracking or crushing of concrete and yielding of steel at any stage during lateral loading up to ultimate load conditions.

Fig (6—4) shows the direction and crack propagation for the various load increments up to failure resulting from the analysis. As might be expected initial cracking is predicted to occur in regions of flexural tensile stress in directions at right angles to the bending stress. The cracks are horizontal for the loaded faces of the walls at base level and vertical at each end of the connecting beams subjected to reverse curvature bending. As applied loading is increased and the flexural cracks penetrate further into the bodies of the walls and depth of lintel beams, they tend to become inclined as the relative importance of the horizontal shearing force increases.

Flexural cracks first appear in the lintel beams at levels (2,3,4,5,6) while the lower beam and the walls are uncracked at a load level of 352 kN. On further loading to 528 kN, flexural cracks appear in both walls and the lintel beam at level 1 and further development of flexural cracks in the depth of the lintel beams at levels 4,5,6 can be noticed. At load 704 kN, flexural cracks develop along the span of the lintel beams and subsequently at 1056 kN shear cracks develop along the height of the wall. Between 1056 kN and 2112 kN, flexural as well as shear cracks extend further into the depth and along the span of lintel beams. Concerning reinforcement, at 1144 kN tensile steel first yields at the left end of lintel beam (3) and both ends of lintel beams 4 and 5. Upon further loading and at 1320 kN, tensile steel yielded at both ends of all lintel beams except at level 1.

At 1496 kN, tensile steel start yielding at the base of both walls.

Failure is predicted at 2288 kN at which level, concrete crushing in both ends of lintel beams at level 3,4,5 is observed as indicated in Fig (6−4). The crushing of concrete occured at the same increment (26) and iteration (4),therefore the sequence of crushing can not be determined. The extent of steel yielding is shown in Fig (6−5) at ultimate conditions.

The lateral load versus top−deflection is shown in Fig (6−3) along with the deformed finite element mesh at failure and the main load levels indicated upto collapse load. It can be noticed from the deformed finite element mesh at failure shown in Fig (6−3) that much higher distortions in the top lintel beams have developed compared to the lower beam at lower levels.

6−2−2 WALL WITH MODERATE COUPLING (d = 90 cm):

The finite element model shown in Fig (6−6) for the wall with moderate coupling is discretized with 760 nodes and 648 elements corresponding to a total of 3040 degree of freedom and 5832 sampling points for numerical integration and monitoring the damage that weakens the reinforced concrete material up to failure.

Crack development and propagation is shown in Fig (6−8) at different intermediate load levels up to failure. The onset of cracking appears in lintels 2,3,4,5 at a load of 352 kN, while the top and lower lintels and the walls are uncracked. At double this initial cracking load (704 kN), flexural cracks extend further into the depth of all lintel beams. Cracks in both walls are flexural and some diagonal cracks appear at the lintel beam−wall junction at the top and lower levels due to stress concentration.

Between 1056 and 1408 kN, shear cracks appear into the depth and along the span of all lintel beams. Further development of flexural and shear cracks along the height of both walls is noticed.

Between 1408 kN and 2464 kN no major change of cracks along the span of lintel beams is observed, however, shear cracks continue to develop into the depth of lintel beams and along the height of the walls. Tensile steel starts yielding at left of end of lintel (4) at a load level of 1320 kN and subsequently at 1408 kN tensile steel yield at both ends of lintel 4,3,2 and 5 (in that order). At 2024 kN tensile steel starts yielding at the base of right wall and at 2112 kN yielding occured at the base of the left wall and compression steel yields at both ends of lintels (3) and (4). At 2816 kN concrete crushes at both ends of lintels 2,3,4 and 5 and the sequence of crushing is indicated in Fig (6—8). Also at 2816 kN compression steel yields at the base of the right wall. Upon further loading and at 2992 kN numerical collapse of the coupled shear walls is observed, at which level crushing of compressive concrete at the base of the right wall as indicated in Fig (6—8) occured. Almost half of the total height of the walls is cracked both flexural and in shear. The deformed finite element mesh at failure is shown in Fig (6—7) along with the lateral load top deflection indicating the main load levels at which steel start yielding and concrete crushing in the lintel beams and walls. The extent and direction of steel yielding at numerical collapse load is shown in Fig (6—9) where tensile and compressive steel have yielded at both ends of all lintel beams.

6—2—3 WALL WITH STIFF COUPLING (d = 150 cm):

The finite element discretization shown in Fig (6—10) is similar to the wall with moderate coupling with a slight modification to discretize the much deeper lintel beams. Due to high depth of the coupling beams, the first cracks are slightly inclined due to shear effects, Fig (6—12). This occurred at levels 1,2,3,4 at load 528 kN. First flexural cracks appear in the right wall at a load level 704 kN. Between 1056 and 3872 kN further flexural as well as shear cracks develop along

the height of both walls and it can be noticed that the right wall has more crack damage than the left one. This is in agreement with what is expected because the walls tend to behave as a monolithic unit where the high degree of inter— coupling produces significant axial tensile and compressive stresses vertically in the walls. For reinforcement, tensile steel starts yielding at 2024 kN at the left end of the lintel beam at level 2. At 2464 kN tensile steel yielded at both ends of lintel beams at levels 1 to 4. Yielding of steel at the base of walls is predicted at 2904 kN for the left wall and 2992 kN for the right wall. At 3432 compression steel yields at both ends of lintel 2 and at 3784 kN compression steel yields at the base of right wall.

Failure is observed at 4312 kN at which stage the right wall is almost completely cracked compared to the left side. Concrete crushing is observed in lintel beams at levels 1,2,3,4 and diagonal cracks spread along the span of all lintel beams except the top story as indicated in Fig (6—12) where the sequence of crushing is also indicated. Crushing at the base of both walls is also observed with more damage in the right wall as shown in Fig (6—12) and fig (6—11) where the deformed finite element mesh at failure reveals high compression at the base of the right wall.

(a) Symmetric

(b) Unsymmetric

(c) Staggered

(d) Stiffened
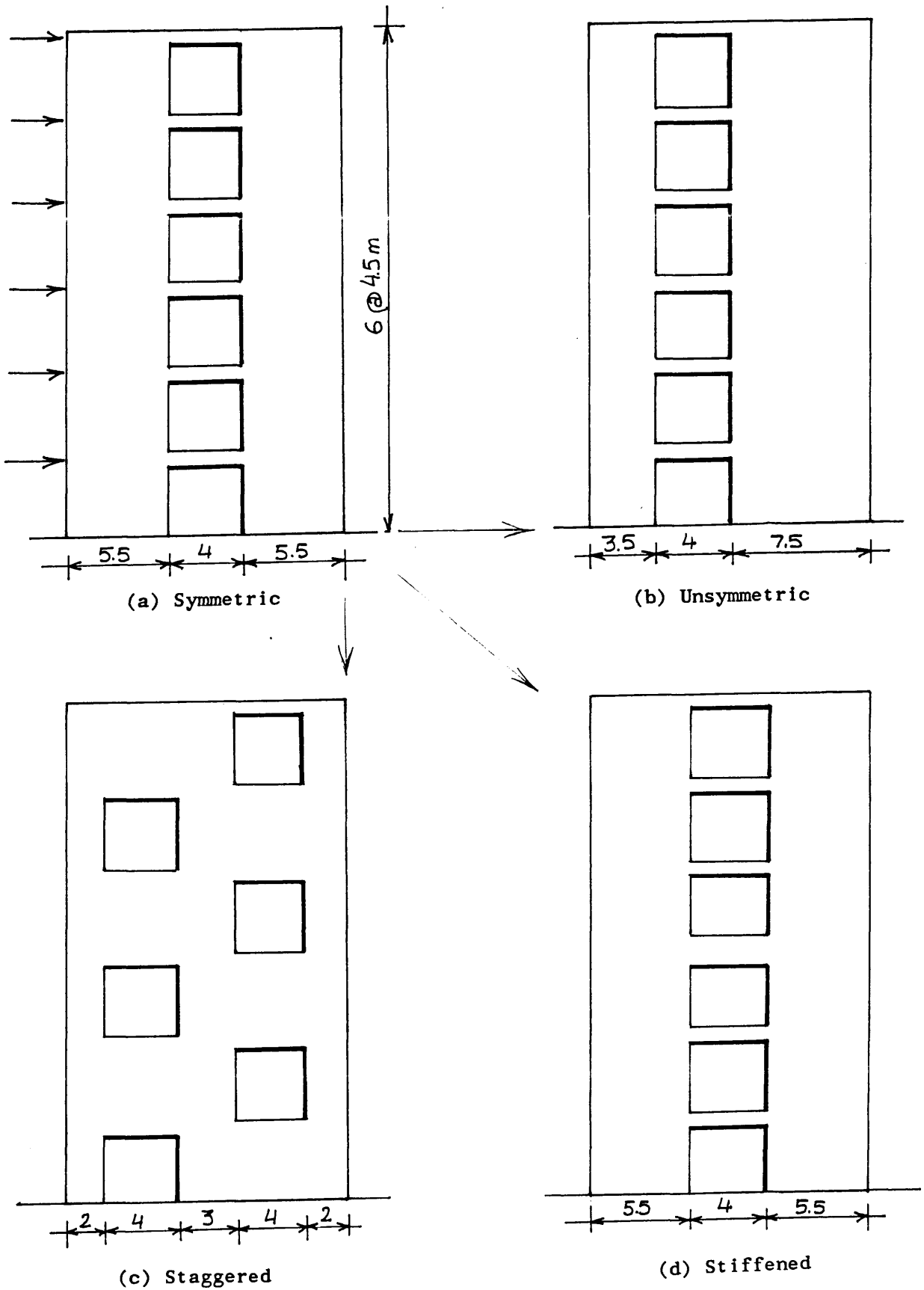
FIG (6-1) REINFORCED CONCRETE SHEAR WALLS ANALYSED
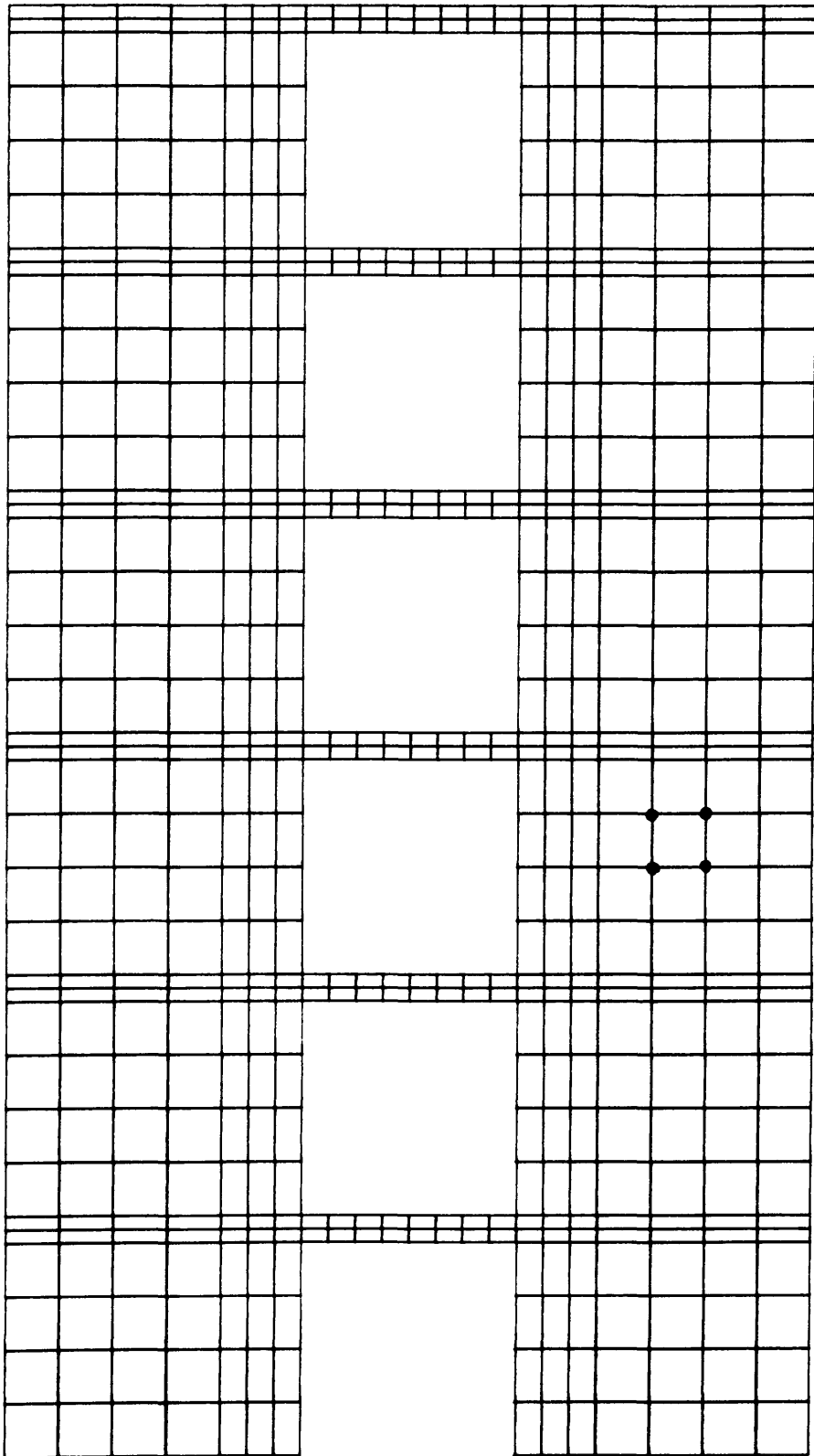
FIG (6-2) FINITE ELEMENT DISCRETIZATION FOR WALL
WITH WEAK COUPLING (d=50cm.)
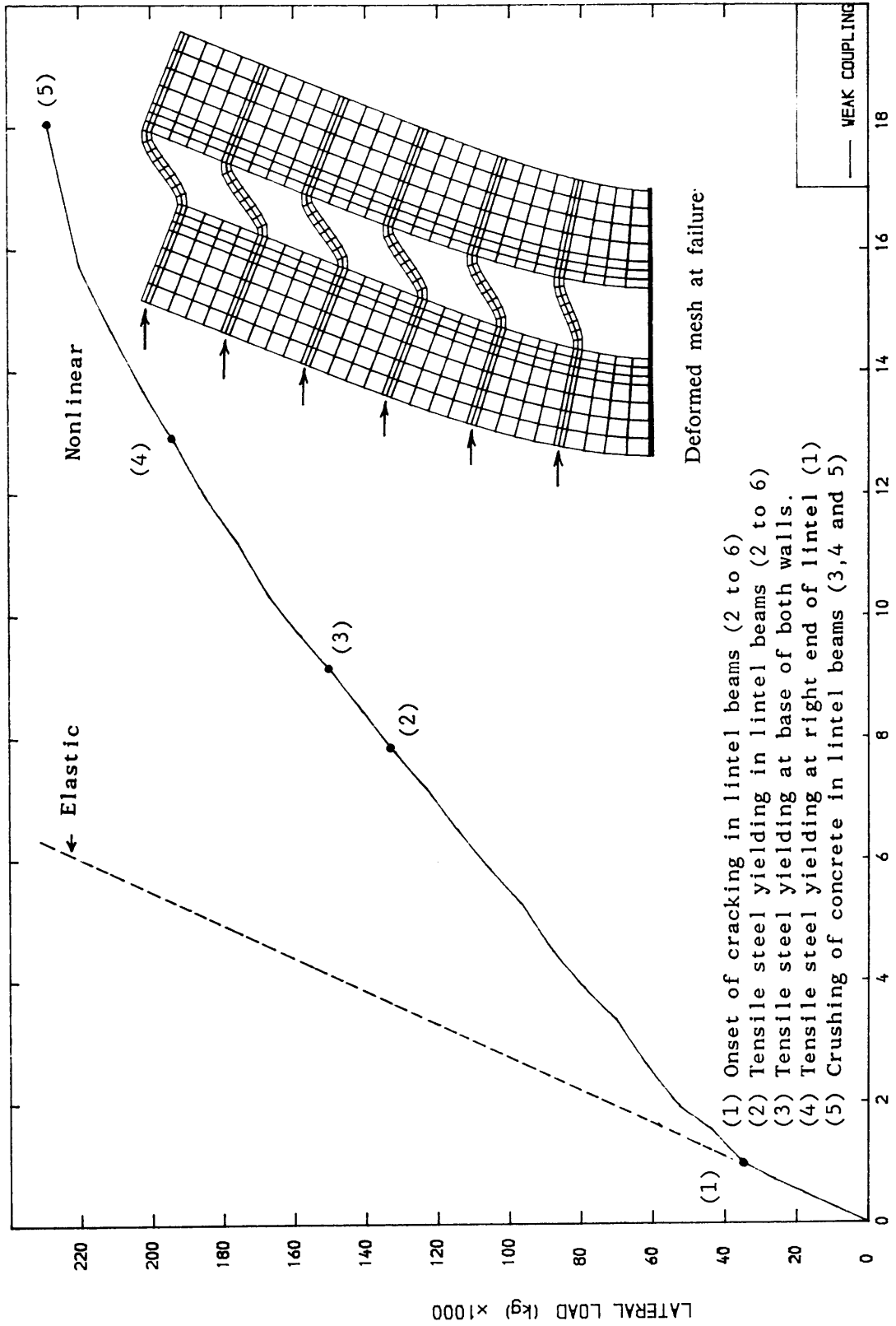
FIG (6-3) *LATERAL LOAD-DISPLACEMENT FOR WALL WITH WEAK COUPLING*

Nonlinear

Elastic

(1) Onset of cracking in lintel beams (2 to 6)
(2) Tensile steel yielding in lintel beams (2 to 6)
(3) Tensile steel yielding at base of both walls.
(4) Tensile steel yielding at right end of lintel (1)
(5) Crushing of concrete in lintel beams (3,4 and 5)

Deformed mesh at failure

LATERAL DISPLACEMENT (cm)

LATERAL LOAD (kg) ×1000

—— WEAK COUPLING

352 kN   528 kN
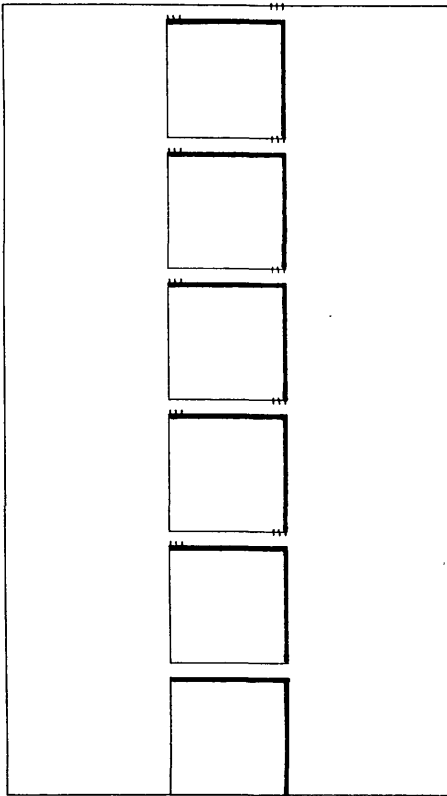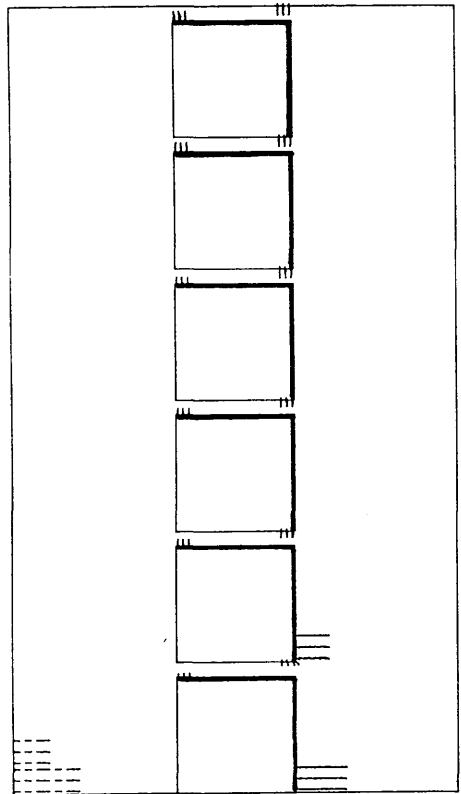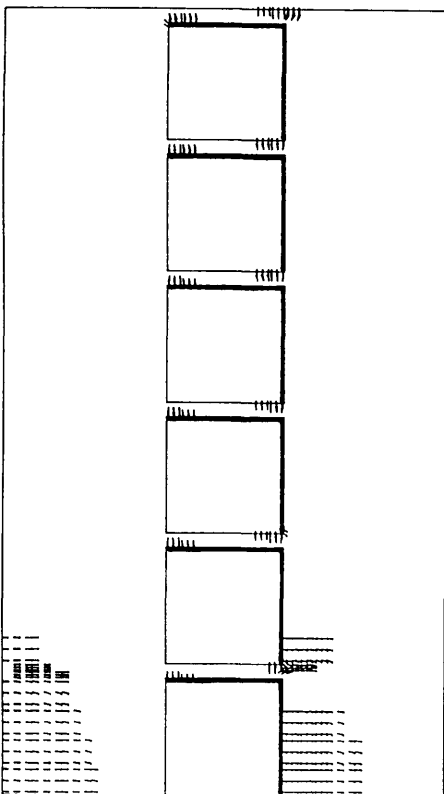
704 kN   1056 kN
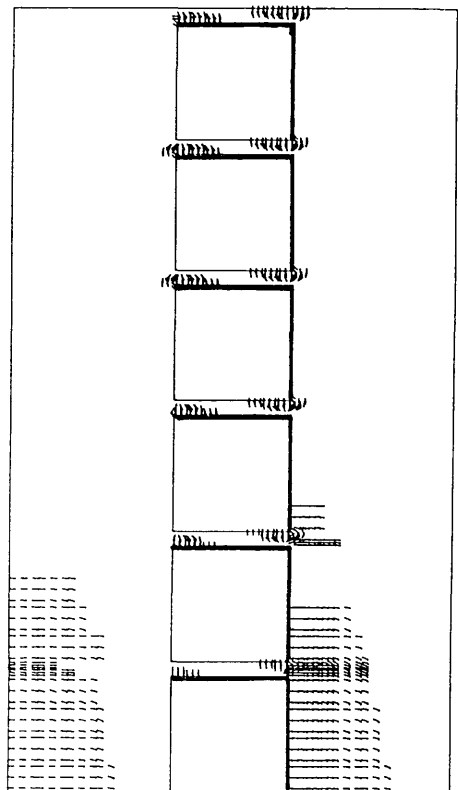
FIG (6-4) CRACK PATTERN AND PROPAGATION FOR WALL
          WITH WEAK COUPLING (d=50cm.)

1408 kN
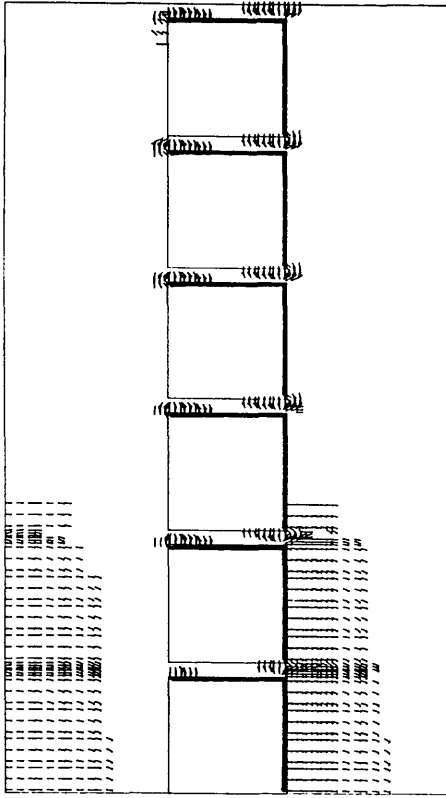
1584 kN
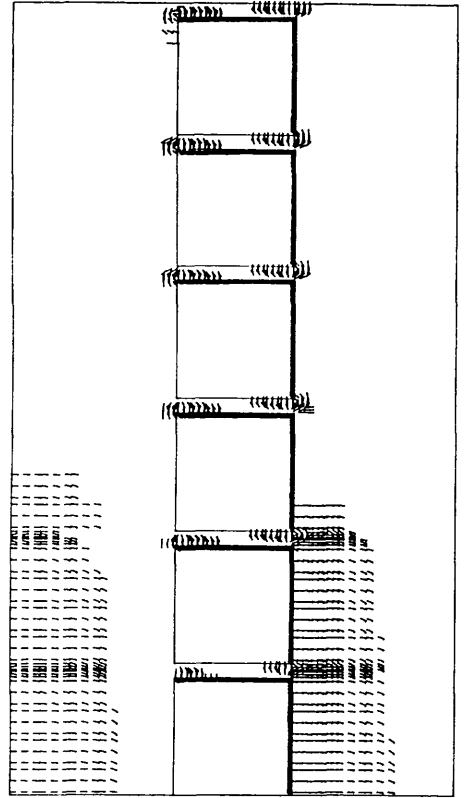
2112 kN
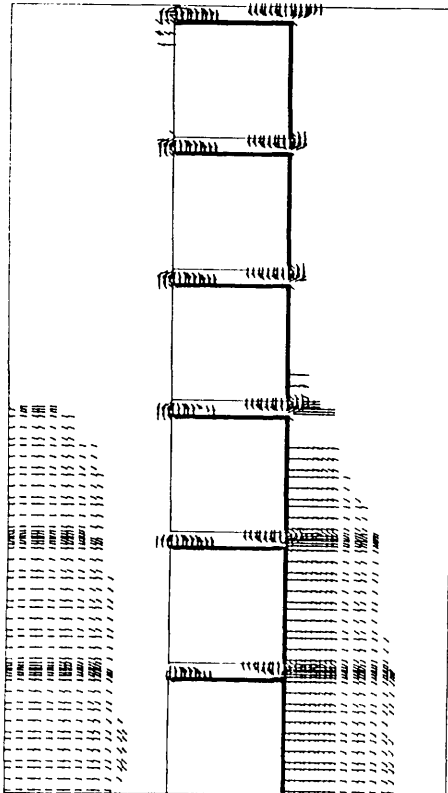
2288 kN
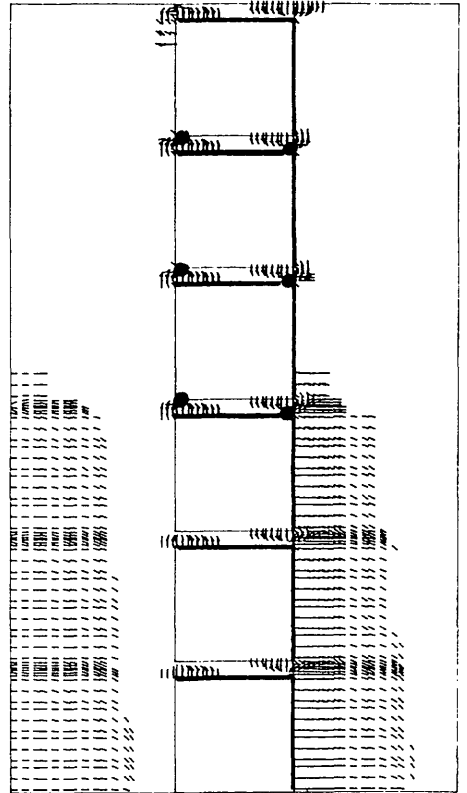
● Crushed concrete

FIG (6-4) .... CONTINUED .
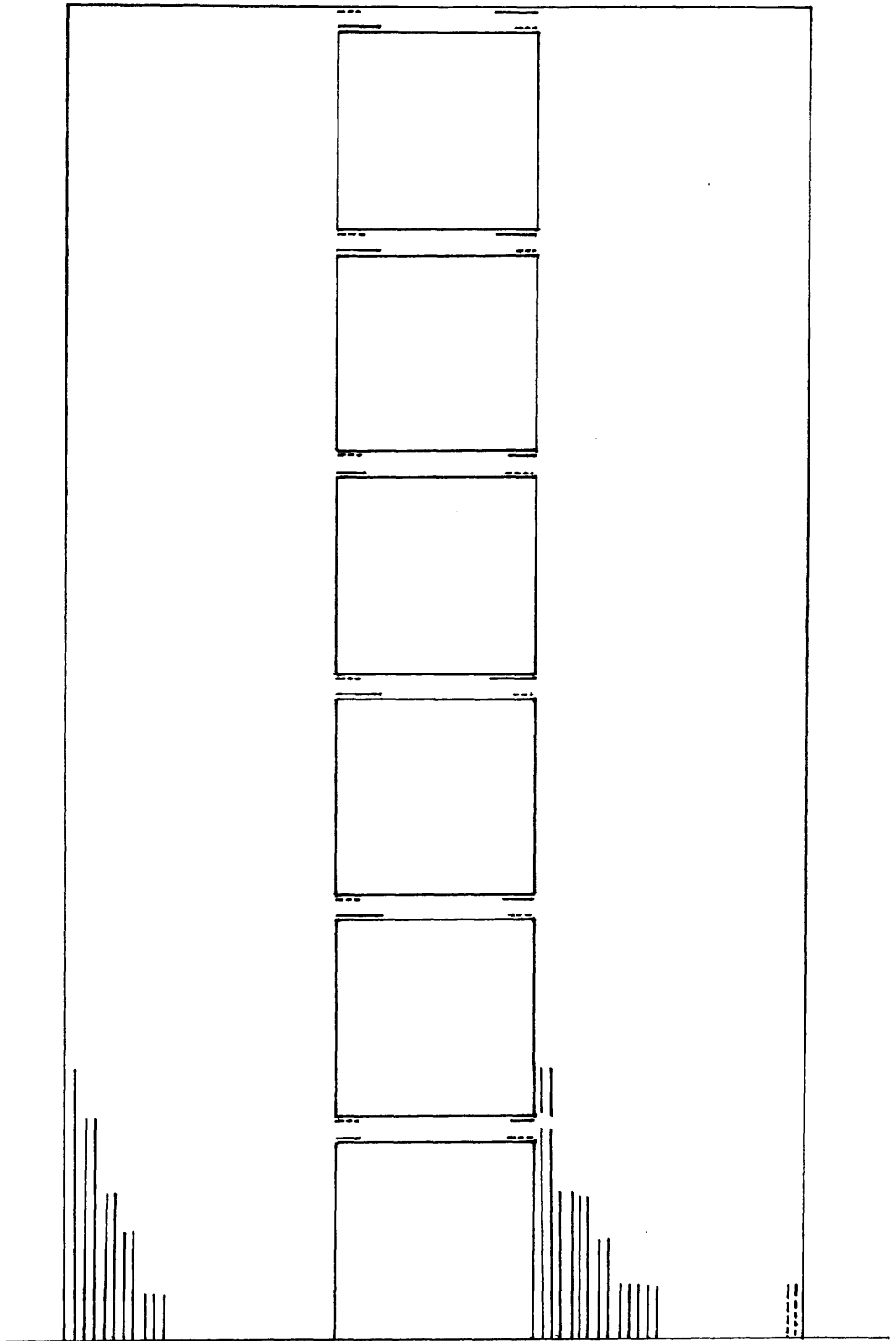
——— Tension   ----- Compression

FIG (6-5) EXTENT AND DIRECTION OF YIELDED STEEL AT ULTIMATE
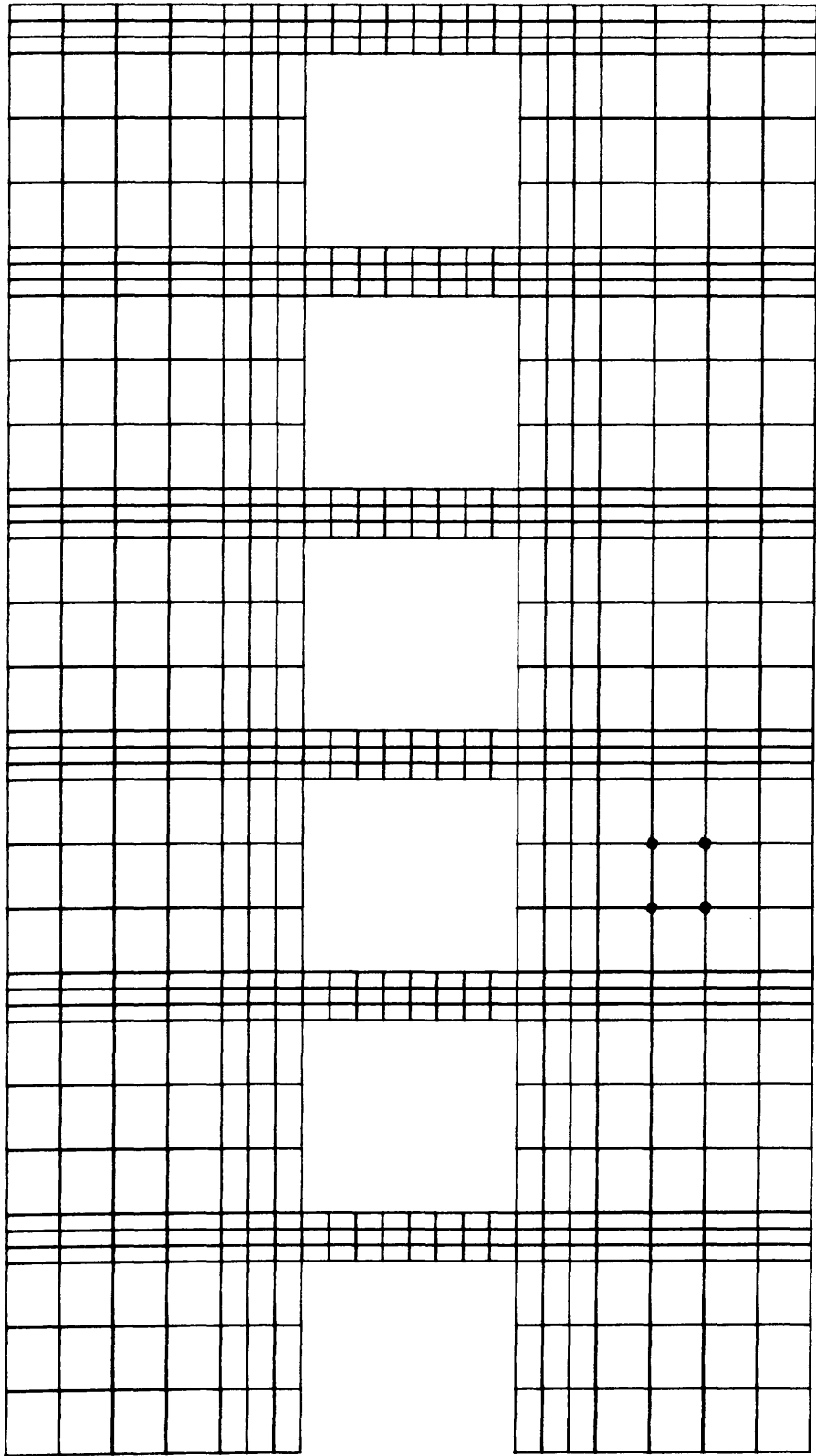
FIG(6-6) FINITE ELEMENT DISCRETIZATION FOR WALL
WITH MODERATE COUPLING (d=90cm.)

Deformed mesh at failure

(1) Onset of cracking in lintel beams 2,3,4 and 5.
(2) Tensile steel starts yielding at left end of lintel 4.
(3) Tensile steel yielding at both ends of lintels 2,3,4 and 5.
(4) Tensile steel yielding at base of both walls.
(5) Crushing of concrete at both ends of lintels 2,3,4 and 5.
(6) Crushing of concrete at base of right wall.
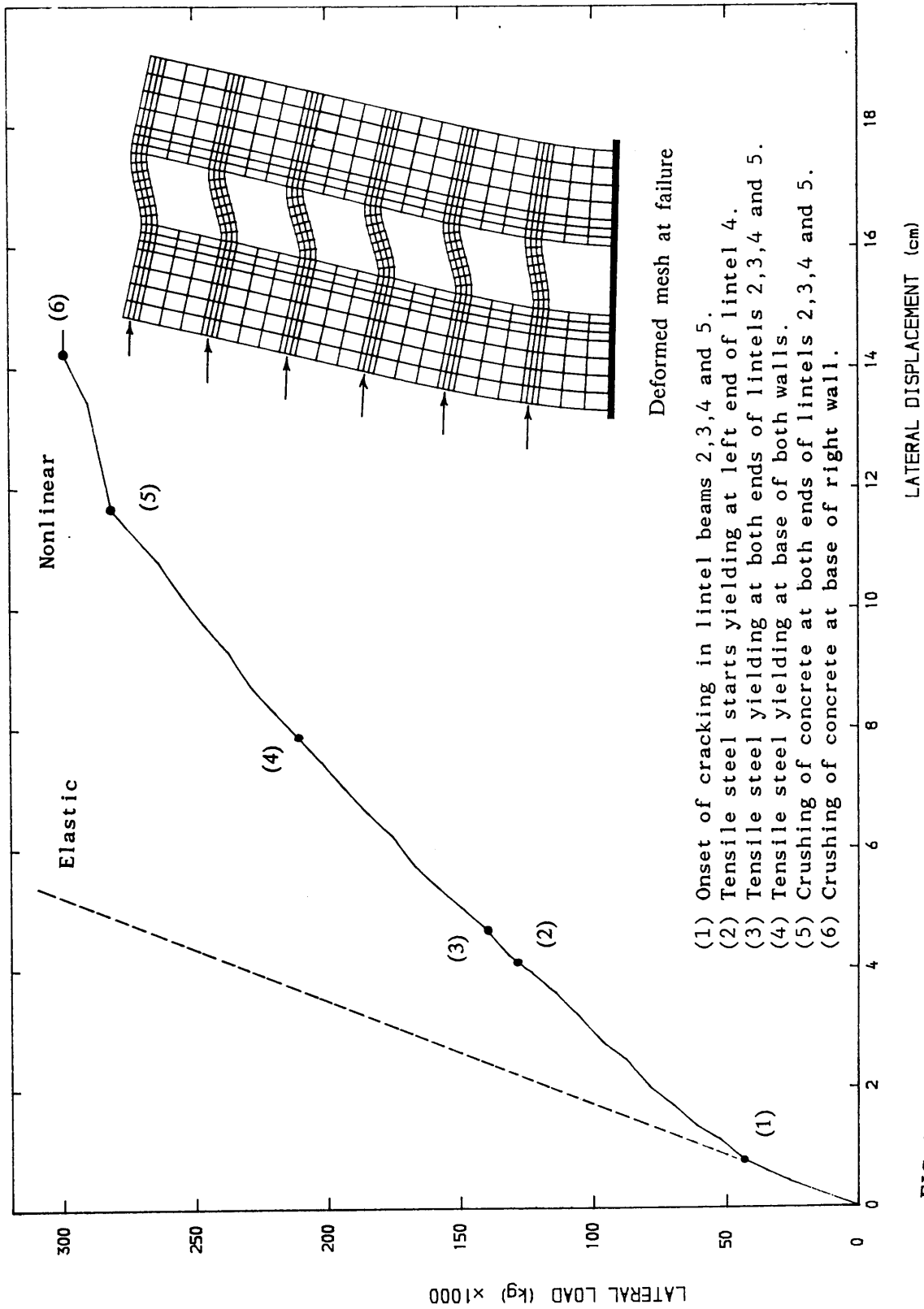
FIG (6-7) *LATERAL LOAD–DISPLACEMENT FOR WALL WITH MODERATE COUPLING*
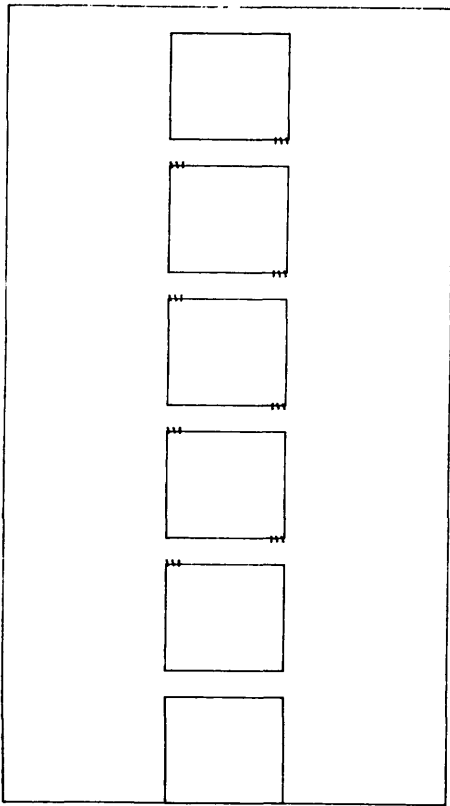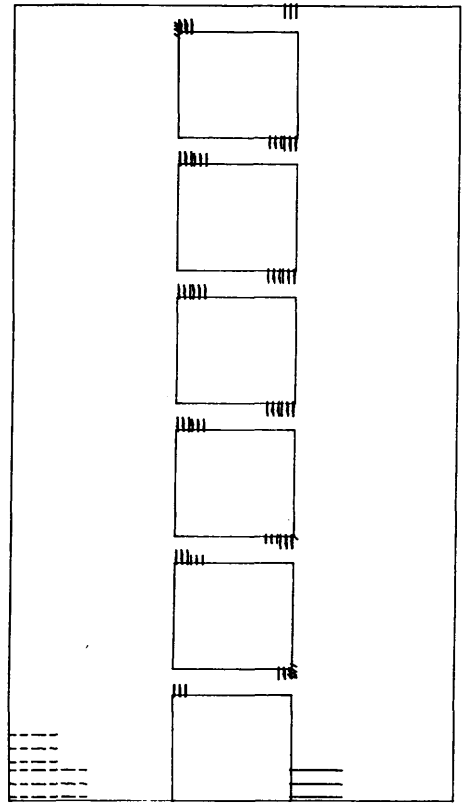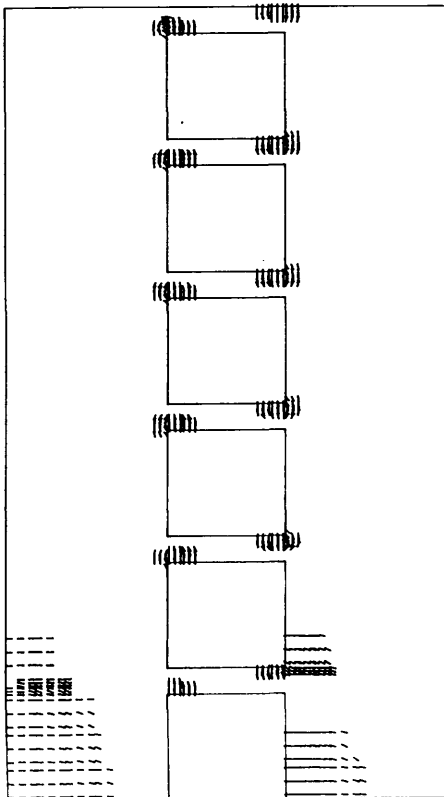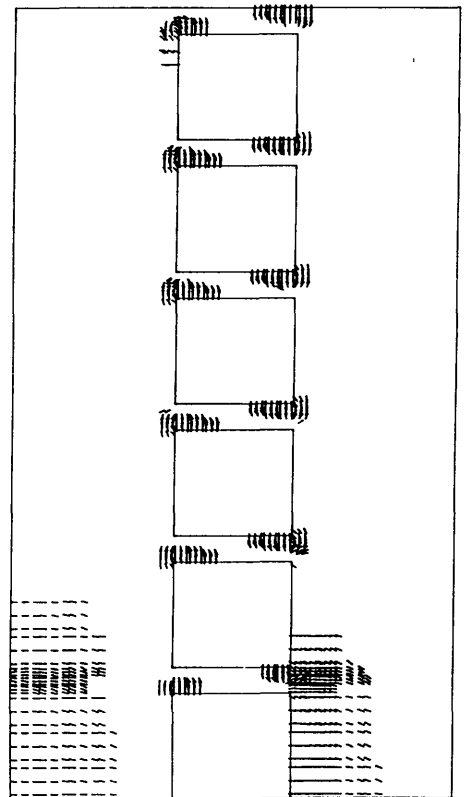
FIG (6-8) CRACK PATTERN AND PROPAGATION FOR WALL
WITH MODERATE COUPLING (d=90cm.)

1760 kN
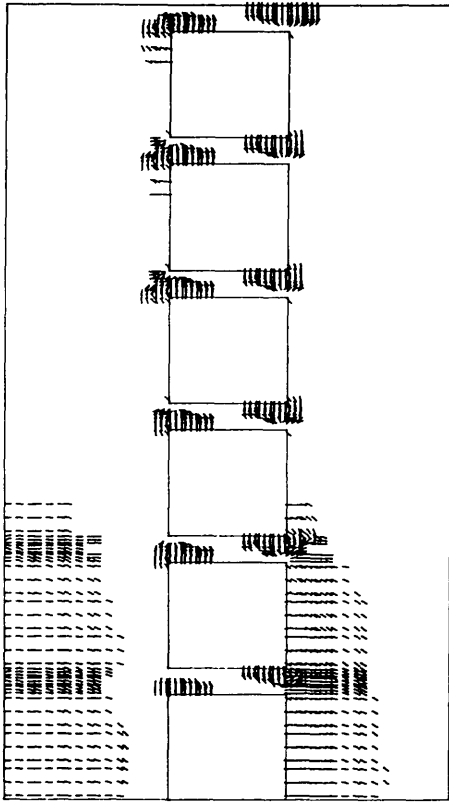
2112 kN
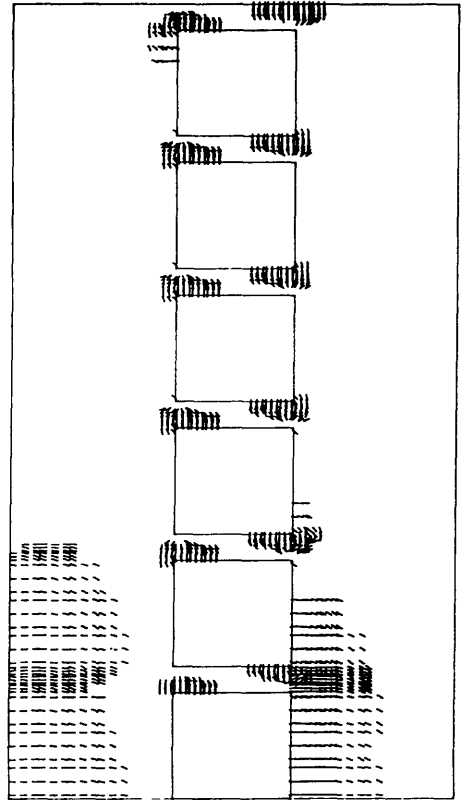
2464 kN
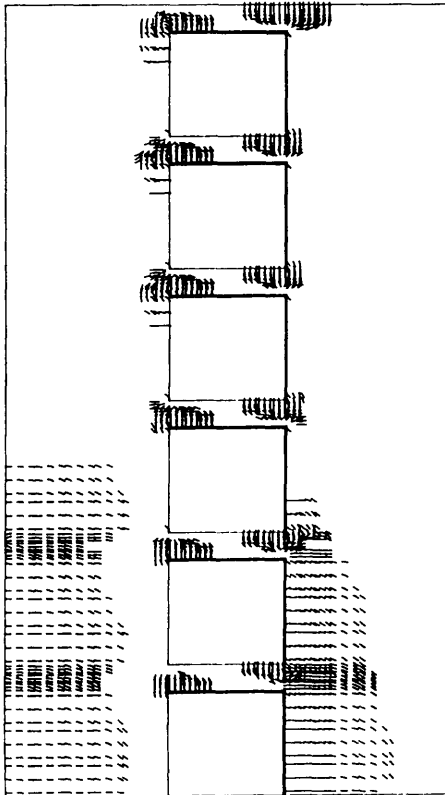
2992 kN
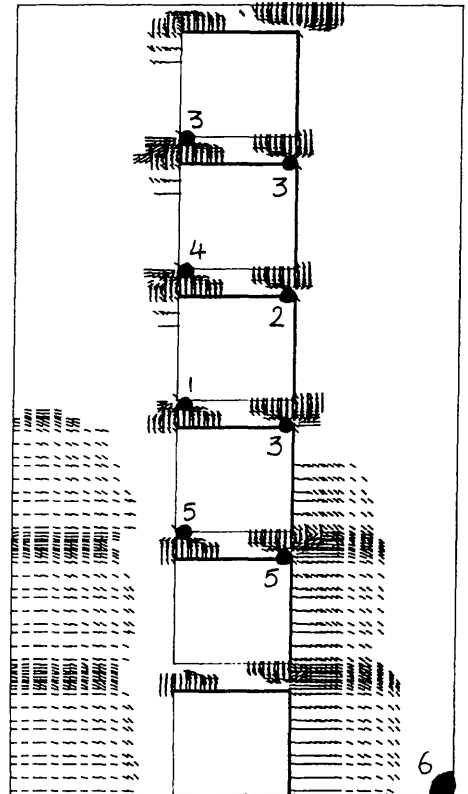
● Crushed concrete

FIG (6-8) .... CONTINUED .
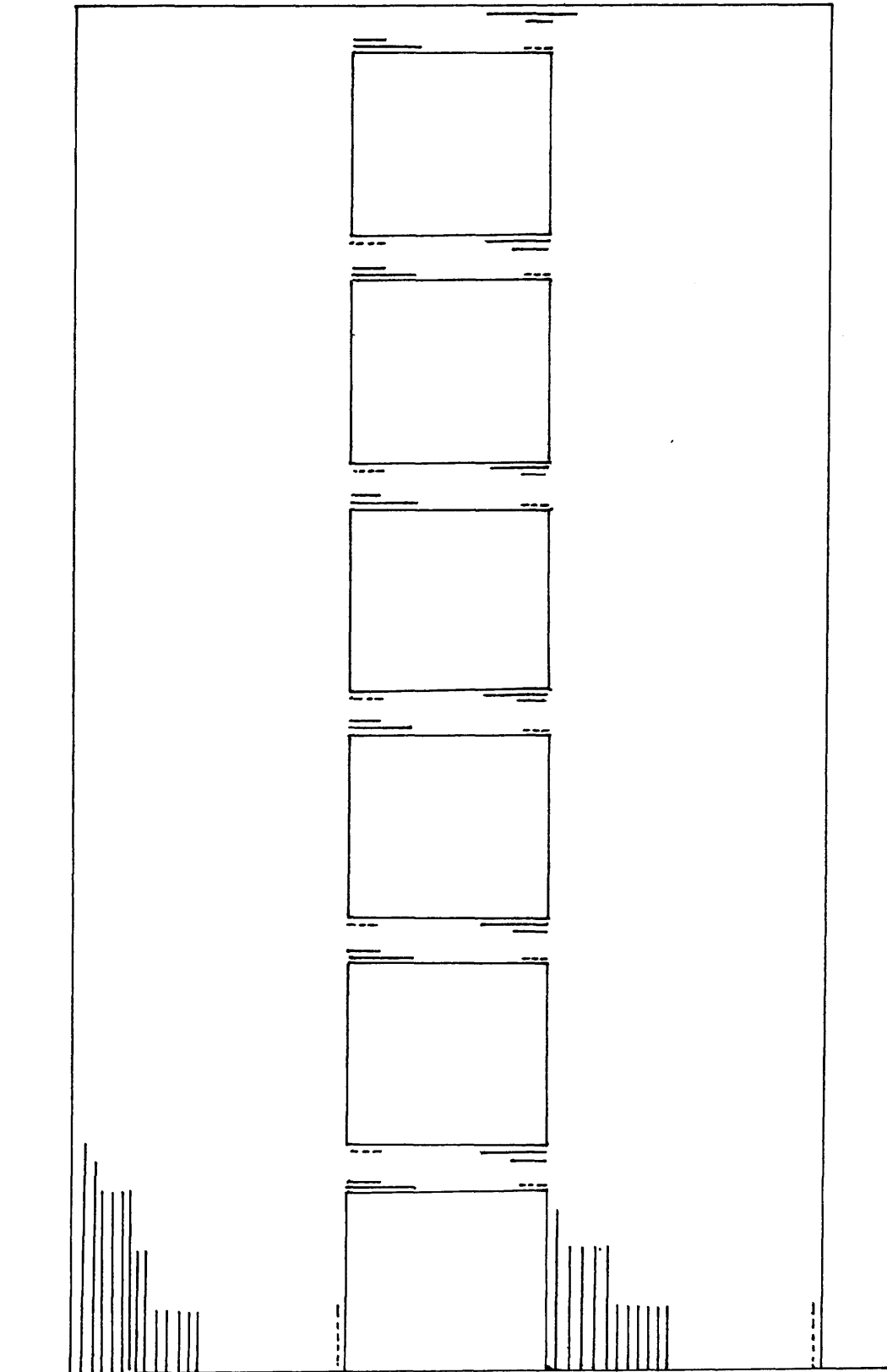
———— Tension   ----- Compression

FIG (6-9) EXTENT AND DIRECTION OF YIELDED STEEL AT ULTIMATE
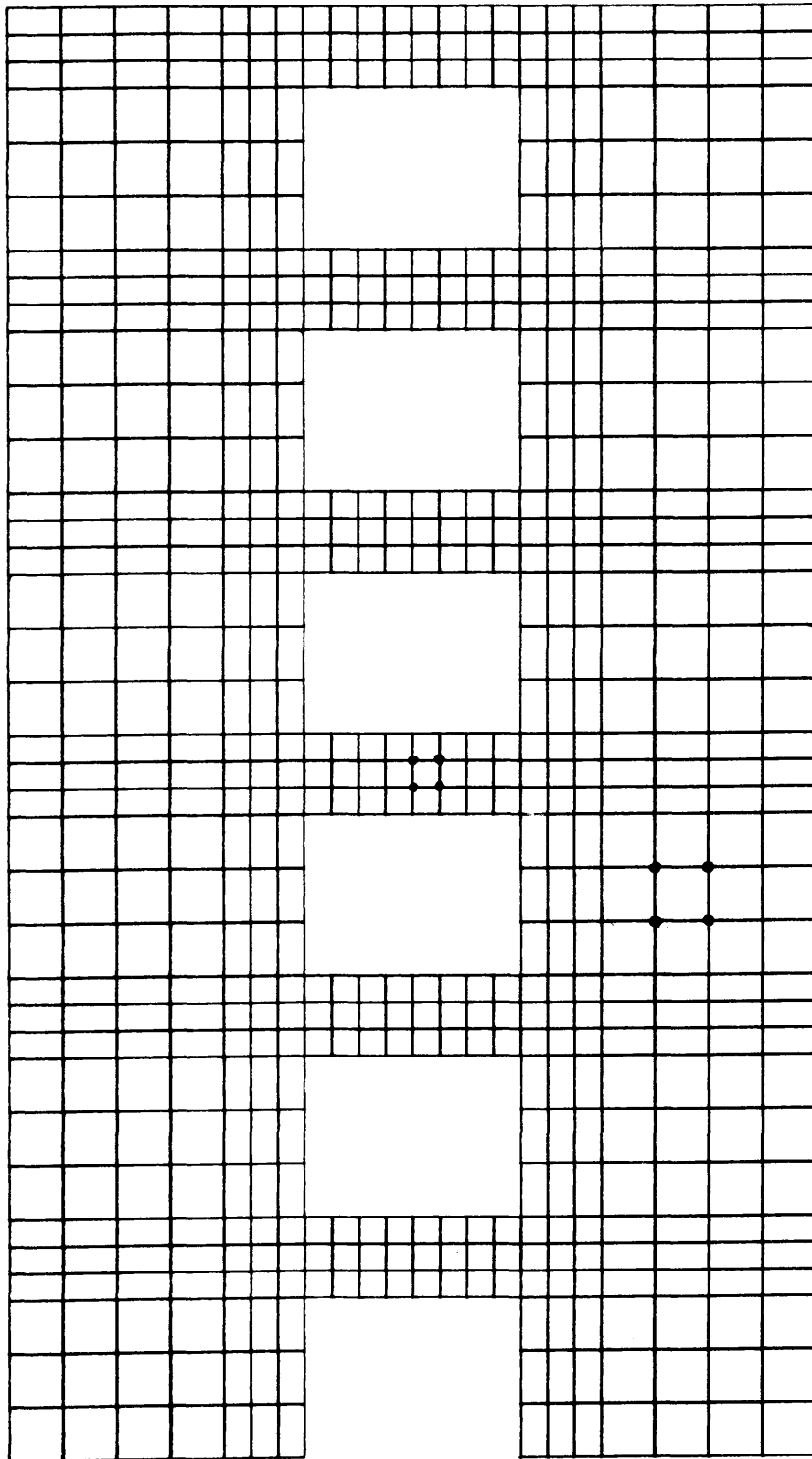
FIG (6-10) FINITE ELEMENT DISCRETIZATION FOR WALL
WITH STIFF COUPLING (d=150cm.)

Deformed mesh at failure
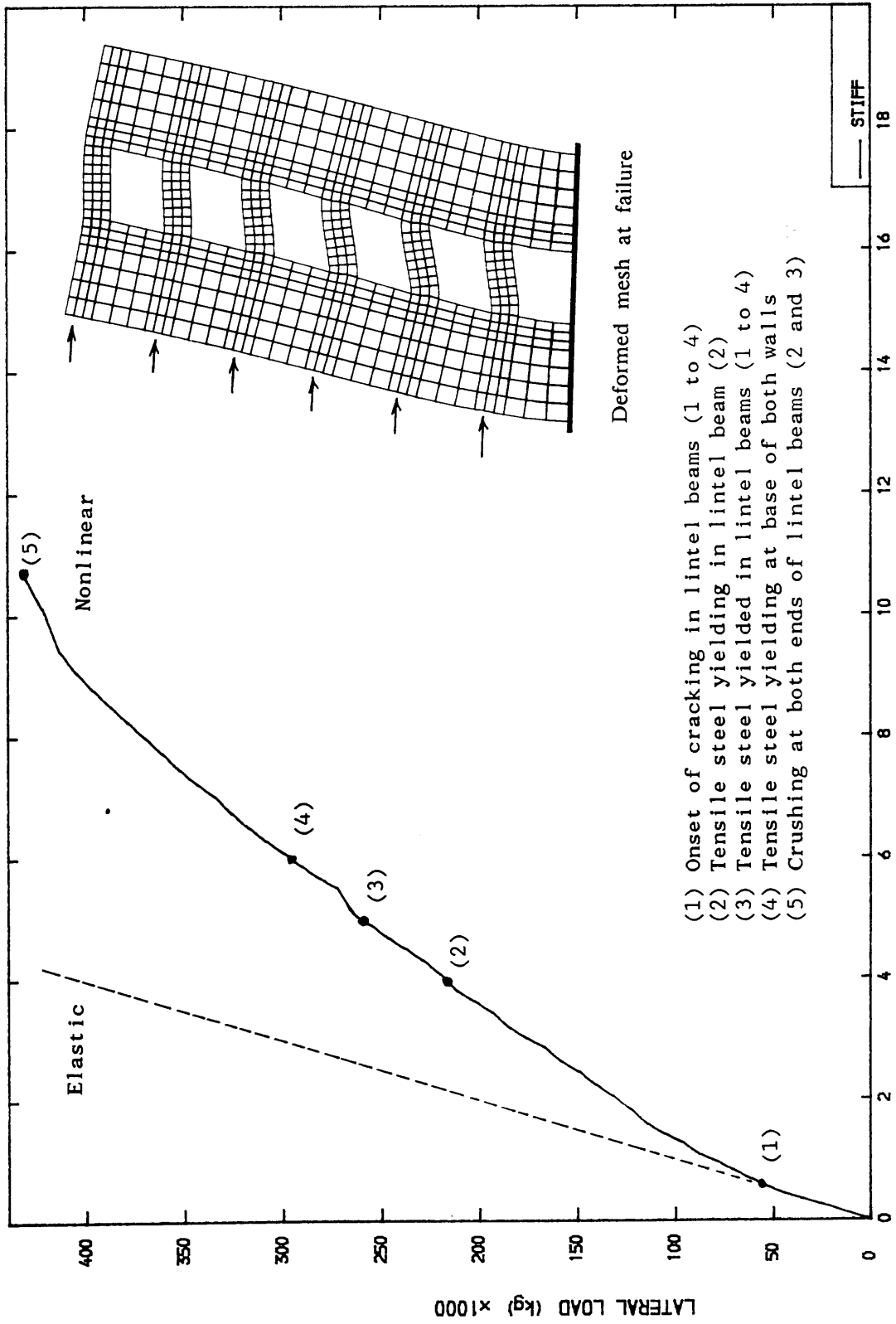
(1) Onset of cracking in lintel beams (1 to 4)
(2) Tensile steel yielding in lintel beam (2)
(3) Tensile steel yielded in lintel beams (1 to 4)
(4) Tensile steel yielding at base of both walls
(5) Crushing at both ends of lintel beams (2 and 3)

Nonlinear

Elastic

—— STIFF

LATERAL DISPLACEMENT (cm)

LATERAL LOAD (kg) ×1000

FIG (6-11) LATERAL LOAD-DISPLACEMENT FOR WALL WITH STIFF COUPLING
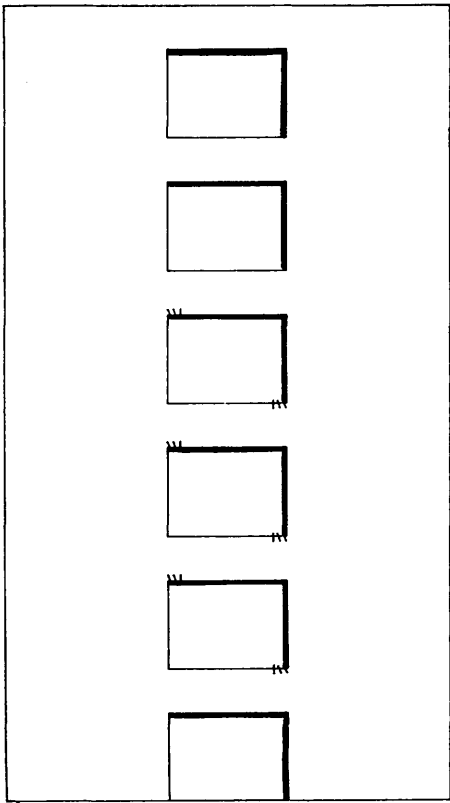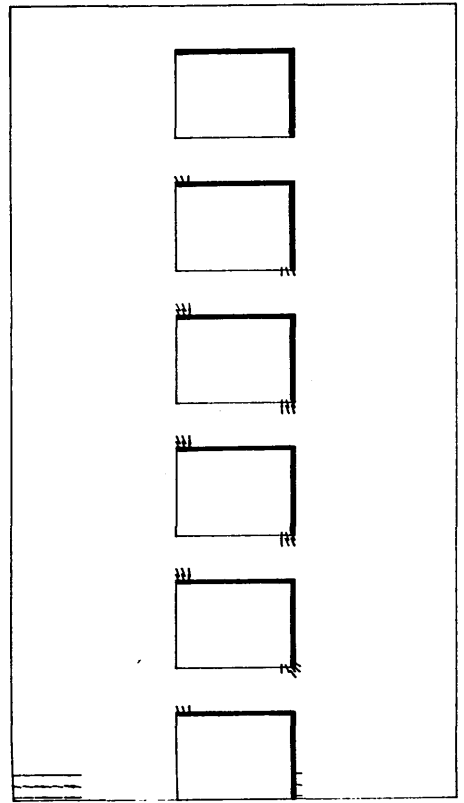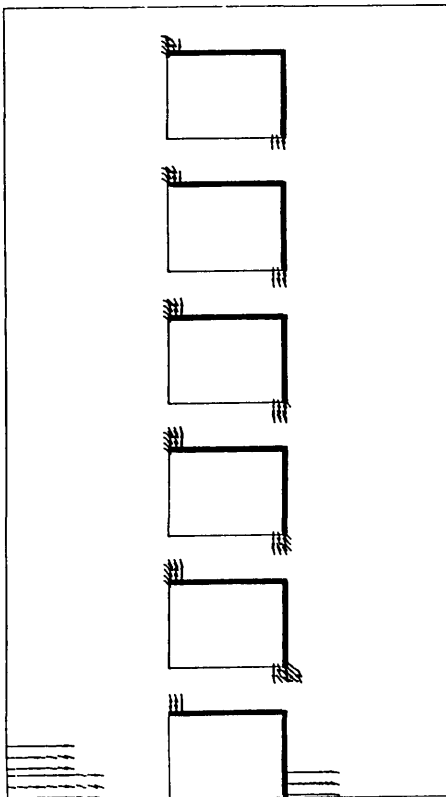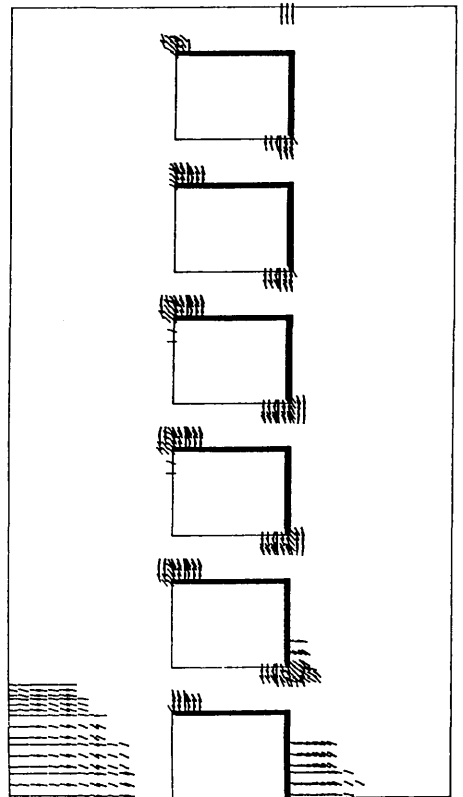
FIG(6-12) CRACK PATTERN AND PROPAGATION FOR WALL
WITH STIFF COUPLING (d=150cm.)

2112 kN
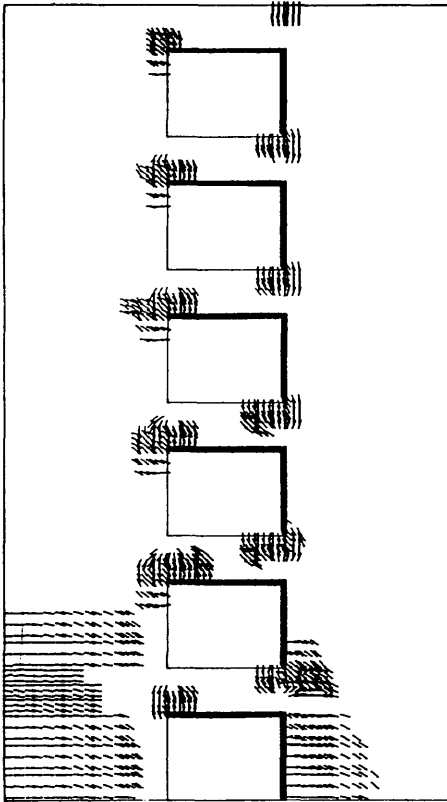
3168 kN
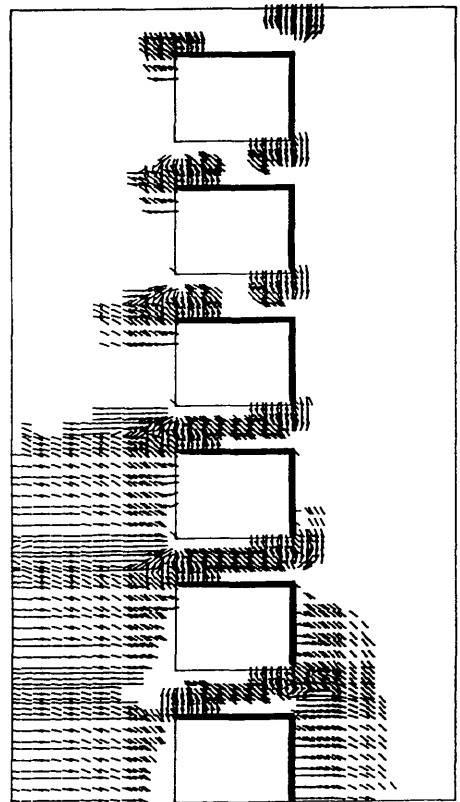
3872 kN
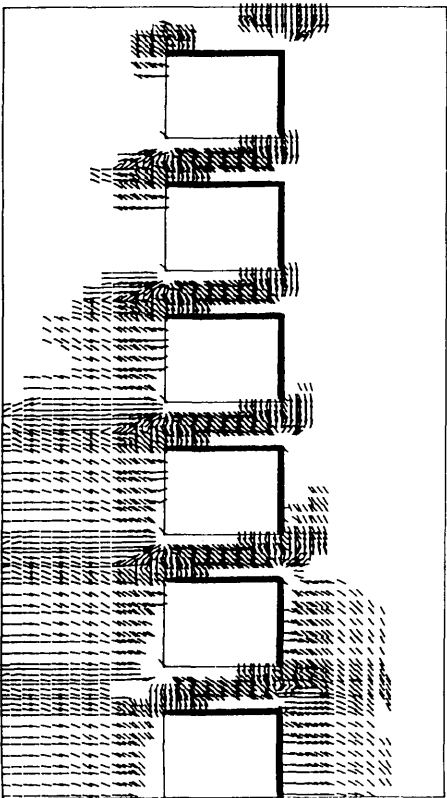
4312 kN
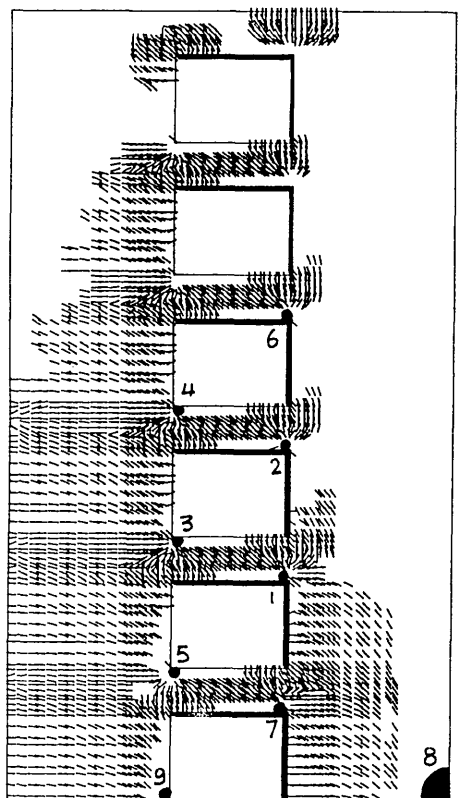
● Crushed concrete

FIG (6-12) .... CONTINUED .

Tension   ----- Compression
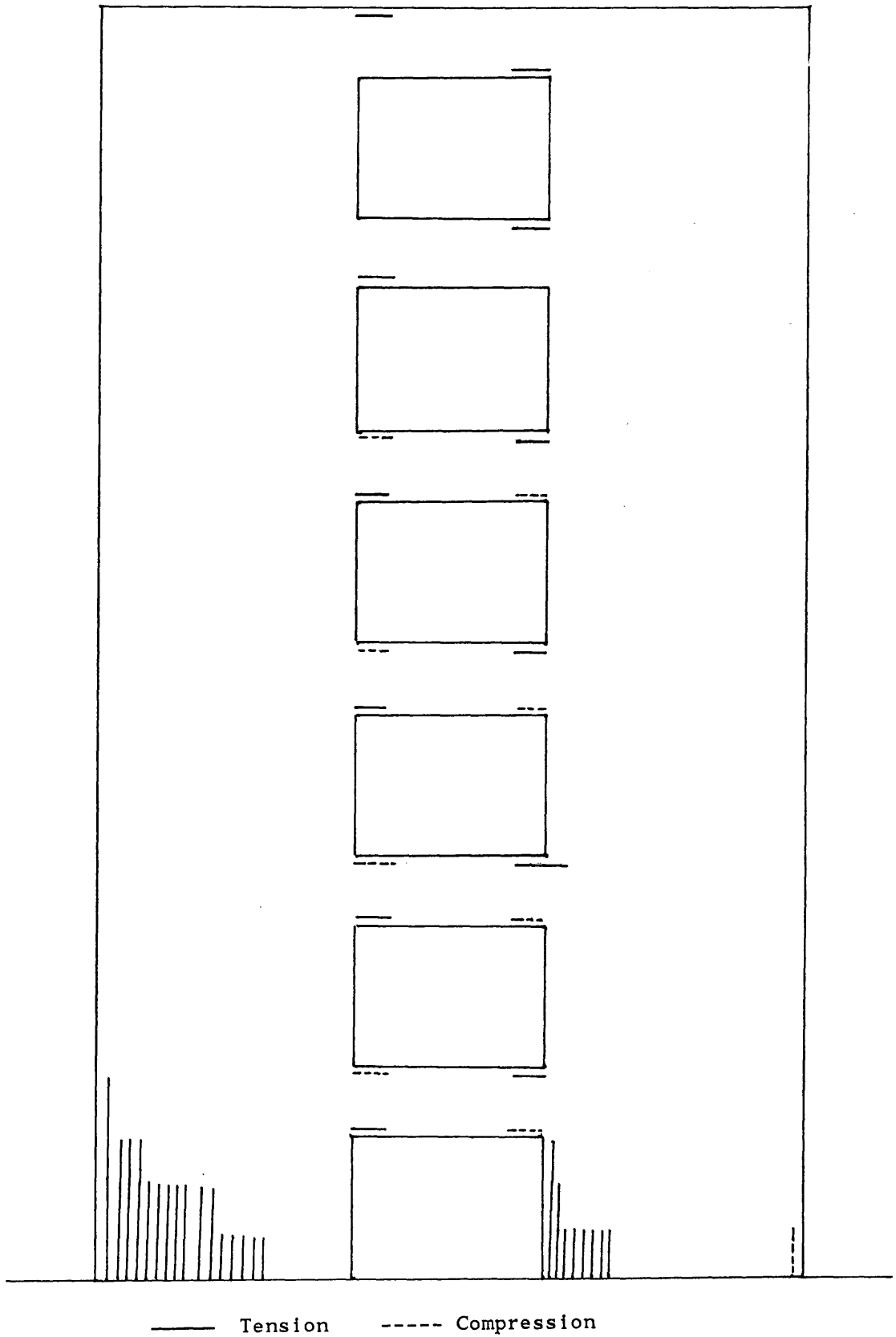
FIG (6-13) EXTENT AND DIRECTION OF YIELDED STEEL AT ULTIMATE

6—3 POSITION OF THE OPENINGS :

In the three examples previously considered, the coupled shear walls were symmetric and the effects of the degree of coupling on the crack distribution, crushing of concrete, yielding of steel and ultimate load and mode of failure were considered. In this section the position of the openings is varied so that two situations are examined. Firstly, the effects of unsymmetrical walls where stiffness of the walls in the ratio (10:1) is considered, and secondly, where the openings are positioned in a staggered arrangement is studied.

6—3—1 UNSYMMETRIC WALLS :

In this case the symmetric coupled shear wall with weak coupling is studied by changing the positions of the openings Fig (6—1b). Because of unsymmetry and nonlinearity two loading cases are considered. The first (case (a)) considers load acting on the left smaller wall, and the second (case (b)) with load acting on the right stiffer wall.

case (a): Load acting on the left smaller wall Fig (6—15)

The finite element mesh chosen for the unsymmetric wall is shown in Fig(6—14) and consists of 718 nodes and 600 elements. Apart from the cracking load and ultimate load of 440 kN and 2552 kN being slightly higher than the corresponding 352 kN and 2288 kN for the symmetric case, comparisons in terms of cracking shown in Fig (6—4) and Fig (6—16) show similar developments and propagation as described in 6—2—1. The only difference is in the unequal cracking of the walls and the lateral deflection exhibiting stiffer behaviour and higher ultimate load of about 12% compared to the symmetric case. At 1408 kN tensile

steel first starts yielding at both ends of lintel 5 and 4 and at 1496 kN this occured at both ends of lintel 3 followed by yielding at left end of lintel 6 during the iterative process. At 1672 kN steel start yielding at left end of lintel 2 , right end of lintel 6 and at the base of the stiffer wall. At 1760 kN compressive steel yields at right end of lintel 3 and at 1936 kN this occured at left end of lintel 3 and both ends of lintels 4 and 5. At 2376 kN tensile steel yields at the base of smaller wall and at 2464 kN compressive steel yields at base of stiffer wall. Concrete crushes at both ends of lintel beams 3 and 4 at 2464 kN. Finally numerical collapse of the wall by crushing at both ends of lintel 2, 5 and 6 and at the base of the right wall is observed at 2552 kN. A summary indicating the main load levels is shown in Fig (6−15) on the lateral load top displacement curve. The extent of steel yielding Fig (6−17) and crack pattern Fig (6−16) reveals that much damage occured in the stiff wall due to its high stiffness in resisting most of the lateral load compared to the smaller wall.

case (b) Load acting on the right stiffer wall Fig (6−18)

Similar crack development and propagation is noticed in Fig (6−19) compared to Fig (6−16) when load acting on the left smaller wall.
At 1320 kN tensile steel starts yielding at both ends of lintel 4 followed by both ends of lintel 5, 3 and right end of lintel 6 at 1408 kN (in that order). At 1496 kN tensile steel starts yielding at right end of lintel 2 and upon further loading at 1584 kN tensile steel yields at base of stiffer wall and left end of lintel 2. At 1672 kN tensile steel yields at left end of lintel 6. At 2200 kN tensile steel yields at base of smaller wall and right end of lintel 1. At 2288 kN compressive steel yields at both ends of lintel 5 and the base of stiffer wall and subsequently at 2376 kN compressive steel yields at both ends of lintels 4 and 3.

6-3-2 STAGGERED OPENINGS :

The staggered finite element discretization is shown in Fig (6-21). Because of unsymmetric geometry and material nonlinearity the same two opposite loading cases considered above will be applied here.

case (a) loading from the left side: Fig (6-22)

The cracking load 528 kN is much higher than for the case of the symmetric wall. Flexural cracks first appear at the base in the left side and the corner of the opening at the first level Fig (6-23). Upon further loading and at 1056 kN the base of the left wall becomes completely cracked and diagonal cracks develop at the corner of the second and third level.

At 1408 kN diagonal shear cracks begin to develop, in the right wall and further diagonal crcaks develop at the corners of the openings at level 2.

At 2112 kN further diagonal shear cracks propagate at the base of the right wall and along the height, This trend continues until numerical failure of the wall at 5368 kN more than double the failure load of 2288 kN for the symmetric wall with weak coupling. Tensile steel starts yielding at the base of the left wall (opposite ends) at 2288 kN. At 2816 kN tensile steel yields at top left corner of the opening at level 2 and at 3432 kN tensile steel yields at the base of the right wall. At 4664 kN the tensile steel at the base of the left wall has completely yielded. Concrete crushing occured at opposite corners of the opening at level 2 as indicated in Fig (6-23). It is noticed that the crack directions in the portions of concrete between the openings are almost 45 degrees as this part is under pure shear with little or negligible axial vertical stress.

case (b) loading on the right wall: Fig (6—25)

First cracks appear at the same load of 528 kN but at the corner of the openings at level 2 and similar crack propagation is observed until failure. At 2376 kN tensile steel starts yielding at top right side of the opening at level 2 and at 2904 kN tensile steel yields in the right wall at 4.0 m above the base where steel starts yielding at a much higher load of 3080 kN. At 3608 kN compression steel yields at the base of the left wall and upon further loading complete crushing of concrete ocured at 4752 kN at the base of the left wall.
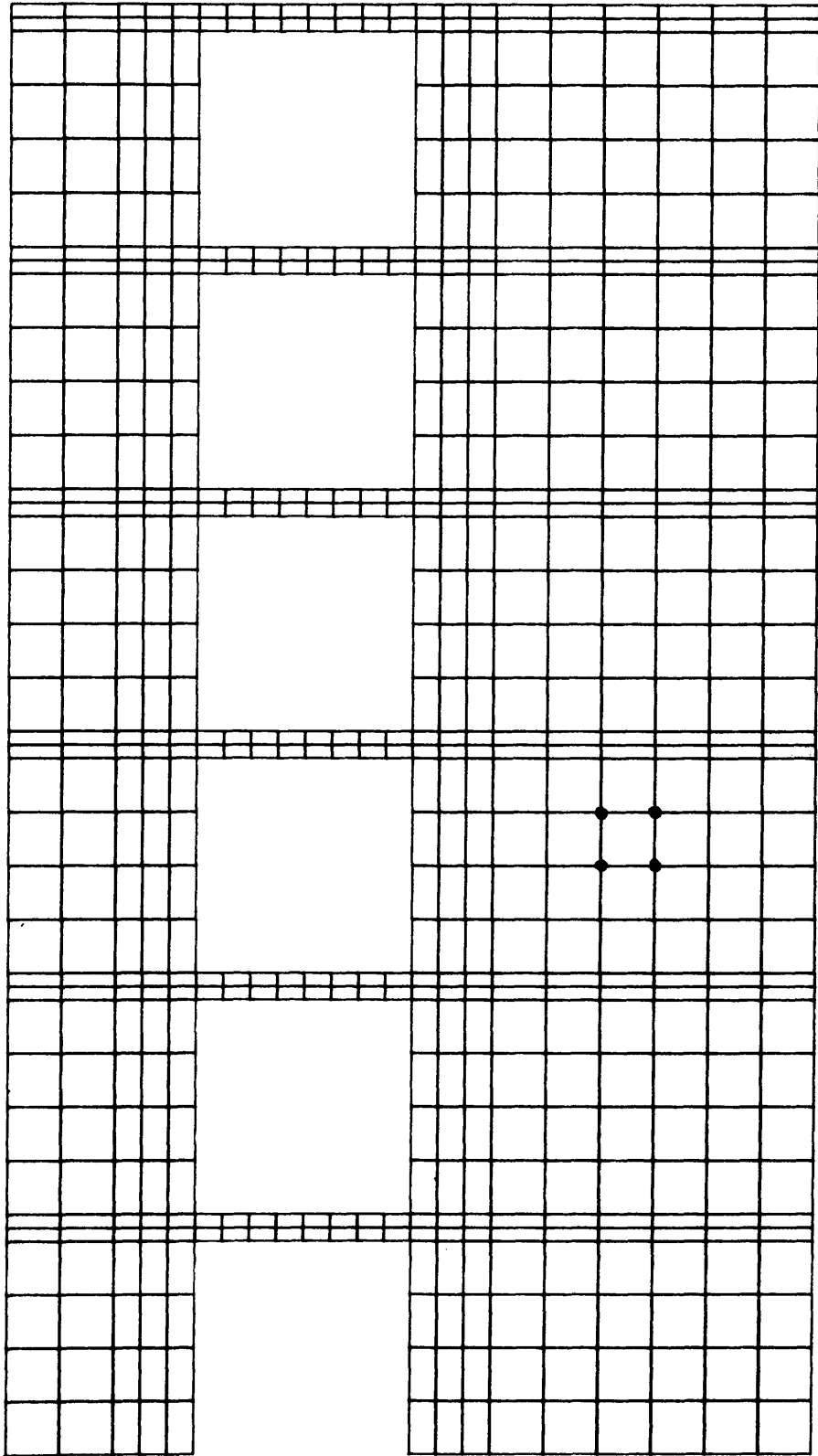
FIG (6-14) FINITE ELEMENT DISCRETIZATION FOR UNSYMMETRIC WALL
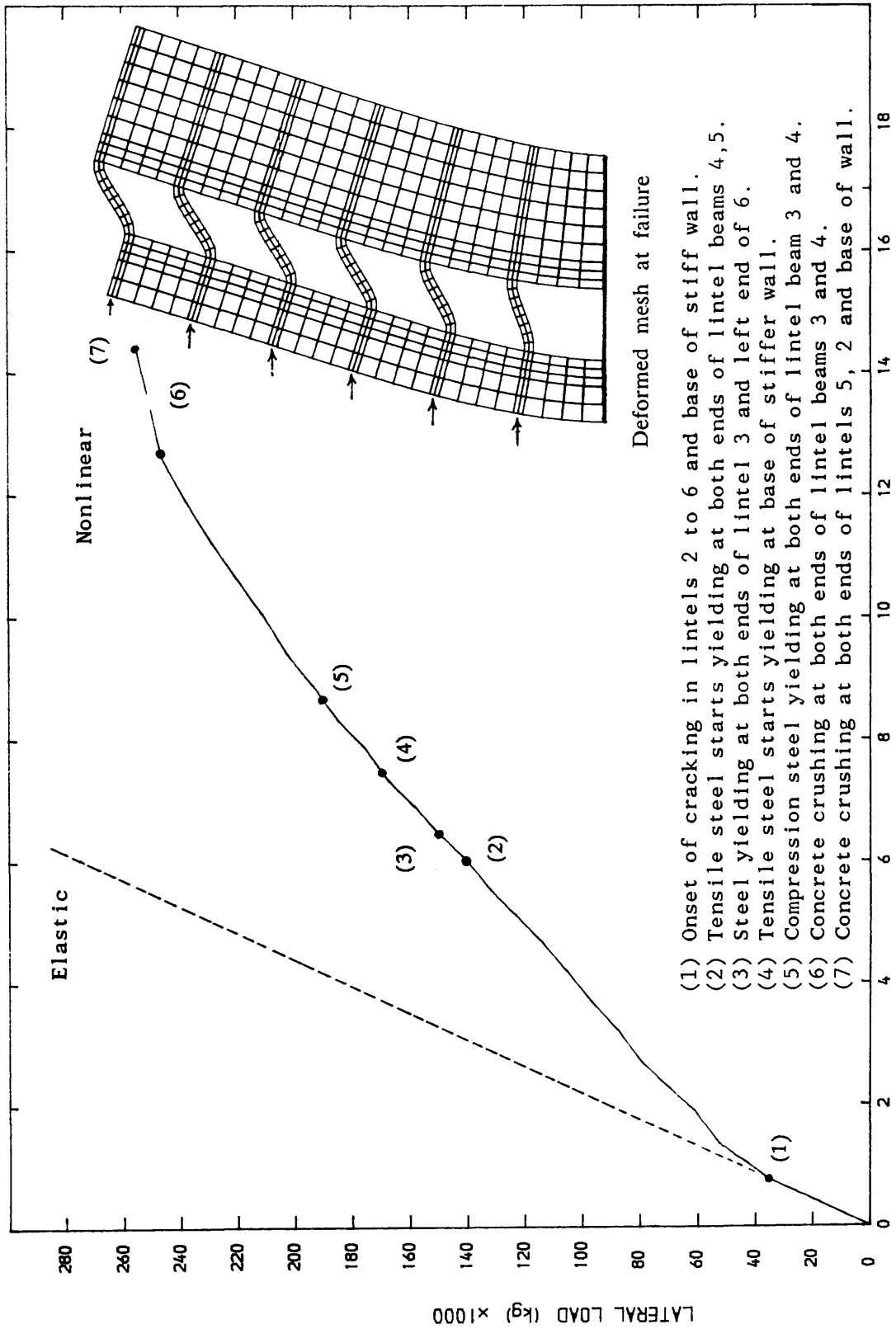
(1) Onset of cracking in lintels 2 to 6 and base of stiff wall.
(2) Tensile steel starts yielding at both ends of lintel beams 4,5.
(3) Steel yielding at both ends of lintel 3 and left end of 6.
(4) Tensile steel starts yielding at base of stiffer wall.
(5) Compression steel yielding at both ends of lintel beam 3 and 4.
(6) Concrete crushing at both ends of lintel beams 3 and 4.
(7) Concrete crushing at both ends of lintels 5, 2 and base of wall.

Deformed mesh at failure

FIG (6-15) *LATERAL LOAD-DISPLACEMENT FOR N-S WALL WITH WEAK COUPLING*

440 kN   528 kN
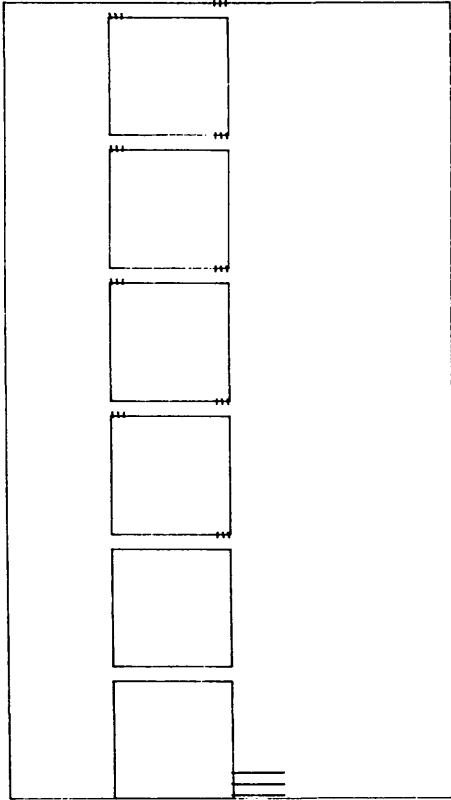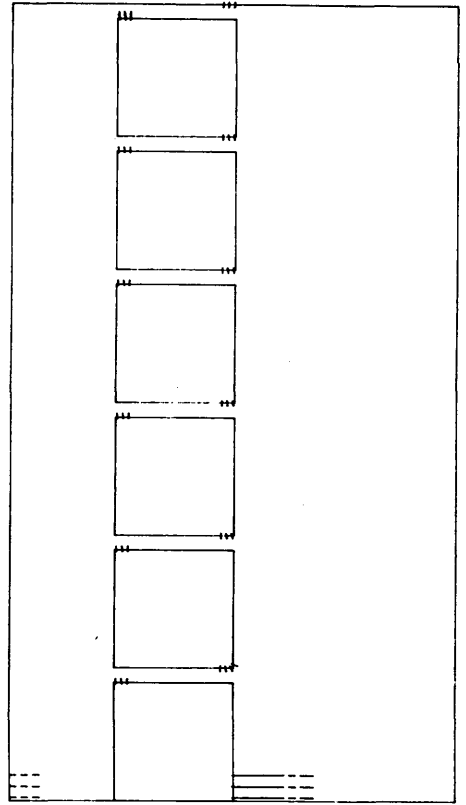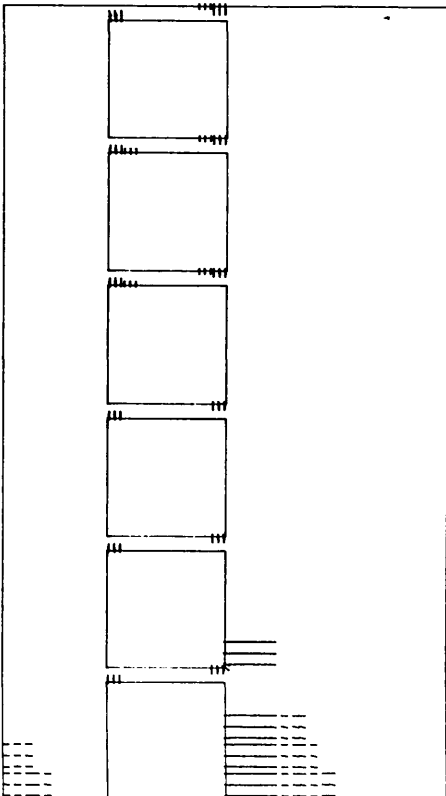
704 kN   1056 kN
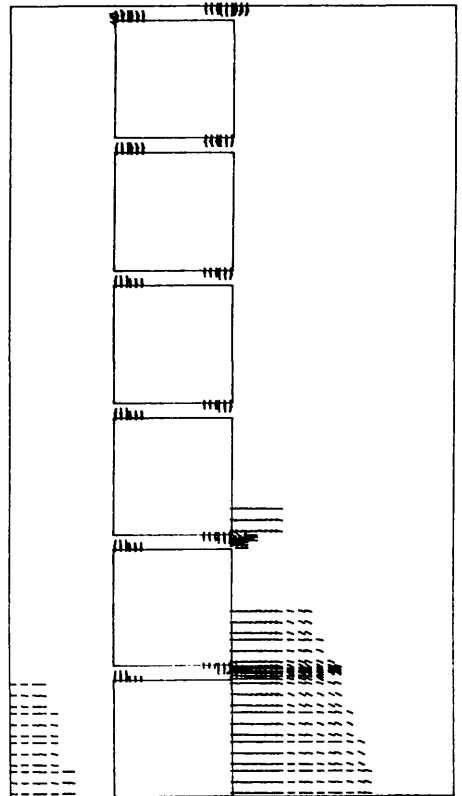
FIG (6-16) CRACK PATTERN AND PROPAGATION FOR UNSYMMETRIC WALL (a)

1408 kN
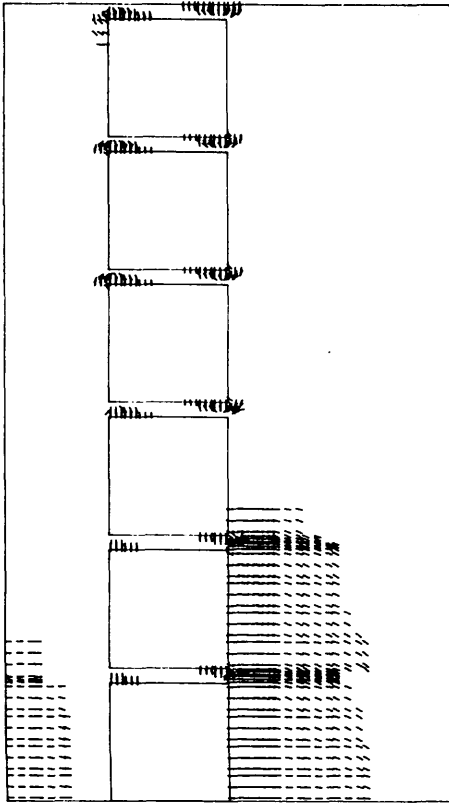
1760 kN
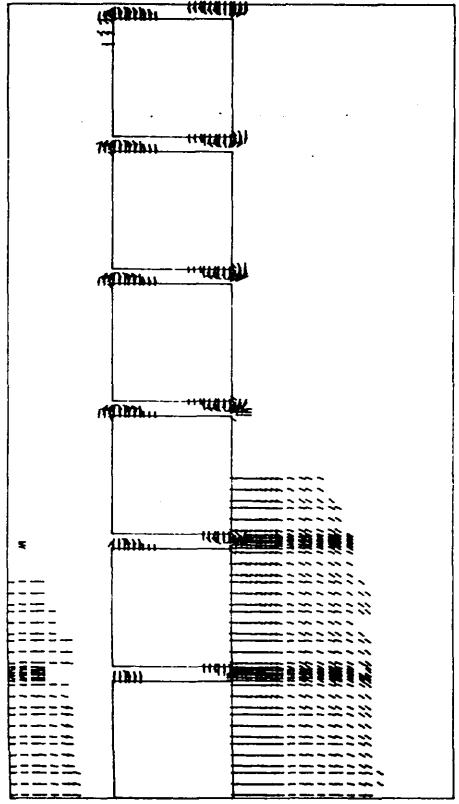
2112 kN
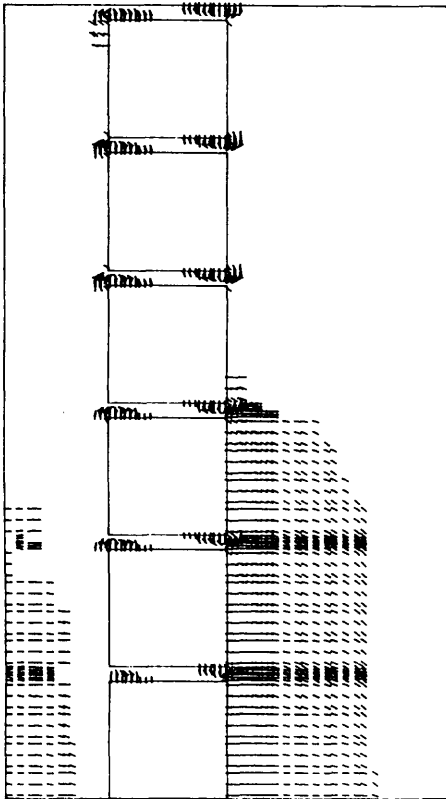
2552 kN
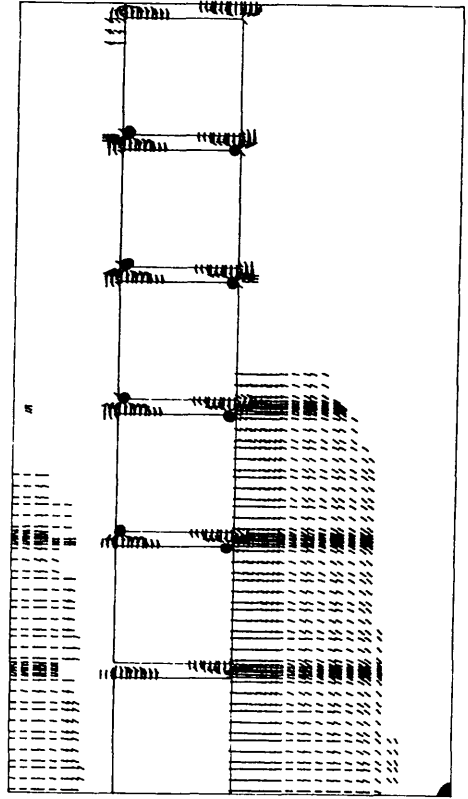
● Crushed concrete

FIG (6-16) .... CONTINUED .

Tension   ----- Compression
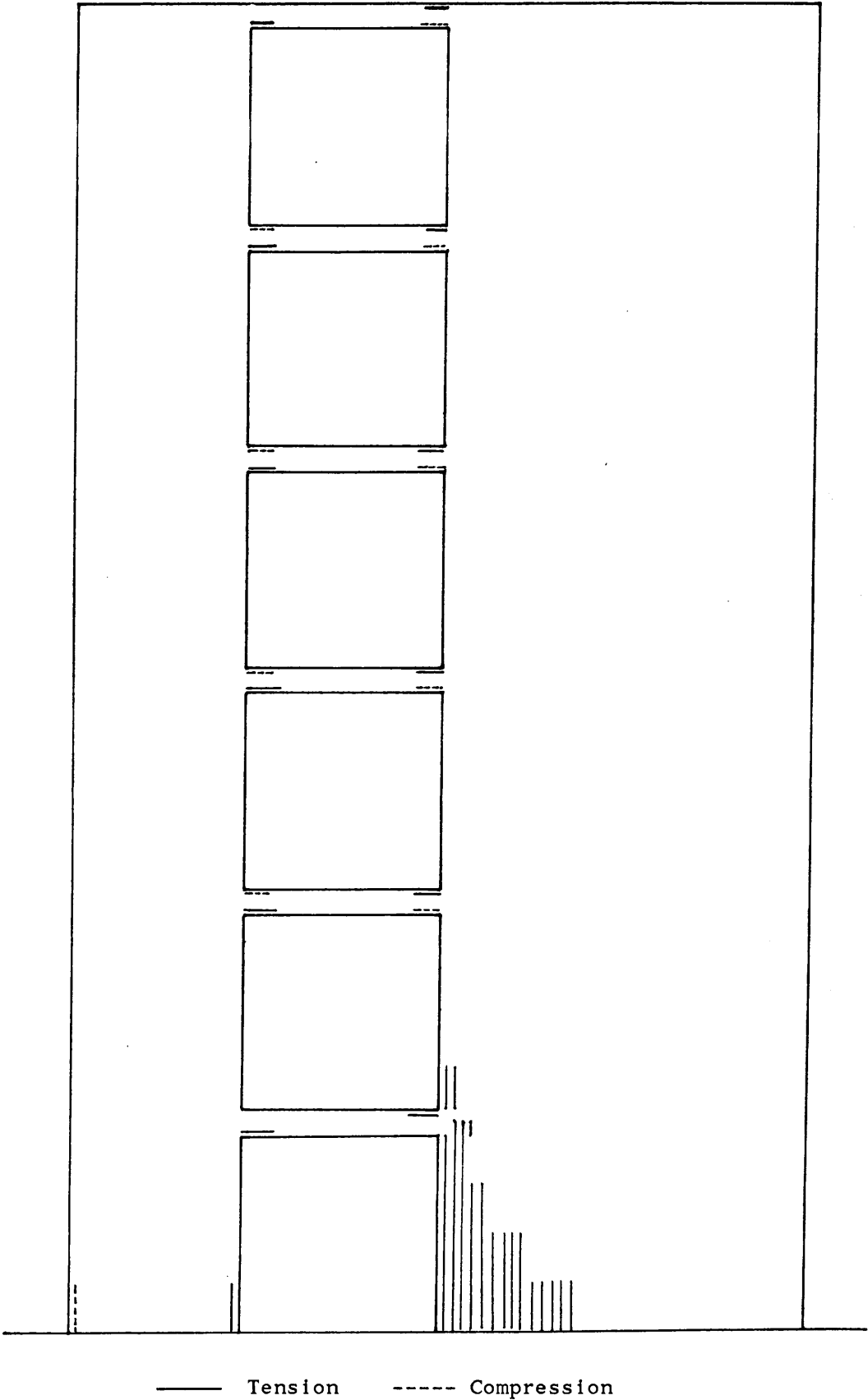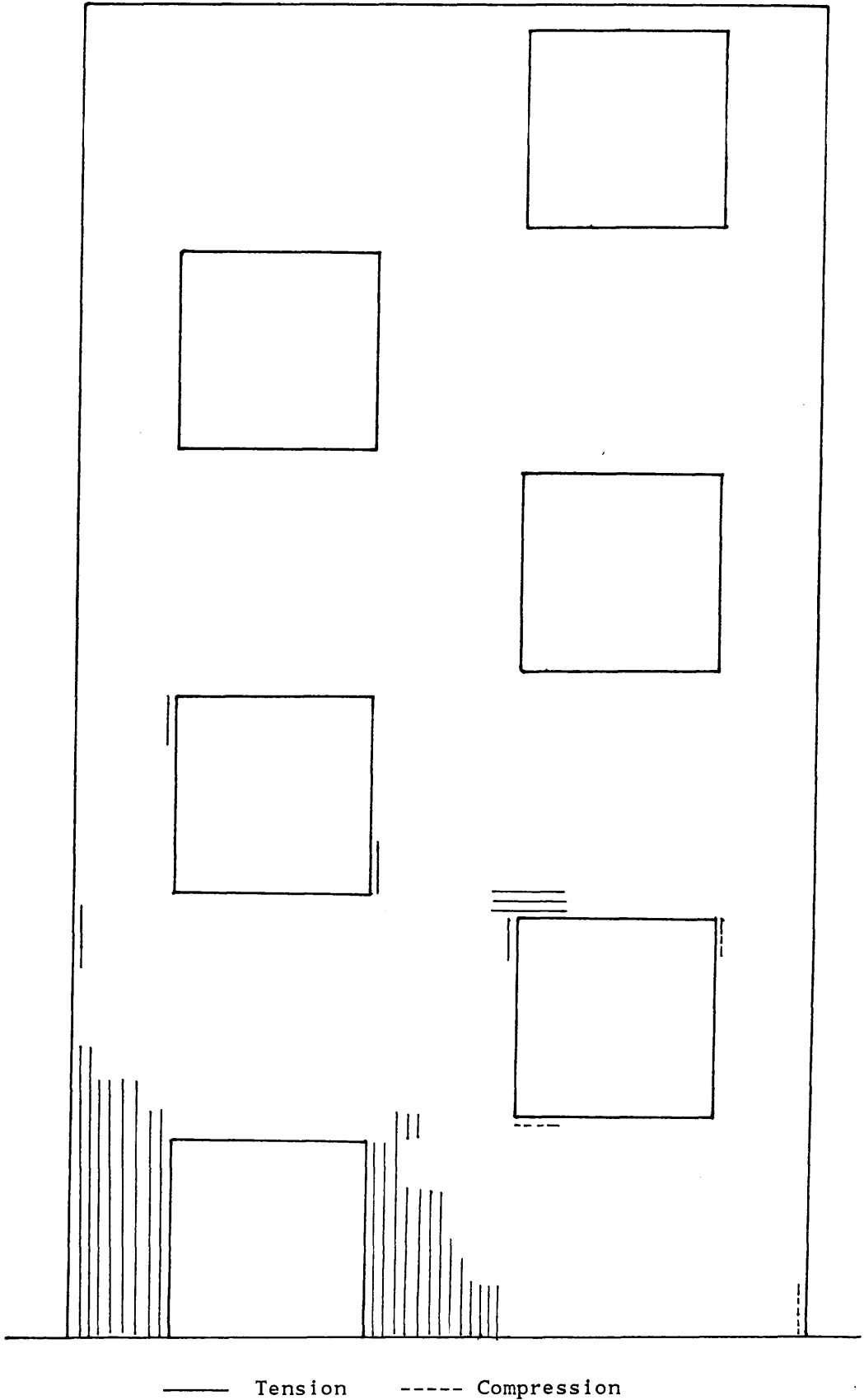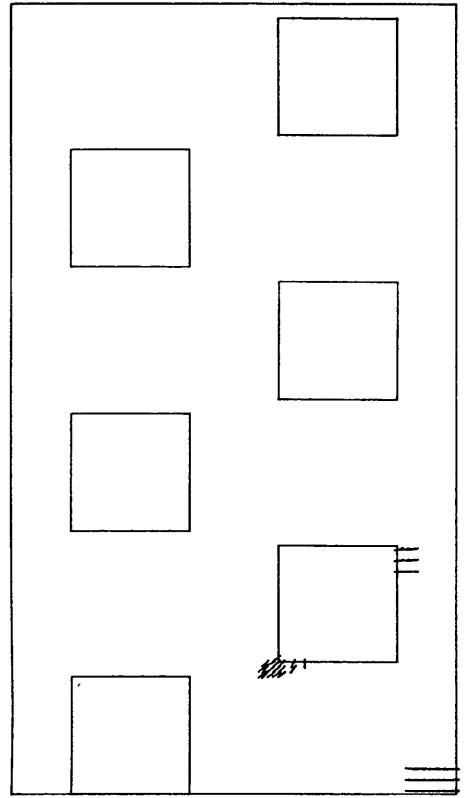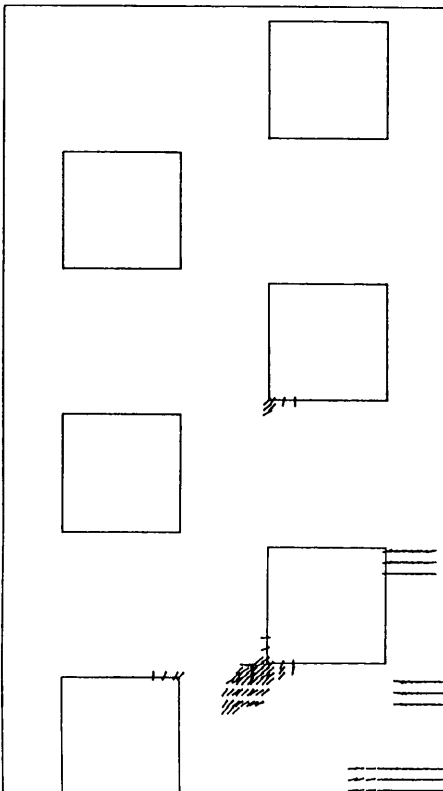
FIG (6-17) EXTENT AND DIRECTION OF YIELDED STEEL AT ULTIMATE
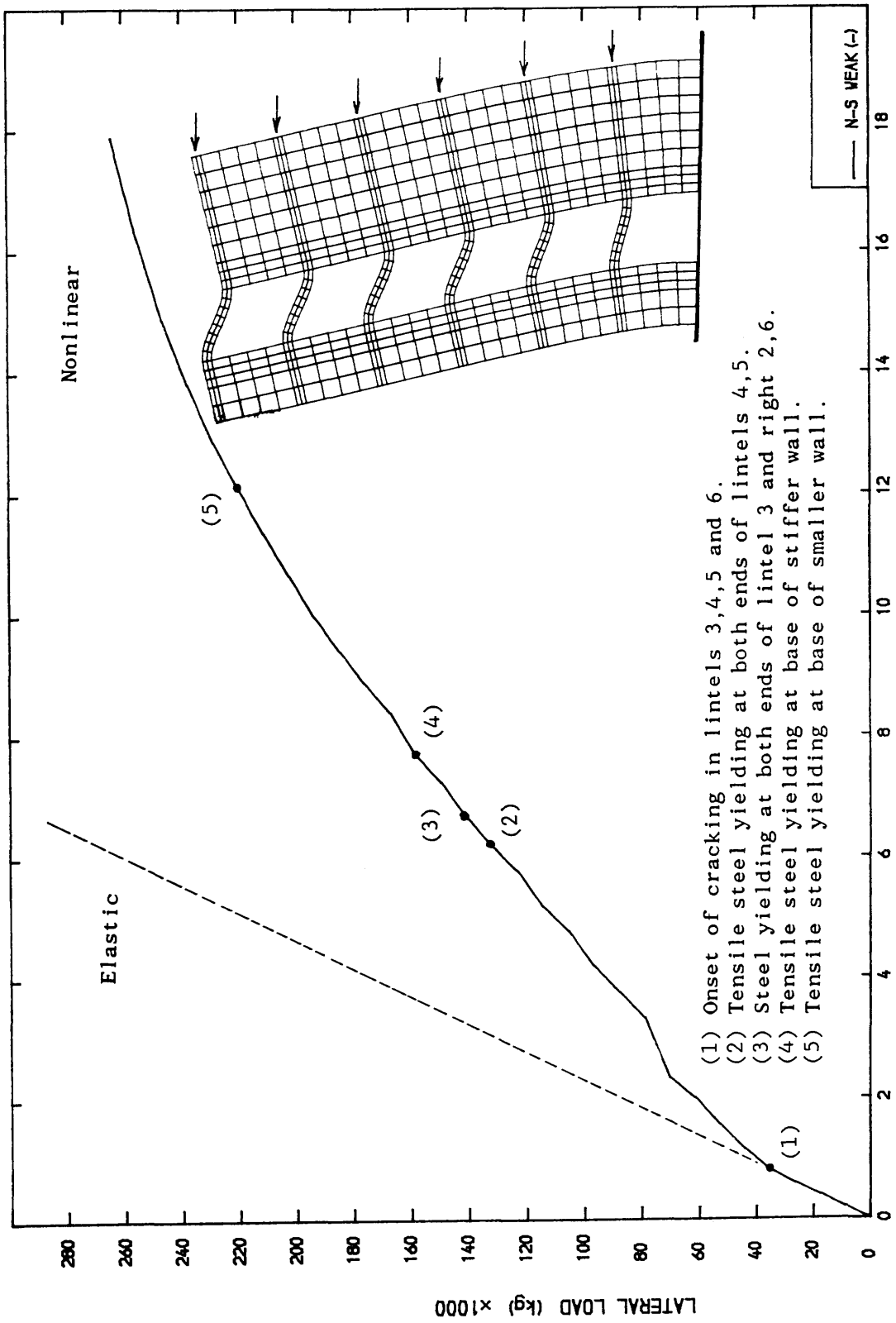
FIG(6-18) *LATERAL LOAD-DISPLACEMENT FOR N-S WALL WITH WEAK COUPLING*

(1) Onset of cracking in lintels 3,4,5 and 6.
(2) Tensile steel yielding at both ends of lintels 4,5.
(3) Steel yielding at both ends of lintel 3 and right 2,6.
(4) Tensile steel yielding at base of stiffer wall.
(5) Tensile steel yielding at base of smaller wall.

— N-S WEAK (-)

352 kN   528 kN
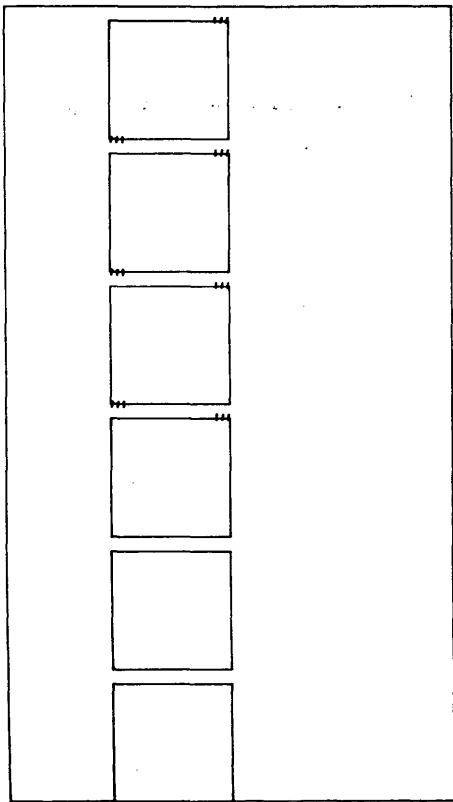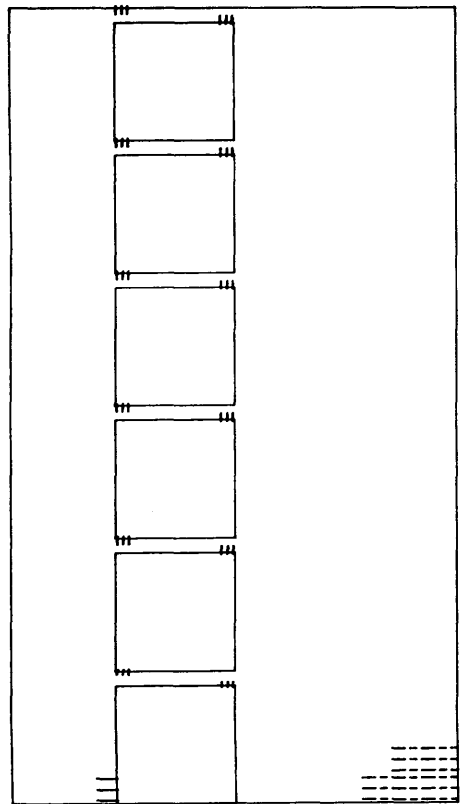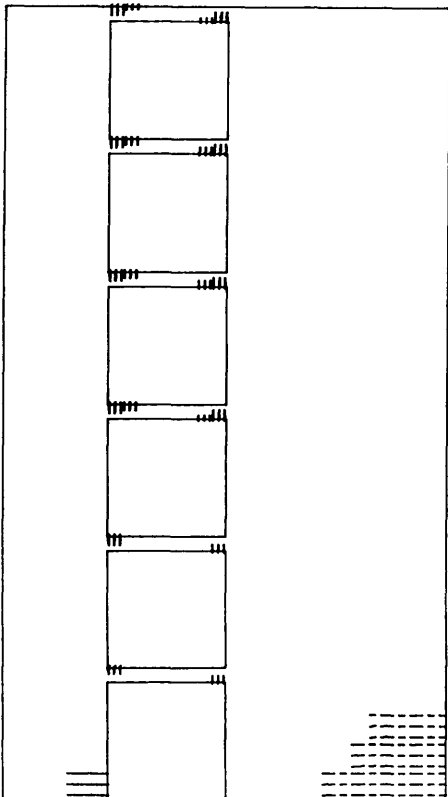
704 kN   1056 kN
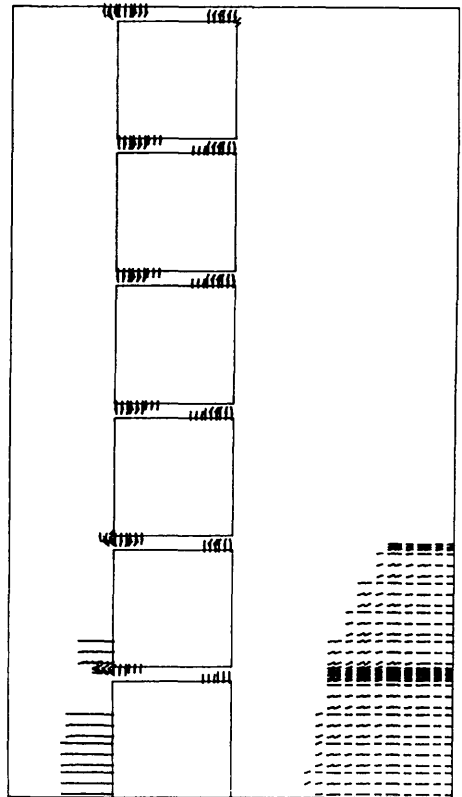
FIG (6-19) CRACK PATTERN AND PROPAGATION FOR UNSYMMETRIC WALL (b)

1408 kN
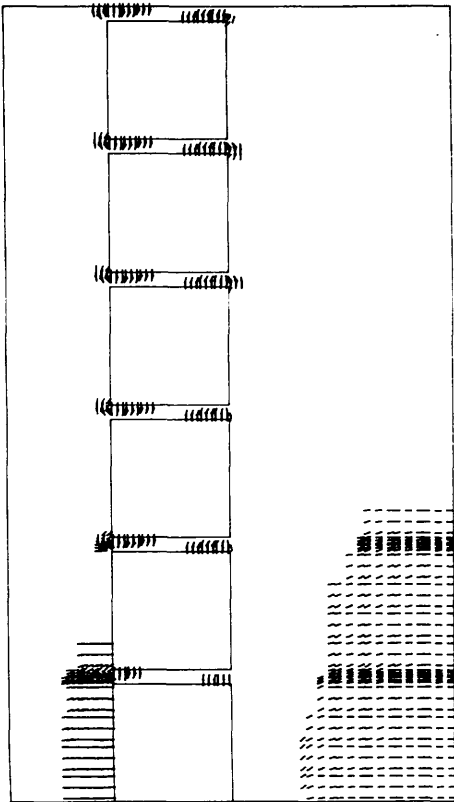
1760 kN
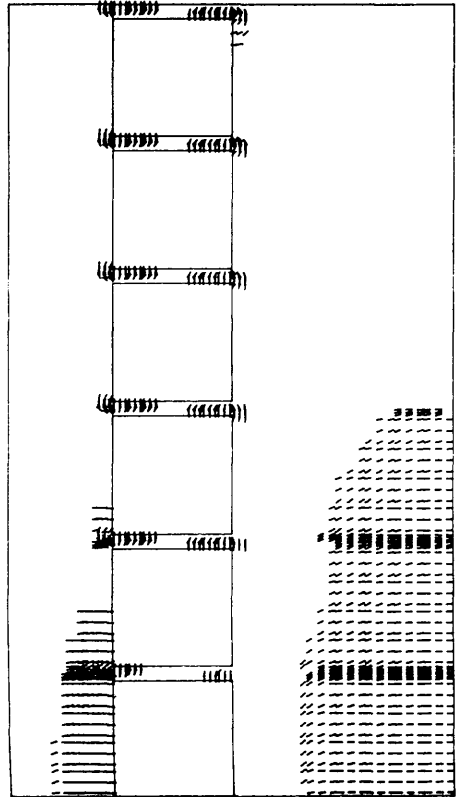
2288 kN
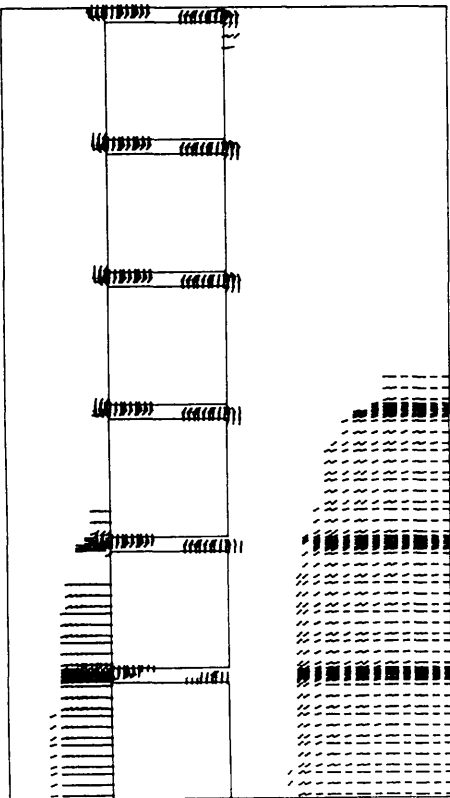
2728 kN

FIG (6-19) .... CONTINUED .

———— Tension   ----- Compression
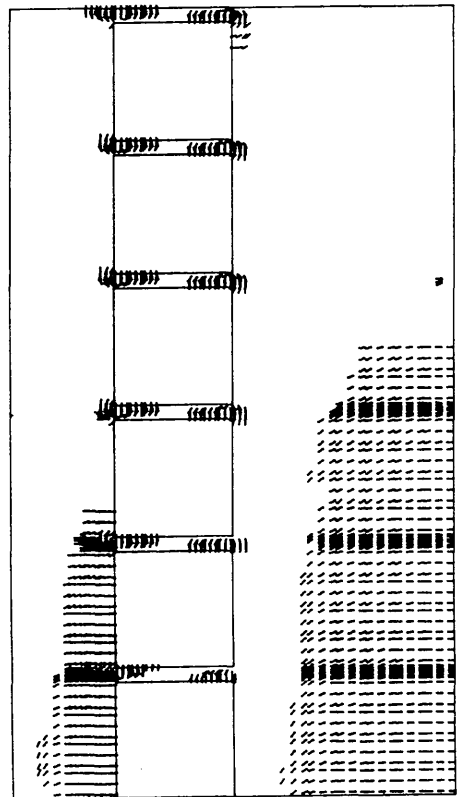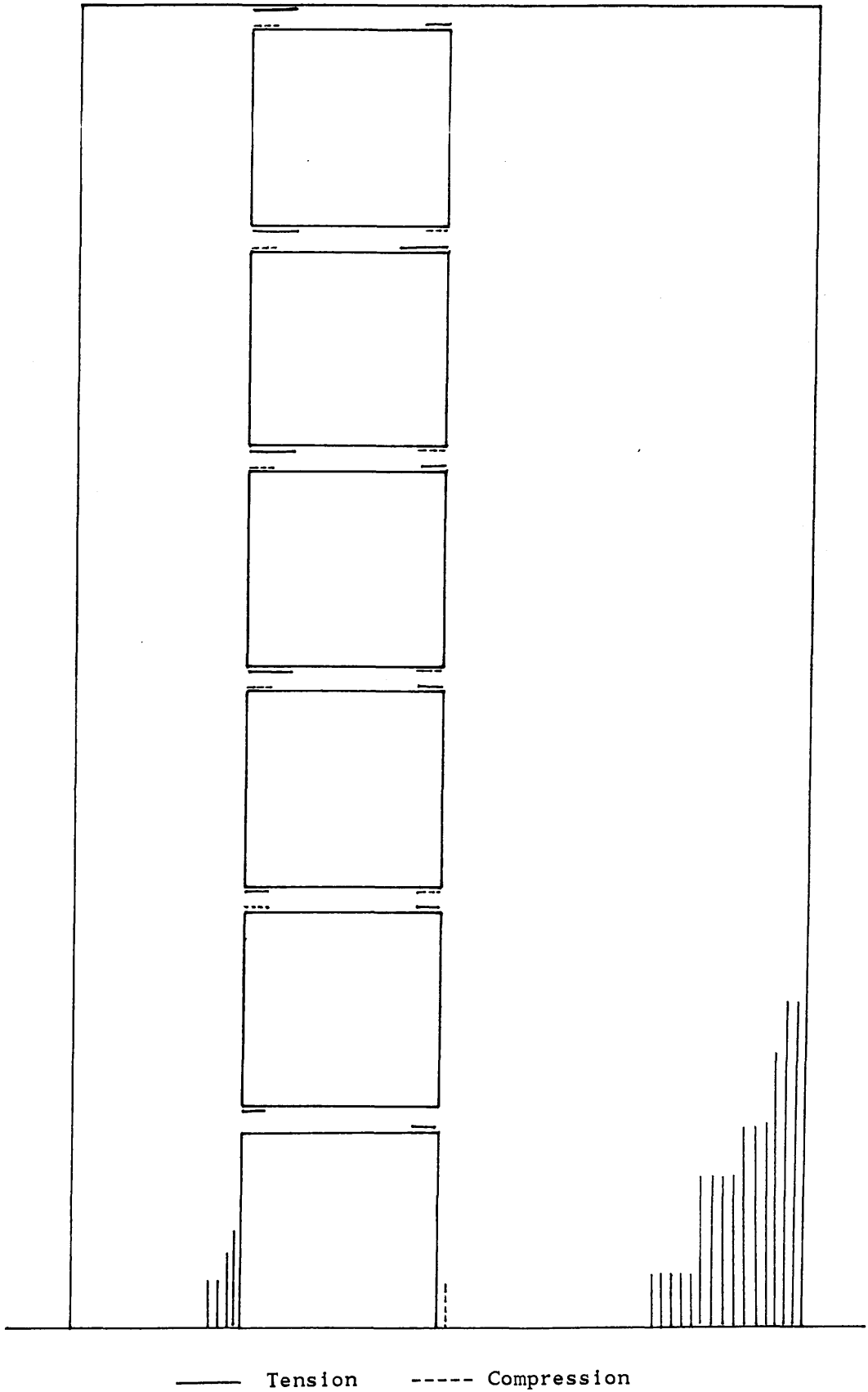
FIG (6-20) EXTENT AND DIRECTION OF YIELDED STEEL AT ULTIMATE
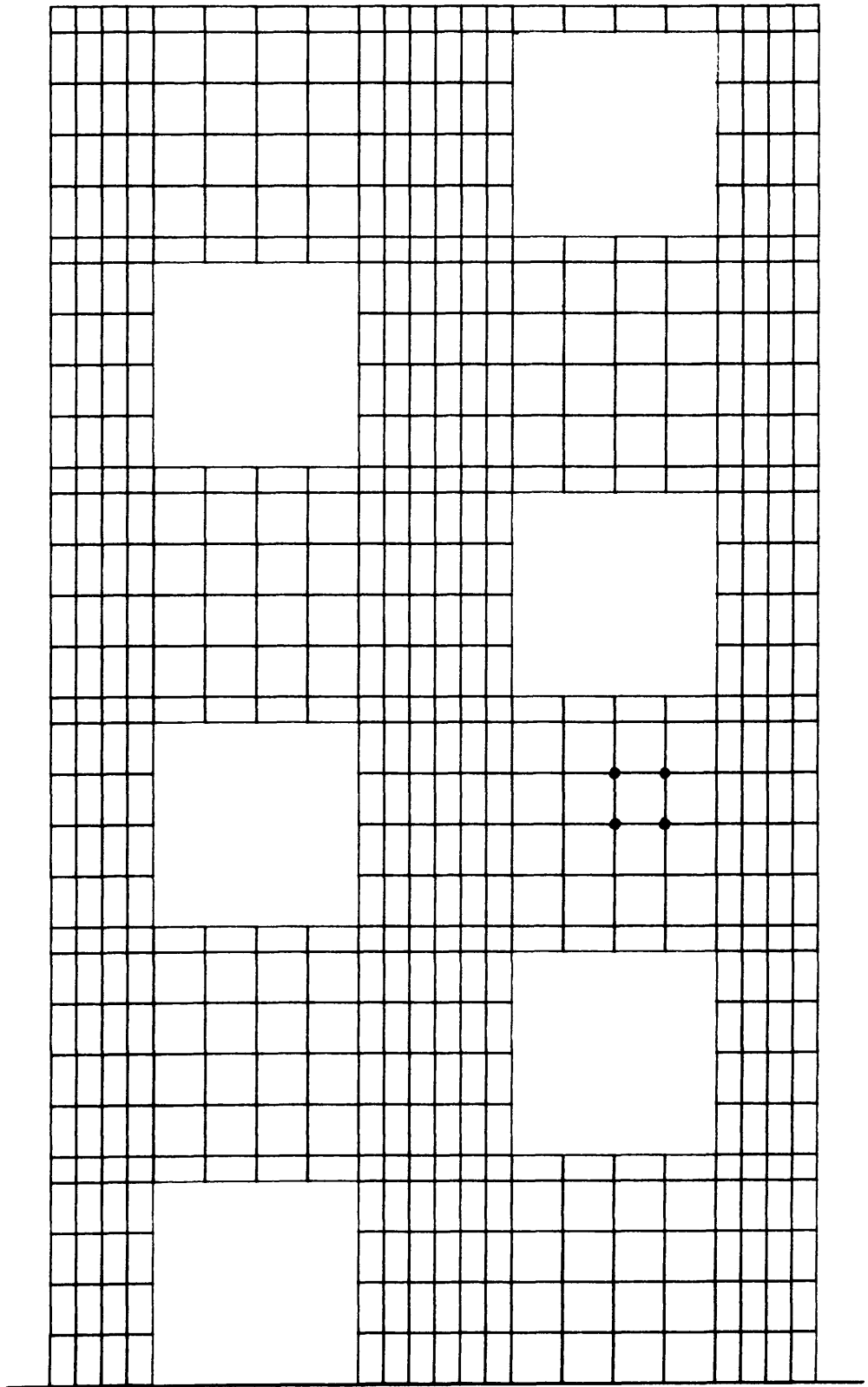
FIG (6-21)   FINITE ELEMENT DISCRETIZATION FOR STAGGERED WALL

Deformed mesh at failure
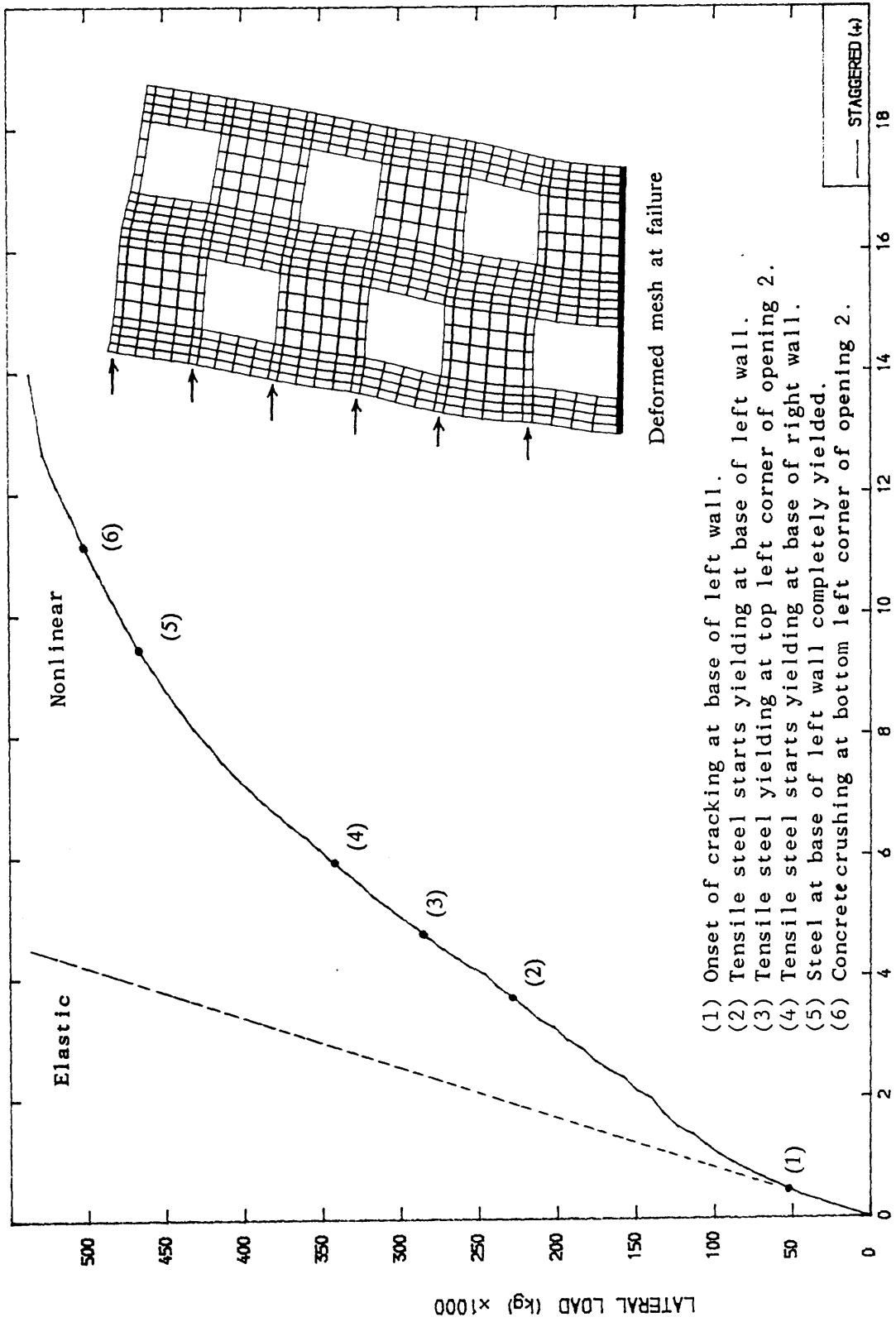
(1) Onset of cracking at base of left wall.
(2) Tensile steel starts yielding at base of left wall.
(3) Tensile steel yielding at top left corner of opening 2.
(4) Tensile steel starts yielding at base of right wall.
(5) Steel at base of left wall completely yielded.
(6) Concrete crushing at bottom left corner of opening 2.

Elastic

Nonlinear

LATERAL LOAD (kg) ×1000

LATERAL DISPLACEMENT (cm)

STAGGERED (+)

FIG (6-22) LATERAL LOAD-DISPLACEMENT FOR STAGGERED WALL

528 kN
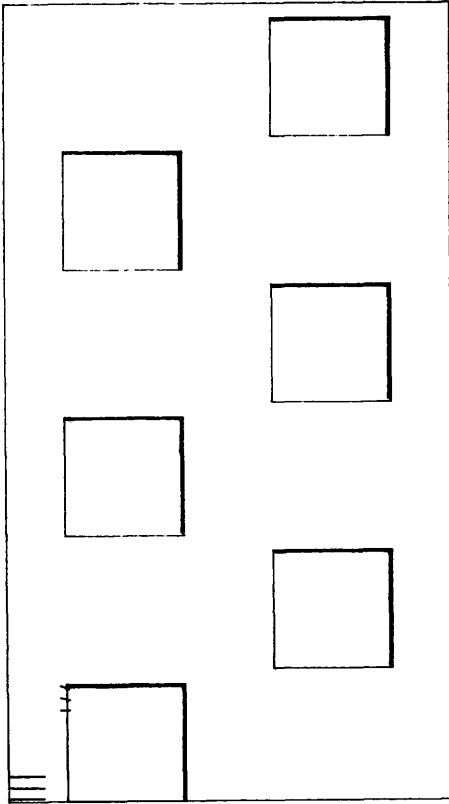
704 kN
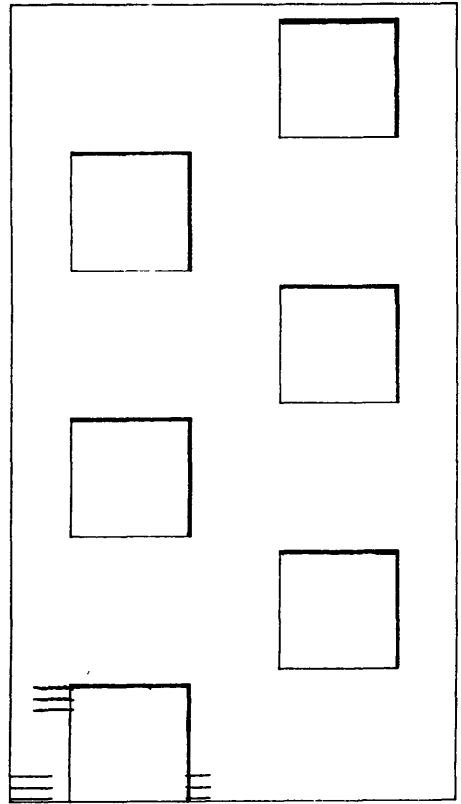
1056 kN
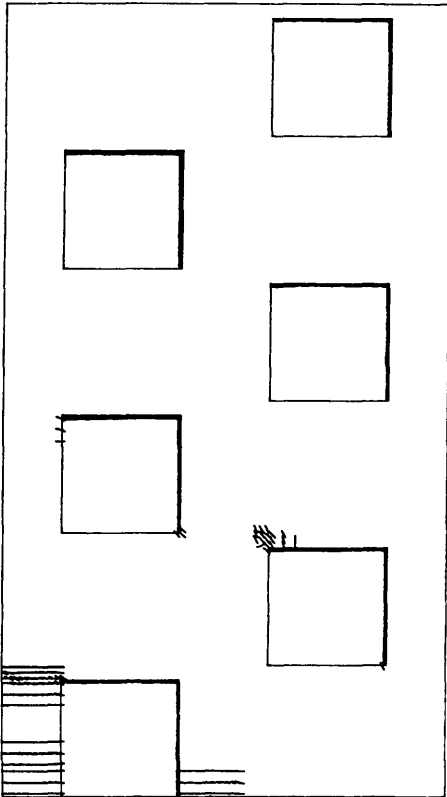
1408 kN
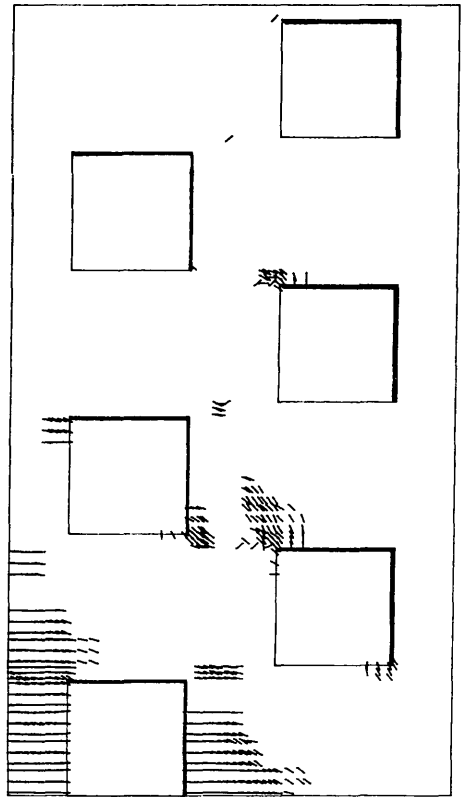
FIG (6-23) CRACK PATTERN AND PROPAGATION FOR STAGGERED WALL (b)

2112 kN
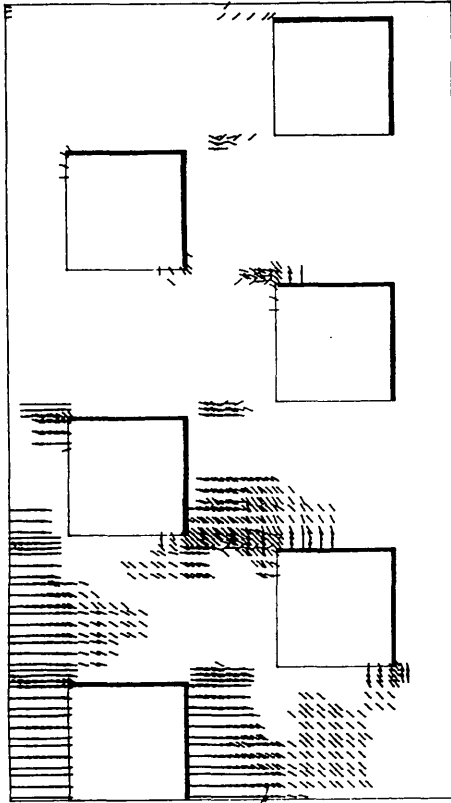
2816 kN
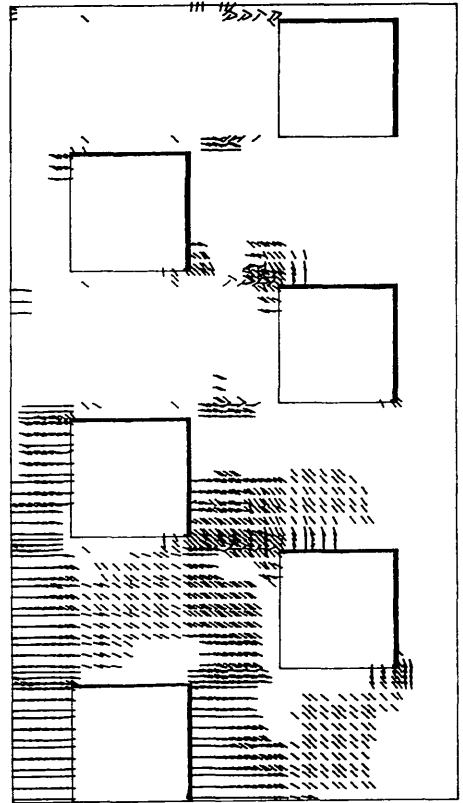
4400 kN
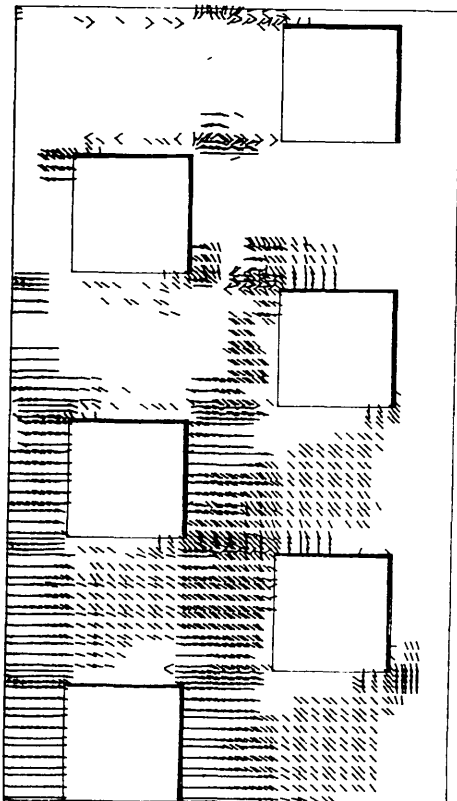
5368 kN

FIG (6-23) .... CONTINUED .

——— Tension   ----- Compression
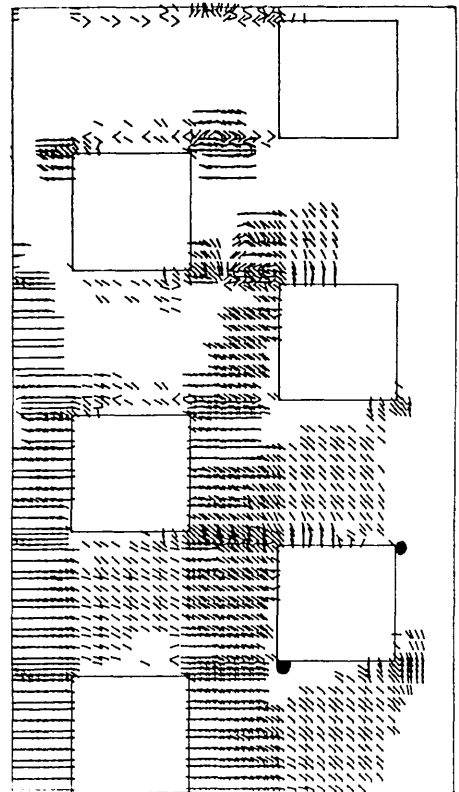
FIG (6-24) EXTENT AND DIRECTION OF YIELDED STEEL AT ULTIMATE

Deformed mesh at failure
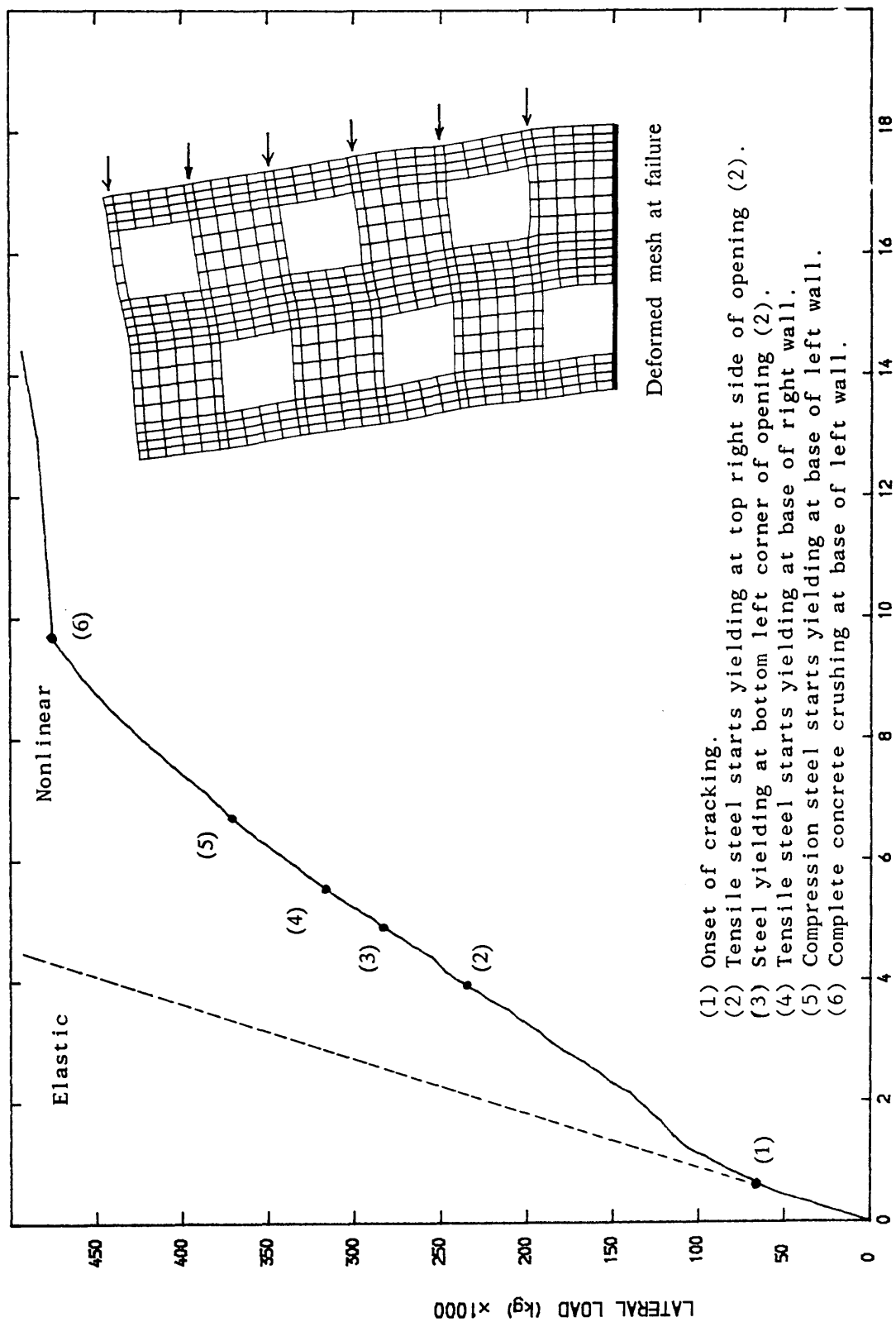
(1) Onset of cracking.
(2) Tensile steel starts yielding at top right side of opening (2).
(3) Steel yielding at bottom left corner of opening (2).
(4) Tensile steel starts yielding at base of right wall.
(5) Compression steel starts yielding at base of left wall.
(6) Complete concrete crushing at base of left wall.

FIG (6-25) LATERAL LOAD-DISPLACEMENT FOR STAGGERED WALL

LATERAL DISPLACEMENT (cm)

LATERAL LOAD (kg) ×1000

528 kN
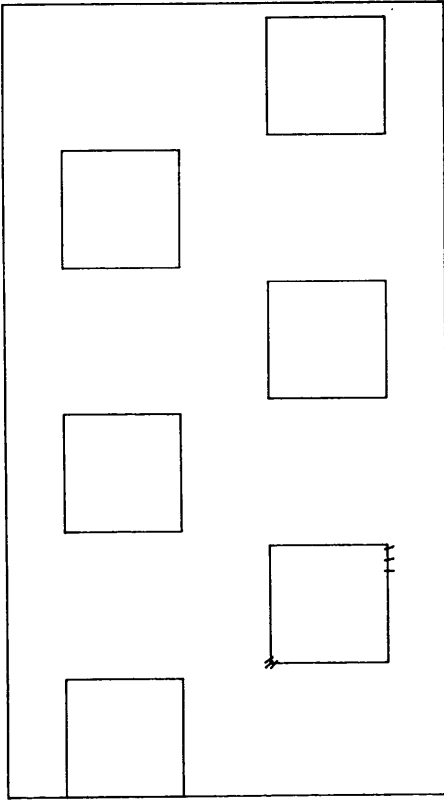
704 kN

1056 kN

1408 kN

FIG (6-26) CRACK PATTERN AND PROPAGATION FOR STAGGERED WALL (a)

2112 kN
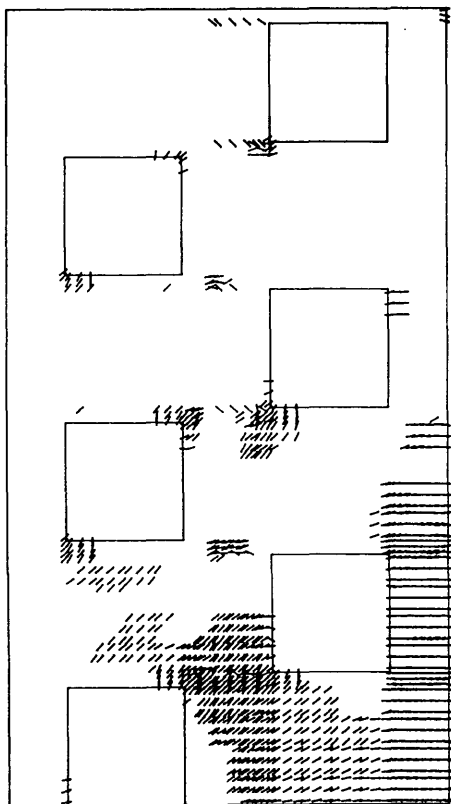
2816 kN
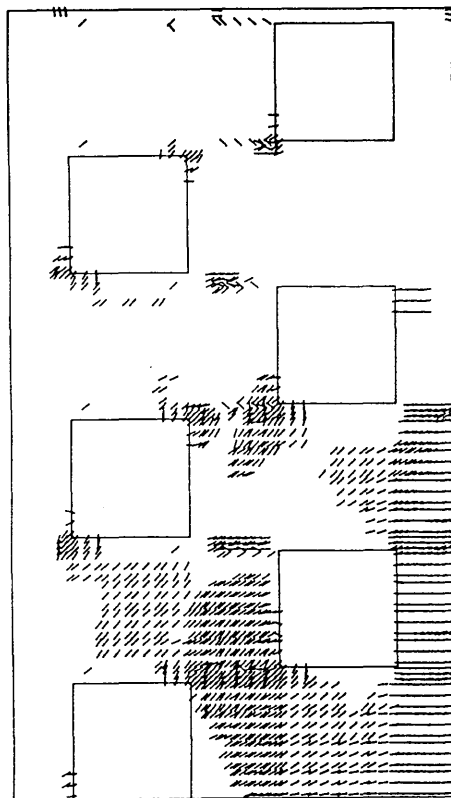
4400 kN
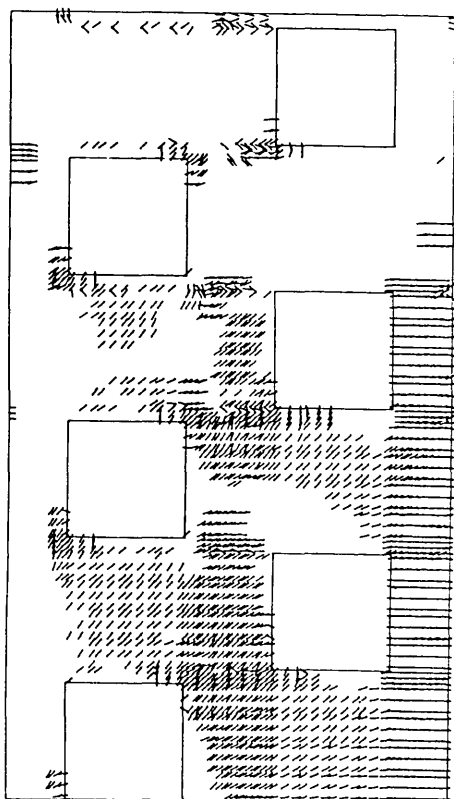
4752 kN

FIG (6-26) .... CONTINUED .

—— Tension ----- Compression
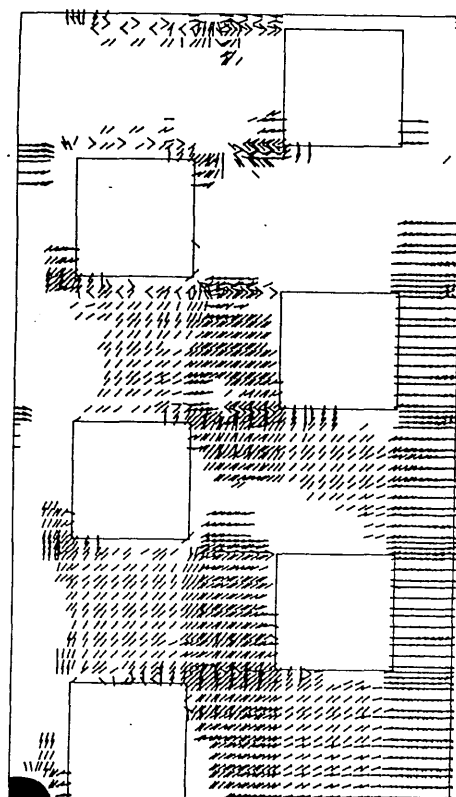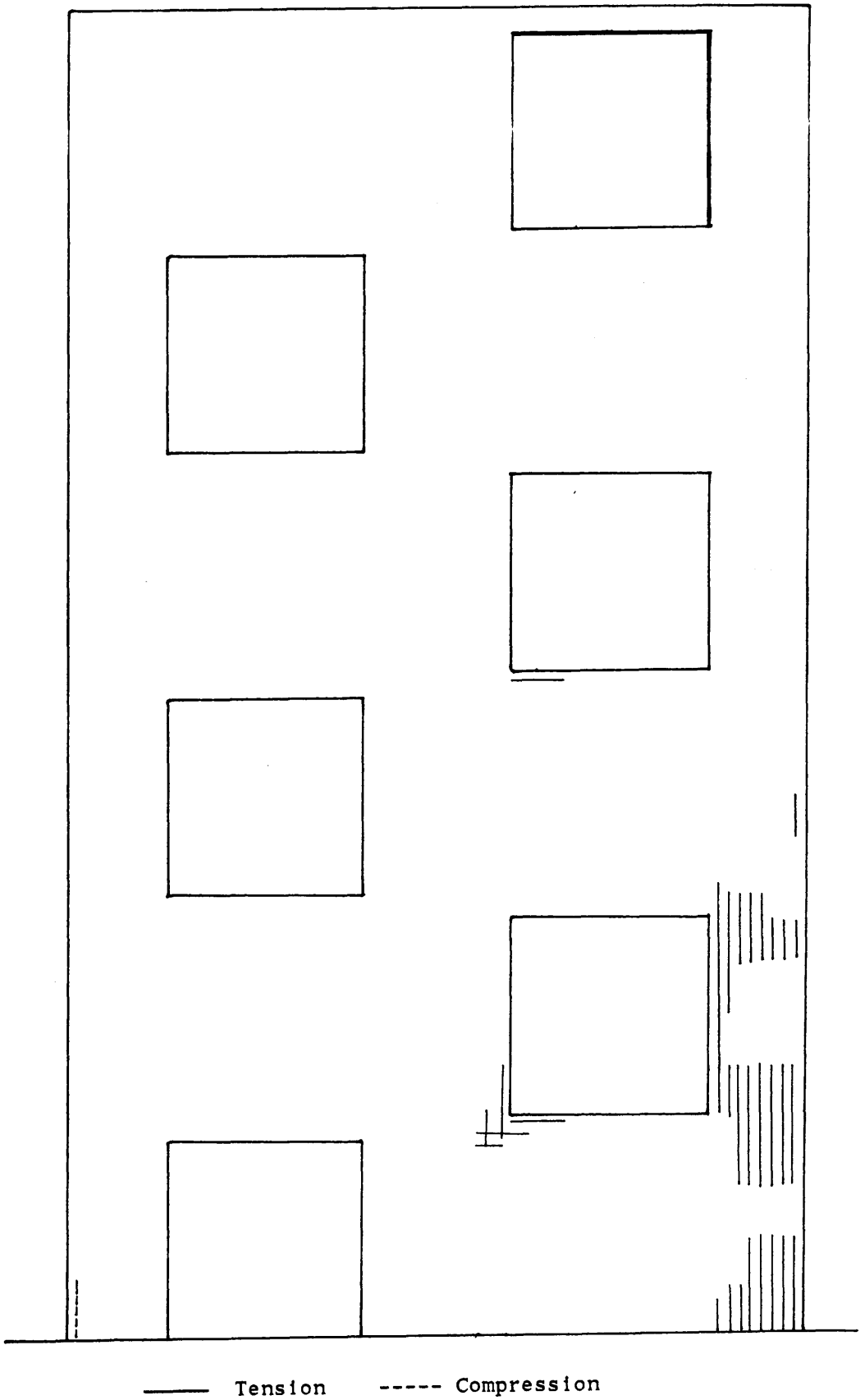
FIG (6-27) EXTENT AND DIRECTION OF YIELDED STEEL AT ULTIMATE

6-4 ADDITION OF STIFFENING BEAM :

Two cases are considered here. A stiff beam is added to the symmetric coupled shear wall with weak coupling. In the first case (a) the stiff beam is located at the top level and in a second case (b) the stiff beam is positioned at mid-height at the third level. The purpose is to observe the effect of the simple additional stiff beam on the crack distribution and ultimate load conditions and how important this effect is. This type of study has been investigated by many workers in the simple elastic case.

6-4-1 Stiffening beam at top : case (a)

The stiff lintel beam first cracks at a load 352 kN similar to the symmetric case and the only noticeable difference is that the lintels at lower levels are uncracked. At 528 kN flexural cracks develop in all lintels and both walls. Between 704 kN and up to 2288kN cracking development is similar to the uniform lintel case. At 2288 kN (the load level at which the wall without the additional stiffening beam collapses by crushing in lower lintels), it can be noticed no crushing occurs and that there is less crack damage along the height of the walls. The cracking in this case extends approximately 1 story less high in comparison with the uniform lintel case at this load level. The wall collapsed at a somewhat higher load of 2640 kN which represents an additional strength of approxiamtely 15 % over the wall with the unstiffened beams.

6-4-2 Stiffening beam at mid-height : Case (b)

Similarly to case (a), cracks first develop at the stiff beam located at mid-height at the same load 352 kN. Upon further loading flexural cracks propagate at the

base of both walls and the remaining lintels at a load level 528 kN. Between 704 kN and up to 2200 kN (almost the collapse load of the wall with uniform lintels), further cracks develop and crushing is observed in both sides of the stiff beam at midheight. Tensile steel starts yielding at both ends of the stiffening beam at 1144 kN. At 1496 kN tensile steel yield at both ends of lintels 4,5 just above the stiffening beam. At 1760 kN tensile steel has yielded at both ends of all lintel beams except at level 1. Tensile steel starts yielding at the base of both walls at 1848 kN, also compressive steel at both ends of the stiffening beam yield. Finally, the numerical collapse of The wall occured at 2464 kN by crushing of concrete at both ends of the stiffening beam which is about 8 % higher than the wall with the unstiffened beams. The extent and direction of steel yielding at ultimate load is shown in Fig (6— 35). The lateral load top deflection up to numerical failure load is shown in Fig (6— 33) along with some main load levels during the analysis and the deformed finite element mesh at failure highlighted. It can be noticed that high compression and traction have developed at failure in the stiffening beam at both ends compared to the other lintels.
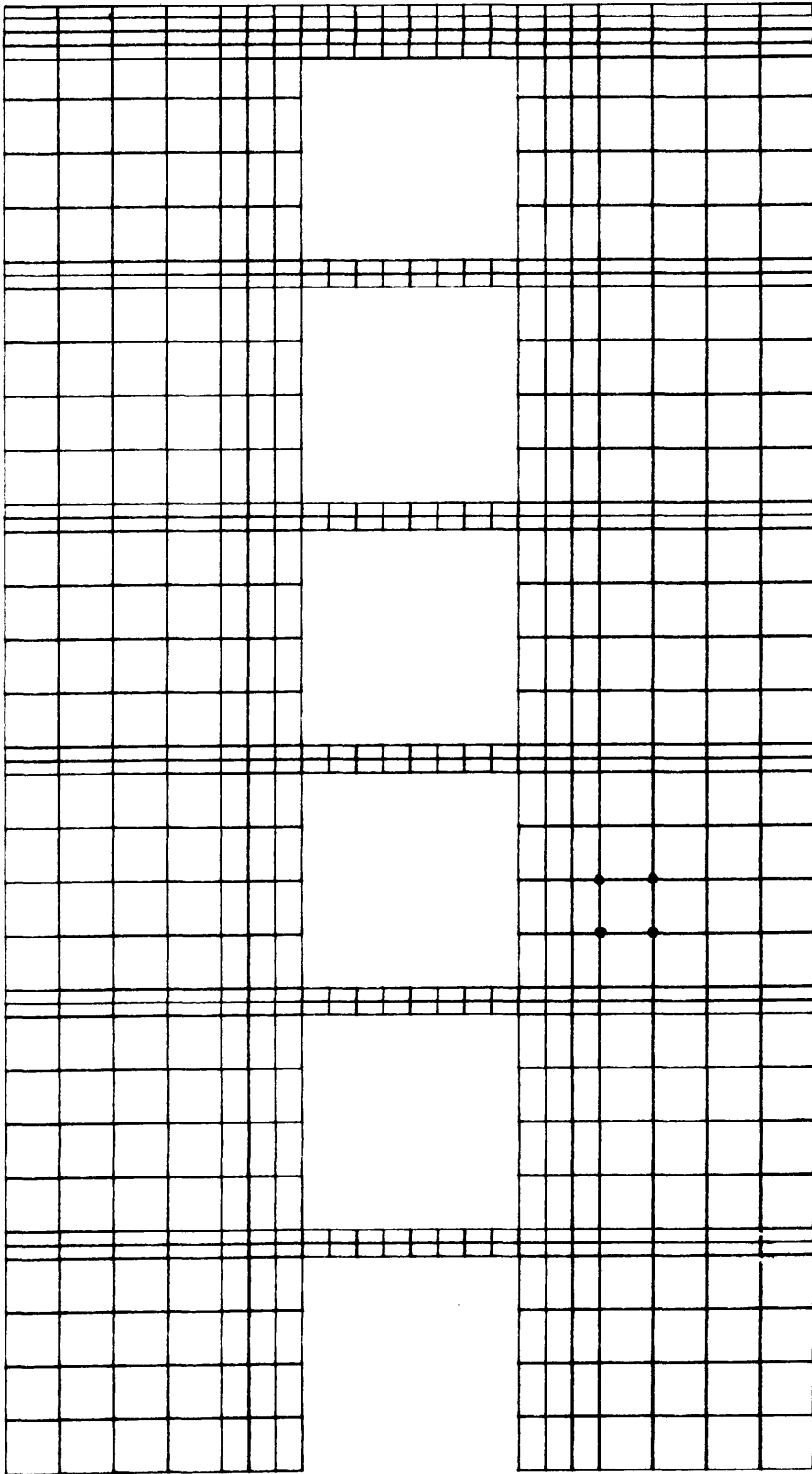
FIG (6-28) FINITE ELEMENT DISCRETIZATION FOR WALL
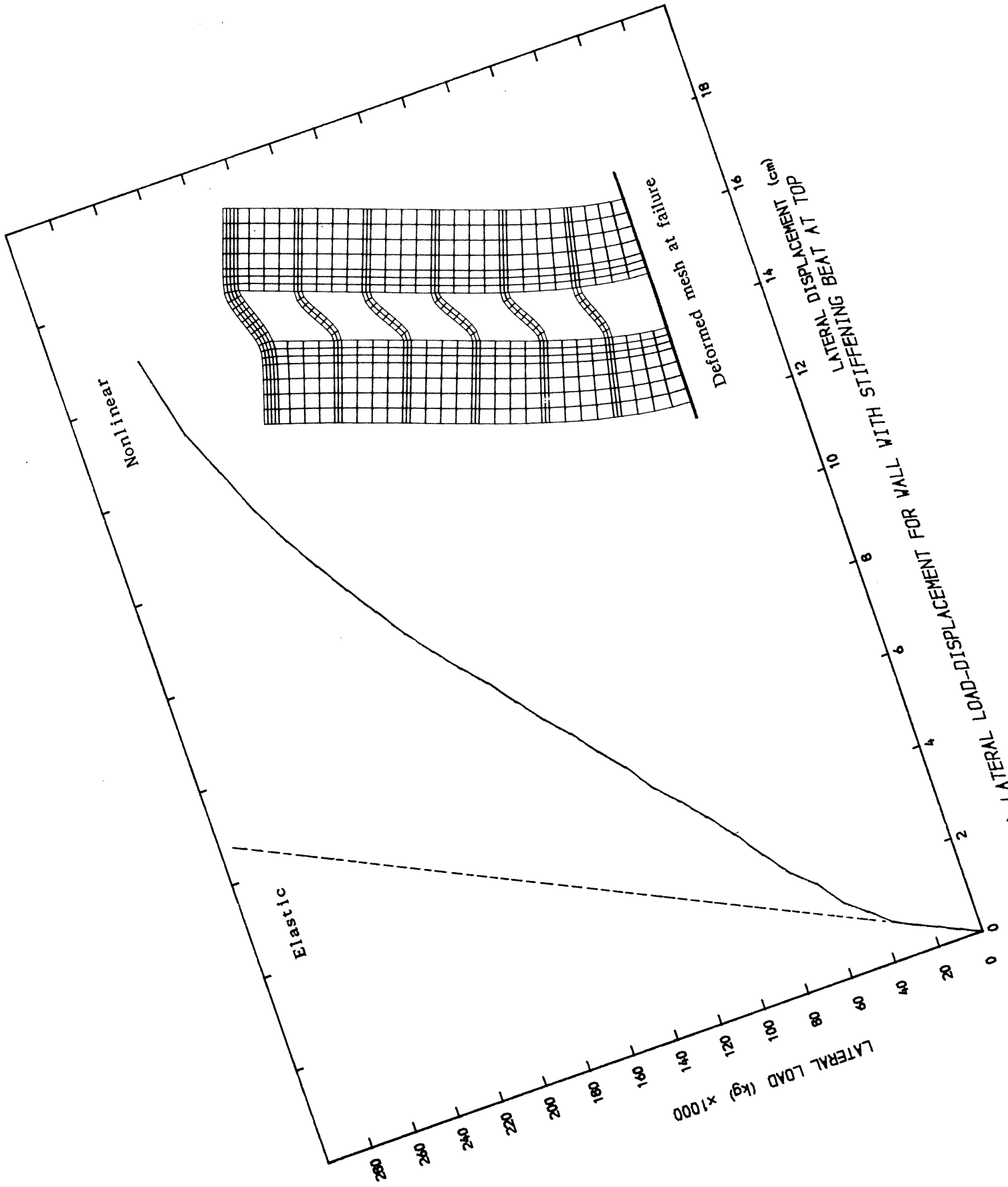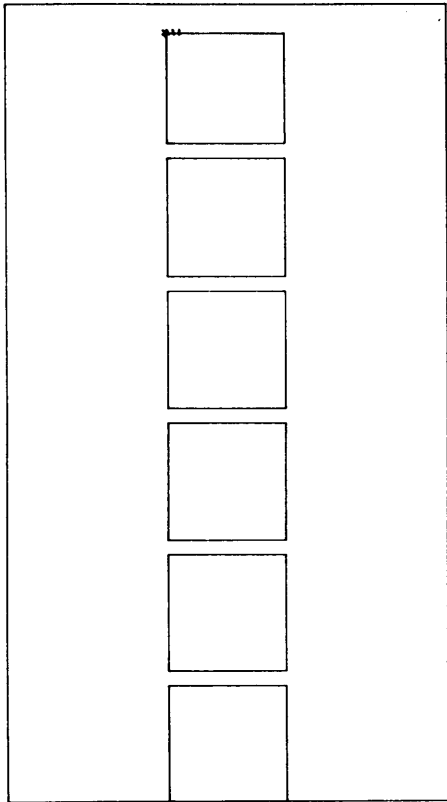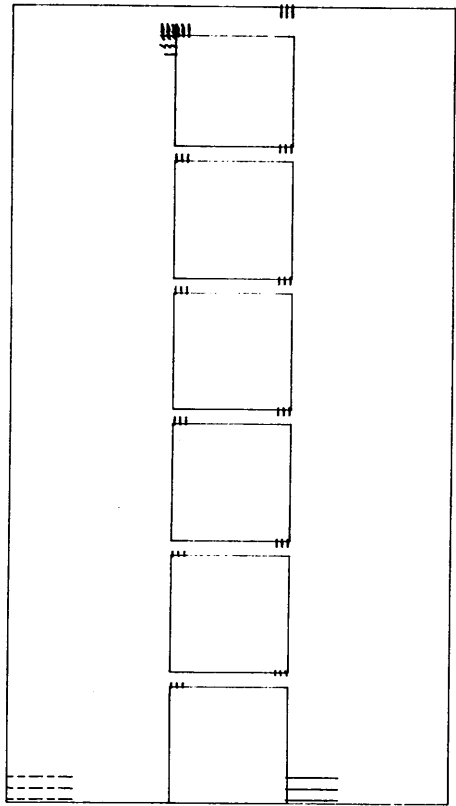WITH TOP STIFFENING BEAM

Deformed mesh at failure

LATERAL DISPLACEMENT (cm)

LATERAL DISPLACEMENT BEAT AT TOP

FIG (6-29) LATERAL LOAD-DISPLACEMENT FOR WALL WITH STIFFENING
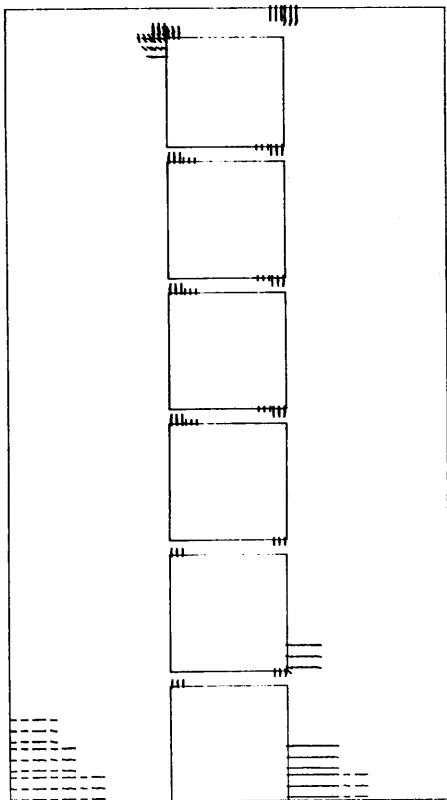
LATERAL LOAD (kg) x1000
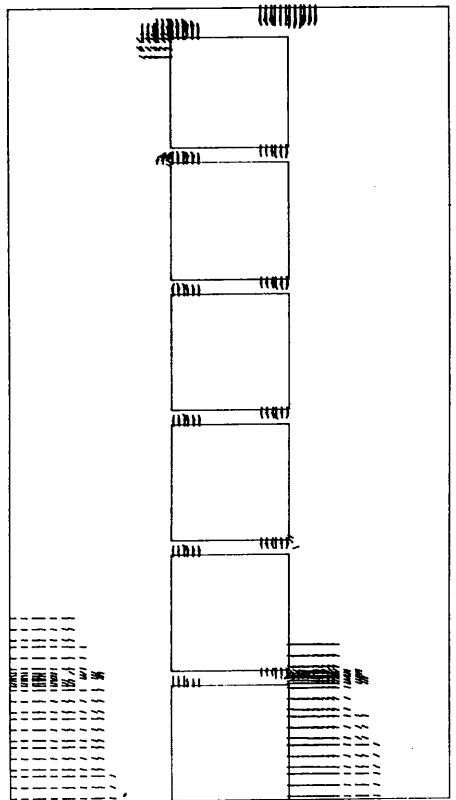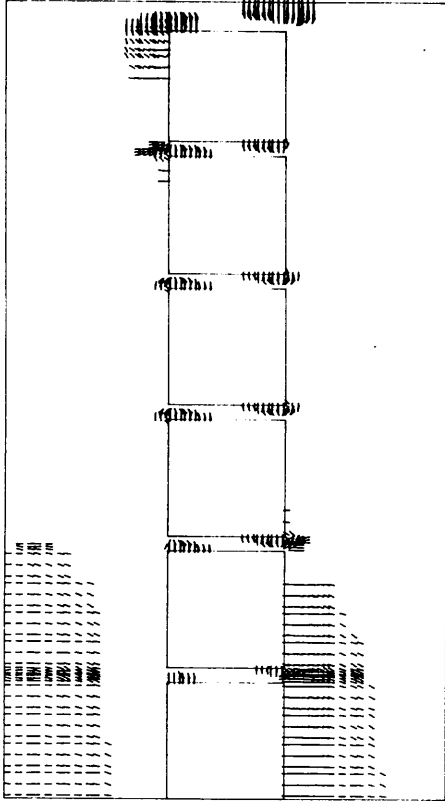
Nonlinear

Elastic

352 kN
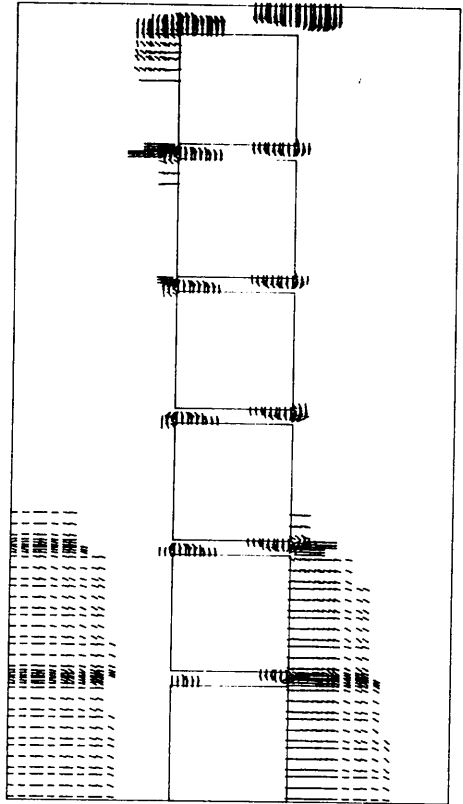
528 kN

704 kN

1056 kN

FIG(6-30) CRACK PATTERN AND PROPAGATION FOR WALL
WITH STIFFENING BEAM AT THE TOP.
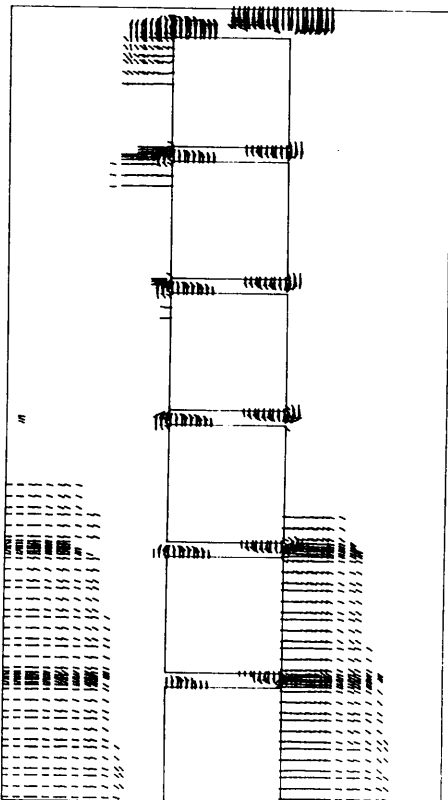
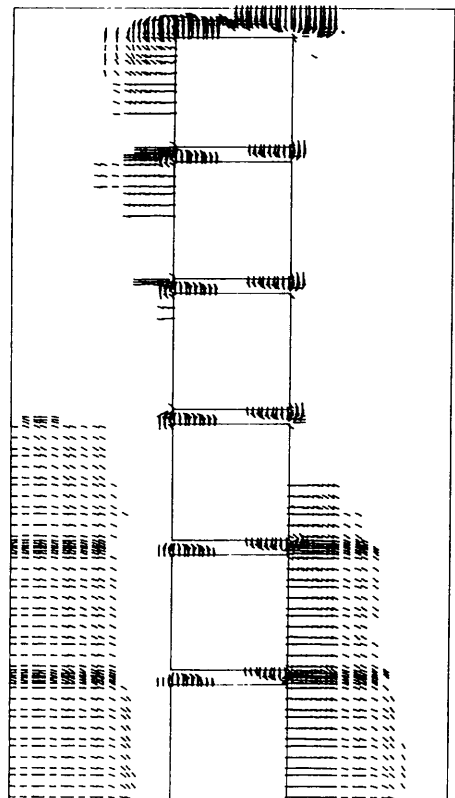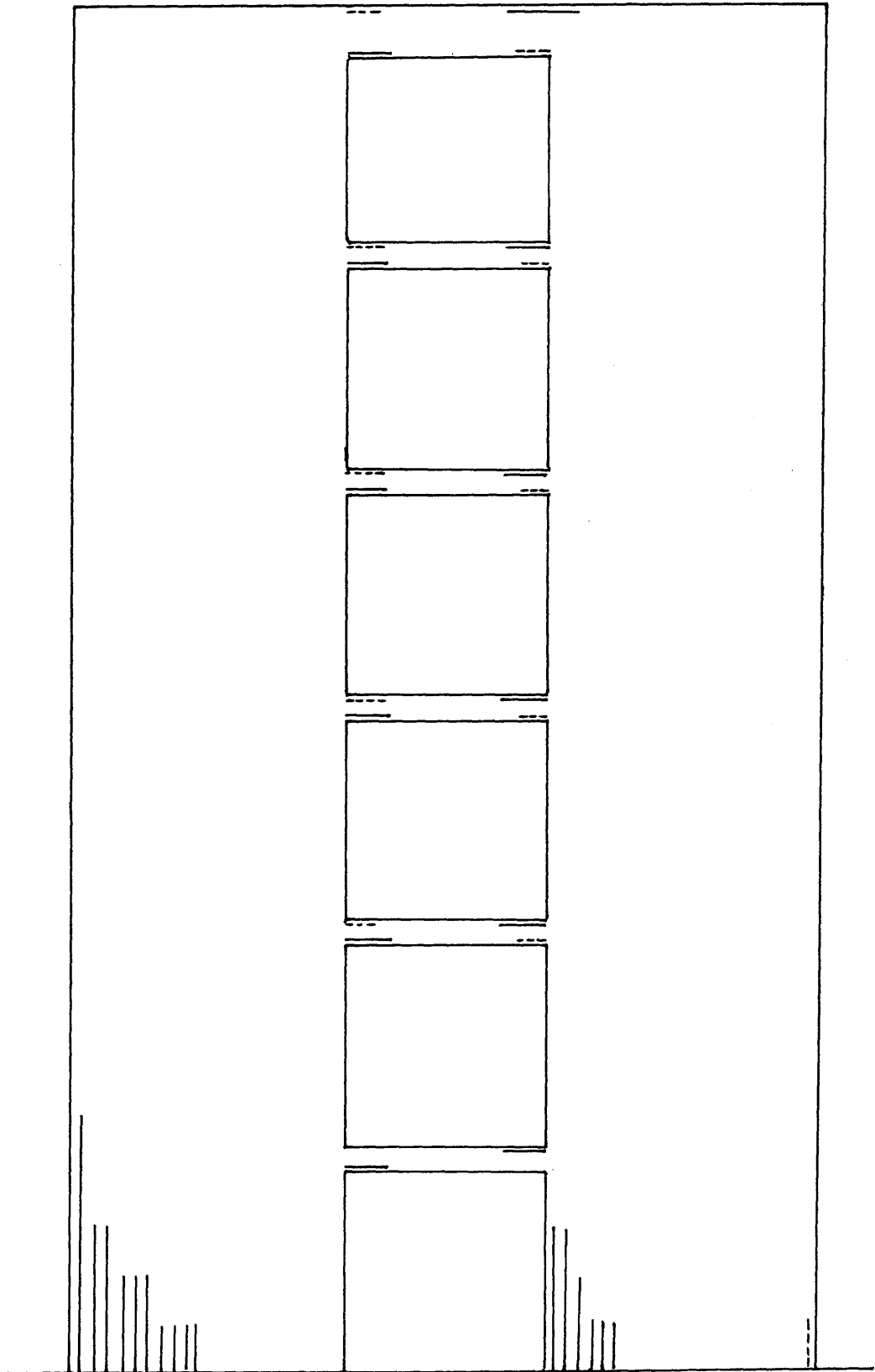## 1408 kN

1760 kN

2288 kN

2640 kN

FIG (6-30) .... CONTINUED .

――― Tension   ----- Compression

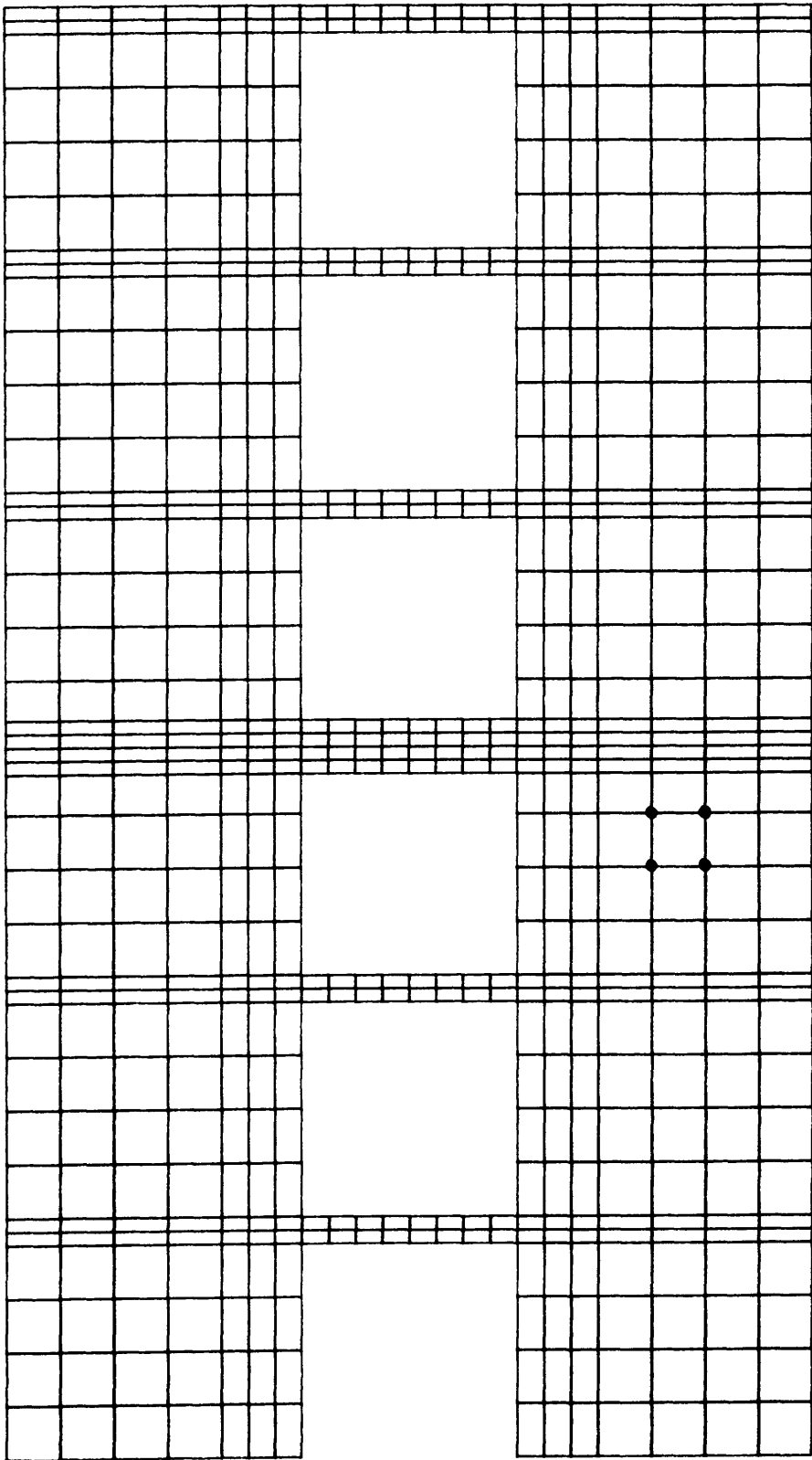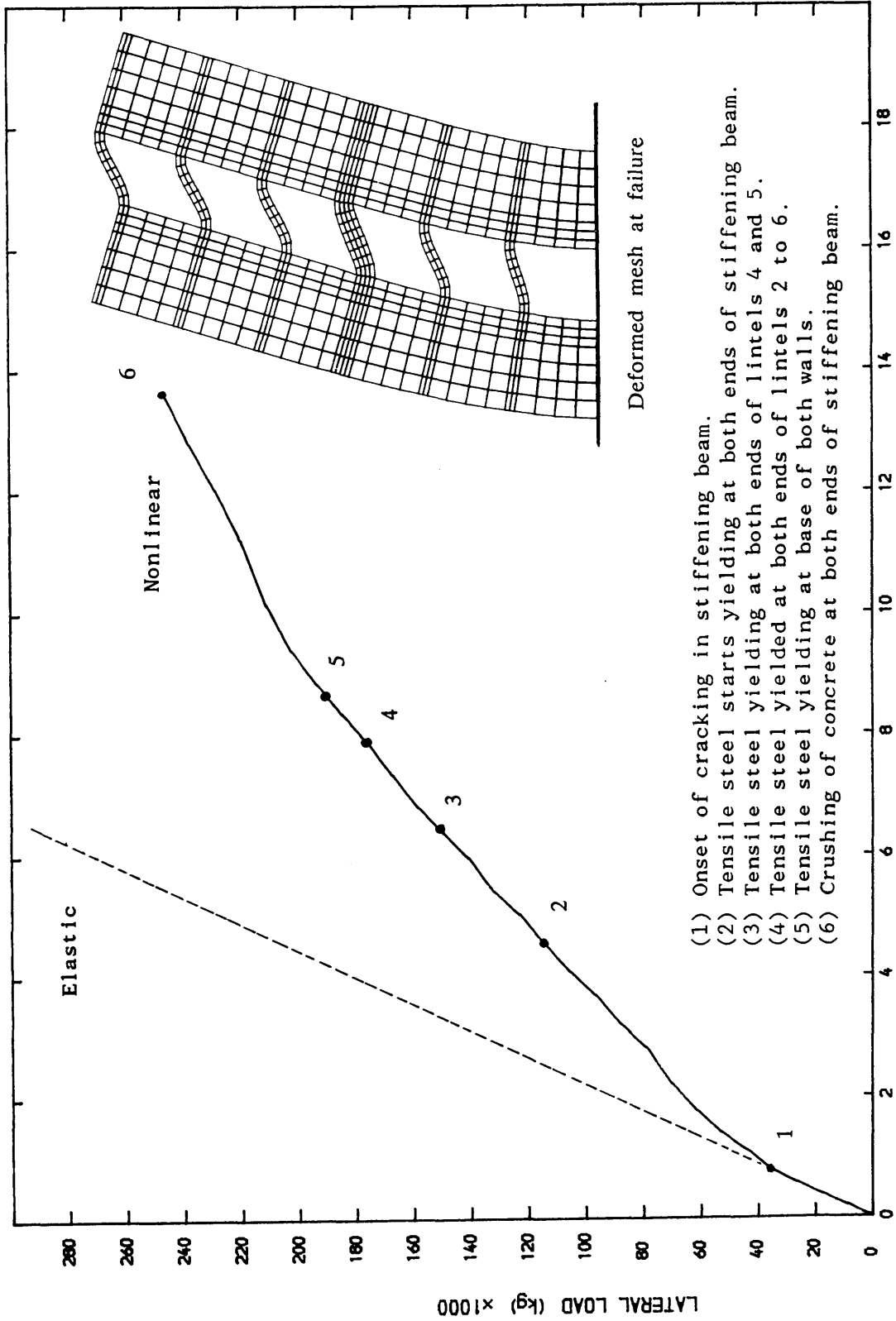FIG (6-31) EXTENT AND DIRECTION OF YIELDED STEEL AT ULTIMATE

FIG (6-32) FINITE ELEMENT DISCRETIZATION FOR WALL
STIFFENING BEAM AT MID-HEIGHT

(1) Onset of cracking in stiffening beam.
(2) Tensile steel starts yielding at both ends of stiffening beam.
(3) Tensile steel yielding at both ends of lintels 4 and 5.
(4) Tensile steel yielded at both ends of lintels 2 to 6.
(5) Tensile steel yielding at base of both walls.
(6) Crushing of concrete at both ends of stiffening beam.

FIG (6-33) *LATERAL LOAD-DISPLACEMENT FOR WALL WITH STIFFENING BEAM AT MIDHEIGHT*
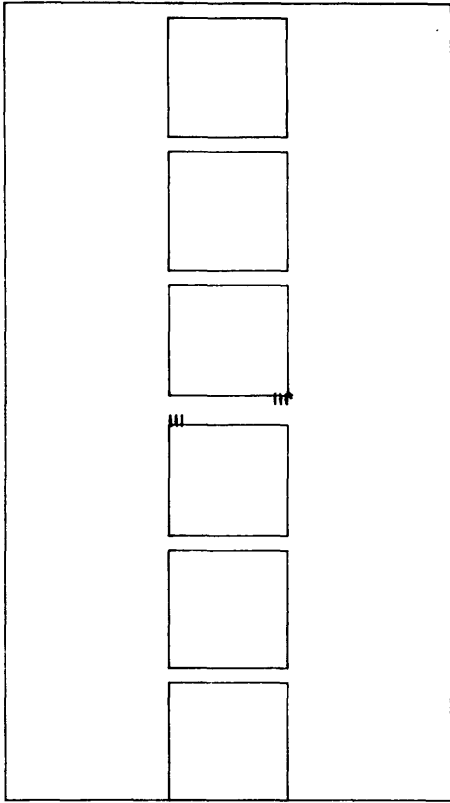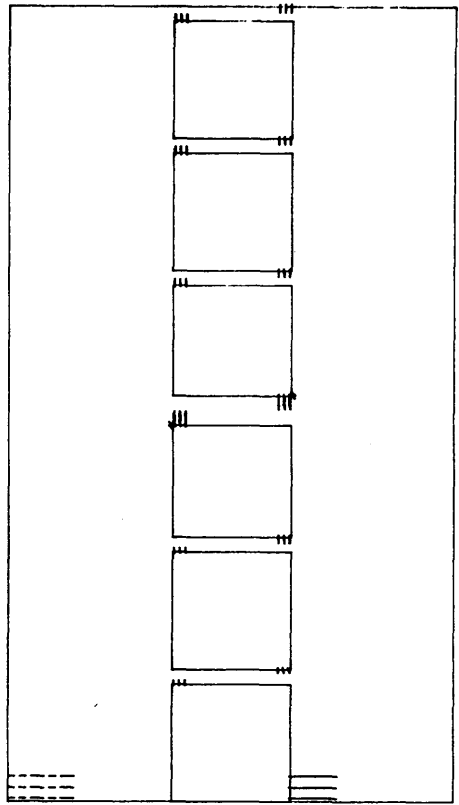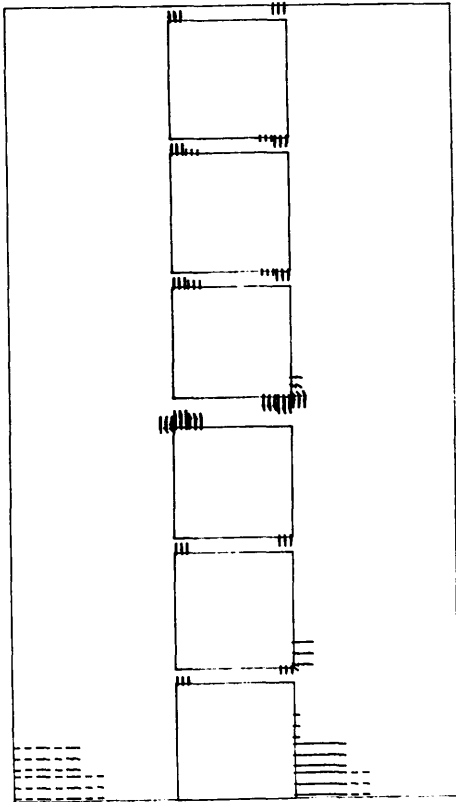
FIG (6-34) CRACK PATTERN AND PROPAGATION FOR WALL
WITH STIFFENING BEAM AT MID-HEIGHT.

1408 kN

1760 kN

2200 kN
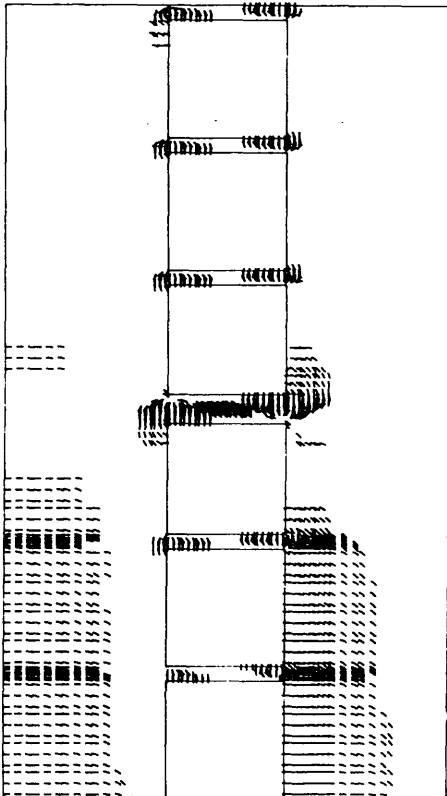
2464 kN
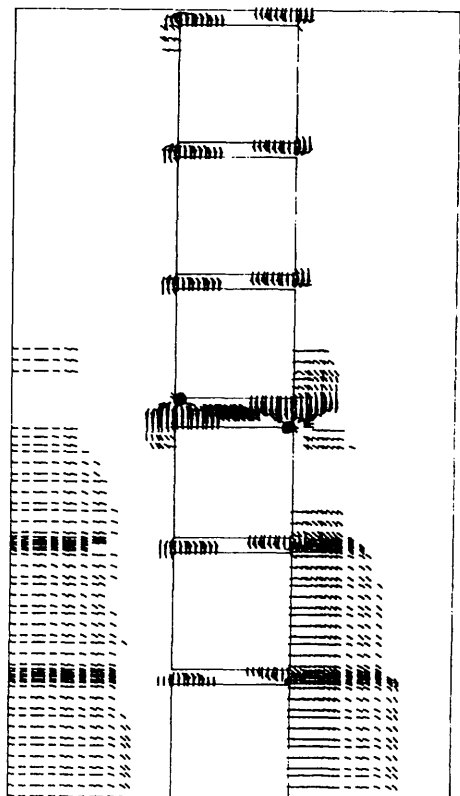
● Crushed concrete

FIG (6-34) .... CONTINUED ..

——— Tension ----- Compression

FIG (6-35) EXTENT AND DIRECTION OF YIELDED STEEL AT ULTIMATE

6-5 MICROCONCRETE MODELS:

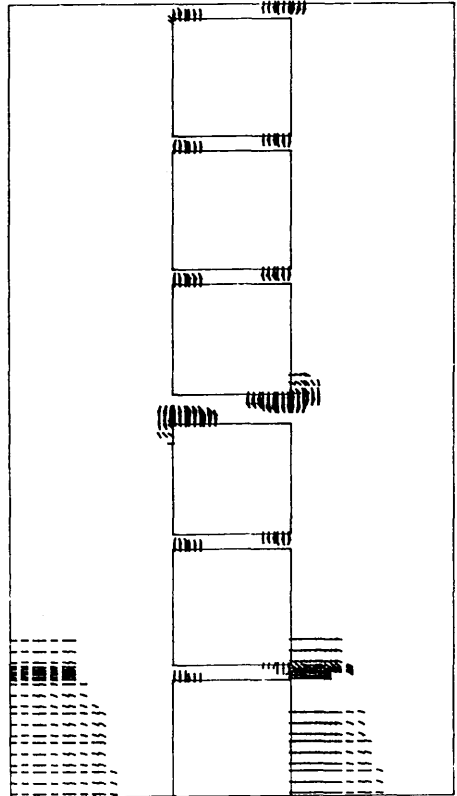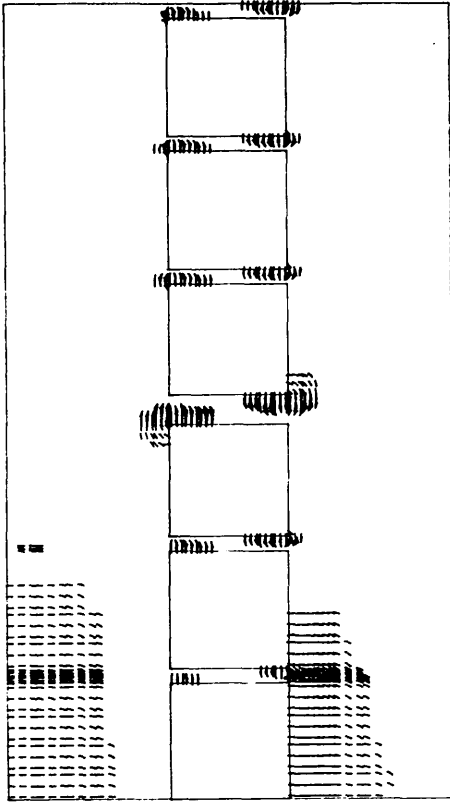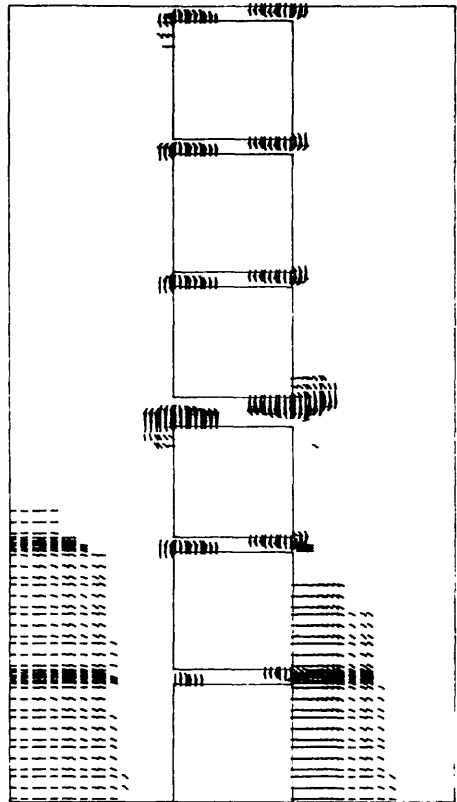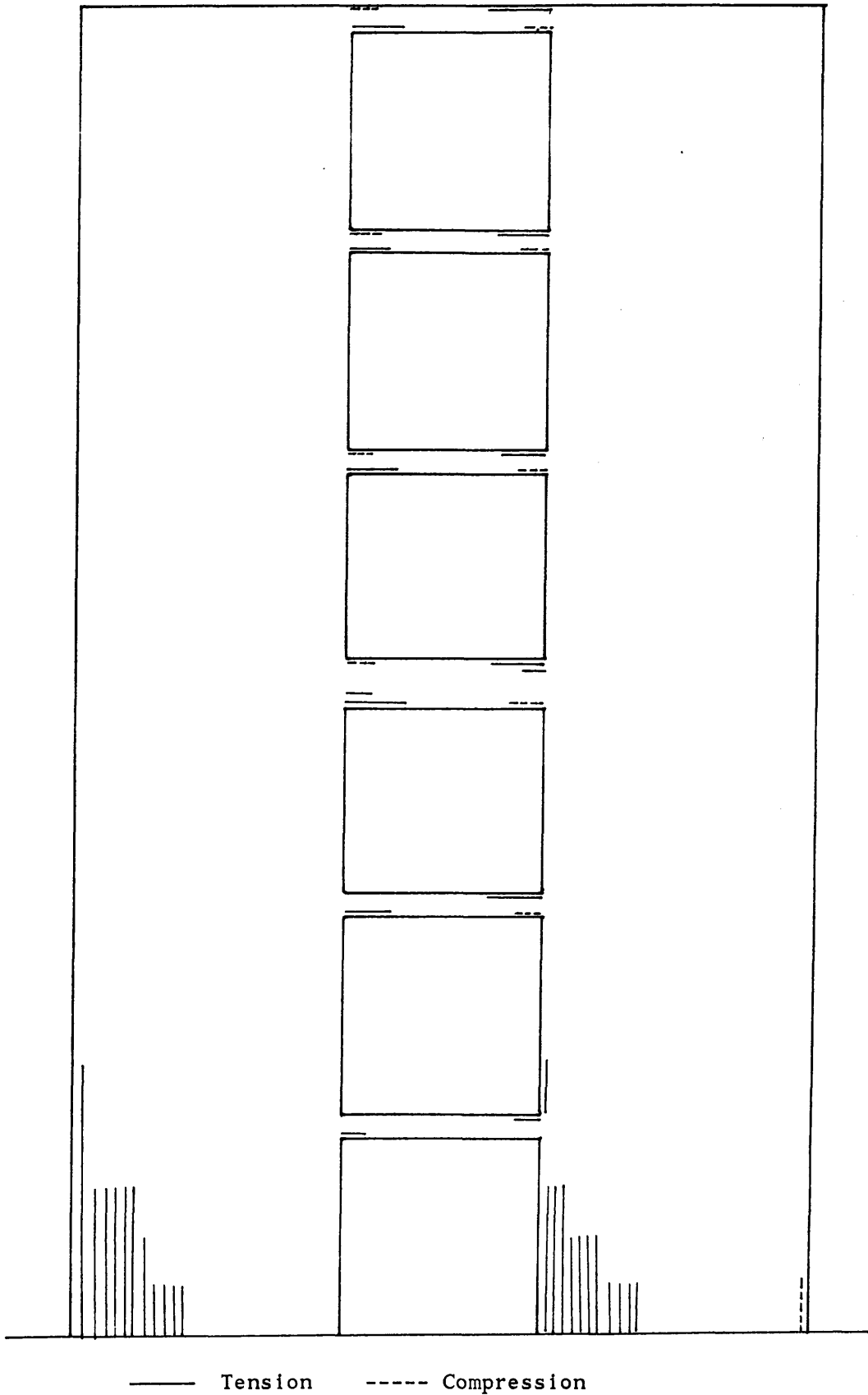Subedi 1991 tested experimentally to failure three microconcrete models of coupled shear walls, representing approximately 1/30 scale of a 15 story building. In the present study Subedi's Model 1 and Model 3 are studied using the present numerical model. Model 1 was made of cement and graded sand with a maximum aggregate size of 2.36 mm. In the case of Model 3, normal concrete with a maximum aggregate size of 5 mm was used. The geometry and reinforcement details of the models were chosen to give different modes of failure, flexure for Model 1 and shear for Model 3. The details of material properties are given below as found in tests by Subedi 1991:

Model 1

$f_c' = 48.3$ N/mm^2

$f_t = 2.3$ N/mm^2

$f_y = 385$ N/mm^2

Model 3

$f_c' = 40.0$ N/mm^2

$f_t = 1.9$ N/mm^2

$f_y = 450$ N/mm^2

Model 1 : The finite element mesh for model 1 is shown in Fig (6-38). Fig (6-39) shows the top lateral deflection at different stages of loading. The onset of cracking is predicted at 500 N in the lintel beams as compared to 1800 N where the first sign of cracks appeared in the experiment. This may be due to the development of microcracks (internal) that cannot be observed by the naked eye during the experiment. At 4300 N crushing of compression concrete in the lintel beams at levels 7 to 14 is observed in the numerical analysis. At 5300 N the numerical model collapses by further crushing at the base of right hand compression wall and yielding of tensile steel at the base of the left tensile wall. The experimentally recorded collapse load is 4950 N where nearly all coupling beams failed in flexure and crushing of the compression wall were observed by

Subedi 1991. It is concluded that both the ultimate load and mode of failure are predicted satisfactorily.

Model 3 : The finite element discretization is shown in Fig (6—41). The mesh might be criticised because the element aspect ratio is relatively high, however due to the size of the problem at hand compromise on the degree of refinement has to be made. Avoiding the aspect ratio problem would lead to either coarse or very refined finite element grid both of which are inefficient from the point of view of reliability and computational cost respectively. Cracks start to develop at 6000 N compared to 18000 N experimentally, difference due to microcracks as suggested above. At 27000 N tensile steel yielded in both walls in the numerical analysis. At 33000 N compressive steel yields in the right wall and at 38000 N the concrete compressive stress reaches f_c' in the right wall. Shortly afterwards at 40000 N concrete crushes in the right wall by compression. The numerical model collapses at 50000 N. Experimentally, the model collapses at 53000 N by beams failing in shear and crushing of compression walls, which is in good agreement with the numerical model.

CONCLUSIONS :

The history and sequence of cracking, crushing of concrete and yielding of steel can be predicted by the use of the finite element up to failure in the analysis of reinforced concrete coupled shear walls.

Severe deviations between an elastic analysis and a full nonlinear analysis are highlighted in the lateral load top deflection curves shown for various reinforced concrete coupled shear walls analysed. This is important even at lower load levels and before any yielding of steel showing the importance of cracking in a realistic

analysis. The crack pattern and direction are in agreement with what would be expected in an experimental test. The comparison of the prediction obtained by the present numerical model and the microconcrete experimental tests of Subedi 1991 presented in this chapter and the numerical tests presented in chapter 5 for the validation of the model suggest that the numerical model developed in the study proved to be a valuable research tool to be used with confidence in conjunction with experimental tests for a further understanding of the nonlinear behaviour of reinforced concrete coupled shear walls. Simplicity yet main nonlinear behaviour of reinforced concrete taken into account was the basis for building the model.

The use of the initial elastic stiffness matrix throughout the nonlinear analysis was found very efficient to reduce the computational cost of the analysis. Furthermore, the use of an updated stiffness matrix during the incremental— iterative process will not only increase the computational cost prohibitively but may fail due to crushing at the ends of lintel beams as the global stiffness matrix approaches singularity and the problem of ill— conditionning may arise leading to a premature numerical collapse.

References

SUBEDI, N. K.
RC coupled shear wall structures II:
Ultimate strength calculations
*Journal of Structural Engineering, A.S.C.E,
Vol. 117, No. 3, pp. 681—898, 1991.*

MODEL 1

① SWG 10   ③ SWG 14
②   12   links   19

Section of wall near base
All dimensions are in mm
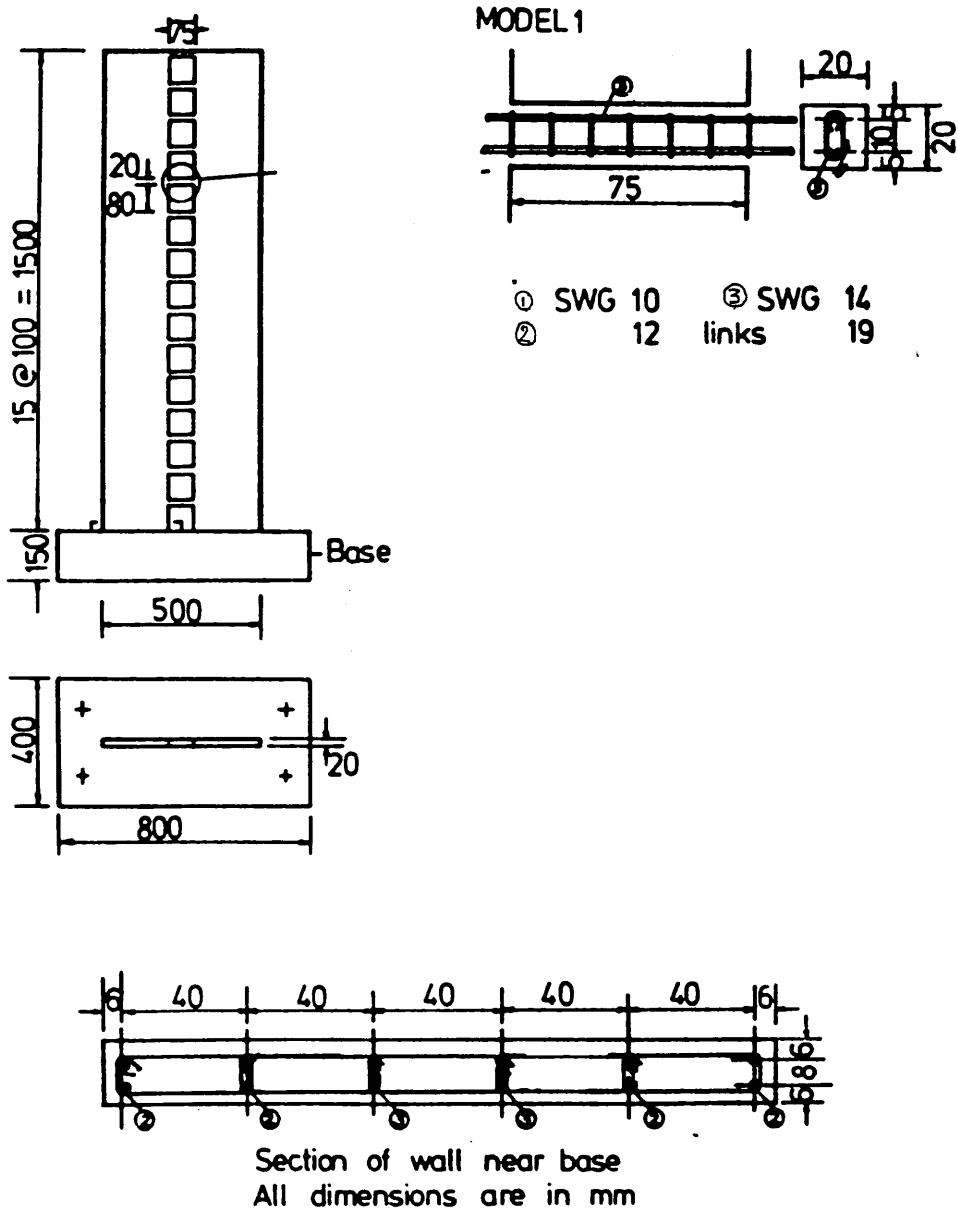
FIG (6-37) SUBEDI'S 15 STOREY MICROCONCRETE MODEL (1)
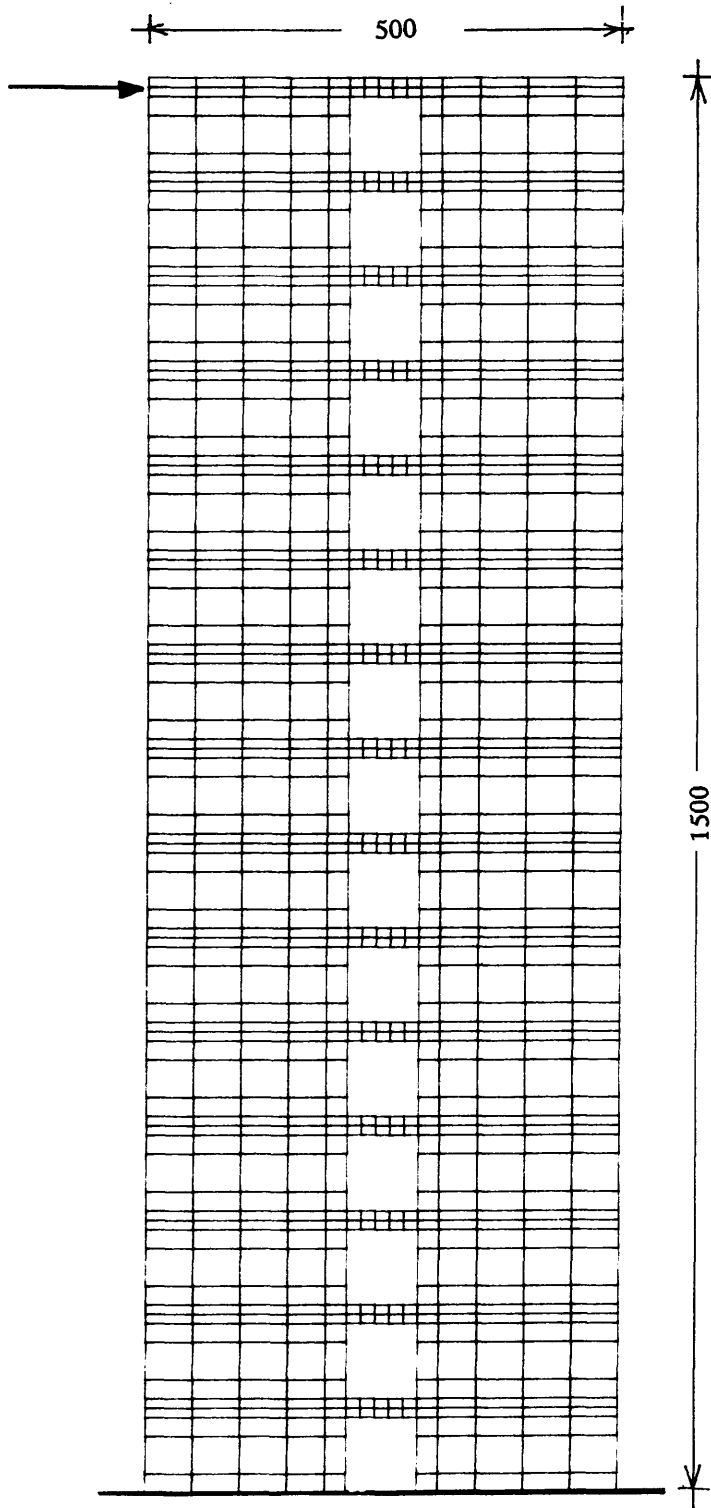
FIG (6-38) FINITE ELEMENT MESH FOR MODEL (1)

Linear elastic

Experimental ultimate load

(3)

(2)

Nonlinear
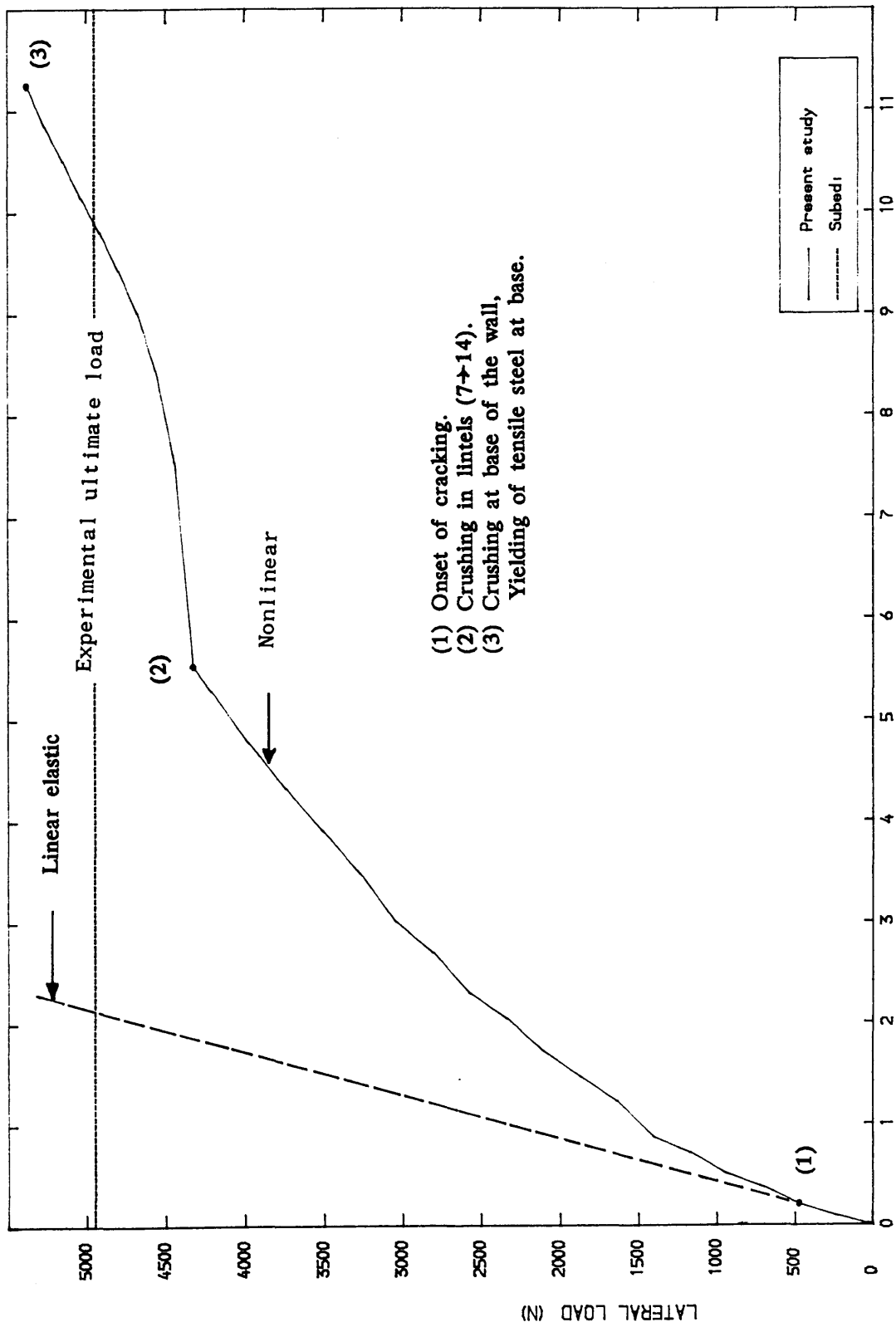
(1) Onset of cracking.
(2) Crushing in lintels (7→14).
(3) Crushing at base of the wall,
    Yielding of tensile steel at base.

(1)

Present study

Subedi

LATERAL LOAD (N)

LATERAL DEFLECTION (mm)

FIG (6-39)   LATERAL LOAD DEFLECTION FOR SUBEDI 15 STOREY RC WALL (MODEL 1)

MODEL 3

All main bars are 4.75 mm ⌀
All dimensions are in mm

Base 1200 × 1200

Section of wall near base

only main bar are shown

2mm ⌀ links
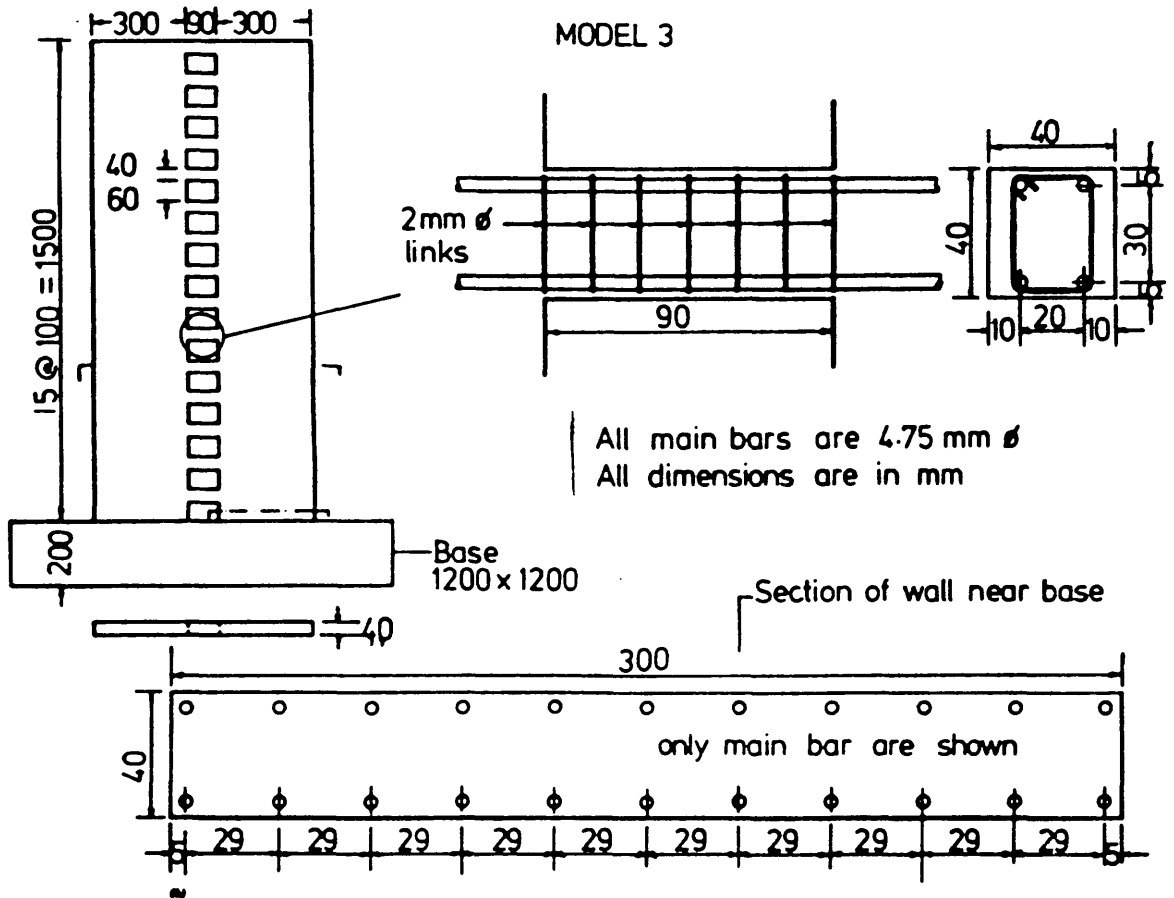
FIG (6-40) SUBEDI'S 15 STOREY MICROCONCRETE MODEL (3)
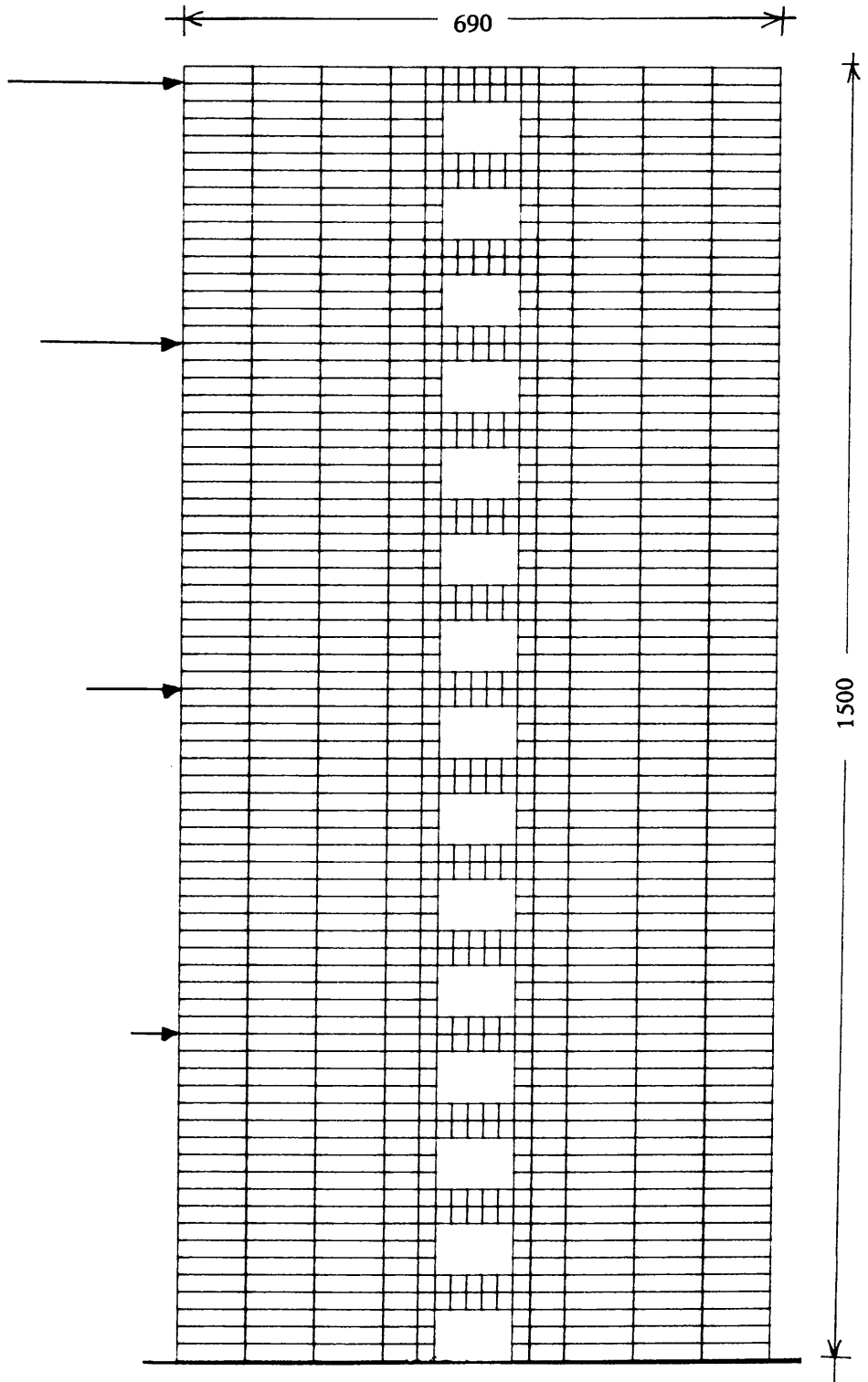
FIG (6-41) FINITE ELEMENT MESH FOR MODEL (3)

Linear elastic

—·—·—·— Experimental ultimate load

Nonlinear

(6)

(5)
(4) .
(3)
(2)
(1)
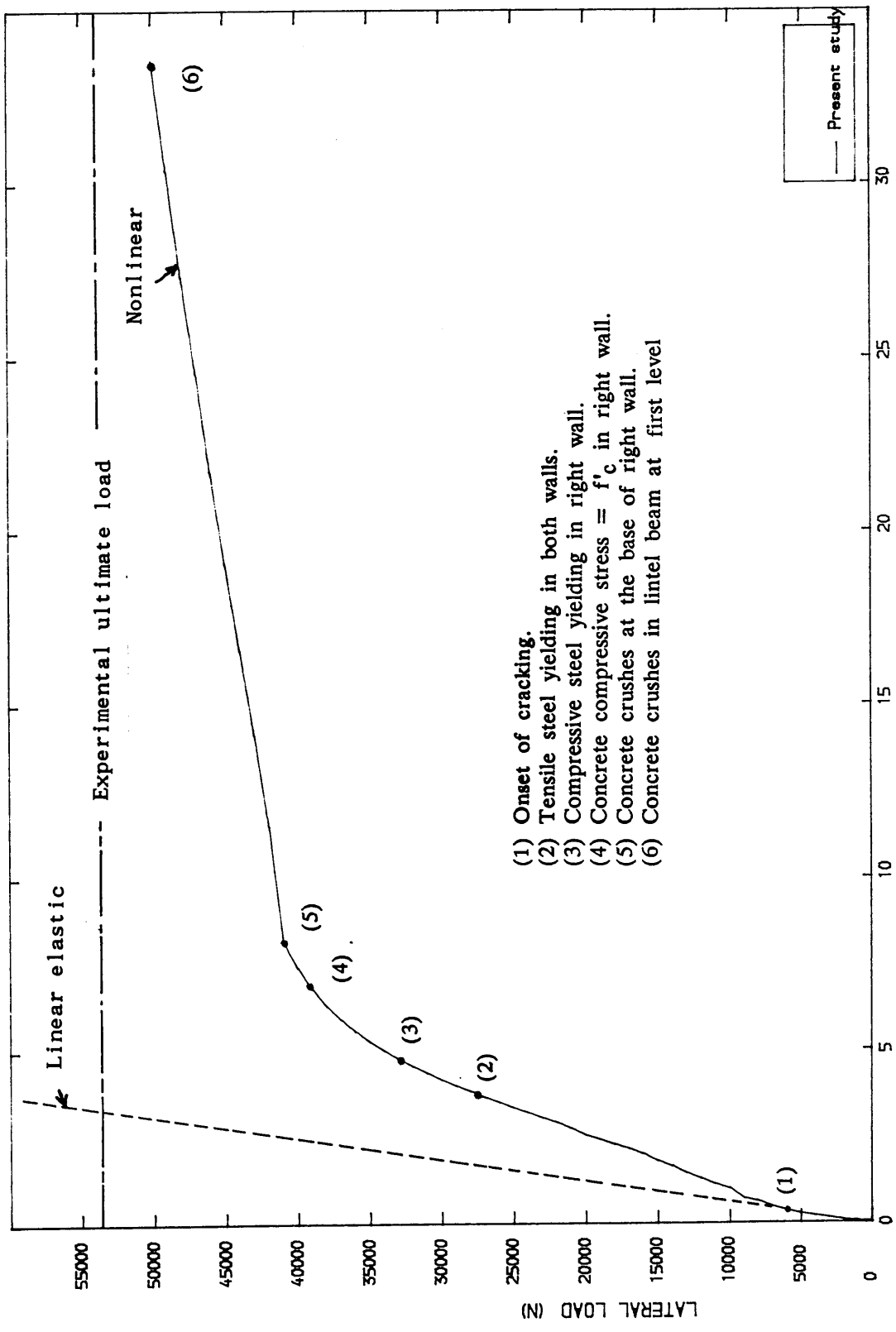
(1) Onset of cracking.
(2) Tensile steel yielding in both walls.
(3) Compressive steel yielding in right wall.
(4) Concrete compressive stress = f'c in right wall.
(5) Concrete crushes at the base of right wall.
(6) Concrete crushes in lintel beam at first level

LATERAL LOAD (N)

55000
50000
45000
40000
35000
30000
25000
20000
15000
10000
5000
0

0   5   10   15   20   25   30

LATERAL DEFLECTION (mm)

——— Present study

FIG (6-42)   LATERAL LOAD DEFLECTION FOR SUBEDI 15 STOREY RC WALL (MODEL3)

CHAPTER 7

CONCLUSIONS AND RECOMMENDATIONS

7-1 general:

The present study started with the development of a simple elastic finite element program for the analysis of coupled shear walls using a suitable higher order element. Comparison of the finite element results with those of the continuum and wide-column frame analogies presented in chapter (2) revealed the superiority (at a much higher computational cost) of the finite element method.

Incorporation of the main features of nonlinear behaviour of concrete and steel into the simple elastic model above, validated in chapter 5 by comparison to other carefully conducted experimental tests proved the suitability of the linear cubic element in modelling reinforced concrete, in contrast to the widely used isoparametric parabolic element.

Numerical simulation tests shown in chapter 6 highlighted the nonlinear behaviour of reinforced concrete coupled shearwalls up to failure. Very few experimental tests are available, the present model as shown in chapter 6 can be used to predict the history of crack propagation, sequence of yielding of steel and crushing of concrete in the lintel beams and walls to assess the overall mode of failure. Although an automatic finite element mesh generator has been developed to facilitate the pre-processing phase, post-processing was found somewhat a difficult task due to the amount of valuable output (in the order of 10^6 lines). Nevertheless, the salient numerical results have been presented in chapter 6.

In this chapter, the main conclusions from the study are presented.

7— 3 Non— elastic analysis of planar reinforced concrete beams and panels:

On the basis of the results presented in chapter 6, the following conclusions regarding the applicability of finite element analysis can be drawn:

(1) The major conclusion from this study is that the finite element method can be used to predict the behaviour of reinforced concrete members subjected to in plane forces if proper account is taken in modelling the material behaviour. The load deflection response, crack pattern, failure load and failure mode can be predicted with an accuracy that is acceptable for engineering purposes.

(2) The expectations from nonlinear finite element analysis of reinforced concrete structures are fulfilled in so far as it appears to be a significant improvement (but no more) over classical methods of analysis of such structures, which are not able to account adequately for important mechanical phenomena in a rational manner.

(3) The simple strength criterion with a fixed smeared crack model is adequate to study global behaviour of many structural problems as demonstrated by the various reinforced concrete structures examined.

(4) Smeared crack approaches are capable of predicting dominant diagonal cracks which occur in shear failure. Reasonable crack patterns were obtained for the sample problems presented in chapter 5 although the numerical model generally predicts a more diffused crack system than the physical reality. This is due mainly to the present limitations of the smeared crack concept.

(5) In shear critical beams, the numerical results and in particular the ultimate load is not greatly sensitive to the shear retention factor adopted. A constant shear retention factor $\beta = 0.5$ was found to lead satisfactory results and therefore has been adopted in this study. Further research should be stimulated to better estimate the complete crack interface

stiffness matrix so as to agree with experimental findings from laboratory tests to replace the simple shear retention factor.

(6) Smeared steel modelling was found to yield satifactory results even for beams reinforced with individual bars, when the finite element grid is appropriately chosen around the bar.

(7) A modified Newton—Raphson algorithm in which the global stiffness matrix is updated in the second iteration of each load increment has been found to be effective for the analysis in most problems investigated.

(8) The numerical tests and results presented in chapter 6 demonstrate the suitability of the concrete model in simulating the dominant behaviour characteristics of reinforced concrete elements.

7-4 Non-elastic analysis of reinforced concrete shear walls:

On the basis of the variety of examples analysed, it can be concluded that the computational model developed in this study is useful for studying complex structural behaviour such as coupled shear walls. The entire structural response of these structures including cracking loads, crack development and crushing of concrete, yielding of steel, ultimate load and the collapse mechanism can be predicted.

(1) The standard Newton-Raphson method, where the initial elastic global stiffness matrix is used throughout the analysis, was found to be efficient in analysing large reinforced concrete structures such as coupled shear walls, reducing the total computational cost, as the formation and factorization of the global stiffness matrix constitutes the majority of the computational effort in such large problems.

(2) The numerical model is shown to be a valuable tool, to be used in combination with experiments on reinforced concrete coupled shear wall structures, permitting more comprehensive investigations.

Finally, the finite element analysis developed for this initial investigation could be used for a more refined and detailed parametric study of shear wall behaviour over the full load range. This could lead to more conclusive suggestions for possible improvements in the design of reinforced concrete coupled shear walls.

7- 5 Suggestions for future study:

A number of areas remain to be examined for the wider, practical application of the finite element method for the prediction of concrete behaviour. Some suggestions are given for possible improvements of the present formulation and extension of this investigation.

(1) It has been observed in analysing coupled shear walls, that the collapse is in fact numerical when crushing occurs in the lintel beams, and the solution process becomes unstable. In fact, even a complete collapse of a few lintel beams does not necessarily mean failure of the structure, as the walls may still be capable of carrying further loading. Therefore, it is suggested that a procedure should be developed by which, a redefinition of the original mesh removing the crushed elements is devised and information about the state of the material transferred from the previous mesh to the new updated mesh.

(2) Because of cracking and the yielding of reinforcement at the base of reinforced concrete shear walls, it might be useful to use a model whereby variable boundary conditions replace the fully fixed conditions assumed at all stages of loading. This can be achieved by assuming two orthogonal springs with softening as a function of the steel strain to model partially fixed wall at high stresses. This problem does not arise for simply supported (point support) structures, but for cantilevers and shear walls where continuous fixed support exists.

(3) The influence of mesh refinement and aspect ratio of the element on the nonlinear behaviour prediction needs to be examined.

(4) A restarting procedure should be useful for the continuation of the nonlinear solution in cases of highly nonlinear problems or when the iterative process fails.

(5) Improvements of the nonlinear solution algorithm to reduce the computer time. Improving the efficiency of the present formulation may be achieved by implementation of

matrix update schemes such as BFGS methods.

(6) Tracing of the structural response beyond the maximum load level is desirable. This can be achieved by including the strain softening behaviour of concrete and using nonlinear numerical procedures such as the arc length methods to trace the post peak behaviour.

(7) The rotating smeared crack model should be implemented as confirmed by the experimental tests of Vecchio and Collins, enabling a better prediction of reinforced concrete membranes.

(8) More accurate deformational response are required for some problems. This may be achieved by a more consistent description of the concrete— reinforcement interaction effects by introducing bond elements to simulate bond— slip.

(9) For reinforced concrete beams the finite element embedded formulation, especially the newly emerged generally orientated with bond slip is more appropriate to analyse reinforced concrete beams.

(10) Extension of the material model to include long term effects on concrete behaviour (Creep and Schrinkage) as well as cyclic loading.

(11) Finally, a macroscopic model using a wide— column frame analogy and including nonlinearities by moment curvature relationships is more attractive from the computational viewpoint and would be more suitable for design office use.